AREVA

Response to RAIs on WCAP-17788 Volume 4 - CE Plants

ANP-3583NP

LICENSING REPORT

Revision 1

December 2017

AREVA Inc.

Nature of Changes

Item	Section(s) or Page(s)	Description and Justification
1	Sect 2.1.2.1	Modify to correct reference to WEC response and to be consistent with WEC response.
2	Sect 2.1.2.3	Updated to be consistent with WEC response.
3	Sect 2.30.2	Added response to part b.

Contents

List of Tables

List of Figures

Nomenclature

Acronym	Definition
AC	Average Core
AFP	Alternate Flow Path
ANS	American Nuclear Society
AOR	Analysis of Record
B&W	Babcock & Wilcox
BAP	Boric Acid Precipitation
BAPC	Boric Acid Precipitation Control
BB	Barrel/Baffle
BE	Best Estimate
BOC	Beginning of Cycle
CC	Central Core
CE	Combustion Engineering
CHF	Critical Heat Flux
CL	Cold Leg
COLR	Core Operating Limits Report
DC	Downcomer
DEG	Double-Ended Guillotine
DH	Decay Heat
ECC	Emergency Core Cooling
ECCS	Emergency Core Cooling System
EM	Evaluation Model
FA	Fuel Assembly
GDC	General Design Criterion
GSI	Generic Safety Issue
HA	Hot Assembly
HL	Hot Leg
HLI	Hot Leg Injection

Acronym	Definition
HPSI	High Pressure Safety Injection
HTC	Heat Transfer Coefficient
INL	Idaho National Laboratory
LAR	License Amendment Request
LBLOCA	Large Break Loss of Coolant Accident
LH	Lower Head
LHGR	Linear Heat Generation Rate
LOCA	Loss of Coolant Accident
LOOP	Loss of Offsite Power
LP	Lower Plenum
LPSI	Low Pressure Safety Injection
LTCC	Long Term Core Cooling
MWR	Metal-Water Reaction
NRC	Nuclear Regulatory Commission
PC	Periphery Core
PCT	Peak Cladding Temperature
PWR	Pressurized Water Reactor
PWROG	Pressurized Water Reactor Owner's Group
PZR	Pressurizer
RAI	Request for Additional Information
RBHT	Rod Bundle Heat Transfer
RCP	Reactor Coolant Pump
RCS	Reactor Coolant System
RHR	Residual Heat Removal
RLBLOCA	Realistic Large Break Loss of Coolant Accident
RV	Reactor Vessel
RWST	Refueling Water Storage Tank
RWT	Reactor Water Tank
SBLOCA	Small Break Loss of Coolant Accident

Acronym	Definition
SE	Safety Evaluation
SG	Steam Generator
SI	Safety Injection
SIRB	Safety Issues Resolution Branch
SIT	Safety Injection Tank
SONGS	San Onofre Nuclear Generating Station
SSO	Sump Switch Over
TH	Thermal Hydraulic
TR	Topical Report
TS	Technical Specifications
UH	Upper Head
UHSN	Upper Head Spray Nozzle
UP	Upper Plenum
V&V	Verification and Validation
WEC	Westinghouse Electric Company

1.0 Summary

In July of 2015, the Pressurized Water Reactor Owner's Group (PWROG) submitted licensing Topical Report (TR) WCAP-17788 "Comprehensive Analysis and Test Program for GSI-191 Closure" intended for Generic Safety Issue (GSI)-191 closure (Reference 1). The TR is an approach to define an in-vessel fibrous debris limit and provides a means for increasing the approved fibrous debris limit used by licensees to resolve GSI-191.

By letter dated August 18, 2016, the Safety Issues Resolution Branch (SIRB) of the Nuclear Regulatory Commission (NRC) provided Requests for Additional Information (RAIs) on Volume 4 of WCAP-17788-P in order to complete their review (Reference 2). This report is intended to capture the response to these RAIs that fall within AREVA's scope of the project.

The results of the original thermal-hydraulic analyses for the Combustion Engineering (CE) plant category are presented in WCAP-17788-P, Volume 4, Section 10. These analyses used a coupled containment code called ICECON to calcualted the containment backpressure in lieu of setting a constant value of 14.7 psia, like the WEC and B&W analyses. In RAI 4.1b, the NRC requested a justification that the use of ICECON was appropriate for use for the GSI-191 analyses. In response to that RAI, a new "base" case was developed that removed ICECON from the analyses and set the containmnet pressure to a constant 14.7 psia. The new case described in the response to RAI 4.1b is used as a basis for all of the other RAI responses, as appropriate. As a consequence of this and other RAI responses, WCAP-17788-P, Volume 4 was extensively revised. The markups from the original submittal are provided separately.

References

1 PWROG letter dated July 17, 2015, Stringfellow, N.J. (PWR Owners Group) to Rowley, J.G. (U.S. NRC), Submittal of WCAP-17788, "Comprehensive Analysis and Test Program for GSI-191 Closure (PA-SEE-1090)," (ML15210A668).

2 NRC letter dated August 18, 2016, Rowley, J.G. (U.S. NRC) to Nowinowski, W.A. (PWR Owners Group), Request for Additional Information Re: Pressurized Water Reactor Owners Group Topical Report WCAP-17788, Comprehensive Analysis and Test Program for GSI-191 Closure (TAC No. MF6536), (ML16195A362).

2.0 REQUESTS FOR ADDITIONAL INFORMATION AND RESPONSES

2.1 RAI 4.1

2.1.1 Statement of RAI 4.1

General Design Criterion (GDC) 35, "Emergency Core Cooling," in Appendix A, "General Design Criteria for Nuclear Power Plants," to Title 10 of the Code of Federal Regulations (10 CFR) Part 50, requires that a single failure be assumed when analyzing safety system performance. Sections 8.2, 9.2, 10.2, and 11.2 present safety system performance analysis results for four different plant categories.

(a) Describe the single failure assumptions implemented in the analyses of the safety system performance for the four analyzed plant categories. Identify the single failure assumption(s) applied in the modeling of the reactor coolant system (RCS) response including the performance of the emergency core cooling system (ECCS). Justify the assumptions by describing pertinent conditions, supporting considerations, and applicable analyses.

(b) The analyses for the Combustion Engineering (CE) plant category were performed with the containment backpressure computed by a coupled containment code. Demonstrate how the single failure assumptions implemented in the RCS response analysis for this plant category, as well as any additional and related assumptions, were considered for the purposes of calculating the containment backpressure response. Verify that treatment is consistent with Assumption No. 6 in Section 4.1, "Major Assumptions," and Input No. 6 in Section 4.2, "Critical Inputs".

(c) Provide information that demonstrates whether plant-specific considerations are necessary to address GDC 35 when considering safety system performance on a plant-specific basis. Explain how the single failure assumptions implemented in the T-H analyses in Sections 8.2, 9.2, 10.2, and 11.2, as considered in the response to Items a and b above, remain valid for each plant category. Describe how it was determined whether additional single failure assumptions and applicable supporting considerations were required for plant specific T-H analyses. If necessary, identify the types of plant specific information related to systems, conditions, parameters, and other relevant items that will need to be considered for adequate implementation of the topical report (TR) with respect to GDC 35 on a plant specific basis.

2.1.2 Response to RAI 4.1

2.1.2.1 Part a

The analyses consider the effect of the limiting single failure on Emergency Core Cooling System (ECCS) performance. The minimum Safety Injection (SI) flow rate and maximum SI delay times are used based on plant technical specification limits from the base plant models selected for each plant category. The base plant models are identified and described in RAI 4.29.

The limiting single failure also takes into account the effect on containment pressure. Failure of an entire safety train would result in the loss of one or several containment spray and fan cooling units, reducing containment cooling, and increasing containment pressure, which will reduce cladding temperatures during a debris-induced secondary heatup. As such, the inputs to the containment pressure are skewed in order to obtain a conservative (low) pressure transient such that cladding temperatures during any calculated debris-induced secondary heatup are maximized.

The single failure assumptions applied during the recirculation phase of the accident are disconnected from those applied during the injection phase of the accident transient. In the simulations, an early sump switchover time is applied that is representative of two trains of safety injection during the injection phase. An early sump switchover time is more limiting for Generic Safety Issue (GSI) -191 scenarios since the decay heat is higher and Reactor Coolant System (RCS) liquid inventory is lower. Sensitivity studies performed by Westinghouse Electric Company (WEC) demonstrate that an earlier arrival of debris results in a higher calculated cladding temperature during the debris-induced secondary heatup (see WEC response to RAI 4.19, Item b). As described in the response to RAI-4.1 Item c., utilities implementing the WCAP-17788 in-vessel debris methodology will need to verify that they fall within the range of conditions considered by the analyses. More details regarding how this check is performed are provided in the response to RAI-4.5 Item a.

2.1.2.2 Part b

Prior to implementing the Realistic Large Break Loss of Coolant Accident (RLBLOCA) Evaluation Model (EM), the break pressure boundary condition for RELAP5 Loss of Coolant Accident (LOCA) analysis had been supplied by use of a time-dependent volume component which simulated the reactor containment. This time-dependent volume supplied either an estimated constant containment pressure, or a time-dependent pressure obtained from a separate containment analysis code. Neither of these methods guaranteed a break pressure boundary condition that was consistent with the actual mass and energy discharge for the specific LOCA being analyzed.

In order to provide a more accurate break pressure boundary condition for S-RELAP5 best estimate LOCA analysis, a detailed containment model was integrated into S-RELAP5. This containment model is derived from the AREVA NP licensing code ICECON (Reference 4.1-1). The fundamental basis of the ICECON computer code is the CONTEMPT/LT-022 code, (References 4.1-2 and 4.1-3) to which an ice condenser model (Reference 4.1-4) was added by Exxon Nuclear Company, a predecessor to AREVA NP.

ICECON calculates the time variation of compartment pressures, temperatures, mass and energy inventories, heat structure temperature distributions, and energy exchange with adjacent compartments. The program is capable of describing the effects of penetration and small crack leakage on containment response. Models are provided to describe fan cooler and cooling spray engineered safety systems. ICECON can be used to model from one to four compartments, and any compartment except the reactor system may have both a liquid pool region and a vapor atmosphere region above the pool. Each region is assumed to have a uniform temperature, but the temperatures of the two regions may be different. The program user defines which compartments are used, specifies input mass and energy additions, defines heat structure and leakage systems, and describes the time advancement and output control.

The S-RELAP5/ICECON code integration executes the ICECON sub-code concurrently with S-RELAP5, providing a calculation of containment pressure that is consistent with the break mass flow rate and specific enthalpy currently being generated by S-RELAP5. With the concurrent execution of S-RELAP5 and ICECON sub-routines, an accurate break pressure boundary condition is always available in S-RELAP5. At each time step, S-RELAP5 performs the necessary data transfers between the main code and the sub-code and calls for execution of the sub-code. After execution of the sub-code, ICECON returns a containment pressure to S-RELAP5 for use in the next time step, and control is returned to S-RELAP5, which continues execution.

In order to obviate the need for a single failure assumption in the containment backpressure calculation, the Combustion Engineering (CE) analysis has been re-executed with a constant containment pressure boundary condition of 14.7 psia after 200 seconds. For the first 200 seconds of the transient the pressure boundary conditions are imposed to be those calculated by the ICECON code in the initial analysis. A maximum baffle resistance is applied for this case, along with a minimum ECCS flow of 827 gpm (representing a minimum total SI flow after sump recirculation begins). The new case starts with the model described in the addendum (Ref. 4.1-5) and includes the following changes:

- The decay heat multiplier is reduced to a value of 1.1 (110%). This change is justified in the paragraph that follows this list of changes.
- The Upper Head Spray Nozzles (UHSNs) leakage path is blocked because this

path is not expected to be open during normal operation for CE plants. This path was inadvertently included in the original CE analyses.

- The core shroud region exit connection is moved from Upper Plenum (UP) to the exit of the Periphery Core (PC) in order to prevent false diffusion of liquid in the UP. The base RLBLOCA model connected the outlet of the shroud region to the upper plenum. For short term core cooling (STCC) analyses, this modeling approach is adequate to obtain the proper core bypass flow rate. However, for GSI-191 applications, this modeling is not strictly correct and leads to artificial entrainment of liquid out the break. As described in the response to Request for Additional Information (RAI) 4.3, there are two possible paths for fluid to exit the shroud region near the top of the core (also see WCAP-17788-P, Volume 4, Figure 3-2). The larger opening is an annular gap below the upper core plate that would allow fluid to flow directly to the core periphery. There is also a small gap around the periphery of the upper core plate that allows flow to the upper plenum. Following complete core inlet blockage upflow in the baffle region will follow the path of least resistance and enter the larger gap below the core plate and into the core periphery. Therefore, this is the path modeled in the GSI-191 analyses and the basis for this change.
- The ECCS temperature will be held constant to 110 °F from 0 to 1200 seconds, with a switch to 212 °F at 1200 seconds. This is an update as the previous analysis conservatively modeled a linear increase in temperature from 110 to 212 °F over this time frame.
- The containment pressure will be set to constant atmospheric pressure (14.7 psia) for the Long Term Core Cooling (LTCC) period.
- The Average Core (AC) exit junction reverse form loss factor is increased to match that of the Central Core (CC). This change conservatively precludes liquid from entering the core from the UP to the AC.
- The maximum time step is reduced to 0.001 s during the post-blockage core uncovery.
- The UP is renodalized to have [ ] below the Hot Leg (HL) in order to reduce numerical diffusion of liquid out the break. Additional discussion on the ramifications of this change are discussed in the response to RAI 4.23.
- The peak Linear Heat Generation Rate (LHGR) is increased to a value of 13.75 $\frac{kW}{ft}$ and the radial peaking factor F_r is increased to a value of 1.81. Power fractions for the core heat structures are adjusted to match the new values for LHGR and F_r. These changes were made to ensure that all CE plants are bounded by the analyses as described in the response to RAI 4.5a.

- The vertical stratification model in the UP is turned off. This change is further discussed in the response to RAI 4.23.
- The transient run time is extended to 30000 seconds. This change ensures that the case is run long enough to show continuous liquid out the break. Additional information is provided in the response to RAI 4.23.

The revised analysis uses the ANS/ANSI-5.1-1979 decay heat model (Reference 4.1-6) with a 1.1 decay heat multiplier. The ANS/ANSI-5.1-1979 decay heat model is part of the base EM (Reference 4.1-7). Reference 4.1-6 notes that the maximum positive uncertainty for periods after shutdown of up to 10^3 seconds is 20% and is reduced to 10% after for time period greater than 10^3 seconds, but less than 10^7 seconds. The major events of interest in this analysis occur at 1200 seconds for Sump Switch Over (SSO) and 20000 seconds for the core inlet blockage. A 1.1 multiplier (10% positive uncertainty) adds additional conservatism to the evaluation, representing the maximum value of uncertainty for the period where relevant phenomena of interest occur, while still being a reasonably high conservative value for the first 1000 seconds, when it amounts to 50% of the maximum positive uncertainty.

The new model described above was used to provide new Analysis of Records (AORs) for the CE plant category. These new analyses will be used to address the RAI responses for the CE-designed plants. For the application of a complete core inlet blockage at 20000 seconds (5.6 hours) after the LOCA (t_{block} case), the core experienced a secondary heatup and a Peak Cladding Temperature (PCT) of 542 °F. All other cases (K_{max}, K_{split}, and m_{split} cases) showed no secondary heatup. Volume 4 will be updated to reflect these new AORs for the CE plant category.

2.1.2.3 Part c

Plant-specific considerations are necessary to address General Design Criterion (GDC)-35. This will be completed by each utility when implementing the WCAP-17788 methodology. Each plant will have to justify applicability of the methodology as part of their plant-specific submittal. Each plant will need to determine their limiting GSI-191 scenario relative to debris accumulation in the reactor vessel, considering appropriate single-failure assumptions. Once the limiting GSI-191 in-vessel debris accumulation scenario is defined, a plant will need to demonstrate that it falls within the bounds of the WCAP-17788 methodology. The response to RAI 4.5 provides details regarding the confirmation checks that each utility must complete to justify applicability of the WCAP-17788 methodology.

References - RAI 4.1

4.1-1 AREVA Inc. Document EMF-CC-039(P), Supplement 1, Revision 5, *ICECON Code Users Manual: A Computer Program Used to Calculate Containment Back Pressure for LOCA Analysis (Including Ice Condenser Plants).*

4.1-2 Richard J. Wagner and Larry L. Wheat Aerojet Nuclear Company Interim Report, I-214-74-12.1, *CONTEMPT-LT Users Manual.*

4.1-3 L. L. Wheat LLW-13-73, Letter to Argonne Code Center, Aerojet Nuclear Company, *CONTEMPT-LT/022 Program Transmittal.*

4.1-4 Exxon Nuclear Company XN-CC-39, Revision 1, *ICECON: A Computer Program Used To Calculate Containment Back Pressure For LOCA Analysis (Including Ice Condenser Plants).*

4.1-5 AREVA letter dated January 22nd, 2016, Page Blair, D. (AREVA) to Boardman, J. (PWR Owners Group), WCAP-17788-P Erratum for Update to CE t_{block}.

4.1-6 American Nuclear Society ANSI/ANS-5.1-1979, *American National Standard for Decay Heat Power in Light Water Reactors.*

4.1-7 AREVA Inc. Document EMF-2103(P)(A), Revision 0, *Realistic Large Break LOCA Methodology for Pressurized Water Reactors.*

2.2 RAI 4.2

2.2.1 Statement of RAI 4.2

Section 6.1 states that "a method was developed to calculate appropriate BB (Barrel/Baffle) flow resistances for use in this analysis" so that all Westinghouse upflow plants in operation in the U.S. are represented. The section further clarifies that "the method and supporting calculations are contained in Reference 6-2, which confirms that the BB flow resistances shown in Table 6-1 bound all Westinghouse upflow plants". With regard to the Westinghouse downflow plant design category, Section 6.2 explains that "a method was developed to calculate appropriate UHSN (Upper Head Spray Nozzle) flow resistances for use in this analysis" and that "the method and supporting calculations are contained in Reference 6-2, which confirms that the UHSN flow resistances shown in Table 6-2 bound all Westinghouse downflow plants". Reference 6-2 is identified in Section 6.5, as follows.

Reference 6-2: [

]

(a) Provide a copy of Reference 6-2.

(b) Include a description of the assumptions used in the maximum and minimum BB flow resistance calculations given in Table 6-1.

(c) Include a description of the assumptions used in the maximum and minimum UHSN calculations provided in Table 6-2.

(d) For Items a and b, describe whether the flow passages between the downcomer and upper plenum regions via the hot leg nozzle gaps were modeled and provide a justification for the modeling approach.

(e) For each Westinghouse unit considered in determining the BB and UHSN resistances in Tables 6-1 and 6-2, provide the following information in a table format, separately for both Westinghouse upflow and downflow plant category. In individual columns, include a description for each of the following items:

(i) Name and rated power

(ii) Identification numbers of design drawings, including the name of the unit for which they were produced, containing the geometric data to calculate the resistance associated with the

i. lower core plate to baffle region gap

ii. former holes including the number of former plates with holes
iii. upper core plate to baffle region gap
iv. UHSNs

(iii) For each category of flow passage, identify all types and sizes of openings that are credited in the resistance calculation. As a minimum, include

i. the number of holes or gaps
ii. hole diameter or gap width and perimeter length
iii. individual hole or gap flow area for each type of holes/gaps
iv. total resulting flow area

(iv) Loss coefficients associated with each category of passage along with the reference flow area

(v) Total unadjusted and adjusted BB/UHSN resistances along with the units

(vi) Assumptions related to the way geometric data in the drawings was treated for the purpose of calculating resistances and assumptions related to the consideration of any other existing flow passages such as pressure relief holes in the baffle plates.

(f) For each table in Item e, include a figure that illustrates the BB region and UHSN region geometries for each Westinghouse plant category and a separate figure showing an example of a BB former region top view for one-quarter of the core region. (Appropriate examples of such figures appear as Figures 1 and 2 in a March 26, 2001, letter by Exelon Generation Company, LLC, ADAMS Accession No. ML010890050.)

(g) During the NRC staff audit of supporting Westinghouse documents and drawings on February 2-4, 2016, it was observed, for the upflow BB plant category, former plate holes of Type 1 were assigned a loss coefficient of [ ] and those of Type 2 were assigned a loss coefficient of [ ]. The staff could not determine the basis for those values. Provide the calculations and supporting documentation for each of these loss coefficients, as well as for other loss coefficients identified in the response to Item e.iv above.

(h) During the NRC staff audit of supporting Westinghouse documents and drawings on February 2-4, 2016, the average loss coefficient for the upflow plant category, K_{AVG}, from former plate holes of Type 1 and Type 2 was computed from the individual loss coefficients, K_i, [

]. Explain the rationale for using an averaging equation to obtain an equivalent loss coefficient value and demonstrate whether physical parameters are preserved by using this method

(e.g., flow or pressure loss). Examine the effects of the averaging method on the resulting resistances for both maximum and minimum resistance cases. If the averaging method is found inconsistent, implement an appropriate approach and update the BB resistance results for the Westinghouse upflow and downflow plant categories.

2.2.2 Response to RAI 4.2

This RAI pertains to the Westinghouse Electric Company (WEC) plant categories and therefore requires no response for the Combustion Engineering (CE) plant category.

2.3 RAI 4.3

2.3.1 Statement of RAI 4.3

Section 6.3, "Combustion Engineering Plant Model," states that a method and supporting calculations for calculating appropriate BB flow resistances that represent all CE plants in operation in the U.S. are contained in Reference 6-3 and Reference 6-4. These two references are identified in Section 6.5 and updated in Letter OG-16-42 dated February 12, 2016, as follows.

Reference 6-3: [

].

Reference 6-4: [

].

(a) Provide copies of References 6-3 and 6-4 listed above.

(b) Provide a description of the assumptions used in the maximum and minimum BB flow resistance calculations provided in Table 6-3.

(c) Identify the physical units for the BB flow resistances in Table 6-3.

(d) Describe whether or not the flow passages between the downcomer and upper plenum regions via the hot leg nozzle gaps were modeled. If they were not, provide a justification for the omission.

(e) Provide the information requested in Items e, f, g, and h in RAI 4.2 as it applies to the CE plant category. As both AREVA and Westinghouse performed BB flow resistance calculation for CE plant units, all requested information from each vendor for the analyzed plant units should be provided.

(f) During the NRC audit of supporting AREVA documents and drawings on March 1-4, 2016, it was found in document [

] that two different values for the maximum BB flow resistance case, [ ], were reported for [ ]. During the audit, it was explained that the values resulted from the calculations performed by AREVA and Westinghouse. This significant difference in resistances is a concern regarding the limiting representative resistances determined for the CE plant category. Provide an explanation for the difference in the BB resistance results for [ ]. Since both results

may be incorrect, examine the methods used by AREVA and Westinghouse. Identify whether deficiencies in the calculational methodologies or differences in geometrical plant data related to the BB region were involved in both analyses. If deficiencies are discovered, provide a description and results of any changes to the methods for the corrected BB resistance calculation(s). Provide full calculations and final results for [ ] using both methods with applicable modifications. Provide the input derived from geometrical plant data related to the BB region for this unit as used in both analyses.

(g) Verify that the issues associated with Item f above do not affect the other plant categories.

2.3.2 Response to RAI 4.3

The response to this RAI will be provided by Westinghouse Electric Company (WEC).

2.4 RAI 4.4

2.4.1 Statement of RAI 4.4

Section 6.4, "Babcock and Wilcox (B&W) Plant Model," states that "the BB design for all B&W plants is the same" and explains that the BB flow resistance shown in Table 6-4 is representative of all B&W plants. It is also explained that the method and supporting calculations confirming the provided BB flow resistance value are contained in Reference 6-3, which is identified in Section 6.5 and updated with Letter OG-16-42 dated February 12, 2016, as follows.

Reference 6-3: [

]

(a) The above identified document appears to be related to the CE plant category. Confirm whether this is the proper reference for B&W plants. If a reference other than Reference 6-3 was used for B&W plants, provide a copy of the document.

(b) Include a description of the assumptions used in the calculation of the BB total flow resistance value provided in Table 6-4.

(c) Identify the physical units for the BB flow resistance shown in Table 6-4.

(d) State whether any other flow passages between the downcomer and upper head/plenum regions were modeled in the analyses. If they were, provide a description of these additional passages and how they are evaluated.

(e) Provide the information requested in Items e, f, g, and h in RAI 4.2 as it applies to the B&W plant design category.

(f) During the NRC staff audit of AREVA documents and drawings on March 1-4, 2016, the NRC staff encountered difficultly in interpreting, following, and confirming calculations and results pertaining to the BB resistance calculations for the B&W plant design category. Therefore, ensure that the information provided in response to Items a through e above include all necessary clarifying and supporting information to support an independent review of the BB resistance calculation methodology and the results documented for the B&W plant category.

2.4.2 Response to RAI 4.4

This RAI pertains to the Babcock & Wilcox (B&W) plant category and therefore requires no response for the Combustion Engineering (CE) plant category.

2.5 RAI 4.5

2.5.1 Statement of RAI 4.5

Tables 6-1 through 6-4 provide a summary of key inputs for each plant category. Provide the following information related to the key inputs for the HLB methodology:

(a) Justify that the values for the parameters listed in Tables 6-1 through 6-4 are bounding or demonstrate that these values can be considered appropriate and applicable for all of the plant units covered by the TR. If certain key input values have not been validated as bounding, state how the use of the TR methodology will ensure that the applicable acceptance criteria are met for the specific plant application. Include enough information for each key parameter so that the NRC staff can verify that they are bounding for the plants intended to use the TR. Ensure that the information includes, as necessary, plant specific characteristics, operating conditions, licensing basis assumptions (including single failure), regulatory limits, operating procedures, technical specifications limits, uncertainties, and full ranges of the inputs and variables that could affect the evaluation. If it is determined that these parameters are valid for plants using the methodology, how will the plants ensure the variables that can affect these parameters are maintained at acceptable values?

(b) Provide graphs of the physical axial power profiles implemented in the plant design analyses in Sections 8 through 11. Provide each physical axial power profile on a separate plot and for each profile show its nodal approximation based on the core axial nodalization.

    (i) Specify the elevation of the axial peak power location associated with the profile described in Table 6-3 for the Combustion Engineering (CE) plant design analysis.

(c) Clarify the approach to determining the axial power shapes simulated in the LOCA analyses. Explain if any bounding, or otherwise considered appropriate, assumptions were introduced to define the shapes requested in Item a. Explain if any physical axial power shapes, representative of individual units for each of the NSSS plant design categories included in Table 3-1 were considered in analyzing and determining the applicability of the simulated axial power profiles. Describe and justify the basis on which a single axial power profile, applied in the analyses for each plant category, can be considered valid and applicable to reactor core conditions across various units represented by each NSSS design category. An axial power profile applied for the purpose of a small-break LOCA analysis using a

model based on 10 CFR Part 50, Appendix K, would represent an acceptable axial power profile on a plant specific basis.

2.5.2 Response to RAI 4.5

2.5.2.1 Part a

Each of the parameters on Table 6-3 is discussed in the order they are presented.

Core Power:

A core power level of 3458 MWt was analyzed in the CE Thermal Hydraulic (TH) analysis. This power level, in and of itself, does not bound all operating CE plants. However, core power alone is not a sufficient metric to ensure that all plants in the CE fleet are bounded. Instead, the combination core power level and Barrel/Baffle (BB) resistance is used. Once a blockage is applied at the core inlet, the flow required through the baffle must at least match the core boiloff flow rate. The core boiloff rate is defined by the core power level and decay heat model selected. The flow through the baffle is defined by the baffle resistance. Therefore, the core power level and baffle resistance must be considered together. In order to represent all CE plants in operation in the U.S., a method was developed to calculate appropriate BB flow resistances for use in this analysis. The method and supporting calculations are contained in Reference 4.5-1, which confirms that the combination of power level and barrel/baffle resistance bounds the entire CE fleet. Therefore, plant-specific confirmation of core power level requires no further validation.

Number of Loops:

All CE plant designs have two hot legs and four cold legs. This configuration is considered in the analysis plant model.

Number of Fuel Assemblies:

The number of fuel assemblies is important when determining the total in-vessel debris load. The parameter K_{max} is applied uniformly across the entire core inlet such that the resistance due to the accumulation of debris is the same at the inlet to all fuel assemblies. In WCAP-17788, Volume 1, K_{max} is related to a physical fibrous debris mass with units of grams per fuel assembly (g/FA). When implementing the WCAP-17788 methodology, plants should confirm that they are using the correct number of fuel assemblies when comparing their in-vessel debris limits to the quantity of fibrous downstream from the sump strainer.

Barrel/Baffle Total K/A^2:

The BB K/A^2 value was selected to bound the CE fleet of plants. As described above for core power level, in order to represent all CE plants in operation in the U.S., a method was developed to calculate appropriate BB flow resistances for use in this analysis. The method and supporting calculations are contained in Reference 4.5-1, which confirms that the combination of power level and BB resistance bounds the entire CE fleet and requires no further validation.

Core Peaking:

The axial power profiles use a high radial peaking factor ($F_r^T = 1.81$), high linear heat generation rate (Linear Heat Generation Rate (LHGR)=13.75 kW/ft), and a skewed to the top power distribution (+20.9% axial offset). F_r^T is the dominant power profile attribute of interest for Long Term Core Cooling (LTCC). The LHGR used in the analyses should be at or above a steady state depletion power distribution. The top-skewed power profile is limiting compared to base load or bottom-skewed power profiles due to the longer time for the quench front to approach the elevations with the highest power and their susceptibility to heatup if the core becomes uncovered or dryout occurs. An axial offset greater than +20.9% and a LHGR greater than 13.75 kW/ft can only occur in rare transient (prior to the Loss of Coolant Accident (LOCA)) conditions. Such an axial offset and LHGR would be temporary and the effects would be limited to the initial stored energy of importance in the short-term LOCA transient but are not indicative of the long-term axial decay heat power distribution of interest for LTCC. Additional justification of the bounding nature of the axial power profiles is as follows:

- Steady-state operation at the Technical Specifications (TS) or Core Operating Limits Report (COLR) nuclear enthalpy rise hot channel factor, F_r^T, is possible and thus; can "burn in" and is the appropriate value to model during LTCC. The value modeled in the CE analyses is, $F_r^T = 1.81$.
- Steady-state operation at the TS/COLR maximum transient linear heat generation rate ($LHGR_{COLR}$) is not sustainable (unstable due to xenon redistribution); thus, an axial power profile based on the TS/COLR value cannot "burn in" and persist into LTCC. The steady state depletion linear heat generation rate ($LHGR_{SS}$), is the appropriate value to model during LTCC. The value modeled in the CE analyses is $LHGR_{SS}$ = 13.75 kW/ft. This value is expected to bound all CE plants. A typical value during steady state depletion is $LHGR_{SS} \approx$ 13.5 kW/ft.
- As with LHGR, steady-state operation is not sustainable with highly skewed axial power profiles and thus, cannot "burn in" and persist into LTCC. The steady state depletion axial offset, AO_{SS}, is the appropriate value to model during LTCC. The axial offset value modeled in the CE analyses is AO_{SS} = +20.9% which is expected

to bound all CE plants. A typical value during steady state depletion is $AO_{SS} \sim +10\%$.

The power profiles used for the CE plant analyses are applicable for an individual plant when the following parameters are met:

- Nuclear enthalpy rise hot channel factor: $F_r^T < 1.81$
- Steady state depletion total peaking factor: $LHGR_{SS} < 13.75 kW/ft$
- Steady state depletion axial offset: $AO_{SS} < +20.9\%$

Individual plants will have to verify applicability of the methodology as part of their plant specific submittals. Furthermore, since the above parameters are dependent on the core design, these parameters will need to be reconfirmed for each reload core to demonstrate the continued applicability of the analyses.

ECCS Recirculation Flow Rate:

The Emergency Core Cooling System (ECCS) injection rate during the transient has a direct effect on the core mixture level and cladding temperature response. Higher flow rates will provide significant excess flow above core boiloff. Lower flow rates may be closer to the core boiloff rate such that when blockage is imposed, decay heat removal may be challenged while the flow through the core is reconfigured to go through the barrelbaffle region instead of the core inlet. Studies presented in WCAP-17788-P, Volume 4 confirmed that lower flow rates are more conservative for the thermal-hydraulic analyses. Therefore, a minimum flow rate for the CE plants was targeted.

ECCS flow for the CE plants consists of flow from the Safety Injection Tanks (SITs), Low Pressure Safety Injection (LPSI) system, and High Pressure Safety Injection (HPSI) system. The SITs flow is passive and occurs early in the event. The SITs are typically empty before 50 seconds for a Large Break Loss of Coolant Accident (LBLOCA). Since SITs are passive, they are not subject to single failure assumptions. Since they empty early in the event (well before a blockage is imposed), they have no effect on the GSI-191 TH analyses. Therefore, no plant-specific validation is required for the SITs.

Before Sump Switch Over (SSO), the flow rate should be minimized to be consistent with Westinghouse Electric Company (WEC) analyses. In this case, it means a single ECCS train from the base plant model. This flow rate is used for all analyses (t_{block}, K_{max}, K_{split}, m_{split}).

After SSO, the LPSI pumps are isolated leaving only the HPSI pumps to supply ECCS flow. For the t_{block} and K_{max} analyses, the limiting single failure is of a train of ECCS. Therefore, after SSO, only a single HPSI pump is available. For the base plant model,

this is 827 gpm[1]. To confirm that a given plant is bounded by the analysis, the following calculation is done to determine an equivalent ECCS flow rate for each plant.

A direct comparison of a given plant ECCS flow rate to the analysis flow rate is difficult given the differences in plant designs among the CE fleet. Specifically, the volume of the Downcomer (DC) and the core power level must be considered to adjust the ECCS flow rate for comparison to the analysis. The sketch in Figure RAI-4.5-1 identifies the scenario that exists during LTCC. ECCS enters the DC from the top. Flow out the bottom is based on the core boiloff rate. The net difference is roughly the time it takes to fill the DC, which can be approximated by

$$t = \frac{V_{DC}}{M_{ECCS} - M_{boil}} \qquad \text{(RAI-4.5-1)}$$

where V_{DC} is the volume of the DC between the bottom of the cold leg nozzle and the bottom of the active core, M_{ECCS} is the ECCS mass flow rate, and M_{boil} is the core boiloff rate.

In order for the plant to be bounded by the analysis, the time to fill the DC must at least be equal between the plant and the analysis.

$$\frac{V_{DC,analysis}}{(M_{ECCS,analysis} - M_{boil,analysis})} = \frac{V_{DC,plant}}{(M_{ECCS,plant} - M_{boil,plant})} \qquad \text{(RAI-4.5-2)}$$

This equation can be rearranged to solve for $M_{ECCS,plant}$.

$$M_{ECCS,plant} = \frac{V_{DC,plant}}{V_{DC,analysis}} * (M_{ECCS,analysis} - M_{boil,analysis}) + M_{boil,plant} \qquad \text{(RAI-4.5-3)}$$

$$M_{boil} = \frac{P_{plant} * P/P_0}{h_{fg}} \qquad \text{(RAI-4.5-4)}$$

where P/P_0 is the decay heat fraction at the time of the blockage based on 1.2 the ANS 1971 DH standard, P_0 is the rated core power plus uncertainties, and h_{fg} is the latent heat of vaporization.

Equations RAI-4.5-3 and RAI-4.5-4 can be used to determine if a the plant ECCS flow rate is bounded by the ECCS flow rate used in the thermal-hydraulic analyses. The inputs needed for the CE plants are:

[1] In the past, the value reported for this analysis was 800 gpm, which corresponds to the ECCS flow rate at a fluid density of 61.9 lbm/ft^3. This density is representative of fluid from the Reactor Water Tank (RWT), which occurs before SSO. After SSO, the density will be closer to 59.8 lbm/ft^3, which is representative of fluid from the containment sump. Consequently, the modeled flow rate is 827 gpm.

- $V_{DC,analysis} = 551 ft^3$
- P/P_0 is 0.0106. t_{block} is applied at 5.33 hours into the transient. The value selected is the P/P_0 at six hours based on Appendix K decay heat, infinite operation, and no actinides. A later time and no actinides are selected to minimize the decay heat contribution to ensure a conservative calculation.
- h_{fg} is 970 BTU/lbm at 14.7 psia.
- $M_{ECCS,analysis} = 827 gpm = 110 lbm/s$

Each utility needs to perform the above calculation to determine $M_{ECCS,plant}$ using plant-specific inputs. If $M_{ECCS,plant}$ is less than the minimum assured ECCS flow rate during sump recirculation at the plant, then the ECCS flow rates used in the analysis results bound the ECCS flow rates at the plant and the thermal-hydraulic analyses can be applied to the subject plant.

For K_{split} and m_{split} analyses, the limiting single failure may be different than for the t_{block} and K_{max} analyses. That is, the analyses described in Volume 1 to calculate the debris limit in the reactor vessel will show limiting results for higher ECCS flow rates. To that end, the K_{split} and m_{split} analyses are done for a range of ECCS flow rates between 3.8 to 11.4 gpm/FA. RAI 4.22 discusses extrapolation beyond this range of applicability.

Containment Pressure During Recirculation:

As described in WCAP-17788, Volume 4, Section 4.2 (under break flow), the containment pressure is set to 14.7 psia to maximize the break flow rate and minimize the vessel inventory (due to higher voiding at lower pressures compared to higher pressures). This is a reasonable lower bound on containment pressure following a LOCA for the operating CE plants. Therefore, this parameter requires no further validation.

ECCS Temperature After Sump Switchover:

CE plant designs lack Residual Heat Removal (RHR) heat exchangers, and after switchover to recirculation high pressure safety injection flow goes directly from sump to the Reactor Coolant System (RCS). Therefore, the use of a saturated liquid at the containment pressure is a reasonable input for the CE plants. Further, a sensitivity study on ECCS temperature during the recirculation phase of the event (RAI 4.16) demonstrated that lower ECCS temperatures during recirculation improved the results. Therefore, the use of 212 °F (saturation temperature at atmospheric pressure) bounds the CE plant results and requires no further validation.

Sump Switchover Time:

As described in the response to RAI-4.1, Item a, an early sump switchover time provides the greatest challenge to long-term decay heat removal because debris arrives at the core inlet earlier in the transient when decay heat is higher. A sump switchover time of 20 minutes is a representatively limiting early switchover time for the CE plants covered by the analyses. No additional validation is required with regard to sump switchover time during plant implementation of the WCAP-17788 methodology.

Figure RAI-4.5-1: Sketch of DC Fill Rate

2.5.2.2 Part b

The plots requested are provided below. All the plots show peak-to-average power density on the ordinate and core elevation on the abscissa. In each plot the vetical dotted lines represent the control volume boundaries, and the horizontal bars represent the power in each heat structure. There are two heat structures for each control volume. The power is peaked at the 9.94-ft elevation.

Figure RAI-4.5-2: CE Base Case – Hot Rod Axial Power Profile

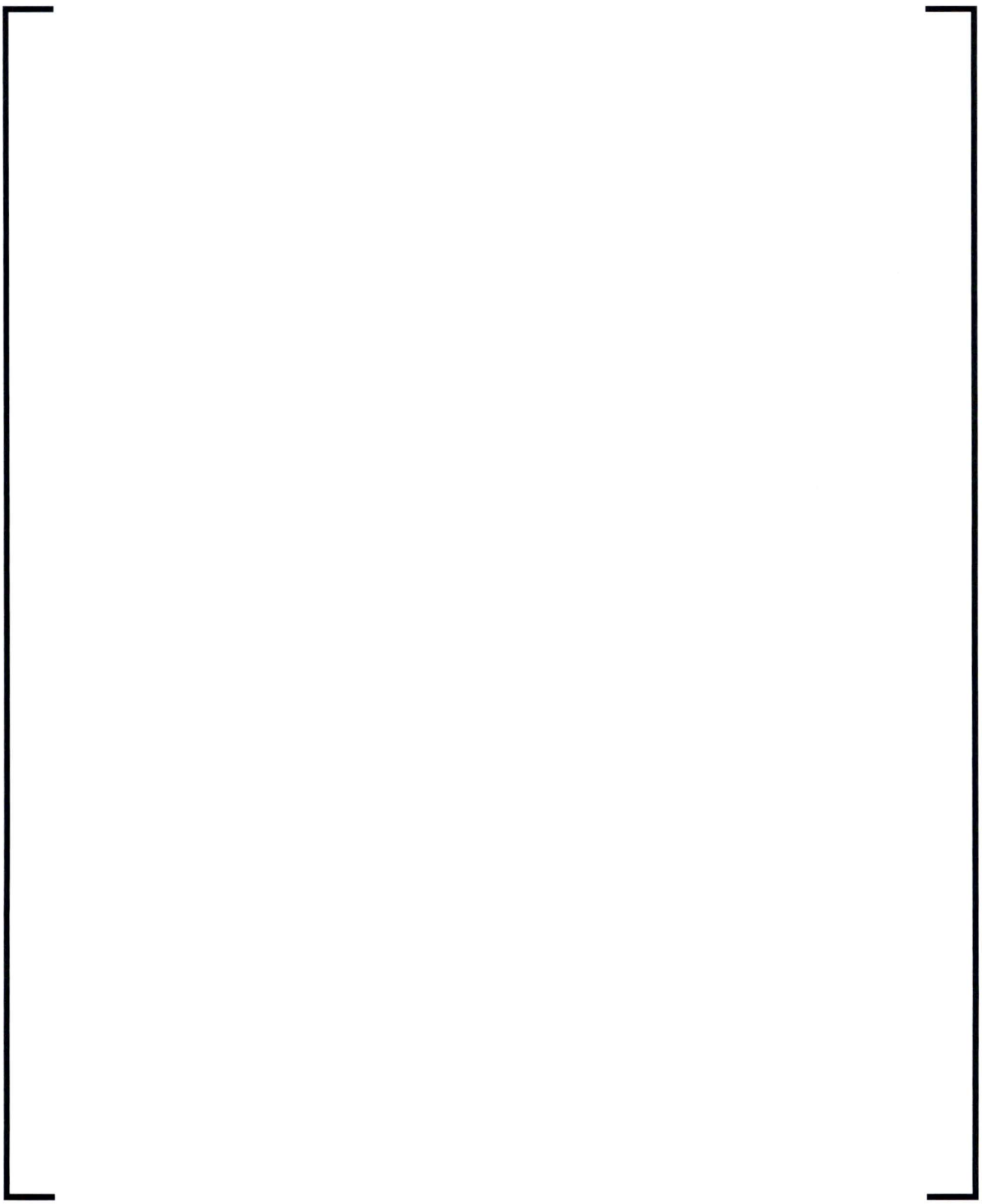

Figure RAI-4.5-3: CE Base Case – Hot Assembly Axial Power Profile

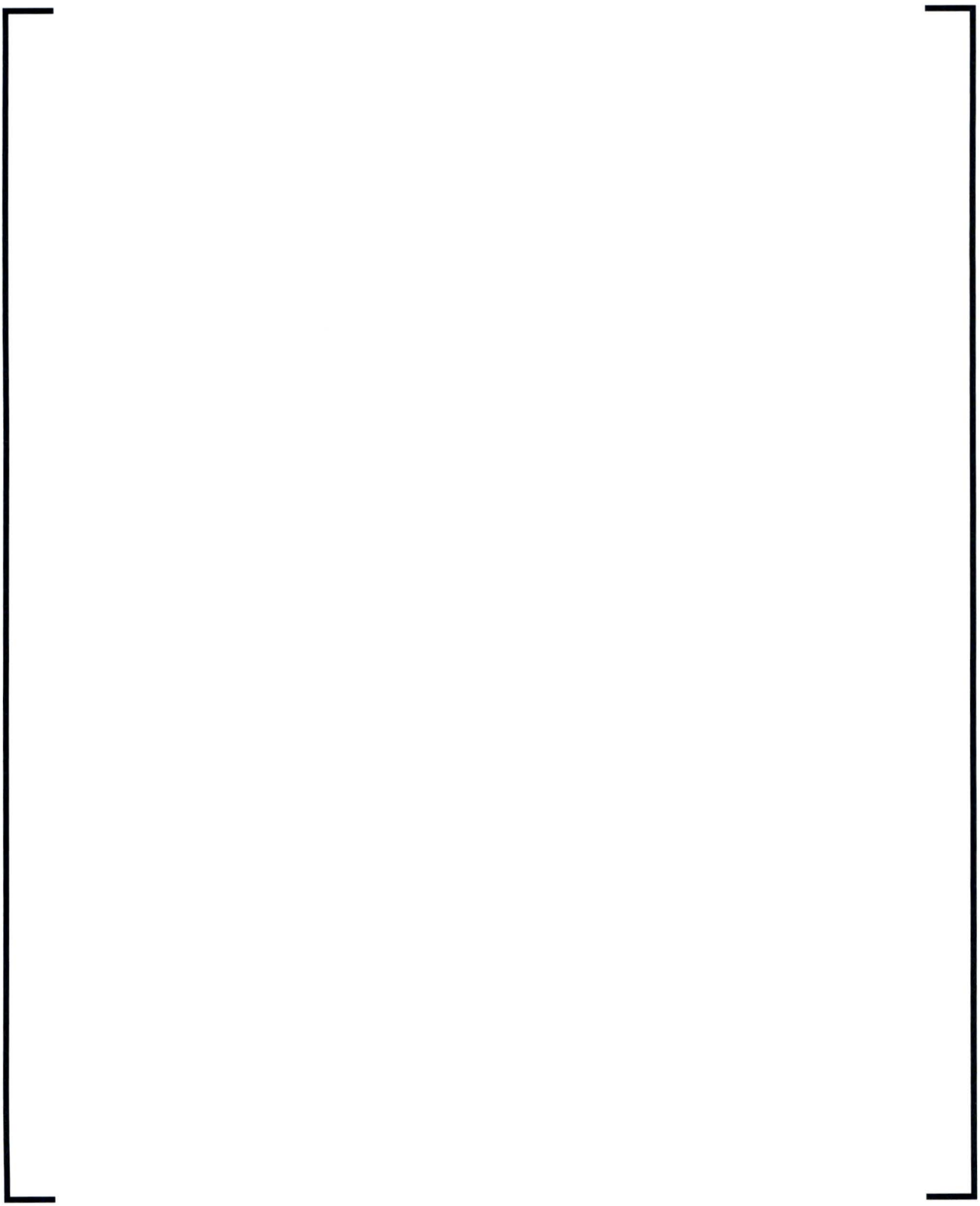

Figure RAI-4.5-4: CE Base Case – Central Core Axial Power Profile

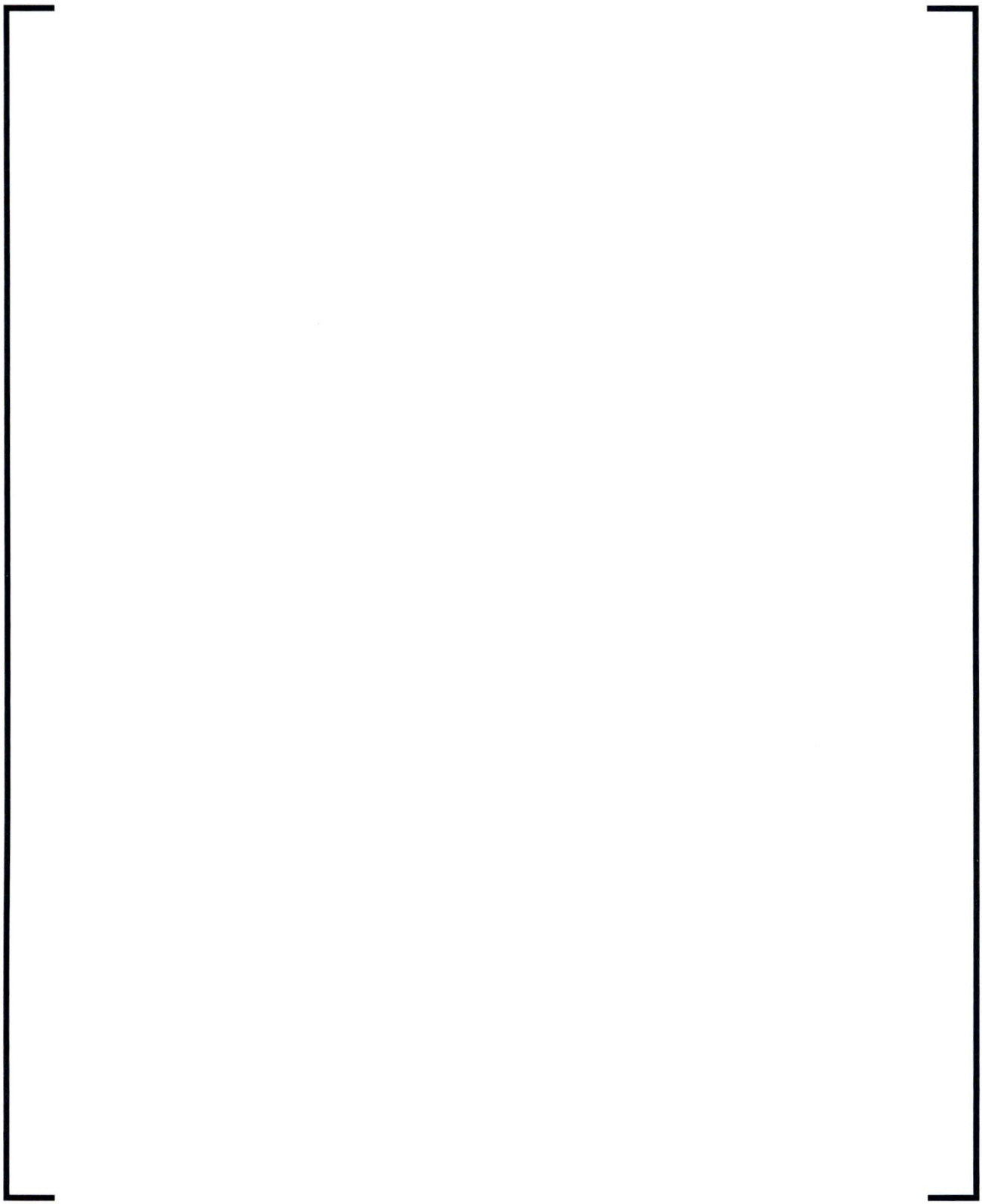

Figure RAI-4.5-5: CE Base Case – Average Core Axial Power Profile

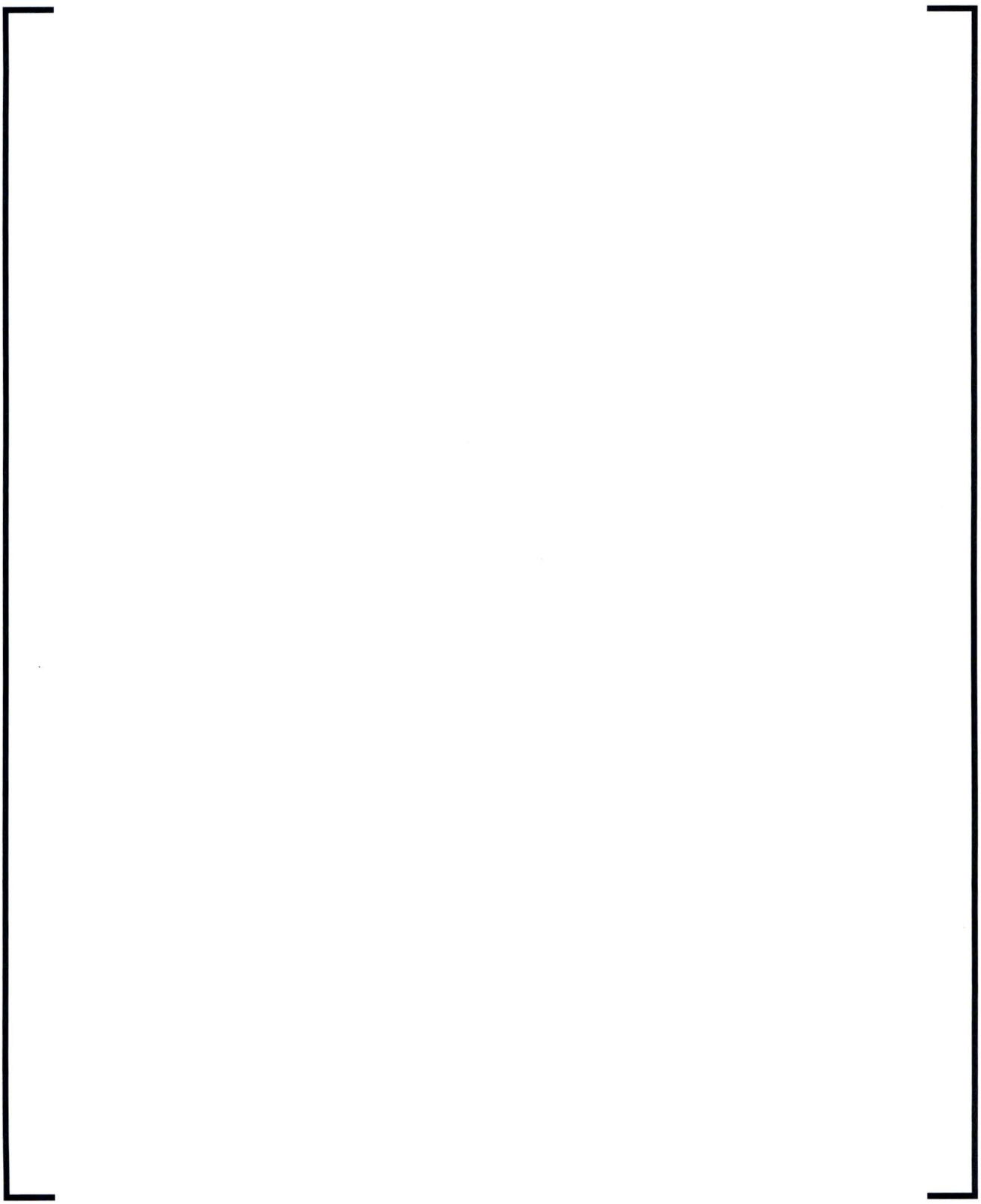

Figure RAI-4.5-6: CE Base Case – Peripheral Core Axial Power Profile

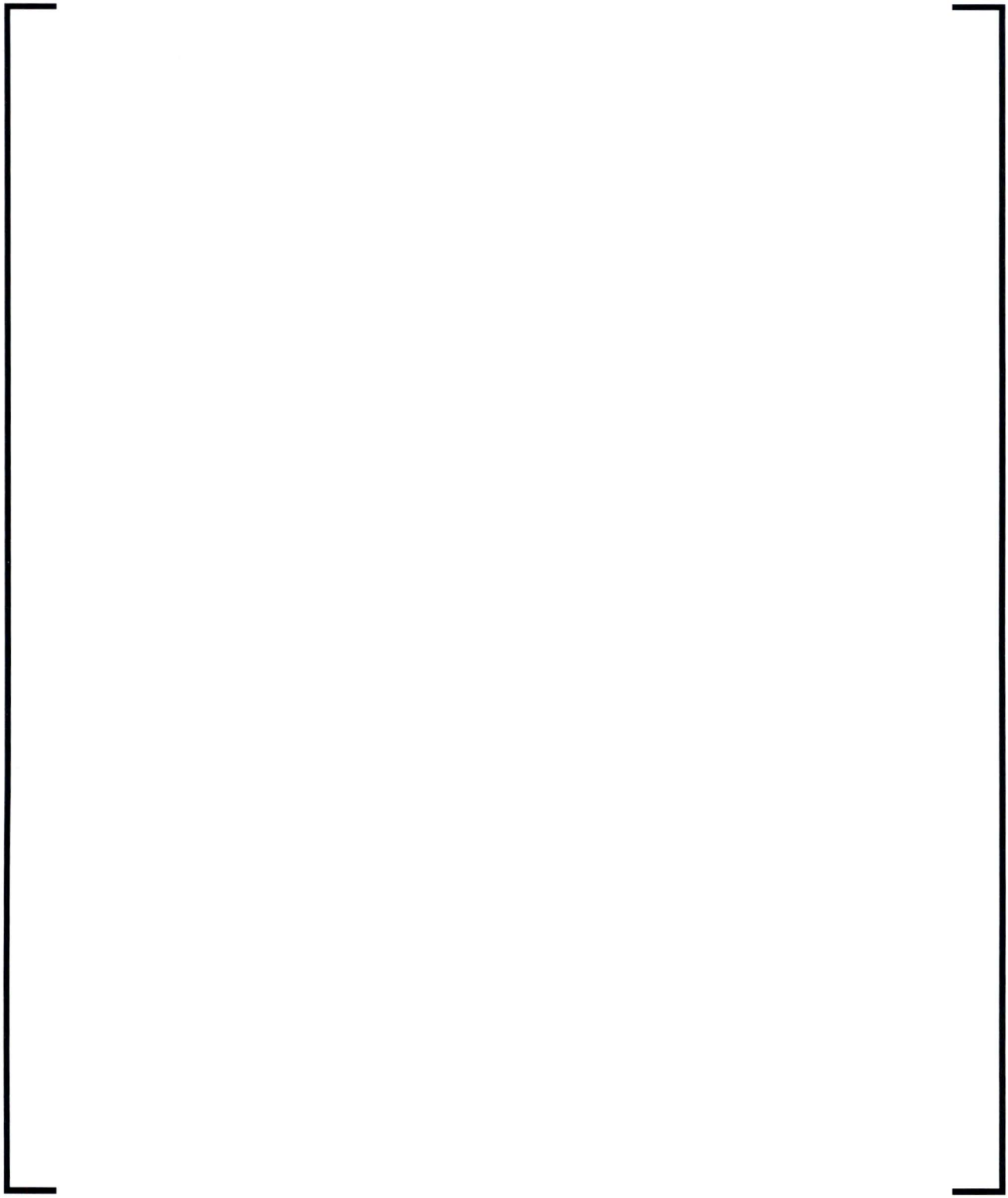

2.5.2.3 Part c

The analyses performed for the CE plants that are included in WCAP-17788-P used a process known as "modal decomposition" when mapping the axial power shape to the S-RELAP5 heat structures. This process was part of the EMF-2103(P)(A), Revision 0 methodology with the "transition package". During the time since the previous analyses for WCAP-17788-P were performed, a 10 CFR 50.46 letter was issued indicating that the "modal decomposition" process can cause artificial peaks and valleys in the axial power shape and has the potential to shift the peak. As a result, a commitment was made by AREVA to replace the "modal decomposition" process with a linear interpolation process for all EMF-2103(P)(A), Revision 0 methodology with the "transition package" analyses moving forward. In order to follow this commitment, the revised CE cases described in response to RAI 4.1b have been updated to use the linear interpolation method for the mapping of the axial power shape. The 10 CFR 50.46 letter related to this change is available in Reference 4.5-2.

A detailed discussion of the generation of the axial power shapes and how those shapes are mapped to S-RELAP5 heat structures is provided in Section A.2.5.10 of Reference 4.5-3. While there are some minor differences between the Revision 0 methodology with the "transition package" used for WCAP-17788-P and what is shown in Reference 4.5-3, the overall approach is the same. The basic difference between the two in this area is the improved rod-to-rod radiation model in Reference 4.5-3, which results in a different number of heat structures. The improved rod-to-rod radiation model from Reference 4.5-3 is not needed in the analyses performed with WCAP-17788-P as the cladding temperatures are low (< 800 °F) and radiation heat transfer between the rods at these temperatures is not a significant contributor at these temperatures.

The approach described in Reference 4.5-3 for the axial power shapes uses Best Estimate (BE) modeling of a hypothetical xenon-driven power oscillation. For the application of WCAP-17788-P, additional conservatisms are added by selecting a bounding value for F_Q and a reasonably conservative top-peaked axial power shape. In addition, the power shapes used in the short-term LOCA calculation, which are generated based on a hypothetical xenon-driven power oscillation, are not expected to persist into the long-term LOCA phase. Additional discussion and justification of this approach is provided as the response to Item a of this Request for Additional Information (RAI).

References - RAI 4.5

4.5-1 AREVA Inc. Document Comparison of Baffle Flow Resistance K/A^2 for the CE Plant Fleet, June 2015.

4.5-2 Letter, Pedro Salas (AREVA Inc.) to Document Control Desk (NRC), "2014 - Annual Reporting of Changes and Errors in Emergency Core Cooling Systems (ECCS) Evaluation Models," NRC:15:006, January 30, 2015.

4.5-3 AREVA Inc. Document EMF-2103(P)(A), Revision 3, *Realistic Large Break LOCA Methodology for Pressurized Water Reactors*.

2.6 RAI 4.6

2.6.1 Statement of RAI 4.6

The evaluation models (EMs) used for the LOCA T-H computational analyses are described in Section 5. The plant models used to perform the analyses for each plant category presented in Sections 8 through 11 are described in Section 6. Table 1 below summarizes the computer codes and models used in these analyses.

Table 1: Identification of Computer Codes and Plant Models Used in the Thermal-Hydraulic Computational Analyses

Code and Plant Model Used	**Plant Category**			
	Westinghouse Upflow BB Plant Category	**Westinghouse Downflow BB Plant Category**	**CE Plant Design**	**B&W Plant Category**
System Code	WCOBRA/TRAC MOD7A	WCOBRA/TRAC MOD7A	S-RELAP5	RELAP5/MOD2-B&W
Code Version	Not provided	Not provided	Provided	Provided
EM Topical Report	WCAP-14747 (CQD), WCAP-16009-NP-A (ASTRUM)	WCAP-14747 (CQD), WCAP-16009-NP-A (ASTRUM)	[ ]	[ ]
Code Modified for WCAP-17788 Methodology	Yes (see Section 5.1)	Yes (see Section 5.1)	Yes	No
Base Plant Model	Westinghouse four-loop BE plant model	Westinghouse three-loop BE plant model	CE high-power BE plant model	B&W high-power Appendix K plant model (SBLOCA)

Provide the following information:

(a) Identify the code version of WCOBRA/TRAC MOD7A used in the analyses in Sections 8 and 9.

(b) Clarify if NRC staff approval of subsequent TRs related to WCOBRA/TRAC, S-RELAP5, and RELAP5/MOD2-B&W can have an impact on the EMs applicability or validity of the T-H analysis results presented in WCAP-17788-P.

(c) As seen in Table 1 above, code modifications were made to both WCOBRA/TRAC and S-RELAP5 for the analyses presented in Volume 4 of WCAP-17788-P. Section 5.1 explains that "in order to simulate transient resistance at the core inlet due to the build-up of debris, it was necessary to modify the baseline WCOBRA/TRAC version". Letter OG-16-42 dated February 12, 2016, described a modification of the

baseline S-RELAP5 code version to produce "a development version of S-RELAP5" that was used to obtain the updated analyses submitted with OG-16-42 to replace the original results in Section 10 of Volume 4. Describe briefly the code changes and provide the validation and verification results for the "single-application" WCOBRA/TRAC code version and the S-RELAP5 "development version". Confirm that the code modifications were performed in conformance with applicable quality assurance procedures and provide references to related documents for both code modifications.

2.6.2 Response to RAI 4.6

2.6.2.1 Response to RAI 4.6a

This RAI pertains to the Westinghouse Electric Company (WEC) plant categories and therefore requires no response for the Combustion Engineering (CE) plant category.

2.6.2.2 Response to RAI 4.6b

The S-RELAP5 system code, whose models and correlations are described in Reference 4.6-2, is used to analyze the CE plant category. The analyses were performed in accordance with the EMF-2103(P)(A), Revision 0 methodology with the "transition package".

For Large Break Loss of Coolant Accident (LBLOCA) related to the S-RELAP5 system code, the only Topical Report (TR) that has been subsequently approved by the NRC since the submission of WCAP-17788-P is EMF-2103(P)(A), Revision 3, "Realistic Large Break LOCA Methodology for Pressurized Water Reactors", which was approved by the NRC staff in June of 2016 (Reference 4.6-1).

The final Safety Evaluation (SE) prepared by the NRC staff for EMF-2103(P)(A), Revision 3, includes a summary of the history of the EMF-2103(P)(A) TR, starting with the approval of EMF-2103(P)(A), Revision 0. Table 1 of the SE lists the changes made as part of the transition package, which is the basis for the work provided in WCAP-17788-P for the S-RELAP5 code and the CE plant-type. Table 2 of the final SE gives the additional changes introduced by Revision 3 of this TR. The upgrades made during the development of EMF-2103(P)(A), Revision 3 primarily relate to statistics of the set of cases analyzed and the heat transfer during the reflood phase. Since WCAP-17788-P is based on a deterministic approach and applies during the longer term (past reflood), the majority of the upgrades included in EMF-2103(P)(A), Revision 3 do not apply.

In addition, the modified code version represents a unique "single-application" code

version, and Nuclear Regulatory Commission (NRC) Staff approval of subsequent TRs related to different versions of S-RELAP5 for different applications will not impact this EM's applicability or validity of the Generic Safety Issue (GSI)-191 analysis results presented in WCAP-17788-P. If code errors are identified, they will be assessed per AREVA's established procedures.

2.6.2.3 Response to RAI 4.6c

System codes, such as S-RELAP5 and WCOBRA/TRAC, are developed and go through Verification and Validation (V&V) process that is consistent with their typical application (LBLOCA, Small Break Loss of Coolant Accident (SBLOCA), non-LOCA, etc. events). As such, there may have been modifications made that might add stability to the code, but these modifications do not have any significant impact to the results in these typical applications. During the development of these codes, it was not envisioned to have the situation presented in the GSI-191 application where a significant loss coefficient in conjunction with low flow rates is applied to a junction.

For GSI-191 applications, a "developmental version" of S-RELAP5 that contains an adjustment to the code to get the correct pressure drop behavior at high resistance/low flow applications was created and was promoted to a conditionally certified use-code, for these applications.

The previous versions of the S-RELAP5 thermal hydraulic code contains a term that is undesirable for the GSI-191 application. From Reference 4.6-2, Section 5.4.4, the code applies a term to the calculation of the form loss to prevent the loss from becoming zero when the velocity is zero. [

]

[ ]

The only change made to the code was the reduction of the multiplier on the athroat value used in the loss factors for the momentum equations.

A test case was run to show the effect of the above change. The test case is defined as follows:

Starting with a time dependent volume, a time dependent junction then sets the velocity boundary condition for the case. This velocity boundary condition is shown graphically in Figure RAI-4.6-1. A middle volume is defined to monitor pressure for the ΔP calculation. Then a simple outlet junction connects to an outlet time dependent volume. Control variables are defined to capture the pressure data.

The test case varies the inlet velocity. The outlet junction is modeled with a high fixed loss coefficient (1.92×10^6). A ΔP is measured across this junction (between the middle volume and the fixed downstream pressure boundary condition). The ΔP is ratioed against the pressure drop predicted by the Darcy pressure drop formulation.

The results (Figure RAI-4.6-2) show that the conditionally certified code version (shown as "DMAY15A" in the figure) consistently produces a pressure drop ratio of 1.0, compared with previous S-RELAP5 use version (shown as "UFEB15" in the figure). Thus, the S-RELAP5 version for GSI-191 applications correctly calculates the pressure drop for the low velocity, high loss coefficient condition.

The AREVA quality assurance program was followed for the S-RELAP5 modification. An internal safety-related calculation that supports the V&V, as well as the other supporting software-related documentation, is available to audit in the AREVA offices.

References - RAI 4.6

4.6-1 AREVA Inc. Document EMF-2103(P)(A), Revision 3, *Realistic Large Break LOCA Methodology for Pressurized Water Reactors.*

4.6-2 AREVA Inc. Document EMF-2100(P), Revision 16, *S-RELAP5 Models and Correlations Code Manual.*

Figure RAI-4.6-1: S-RELAP5 Code Test Inlet Velocity

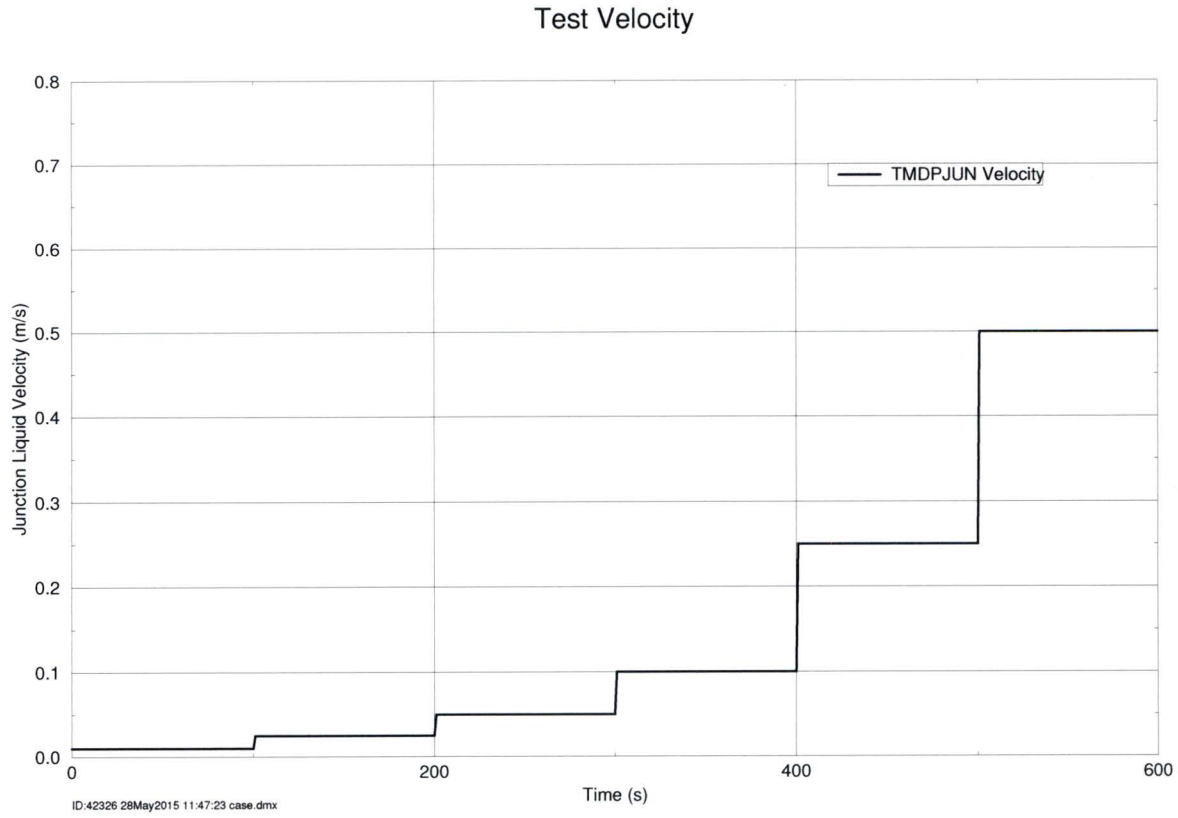

Figure RAI-4.6-2: Ratio of Calculated vs. S-RELAP5 Pressure Drop

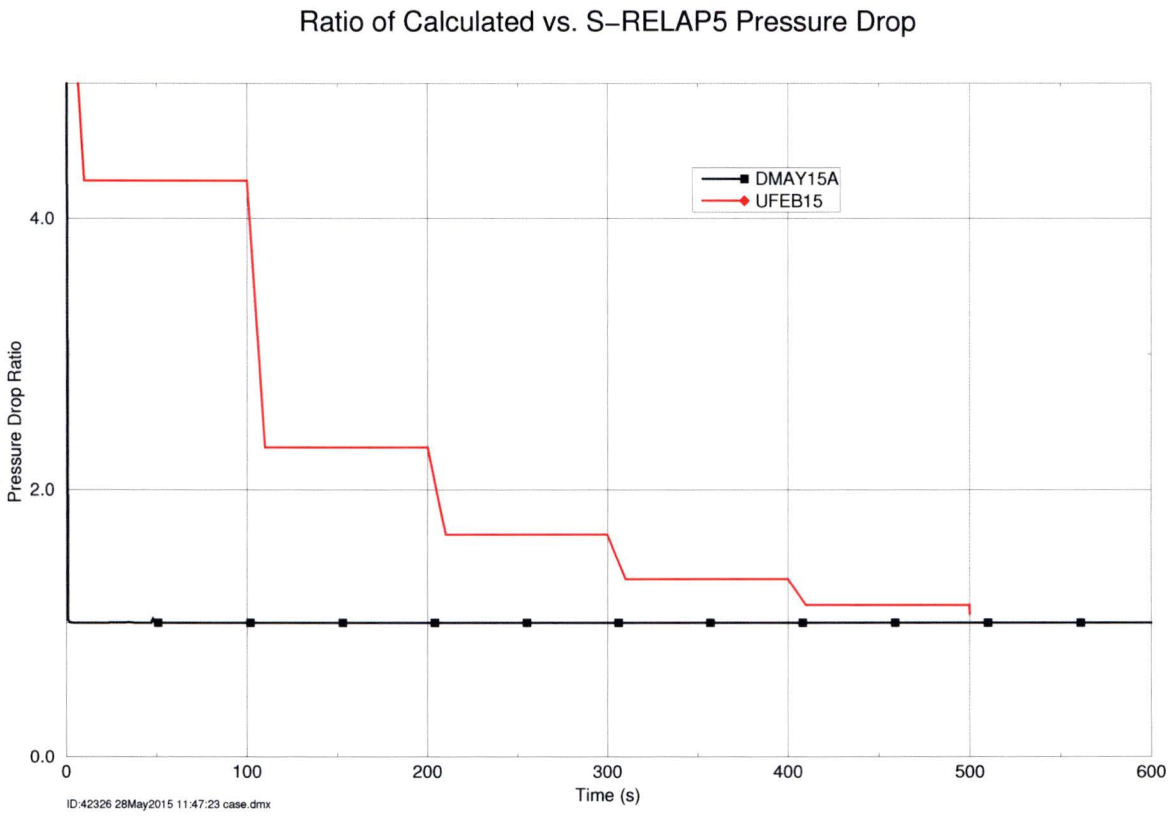

2.7 RAI 4.7

2.7.1 Statement of RAI 4.7

Section 4 states "it was determined that all computer codes and methods utilized have the ability to accurately predict the RCS response to simulated core inlet blockage during the sump recirculation phase of the post-LOCA transient". Describe the technical basis for this determination for each code methodology used in the analyses. Include identification and description of key governing processes and explain how the code capabilities were evaluated in terms of adequacy for the modeling of such processes. Explain how the code capabilities and accuracy in predicting the system and core response, including important parameters associated with the consequences of core inlet blockage, were evaluated. Include comparisons and assessments using experimental data as applicable.

2.7.2 Response to RAI 4.7

The S-RELAP5 system code goes through an extensive Verification and Validation (V&V) process for every use-code version that is developed and released for use. The V&V process includes benchmarks to a wide range of experimental facilities, as well as, some plant transients. Examples of benchmarks used in this V&V process are described in Reference 4.7-3, as well as in Section 8 of Reference 4.7-2. This extensive V&V process covers Small Break Loss of Coolant Accident (SBLOCA), Large Break Loss of Coolant Accident (LBLOCA), and non-LOCA events and related phenomena. Most of the phenomena modeled in the short-term phase of a Loss of Coolant Accident (LOCA) are generally significantly more complex than the phenomena that occur in the post-quench scenario seen in the WCAP-17788-P application. All of these benchmarks performed with S-RELAP5 show an acceptable agreement between the code and the tests.

The typical benchmarks performed as part of the standard S-RELAP5 system code V&V cover high pressures (~2000 psia), medium pressures (~1000 psia), and low pressures (reflood conditions), with pressures in between, depending on the event simulated. Additional benchmarks at low pressure/low power conditions, which are more consistent with the conditions modeled within WCAP-17788-P, are discussed in the response to RAI 4.8. The response to RAI 4.8 shows reasonable to excellent agreement between the S-RELAP5 code prediction and experimental results.

For the process in the WCAP-17788-P application, after the short-term LOCA phase (after core quench), the system is in a quiescent state with the steam production matching decay heat, a nearly constant mixture level that is into the Hot Legs (HLs), and a nearly constant liquid level in the Downcomer (DC) providing flow into the core. The

flow pattern in the core is expected to be upward in the higher power regions in the core and downward in the periphery. The conditions present in the WCAP-17788-P application for this phase are quasi-steady, until the blockage of the core is applied. This phase (after the short-term LOCA phase) is a boiling pot, where the phenomena is not complex and is easily within the code predictive capabilities.

Once the blockage of the core occurs, more flow will be forced to the Alternate Flow Path (AFP). During the initial phase after blockage, the mixture and collapsed levels may decrease in the core region as the initial flow through the AFP is typically not enough to make up for the boil-off due to decay heat. In addition, the DC level will rise due to the increased resistance to the core. At some point, the flow through the AFP will catch up and exceed what is needed to make up for the boil-off from decay heat. Mixture and collapsed levels then recover and cool the core. As the flow through the AFP to make up for decay heat is relatively low compared to the core flow area, the flow from the AFP is expected to fall downward in the outermost assemblies in the core periphery. Prior to core blockage, the flow pattern is expected to be downward in the core periphery as well. This means that the flow from the AFP will combine with the downward flow due to recirculation in the core. These flows will mix and then move upward in the higher power core regions. As such, the core flow pattern is not expected to change after the blockage and the code can predict such a scenario. The flow split between the AFP and the core inlet is a simple flow network calculation, which a system code like S-RELAP5 can predict. An example of the S-RELAP5 code being benchmarked for its multi-dimensional flow capabilities is provided in Section 8.2.14 of Reference 4.7-2 and in Section 3.12 of Reference 4.7-3.

The main phenomena that control the WCAP-17788-P application are as follows:

- **Void distribution/mixture level swell** - Capturing the void distribution in the core region, as well as the resulting mixture level swell, is an important phenomenon for this event. The amount of mixture level swell during the transient progression determines whether the core will uncover as well as the duration of any core uncovery. This is directly tied to the Peak Cladding Temperature (PCT) limits imposed for this analysis. Some examples of the S-RELAP5 predictive capabilities relating to void distribution and mixture level swell are provided in Sections 3.1 and 3.6 of Reference 4.7-3, Sections 8.2.1 and 8.2.8 of Reference 4.7-2, and in the response to RAI-4.8 (see Section 2.8.2).

- **Steam cooling during core uncovery** - Steam cooling heat transfer is an important process if the core uncovers. The S-RELAP5 code has been benchmarked against a variety of steam-cooling tests. Details of the FLECHT-SEASET steam-cooling benchmarks at reflood pressures are available in Section 8.2.4 of Reference 4.7-2 and in Section 3.16 of Reference 4.7-3. Benchmarks against the THTF level swell tests were also performed (Section 8.2.1

of Reference 4.7-2), which provide additional steam temperature comparisons between the measured and calculated values. These THTF benchmarks are at higher pressures and cover the range of steam temperatures up to about 1200 °F.

In addition, the response to RAI 11 in Reference 4.7-2 (pg. 2-113 of Appendix A) compares the S-RELAP5 code against the FLECHT-SEASET steam-cooling tests using either the Sleicher-Rouse or the Wong-Hochreiter vapor convection heat transfer correlation. Either correlation used produced good agreement between the code and the experiments over the Reynolds number span of the test data considered.

- **Decay heat modeling** - The amount of decay heat controls the steam production rate, as well as the rate of cladding heatup if the core uncovers. The S-RELAP5 code has several of the American Nuclear Society (ANS) Standards for decay heat built in and has the ability to include a multiplier on the decay heat. The code follows the 1979 ANS decay heat Standard (Reference 4.7-1) with a 1.1 (for t_{block} case) or 1.2 (for K_{max}, K_{split}, or m_{split} cases) multiplier with an infinite operation assumption with all fissions coming from U-235 with a fission energy of 200 MeV/fission for the WCAP-17788-P approach. In addition, actinide capture decay power is computed from the 1979 ANS decay heat Standard equations, along with the addition of decay heat from neutron capture in fission products and is also included in the analyses performed with the WCAP-17788-P approach. The decay heat is directly modeled per the 1979 ANS decay heat Standard, without additional approximations.

- **Liquid carryover from Upper Plenum to Hot Leg** - The amount of liquid that is carried to the HL and out the break is important both from a Reactor Vessel (RV) inventory (potential PCT impact) and a Boric Acid Precipitation (BAP) control point-of view. A detailed discussion of the liquid carryover from the Upper Plenum (UP) is provided in the response to RAI 4.23.

- **Upper Plenum Counter-Current Flow Drain/Fallback** - Liquid has the potential to collect and be retained in the UP during the period before core blockage is applied. After the core blockage is applied, the mixture and collapsed liquid levels in the core begin to decrease as the flow through the AFP is initially not sufficient to replace the boiloff due to decay heat. As the level decreases, the core may uncover, leading to a heatup of the cladding. If the stored liquid in the UP was to drain, this could lead to a top-down quench and limit the PCT calculated. The base methodology used in WCAP-17788-P (EMF-2103(P)(A), Revision 0 plus "transition package") prohibits top-down quench as one of the Safety Evaluation (SE) restrictions. The base methodology uses techniques to preclude a top-down quench. The same modeling to prevent the fallback from the UP to the hottest parts of the core is retained in WCAP-17788-P for the Combustion Engineering

(CE) plant-type. As described in the response to RAI 4.1b, this modeling is extended to include preventing fallback in the average core as well.

- **Core inlet resistance due to debris accumulation** - The value of the resistance applied at the core inlet due to debris, as well as how the resistance is increased, is an important factor for the WCAP-17788-P analysis.

  The amount of resistance sets how blocked the core really is and the amount of makeup flow that can enter from the bottom. Perhaps even more important is the rate at which the core blockage is applied. If the build up of debris is slow, the core may never uncover as the flow can have time to increase through the AFP and can be enough to exceed the boil-off rate due to decay heat before the core can uncover. A fast increase in the blockage abruptly restricts flow through the core inlet. The flow then has to start to divert through the AFP, which has a higher resistance than an unblocked core. In order for sufficient flow to get through the AFP, the level in the DC needs to build. The rate of level increase in DC depends greatly on the amount of Emergency Core Cooling System (ECCS) flow available. While the DC level builds, the amount of flow through the AFP is insufficient to cover the core boil-off due to decay heat. The collapsed and mixture levels in the core decrease during this period and potentially cause the core to uncover. Once the DC level builds to where the AFP flow can exceed the boil-off rate due to decay heat, the core has to refill. Once the mixture level is restored to the top of the heated core, a quasi-steady condition is re-established with no further heatup. Once the mixture level returns to the HLs, any accumulated boron concentrations will be flushed out to the break. Due to these reasons, the WCAP-17788-P analysis assumes an instantaneous ramp (applied over 60 seconds) for the core blockage in the t_{block} case as a conservative assumption. On the other hand, the analysis for K_{max} uses a more realistic ramp rate than the nearly instantaneous ramp used in the t_{block} case. Additional details of the selection of the ramp rates for the various analyses is provided in the response to RAI 4.26 (see Section 2.26.2).

  The S-RELAP5 code will directly use the resistance values and ramp rate entered. These single-phase flow pressure drops at high resistance and low flow conditions can be properly predicted by the code. The response to RAI 4.6c provides a code-to-theory comparison for a high resistance scenario at a variety of flow rates.

- **AFP ΔP form losses** - The ΔP form losses of the AFP is important as it determines how much the DC level has to build before sufficient flow is available through the AFP after the core blockage occurs.

  The S-RELAP5 code will directly use the form losses provided by the analyst. The corresponding single-phase flow pressure drops are modeled by the code based on the well understood theory of single-phase flow.

- **Single-phase flow split between core and Barrel/Baffle (BB)** - Related to the previous two bullets, the code must be able to partition the flow coming from the DC and lower plenum between the inlet of the core and the AFP. The flow is single-phase liquid. The partitioning of the flow is a basic flow network with the various resistances modeled and can be modeled with a system code like S-RELAP5 without any difficulties.

References - RAI 4.7

4.7-1 American Nuclear Society ANSI/ANS-5.1-1979, *American National Standard for Decay Heat Power in Light Water Reactors.*

4.7-2 AREVA Inc. Document EMF-2103(P)(A), Revision 3, *Realistic Large Break LOCA Methodology for Pressurized Water Reactors.*

4.7-3 AREVA Inc. Document EMF-2102(P), Revision 1, *S-RELAP5: Code Verification and Validation.*

2.8 RAI 4.8

2.8.1 Statement of RAI 4.8

Adequate prediction of the two-phase mixture level swell under core pool boiling conditions at atmospheric or close to atmospheric pressures during the long term core cooling (LTCC) phase of a PWR LOCA is of primary importance for demonstrating adequate core cooling in association with core inlet blockage. Sections 6.1 and 6.2 state "it is known that the version of WCOBRA/TRAC utilized tends to over predict two-phase mixture level swell in the core under low pressure pool boiling conditions (Reference 6-1). To account for this, a multiplier on the core axial interfacial drag is applied consistent with the approach taken in Reference 6-1". Reference 6-1 is listed in Section 6.5 as follows.

Reference 6-1: WCAP-15644-P, Rev. 2 (Proprietary) and WCAP-15644-NP, Rev. 2 (Non Proprietary), "AP1000 Code Applicability Report," March 2004.

Revised Section 7.1.1, "Debris Collection at the Core Inlet," of WCAP-17788-P Vol. 1, provided with Letter CAW-15-4339 dated November 24, 2015, further clarifies that an "interfacial drag multiplier of 0.8 x nominal" was used to analyze a double-ended cold leg break in a three-loop Westinghouse plant "consistent with Westinghouse NSSS analyses in WCAP-17788, Volume 4". Sections 8 through 11 of Vol. 4 provide no information relative to the capabilities of the other codes used for the analyses to predict two-phase mixture level swell in the core under low pressure pool boiling conditions. Also, Reference 6-1 has not been approved by the NRC.

(a) Provide assessment results that demonstrate the codes used for the analyses documented in Sections 8 through 11 adequately predict two-phase mixture level swell under core pool boiling conditions at pressures close to atmospheric. These results should be based on level swell test data relevant to the analyzed plant conditions. Provide figures comparing code predictions to low pressure test data. Include tables identifying the test facilities, test runs, test flow conditions, measured void fractions, and predicted void fractions for the code assessments performed.

(b) Clarify whether the "interfacial drag multiplier of 0.8 x nominal" identified in revised Section 7.1.1 was used in the HLB LOCA analyses in WCAP-17788-P Vol. 4 performed with WCOBRA/TRAC. If the multiplier was used in the analyses presented in Vol. 4:

  (i) Describe the basis for determining the multiplier value.

  (ii) Provide data assessments and the established range for this multiplier.

  (iii) Demonstrate the applicability of the multiplier value to near-atmospheric pressure conditions.

(iv) Explain whether the multiplier has a significant impact on t_{block}, K_{max}, K_{split}, and m_{split}. Use results of sensitivity studies, if necessary, to demonstrate the acceptability of the results in Section 8 and 9 in this regard.

(c) Explain how interfacial drag was treated in the codes used for the CE and B&W analyses in Sections 10 and 11, respectively. Provide the information requested in Item b above as it applies to the EMs used for the analyses of the CE and B&W design categories.

2.8.2 Response to RAI 4.8

2.8.2.1 Part a

The prediction of the mixture level, the void distribution below the mixture level, and the cladding thermal response above the mixture level in the core during the core uncovering following a Loss of Coolant Accident (LOCA) are of paramount importance under low flow conditions. During the post core quench, the superficial liquid velocities in the core are small. Consequently, the acceleration and viscous forces will be negligible compared to the buoyancy force in predicting the two-phase flow distribution in the core. As a result, a simplified approach can be used to extend the bundle boil-off benchmark results to different decay heat power levels.

S-RELAP5 (References 4.8-1 and 4.8-2) has been extensively benchmarked against a wide range of test facilities. These benchmarks demonstrate that the code can predict the thermal-hydraulic response within the core region during core uncovering following a Small Break Loss of Coolant Accident (SBLOCA) and during the reflooding phase of a Large Break Loss of Coolant Accident (LBLOCA) for a Combustion Engineering (CE) or a Westinghouse 3- and 4-loop Pressurized Water Reactor (PWR) with cold leg Emergency Core Cooling System (ECCS) injection. The LOCA benchmarks simulated using S-RELAP5 also demonstrate that the code can predict the core thermal responses during the Long Term Core Cooling (LTCC) phase of the event, as long as the system pressure does not fall below the benchmark pressure range (typically 20 to 30 psia).

To extend the range of applicability of S-RELAP5 to low pressure (<20 psia) and low power levels, seven Rod Bundle Heat Transfer (RBHT) (References 4.8-3 and 4.8-4) bundle boil-off tests were simulated using S-RELAP5. These tests used low bundle inlet flow rates, an upper plenum pressure of approximately 20 psia, and power levels equivalent to the decay heat at 2000 to 4000 seconds after reactor shut down.

The test conditions used in the seven tests are as follows:

Upper plenum pressure (psia)	19.4 – 29.4
Bundle power (kW)	54 – 77
Inlet mass flow rate (lbm/s)	0.039 – 0.164
Inlet fluid temperature (F)	131 – 205

Figure RAI-4.8-1 shows the calculated versus measured void fraction for all the seven tests. A twenty second running average is used in obtaining the calculated void fraction. The plot shows reasonable to excellent agreement, with most of the points within a ± 20 percent relative error band.

Bundle uncovering was noted in the four RBHT tests benchmarked using S-RELAP5. In these cases, the code predicted rod surface temperatures in all four tests were [ ] the test data. From the RBHT tests benchmarks it is also concluded that S-RELAP5 will calculate higher cladding thermal response in the event of core uncovering.

From a review of the available literature, it was found that very few bundle boil-off tests are available to benchmark the codes at 20,000 to 30,000 second decay heat levels. Therefore, a simple phenomenological approach was developed to extend these benchmark results to lower decay heat levels (20,000 to 30,000 seconds after reactor shut down). Several pool void fraction correlations were reviewed. It was found that for a given plant case with constant containment pressure, the functional relationship between the void fraction and the superficial steam velocity given by,

$$\alpha_g = f(j_g), \qquad \text{(RAI-4.8-1)}$$

can be used to extend the benchmark results to different decay heat power levels. This approach was verified by sensitivity studies using an RBHT test benchmark case and by the evaluation of a CE plant case described in the response to RAI 4.1b. Wilson (Reference 4.8-5) and Cunningham-Yeh (Reference 4.8-6) correlations were also used in the evaluation.

It should be noted that the majority of the correlations used in calculating the flow regimes and the interphase drag correlations were developed by the well-known researchers like Taitel, Wallis, Wilson, and Ishii using primarily air-water test data. Therefore, these correlations are appropriate in the calculation of the void fractions in the core and in the Upper Plenum (UP) during the long-term core cooling following a LOCA. In addition, since α_g is primarily a function j_g, the majority of the parameters used in various sensitivity studies conducted in responding to several RAIs will have only secondary effects in the core and in the UP thermal-hydraulic behavior.

From the RBHT tests benchmarks, and the approach developed to extend the benchmark results to lower power levels, it is concluded that S-RELAP5 will correctly

predict the void distribution in the core during post core quench following a Double-Ended Guillotine (DEG) cold or hot leg break in a CE- or Westinghouse-designed plant.

Figure RAI-4.8-1: RBHT Summary S-RELAP5: Calculated vs. Measured Void Fraction for Seven RBHT Tests

2.8.2.2 Part b

This RAI pertains to the Westinghouse Electric Company (WEC) plant categories and therefore requires no response for the CE plant category.

2.8.2.3 Part c

S-RELAP5 is extensively benchmarked for LBLOCA (short term), SBLOCA, and non-LOCA events. These benchmarks cover pressures from 2000 psia down to reflood conditions. The S-RELAP5 range of applicability relative to level swell predictions was validated at low pressures in conjunction with low power decay heat levels corresponding

to conditions at approximately 1,000 seconds after a reactor trip during a LOCA event, which is near the time of sump switchover for Generic Safety Issue (GSI)-191 applications. Details of the benchmarks against RBHT tests and the corresponding test conditions and results are provided in the response to Request for Additional Information (RAI) 4.8a.

The prediction of the mixture level, the void distribution below the mixture level and the cladding thermal response above the mixture level in the core during the core uncovery following a LOCA is of paramount importance under very low flow conditions. When the mass flow rate in the core is small, the buoyancy force is more dominant compared to acceleration and viscous forces. The RBHT benchmarks demonstrate that S-RELAP5 can predict the void distribution and the mixture levels correctly under low flow/low pressure conditions. It should be noted here that, as pressure decreases, the density ratio between vapor in liquid changes dramatically, resulting in more swell, and having a benchmark like RBHT helps to make sure that the code is predicting the right swell under these conditions.

Result for S-RELAP5 benchmarks indicate that the code calculated results show reasonable to excellent agreement to the test data for the parameters of interest identified in the acceptance criteria, i.e. void fraction and superficial steam velocity as function of elevation. Given the demonstrated capability and the robustness of the S-RELAP5 predictions for these benchmarks, no interfacial drag multiplier is necessary.

References - RAI 4.8

4.8-1 AREVA Inc. Document EMF-2103(P)(A), Revision 0, *Realistic Large Break LOCA Methodology for Pressurized Water Reactors*.

4.8-2 AREVA Inc. Document EMF-2328(P)(A), Revision 0, Supplement 1(P)(A), Revision 0, *PWR Small Break LOCA Evaluation Model, S-RELAP5 Based*.

4.8-3 Hochreiter, L. E., et al., Rod Bundle Heat Transfer Facility Two-Phase Mixture Level Swell and Uncovery Test Experiments Data,. NUREG/CR-7218, Volume 1, September 2016.

4.8-4 Hochreiter, L. E., et al., Rod Bundle Heat Transfer Facility Two-Phase Mixture Level Swell and Uncovery Test Experiments Data,. NUREG/CR-7218, Volume 2, September 2016.

4.8-5 R.J. Grenda J.F. Wilson and J.F. Patterson ANS Transactions, Vol 5, *The Velocity of Rising Steam in a Bubbling Two-Phase Mixture*.

4.8-6 Cunningham, J. P., and Yeh, H. C., .Experiments and Void Correlations for PWR Small-Break LOCA Conditions,. Trans. Amer. Nucl. Soc., Vol 17, pp. 370-371, 1973.

2.9 RAI 4.9

2.9.1 Statement of RAI 4.9

Sections 8 through 11 provide LOCA T-H analysis results for determining the earliest transient point in time, t_{block}. T_{block} is defined so that the acceptance criteria for maintaining LTCC would be satisfied should complete core inlet blockage occur at or after this point in time following a HLB LOCA. Figures 8-16 (Case 1B), 9-15 (Case 1A), 10-13 (Case 1), and 11-9 (Case 1) show the core peak cladding temperature (PCT) responses following the application of complete core inlet blockage with temperature excursions being observed in Figures 8-16 and 9-15. Provide the following information in a table format (where applicable) for the limiting analyses. For example, Case 1B in Section 8 and Case 1A in Section 9 for each plant category. Include the axial void fraction profile results (Item c) in separate tables. If a parameter exhibits an oscillatory behavior within the vicinity of the time point of interest, include the parameter's variation range along with the observed predicted value itself.

(a) Provide the following prediction results relative to the PCT excursions:

  (i) Time of PCT (relative to break opening)
  (ii) PCT
  (iii) The core channel and axial elevation associated with the PCT location

(b) Provide the following results relative to the axial elevation in the channel where the PCT was observed and the timing of PCT:

  (i) Fuel rod local linear heat generation rate
  (ii) Predicted two-phase flow regime
  (iii) Vapor/liquid mass flow rates and mass fluxes for predicted continuous/dispersed flow fields (axial and cross-flow)
  (iv) Vapor/liquid phase velocities for predicted continuous/ dispersed flow fields (axial and cross-flow)
  (v) Wall heat transfer mode
  (vi) Fuel rod heat transfer fluxes to continuous/dispersed flow fields (clarify if any radiation heat transfer of significance was predicted)
  (vii) Heat transfer coefficients to continuous/dispersed flow fields.

(c) Provide the axial void fraction distribution in the channel where the PCT was observed at the time when the PCT occurred and corresponding predicted two-phase mixture level in the channel.

(d) Identify the closure heat transfer correlations associated with the heat transfer regimes identified as controlling with regard to the PCT values in Figures 8-16 and 9-15. Provide the ranges of applicability of these correlations and compare them against the predicted core limiting T-H parameters.

(e) Identify the constitutive correlations for computing void fraction and any predicted entrained droplets/liquid film fields, as applicable, associated with the two-phase flow regime predicted at the PCT location and time of its occurrence. Provide their ranges of applicability and compare them against the predicted core limiting T-H parameters.

2.9.2 Response to RAI 4.9

2.9.2.1 Part a

The post-blockage Peak Cladding Temperature (PCT) of 542 °F occurs at about 20580 seconds after the break opening, in a Fresh UO_2 hot rod, and at an axial elevation of 12.135 ft. The thermal-hydraulic boundary conditions for the PCT rod are provided by the Hot Assembly (HA) channel.

2.9.2.2 Part b

As noted in the response to Part a, the PCT occurs around 20580 seconds. The flow regime at the PCT node is expected to be mist flow and the heat transfer conditions to correspond to single-phase vapor, as illustrated below in Figures RAI-4.9-1 and RAI-4.9-2. The data requested is provided for the 20600 seconds major edit for data extraction convenience. At 20600 seconds the cladding temperature at the PCT node is 540.9 °F, with the temperature excursion still close to the peak and thermal-hydraulic conditions similar to the time of PCT. The data requested are summarized in table RAI-4.9-1.

Table RAI-4.9-1: CE Base Case – Results observed at the PCT axial elevation, at 20600 seconds

Parameter	Value	Comments
Fuel rod local linear heat generation rate (kW/ft)	0.073	
Predicted two-phase flow regime	Mist flow	Figure RAI-4.9-2
Axial vapor mass flow rate - inlet (lbm/s)	0.2402	Figure RAI-4.9-3
Axial vapor mass flux - inlet (lbm/s-ft^2)	0.9653	Figure RAI-4.9-4
Axial vapor mass flow rate - outlet (lbm/s)	0.1866	Figure RAI-4.9-5
Axial vapor mass flux - outlet (lbm/s-ft^2)	0.7501	Figure RAI-4.9-6
Axial liquid mass flow rate (lbm/s)	0	
Axial liquid mass flux (lbm/s-ft^2)	0	
Cross-flow vapor mass flow rate (lbm/s)	0.0532	Figure RAI-4.9-7
Cross-flow vapor mass flux (lbm/s-ft^2)	0.1586	Figure RAI-4.9-8
Cross-flow liquid mass flow rate (lbm/s)	0	
Cross-flow liquid mass flux lbm/s-ft^2	0	
Axial vapor velocity (ft/s)	23.65	in the node
Axial liquid velocity (ft/s)	0	no liquid present
Cross-flow vapor velocity (ft/s)	24.72	at the junction
Cross-flow liquid velocity (ft/s)	0	no liquid present
Wall heat transfer mode	Single-phase vapor	Figure RAI-4.9-1
Fuel rod heat transfer flux to vapor(BTU/s-ft^2)	0.4761	no radiation
Fuel rod heat transfer flux to liquid (BTU/s-ft^2)	0.0	
Heat transfer coefficient to vapor (BTU/s-ft^2-°F)	1.932E-3	
Heat transfer coefficient to liquid (BTU/s-ft^2-°F)	0	

Figure RAI-4.9-1: CE Base Case – Heat Transfer Mode at the PCT Node

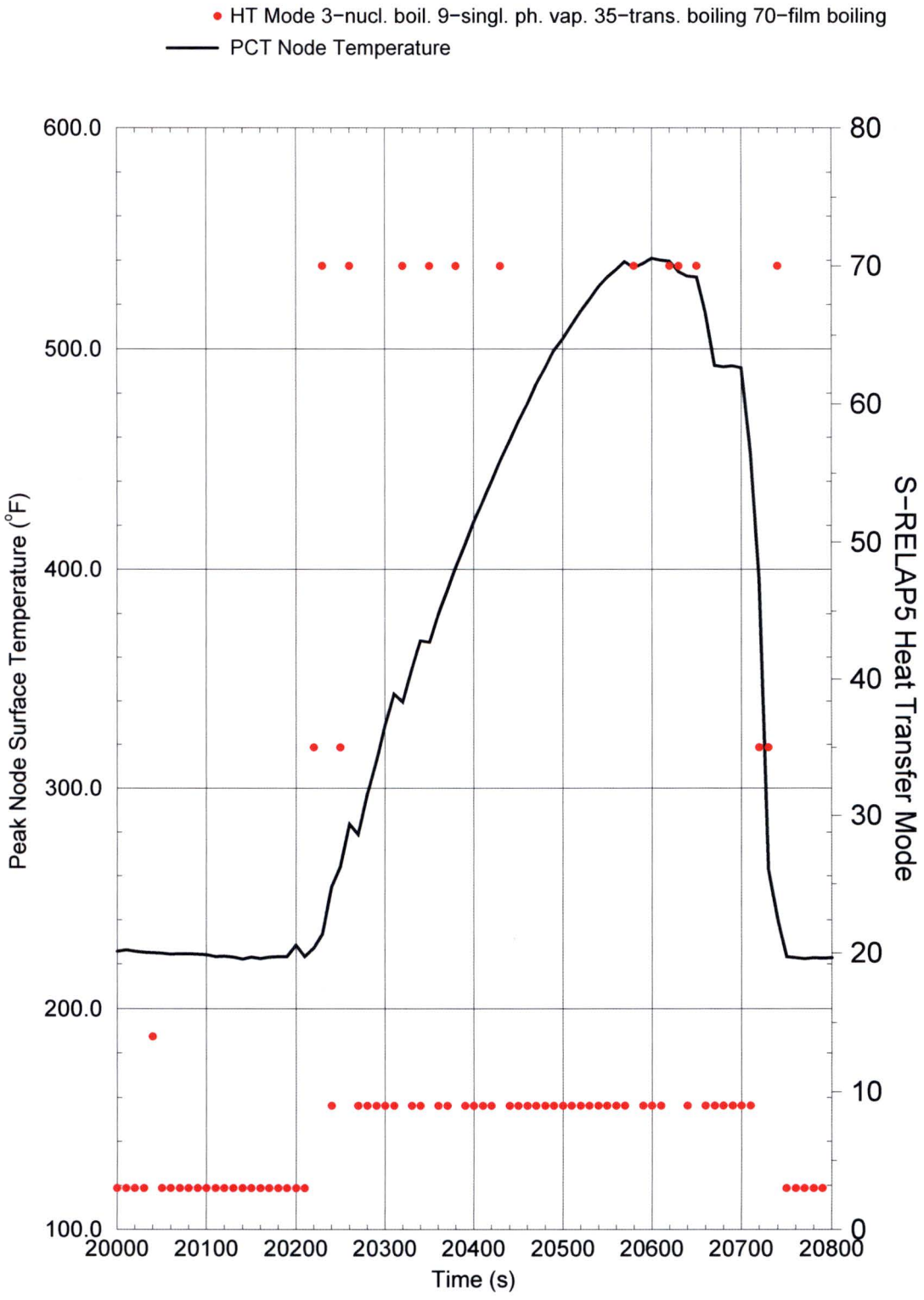

Figure RAI-4.9-2: CE Base Case – Flow Regime at the PCT Node

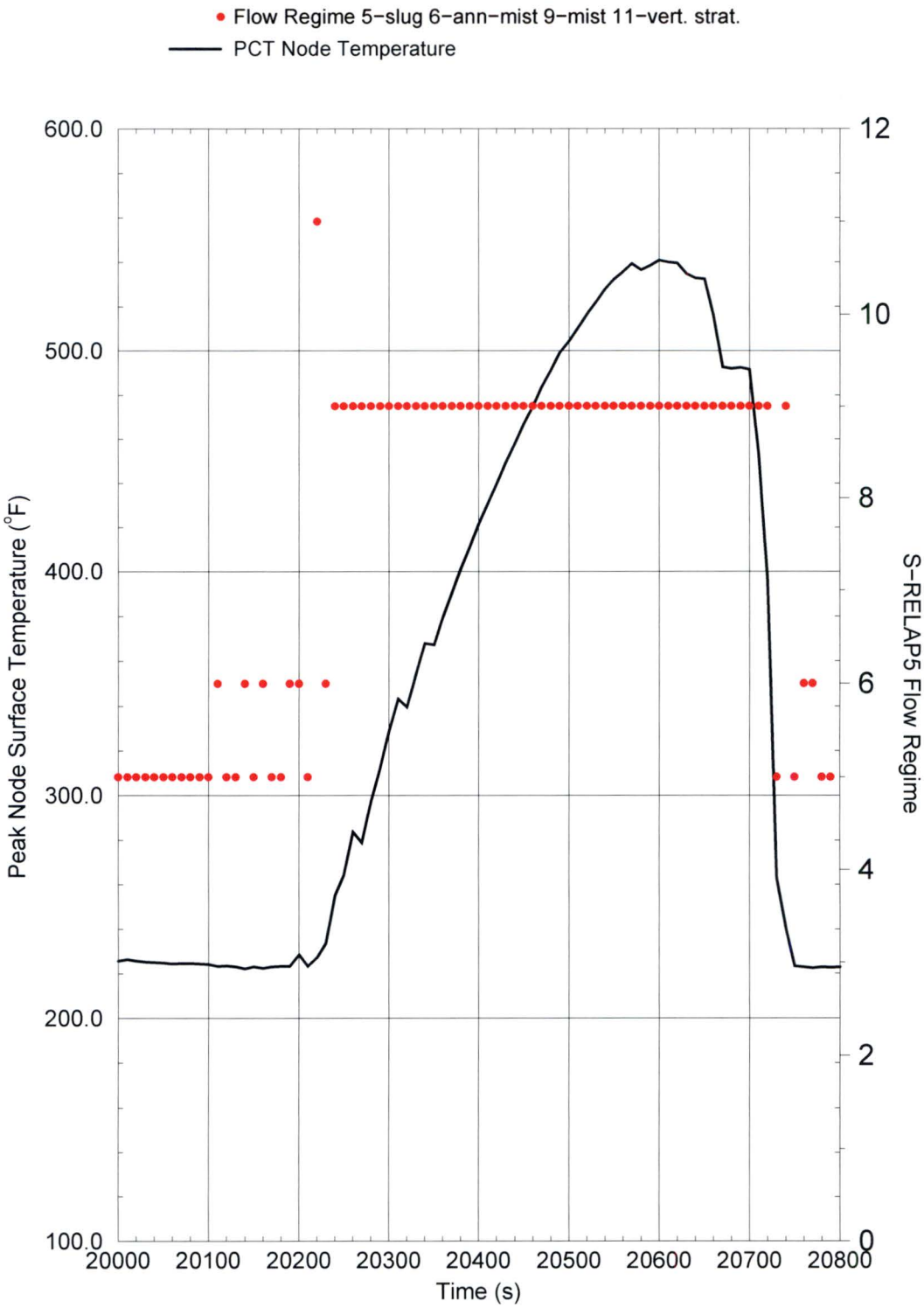

Figure RAI-4.9-3: CE Base Case – PCT Node Axial Inlet Mass Flow Rate

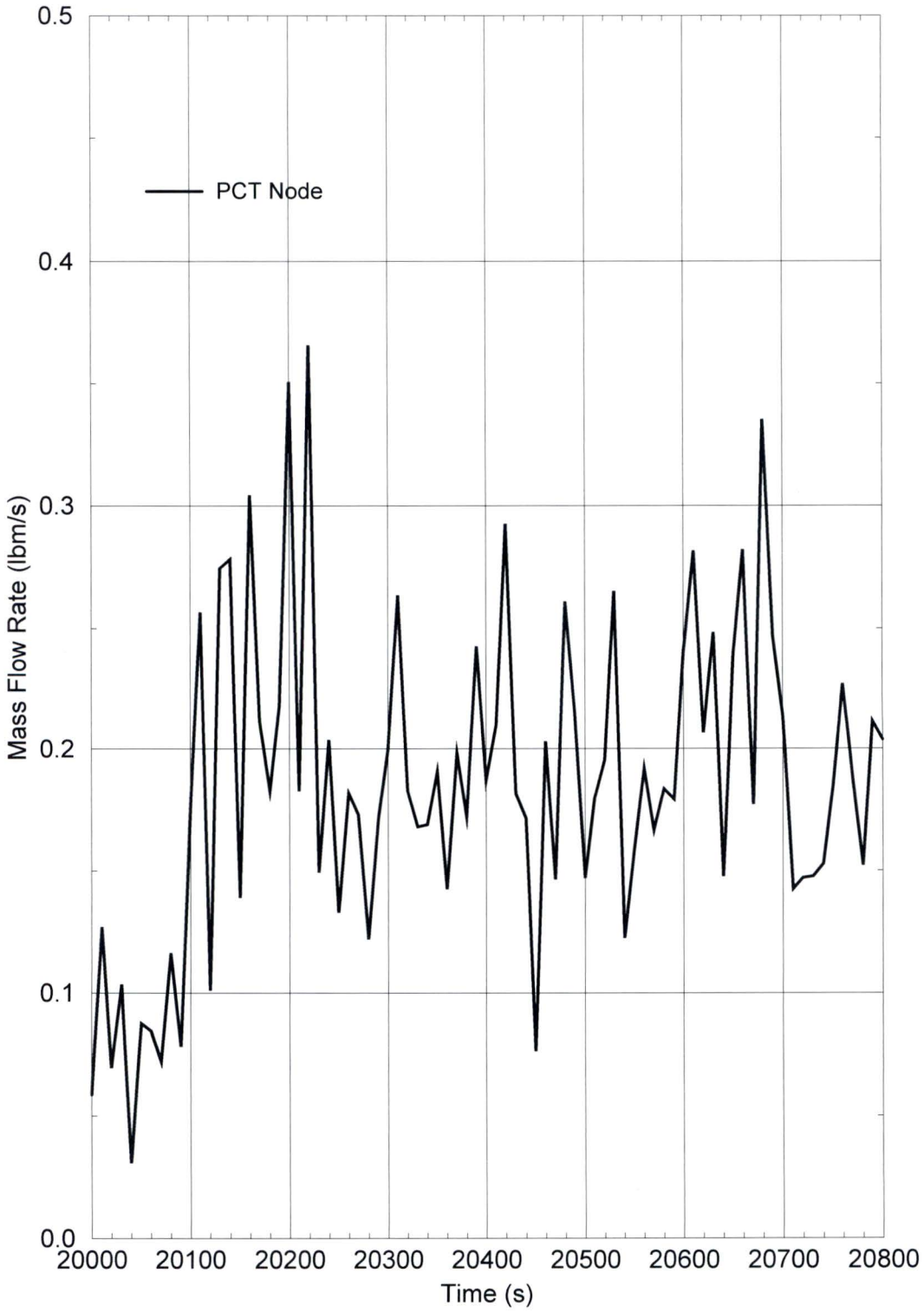

Figure RAI-4.9-4: CE Base Case – PCT Node Axial Inlet Mass Flux

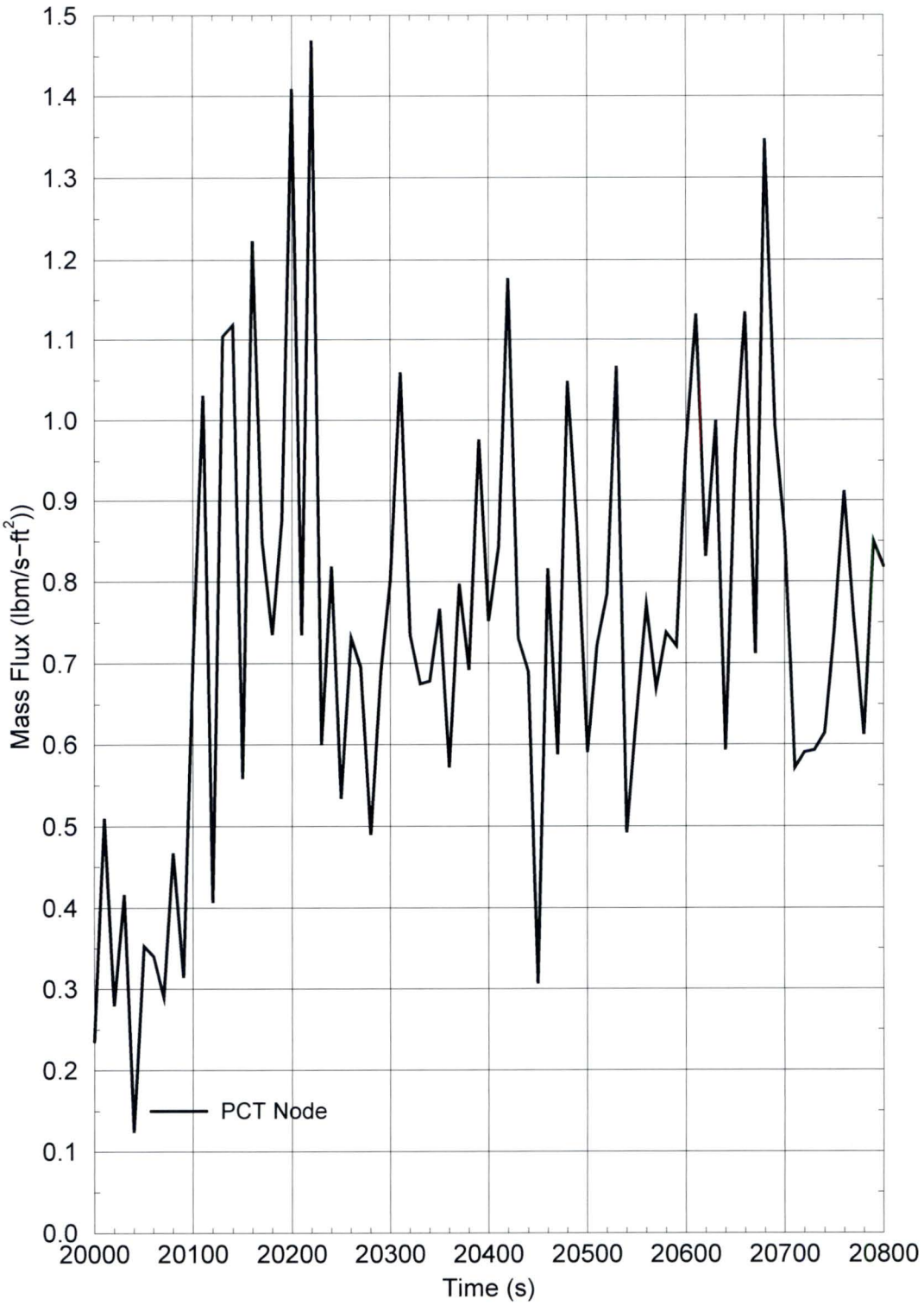

Figure RAI-4.9-5: CE Base Case – PCT Node Axial Outlet Mass Flow Rate

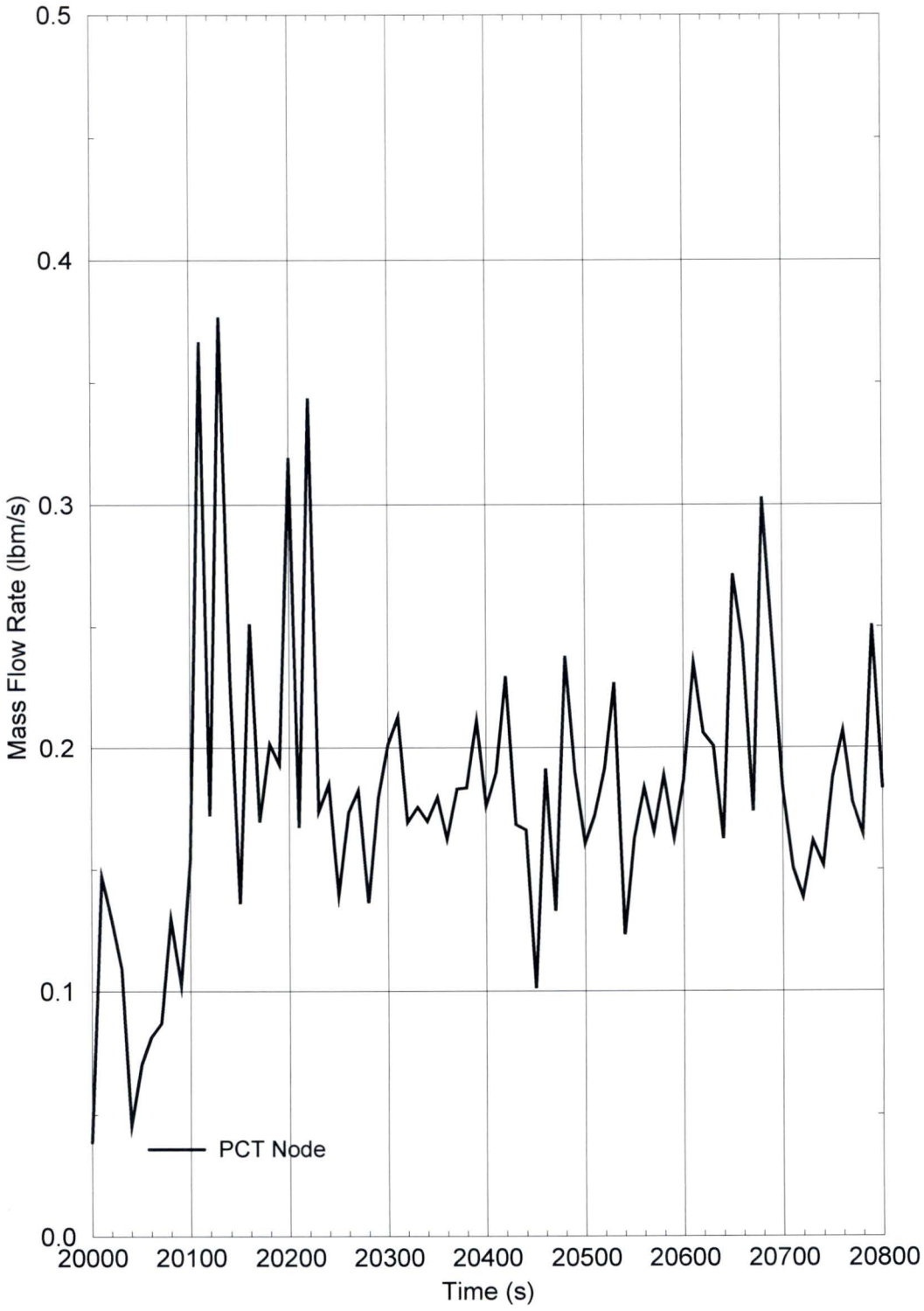

Figure RAI-4.9-6: CE Base Case – PCT Node Axial Outlet Mass Flux

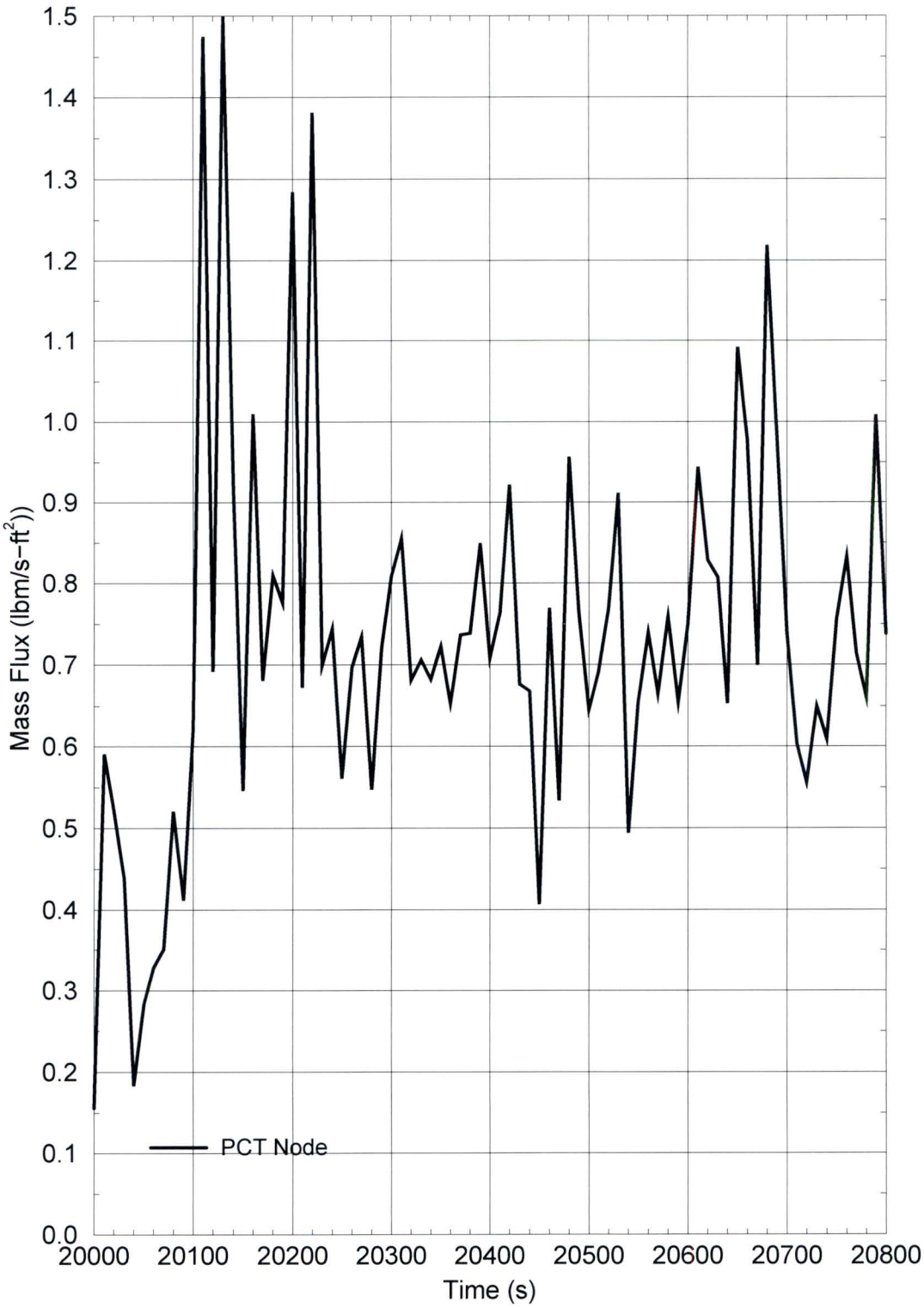

Figure RAI-4.9-7: CE Base Case – PCT Node Cross-flow Mass Flow Rate

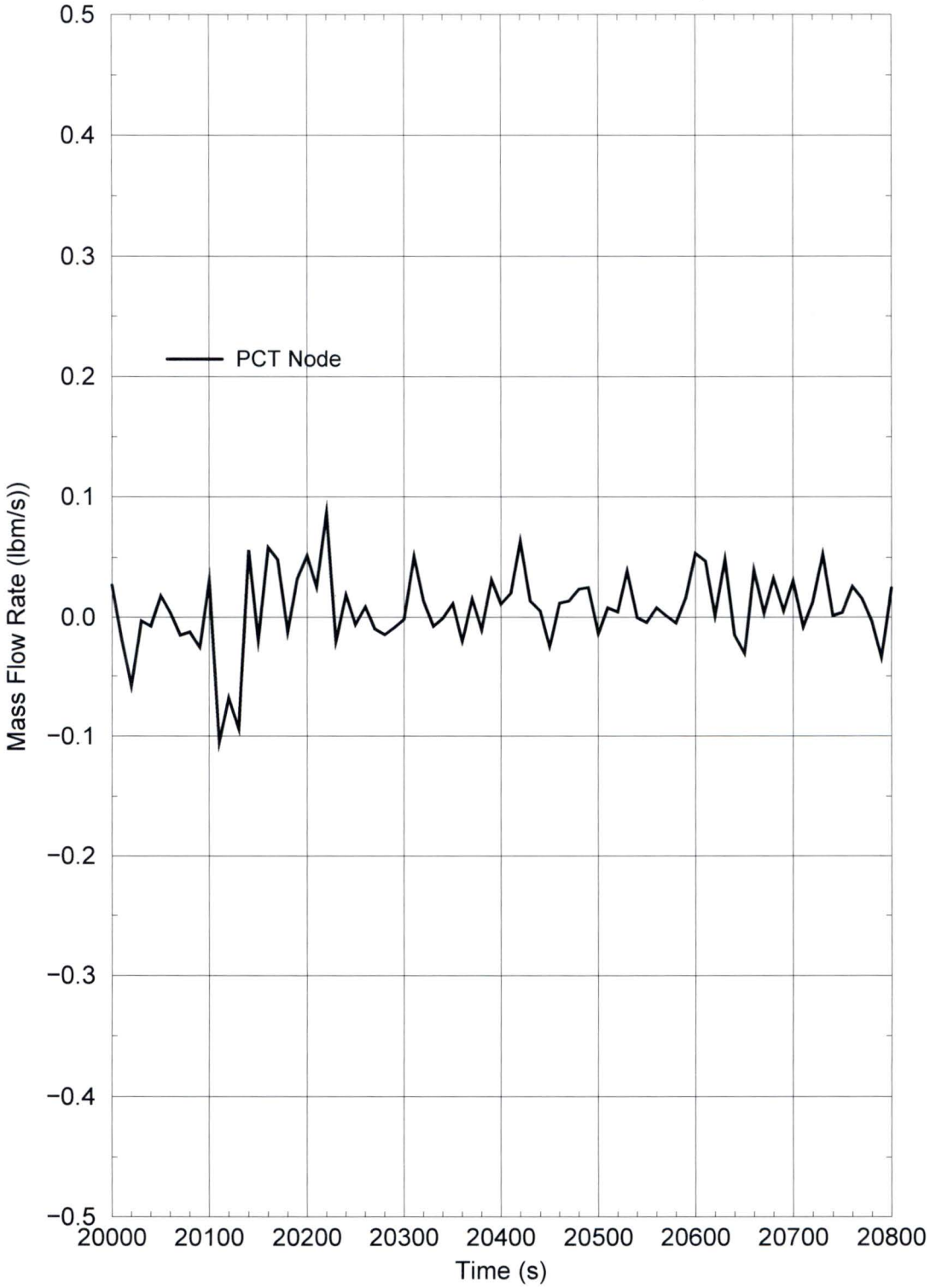

Figure RAI-4.9-8: CE Base Case – PCT Node Cross-flow Mass Flux

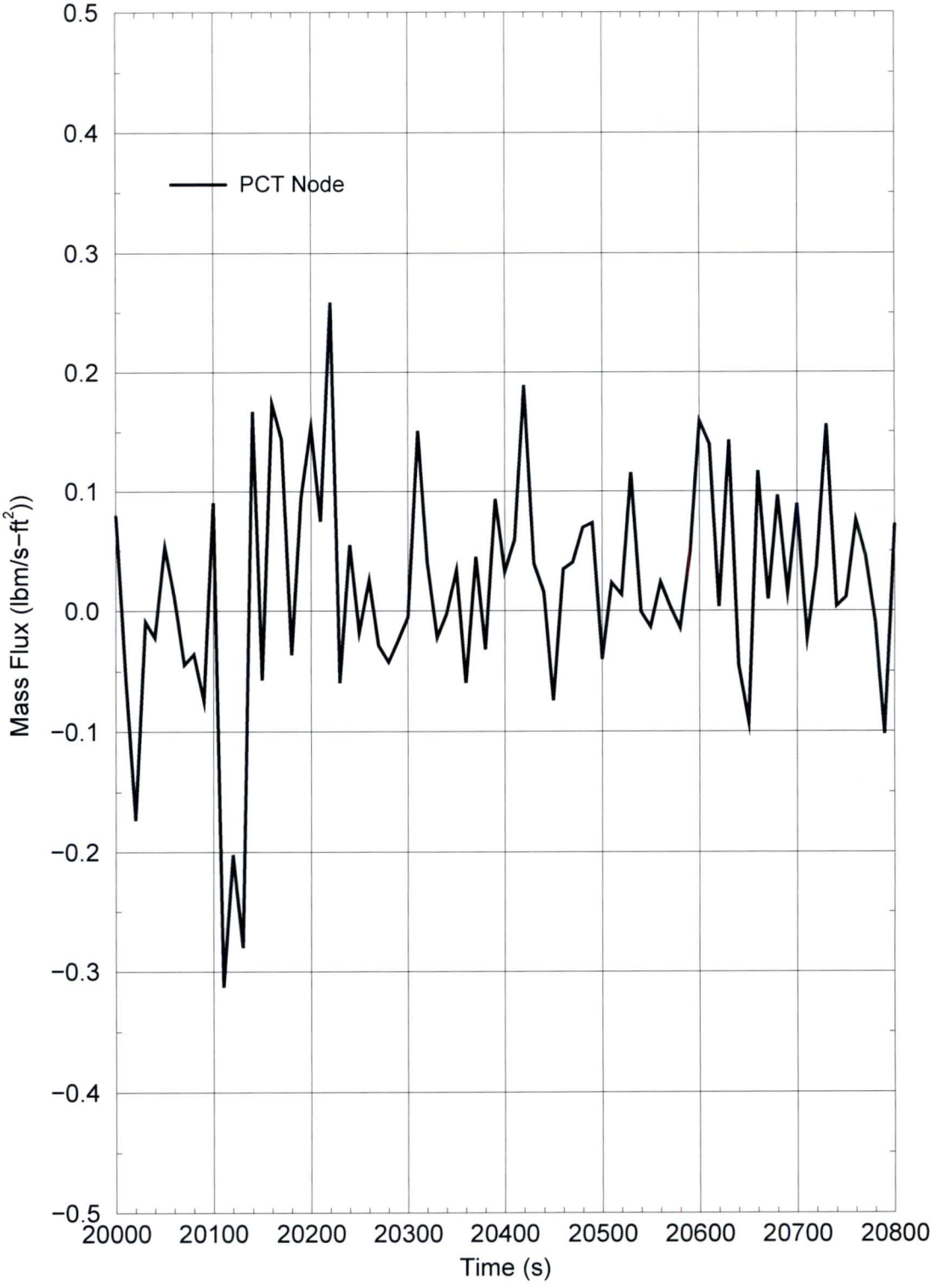

2.9.2.3 Part c

As for Part b above, the data requested is provided for the 20600 seconds major edit for data extraction convenience. The axial void fraction distribution in the HA and the Average Core (AC) at 20600 seconds is provided in Table RAI-4.9-2, for instantaneous values, and Table RAI-4.9-3 for running average values. A plot of the running average void fraction at the PCT location is provided in Figure RAI-4.9-9. As can be seen by the void fraction, the mixture level is between the 11.5 and 12 foot elevation in the core.

Table RAI-4.9-2: CE Base Case – HA and AC instantaneous void fraction distribution at 20600 seconds

Elevation (ft)	HA Void Fraction (-)	AC Void Fraction (-)
0.51	0.00	0.00
1.02	0.01	0.00
1.54	0.13	0.04
1.97	0.25	0.09
2.41	0.34	0.14
2.84	0.37	0.18
3.28	0.46	0.23
3.72	0.52	0.29
4.15	0.51	0.36
4.59	0.59	0.47
5.03	0.62	0.57
5.46	0.58	0.59
5.90	0.55	0.58
6.34	0.51	0.52
6.77	0.48	0.39
7.21	0.44	0.29
7.65	0.42	0.73
8.08	0.61	0.86
8.52	0.65	0.83
8.96	0.70	0.84
9.39	0.74	0.83
9.83	0.75	0.81
10.27	0.74	0.77
10.70	0.70	0.71
11.14	0.62	0.64
11.58	0.70	0.71
12.01	1.00	1.00
12.50	1.00	1.00

Table RAI-4.9-3: CE Base Case – HA and AC running average void fraction distribution at 20600 seconds

Node elevation (ft)	HA Void Fraction	AC Void Fraction
0.51	0.01	0.01
1.02	0.05	0.01
1.54	0.15	0.03
1.97	0.26	0.10
2.41	0.34	0.16
2.84	0.38	0.21
3.28	0.44	0.27
3.72	0.50	0.33
4.15	0.51	0.38
4.59	0.54	0.43
5.03	0.55	0.47
5.46	0.50	0.50
5.90	0.48	0.53
6.34	0.45	0.57
6.77	0.42	0.60
7.21	0.46	0.63
7.65	0.53	0.66
8.08	0.59	0.68
8.52	0.60	0.69
8.96	0.63	0.71
9.39	0.66	0.72
9.83	0.66	0.72
10.27	0.72	0.73
10.70	0.77	0.75
11.14	0.84	0.81
11.58	0.93	0.92
12.01	0.98	0.98
12.50	1.00	1.00

Figure RAI-4.9-9: CE Base Case – Running Average Void Fraction at the PCT Node Exit

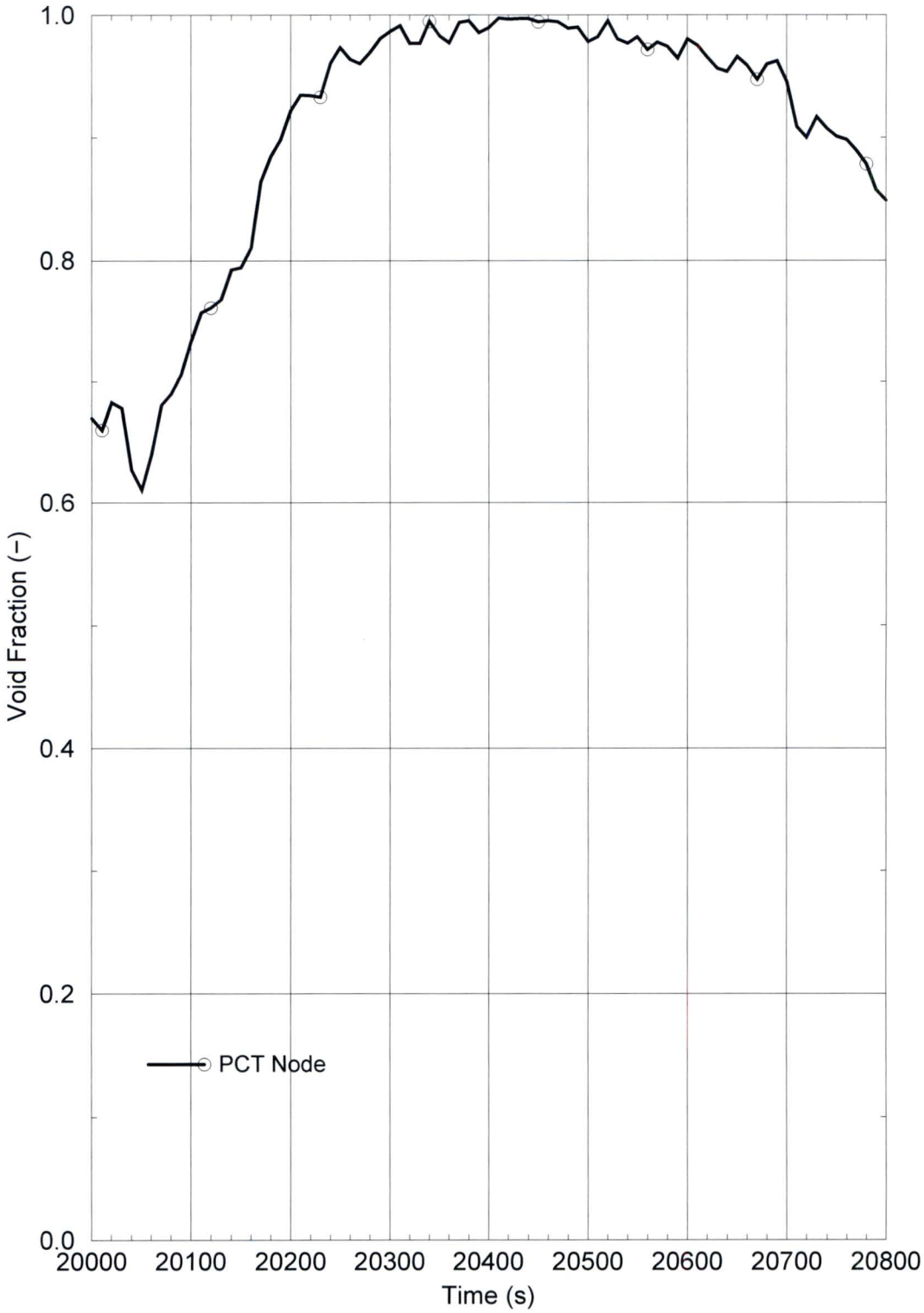

2.9.2.4 Part d

In mist flow regime (dry wall) and single-phase vapor, the heat transfer coefficient is the maximum of the Sleicher-Rouse correlation for forced flow regimes (turbulent and laminar) and the turbulent natural convection heat transfer recommended by Holman (see Reference 4.9-1, Section 4.4.2.1). In general, the Sleicher-Rouse correlation determines the heat transfer. The effects of radiation heat transfer also are considered if the wall temperature exceeds 650 K. A discussion of the ranges of applicability is provided in Reference 4.9-1, Section 4.4.2.1.

2.9.2.5 Part e

As noted above, around the time of PCT, the flow regime at the PCT node is mist flow and the heat transfer mode is single-phase vapor. The void fraction in the node is 1.0, and, there are no liquid droplets being entrained from below due to the fact that steam velocity is below the droplet entrainment limit.

The S-RELAP5 code solves a two-fluid, six equation model plus one continuity equation of noncondensible gas and a boron tracking equation for flow of a two-phase steam-water mixture which can contain a noncondensible in the vapor phase and a soluble in the liquid phase. The void fraction is one of the primary dependent variables for the eight field equations solved by the code. Reference 4.9-2, Section 7.4 includes a detailed discussion of the two-fluid field equations and the solution methods. The interphase coupling terms and the wall friction terms in the fluid field equations are described in Reference 4.9-2, Section 7.5. The constitutive correlations describing the wall frictions, the interphase processes and the interactions between fluid and heat conduction are presented in Reference 4.9-2, Sections 7.6 and 7.7.

References - RAI 4.9

4.9-1 AREVA Inc. Document EMF-2103(P)(A), Revision 0, *Realistic Large Break LOCA Methodology for Pressurized Water Reactors.*

4.9-2 AREVA Inc. Document EMF-2103(P)(A), Revision 3, *Realistic Large Break LOCA Methodology for Pressurized Water Reactors.*

2.10 RAI 4.10

2.10.1 Statement of RAI 4.10

Provide plots showing the heat generation rates from the decay heat models that were used in the LOCA T-H analyses documented in Sections 8 through 11. Show the decay heat rates as a function of transient time with time zero corresponding to the break opening. Display the decay heat rate in relative dimensionless units using a linear scale with a range from null to 1.2. Plot the time axis in a logarithmic scale in units of seconds. Use a common time range that starts at one second after break opening and ends when the longest analyzed LOCA transient case ends.

2.10.2 Response to RAI 4.10

The plot requested is provided in Figure RAI-4.10-1.

Figure RAI-4.10-1: Normalized Decay Heat Power for CE Analyses

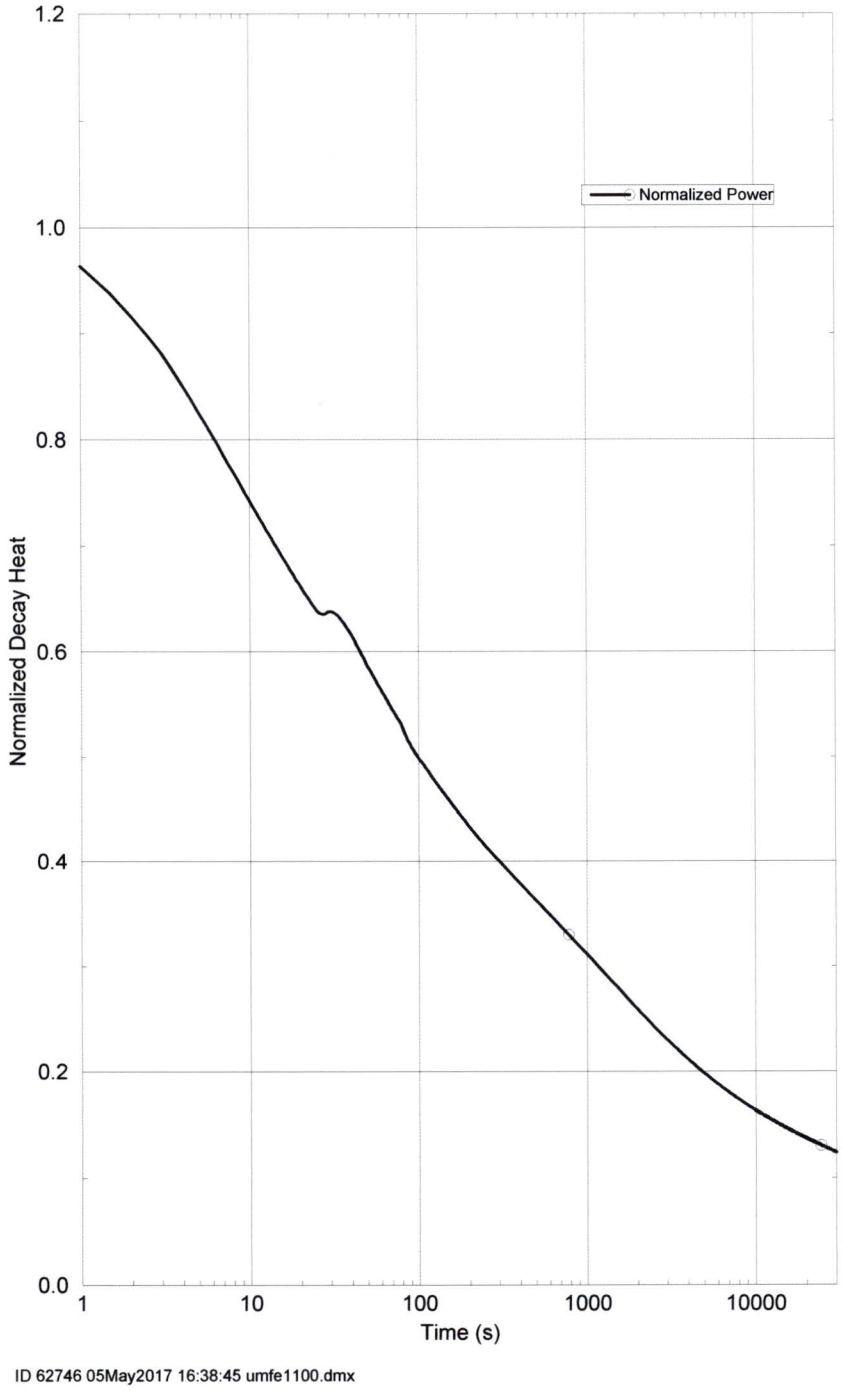

2.11 RAI 4.11

2.11.1 Statement of RAI 4.11

Section 5.4 states that "the analysis completed by AREVA using S-RELAP5 produced results that compared reasonably well to those predicted by WCOBRA/TRAC, which are described in Section 9". The section also explains that "the plant and transient condition analyzed was identical to that used by Westinghouse;" however, "the plant models used for each analysis were developed independently following different methods and techniques". Section 5.4 concludes that "irrespective of the computer codes and methods used, the resulting code predictions are expected to be consistent".

(a) Define the simulated LOCA transient and provide a summary description of the analyses. Provide a table that documents and compares key inputs and modeling features for both studies and explain how this information relates to key inputs provided in Table 6-2 for the Westinghouse downflow plant design analysis.

(b) Provide comparisons of key results from the analyses. Explain any significant discrepancies between the results from the studies and provide an assessment of the degree of conservatism reflected in each of the analyses. Discuss how differences in the prediction results relative to t_{block}, K_{max}, K_{split}, and/or m_{split} could be caused or explained by differences in the applied methodologies, plant model features (such as core nodalization), assumed key inputs, and other relevant conditions.

(c) Provide references for the technical documents containing the calculation notebooks documenting the analyses in Items a and b and confirm that the analyses were quality assured.

2.11.2 Response to RAI 4.11

2.11.2.1 Part a

As discussed in WCAP-17788, Volume 4, Section 5.4, during the initial development of this project, a comparison of analysis results using the AREVA code to the Westinghouse Electric Company (WEC) code for a plant under identical conditions was done. The model selected for comparison did not represent the base model used for either the WEC or CE plant categories. Instead, a plant was selected for which both AREVA and WEC had a model already developed.

This preliminary evaluation of a singular point was useful as an initial comparison of the codes to ensure that AREVA and WEC were using similar approaches and initial and boundary conditions at the outset of the program. After this comparison was made, the PWROG program continued to evolve. As a result of continued analysis of the results, interaction with the NRC staff via public meetings and audits, and technical review, changes were made to the methods and models.

Since the models used in the comparison analysis did not represent a base model in either of the plant categories, they did not evolve with the program. To that end, this comparison is no longer of sufficient exactitude to be meaningful. Further, this initial comparison met the objective of ensuring that AREVA and WEC technical teams were aligned and that they continued to interact to keep the programs aligned. Therefore, the need for this type of comparison provided in Section 5.4 is no longer required, and Section 5.4 is being deleted from WCAP-17788, Volume 4.

2.11.2.2 Part b

As described in the response to part "a" above, Section 5.4 is being deleted from WCAP-17788, Volume 4. Therefore, the requested comparison of results in no longer necessary.

2.11.2.3 Part c

As described in the response to part "a" above, Section 5.4 is being deleted from WCAP-17788, Volume 4. Therefore, reference to the technical documents in no longer necessary.

2.12 RAI 4.12

2.12.1 Statement of RAI 4.12

The UPI plants were not considered as part of the analysis due to their ECCS configurations. Provide justification that plants with the UPI configurations do not require T-H analyses to demonstrate that the acceptance criteria defined in WCAP-17788 are satisfied and that the TR is applicable to their specific plant designs including applicable ECCS features.

2.12.2 Response to RAI 4.12

This RAI pertains to the Westinghouse Electric Company (WEC) plant categories and therefore requires no response for the Combustion Engineering (CE) plant category.

2.13 RAI 4.13

2.13.1 Statement of RAI 4.13

Figure 8-13 shows the mid-core velocity in the BB channel going from negative, interpreted as downward, to about zero very rapidly before switchover time. The plotted BB inlet velocity remains stable at near zero or around a slightly negative value throughout the exhibited part of the transient while the BB exit velocity remains stable at a low negative value. In addition, the BB exit velocity is large in magnitude compared to the BB inlet velocity. Provide an explanation for this behavior.

2.13.2 Response to RAI 4.13

This RAI pertains to the Westinghouse Electric Company (WEC) plant categories and therefore requires no response for the Combustion Engineering (CE) plant category.

2.14 RAI 4.14

2.14.1 Statement of RAI 4.14

Figures 8-16 and 8-25 show a spike in PCT occurring while the downcomer fills. Once the flow begins exiting the BB region, the core begins to cool again and PCT decreases. Were the potential range of flow rates for downcomer fill considered in the analyses? Explain how the analysis accounts for potential uncertainties or variability in the downcomer fill time. If the analysis does not account for such uncertainty/variability, explain how the behavior (PCT spike) would be affected by different downcomer fill times.

2.14.2 Response to RAI 4.14

This RAI pertains to the Westinghouse Electric Company (WEC) plant categories and therefore requires no response for the Combustion Engineering (CE) plant category.

2.15 RAI 4.15

2.15.1 Statement of RAI 4.15

Provide the results of Figures 9-9 and 9-10 on the same graph. Normalize the integrated mass flow on an average channel basis so that a meaningful comparison can be made.

2.15.2 Response to RAI 4.15

This RAI pertains to the Westinghouse Electric Company (WEC) plant categories and therefore requires no response for the Combustion Engineering (CE) plant category.

2.16 RAI 4.16

2.16.1 Statement of RAI 4.16

Assumption 6 in Section 4.1 states that "ECCS temperature during sump recirculation will be set at or near saturation temperature at containment pressure" and explains that "neglecting the presence of subcooling is conservative because it maximizes the steaming rate in the core and minimizes the cooldown rate of the reactor vessel (RV) and steam generators (SGs)". Tables 6-1 through 6-4 include the parameter "ECCS temperature during recirculation phase" as a key input. The CE plant category stands apart in the sense that this input is set at a temperature of 212 °F with the "containment pressure during recirculation phase" specified as "dynamically calculated" according to Table 6-3. During the NRC audit of the AREVA T-H analyses for the CE plant category, it was clarified that S-RELAP5 was used in a coupled mode with the ICECON containment code to calculate the containment backpressure.

(a) Identify contributing physical processes that are dependent on the degree of ECCS fluid temperature subcooling and explain the effects associated with these processes with regard to core cooling. In addition to core steaming, explain whether processes such as condensation, downcomer boiling, liquid entrainment, and boiling in SG tube bundles (if engaged) were considered among such processes. State whether these effects are considered conservative or non-conservative and provide justifications for the conclusions.

(b) Identify the coupled S-RELAP5/ICECON methodology by providing a reference to the technical document that describes it. Explain whether the methodology was validated and assessed for applications similar to the LOCA analyses documented in Vol. 4 for the CE plant category. Clarify whether the coupled code methodology and/or application analyses obtained with this methodology have been reviewed and/or approved by NRC. Provide the key inputs and assumptions relative to the containment model. Explain which of these input parameters were modeled in a bounding manner along with the ranges considered in determining the input values for the parameters.

(c) In order to assess the effect from the major assumption regarding the ECCS temperature subcooling, the NRC staff recommends performing two re-analyses for Cases 1 and 2 documented in Section 10 using S-RELAP5 in a stand-alone mode. For the purpose of these re-analyses it is suggested that an "ECCS temperature during recirculation phase" of 212 °F along with a "containment pressure during recirculation phase" of 14.7 psia consistent with the key inputs applied for the Westinghouse upflow and downflow plant categories is used. Verify that there is

little impact on the K_{max} and t_{block} results compared to the results documented in Section 10.

(d) Tables 6-1 through 6-4 do not provide information regarding the ECCS temperatures prior to sump switch over (SSO). Section 9.3 states that "during transfer to sump recirculation, the ECCS coolant temperature is set to 212 °F". Explain how the ECCS temperatures prior to SSO were defined for the purposes of the analyses and provide the values used for the analyses in Sections 8, 10, and 11. Clarify whether the ECCS temperature prior to SSO should also be considered a contributing factor for the purposes of the T-H analyses in Vol. 4 and justify the response. Describe the effects that the ECCS temperature assumption prior to sump switchover can have on other processes (i.e., voiding, swelling, etc.) if it is found to have a significant impact on the results.

2.16.2 Response to RAI 4.16

2.16.2.1 Part a

The important physical processes applicable to the Combustion Engineering (CE)-designed plants were identified in the response to Request for Additional Information (RAI) 4.7. In the long-term following a hot leg break, the Emergency Core Cooling System (ECCS) flow rate exceeds what is needed to replace that which is boiled off due to decay heat such that the core remains covered. To that end, the Reactor Coolant System (RCS) system response will be controlled by the core decay heat. That is, the boiloff defines the core void fractions and liquid volume, the Downcomer (DC) level will be balanced with the core level, and the excess ECCS flow will exit the break.

After the core has recovered and the system transitioned to the Long Term Core Cooling (LTCC) phase of the event, the heat removal from the RV wall has become conduction limited. While some amount of boiling may occur in the DC, the consequences are insignificant because the DC level quickly adjusts to the additional voiding (boiling) to balance the core liquid level. Since the ECCS flow rate exceeds that needed to match the core boiloff, DC boiling (if present) will have no effect on the core response.

Several sensitivity studies were performed to investigate the effects of the degree of ECCS fluid temperature subcooling after Sump Switch Over (SSO). Table RAI-4.16-1 lists the cases evaluated. The analysis show that, comparing case 04 and case 25, on one hand, and case 07 to case 12, on the other, a lower ECCS fluid temperature after SSO has a beneficial effect and lowers the post-blockage Peak Cladding Temperature

(PCT). These cases have identical ECCS conditions, except the fluid temperature after SSO. The higher condensation potential of the fluid with a lower temperature (cases 25 and 12) requires a slightly higher DC level (Figures RAI-4.16-1 and RAI-4.16-2), which will determine a slightly higher liquid level in the core, too (Figure RAI-4.16-3). Boiloff rates are mainly determined by the decay heat level, with higher rates for the cases with a 1.2 decay heat multiplier (cases 07 and 12 - Figure RAI-4.16-5). The cases analyzed had different condensation potentials associated with ECCS fluid at lower temperature. The ECCS temperature changes the density and the amount of hydrostatic head in the downcomer pushing liquid into the core and the amount of liquid boiled-off in the core. Small variations between the four cases are noted in the Reactor Vessel (RV) mass (Figure RAI-4.16-4), as cases with subcooled ECCS fluid conditions show slightly higher inventory being accumulated. In all cases, the DC level rose to the height needed to push all the ECCS plus condensate into the core region. The condensation does not detrimentally alter the system response because all the ECCS flow reaches the core providing better cooling for the cases with lower ECCS temperature following core inlet blockage. Boundary conditions are similar between the cases, with ECCS mass flows identical (Figure RAI-4.16-6), while differences can be noted in the integrated vapor break flow (Figure RAI-4.16-7) and the integrated liquid break flow (Figure RAI-4.16-8), a reflection of the higher boil-off rates for the cases with a higher decay heat multiplier. These results confirm that the use of ECCS fluid at saturation temperature is appropriate for the base analysis. CE plant designs lack Residual Heat Removal (RHR) heat exchangers, and after switchover to recirculation, High Pressure Safety Injection (HPSI) flow goes directly from sump to the RCS (see RAI 4.5a for additional information), which means that the ECCS fluid is expected to be saturated in the actual plant under these conditions.

Table RAI-4.16-1: ECCS Flow and Temperature Sensitivity Cases

Case	ECCS Temperature before SSO (°F)	ECCS Temperature after SSO (°F)	Decay Heat Multiplier	PCT (°F)
04	110	212	1.1	542
25	110	200	1.1	no clad heatup
07	110	212	1.2	788
12	110	200	1.2	557

Figure RAI-4.16-1: Average Downcomer Collapsed Liquid Level

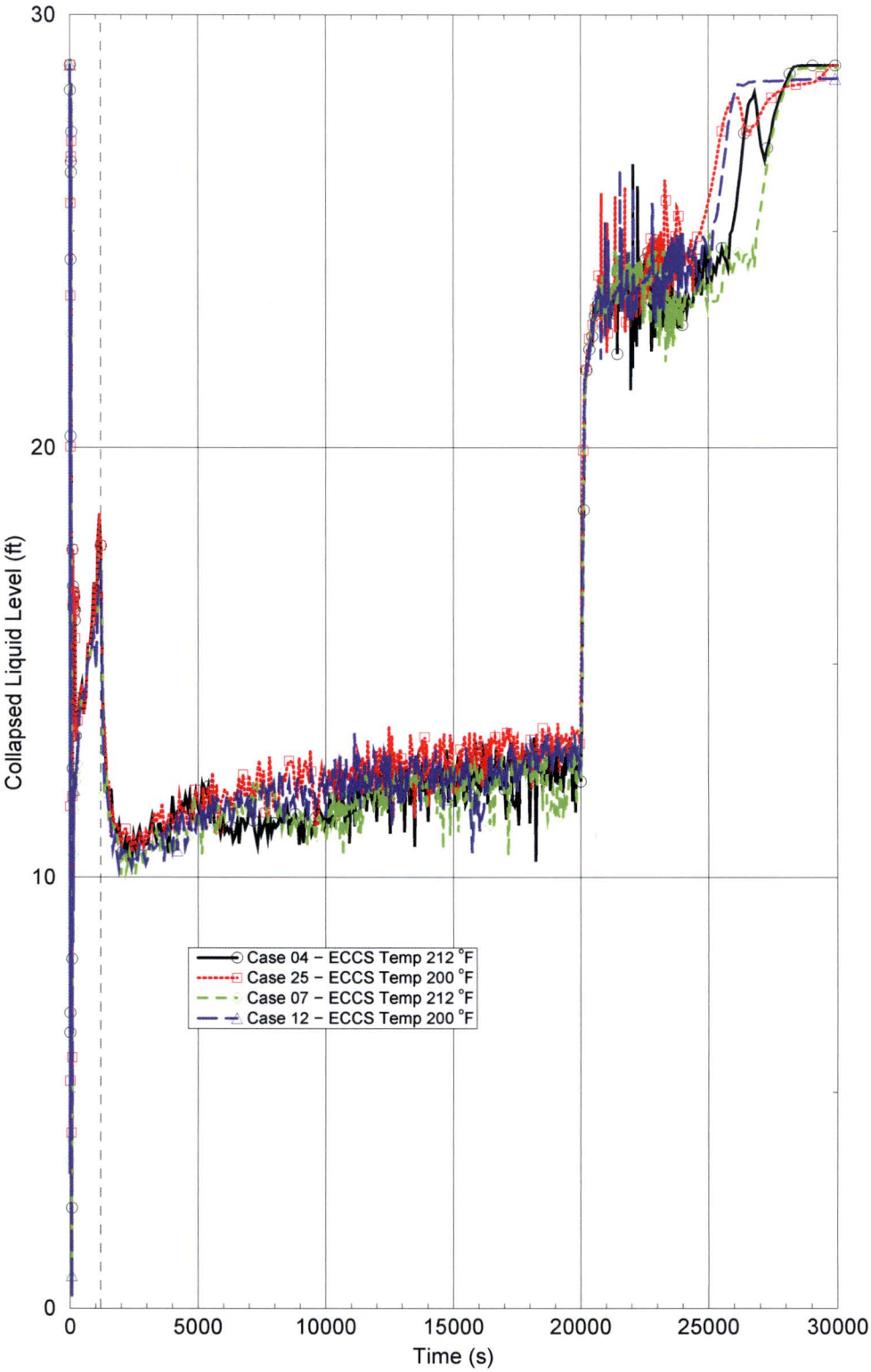

Figure RAI-4.16-2: Downcomer Total Mass

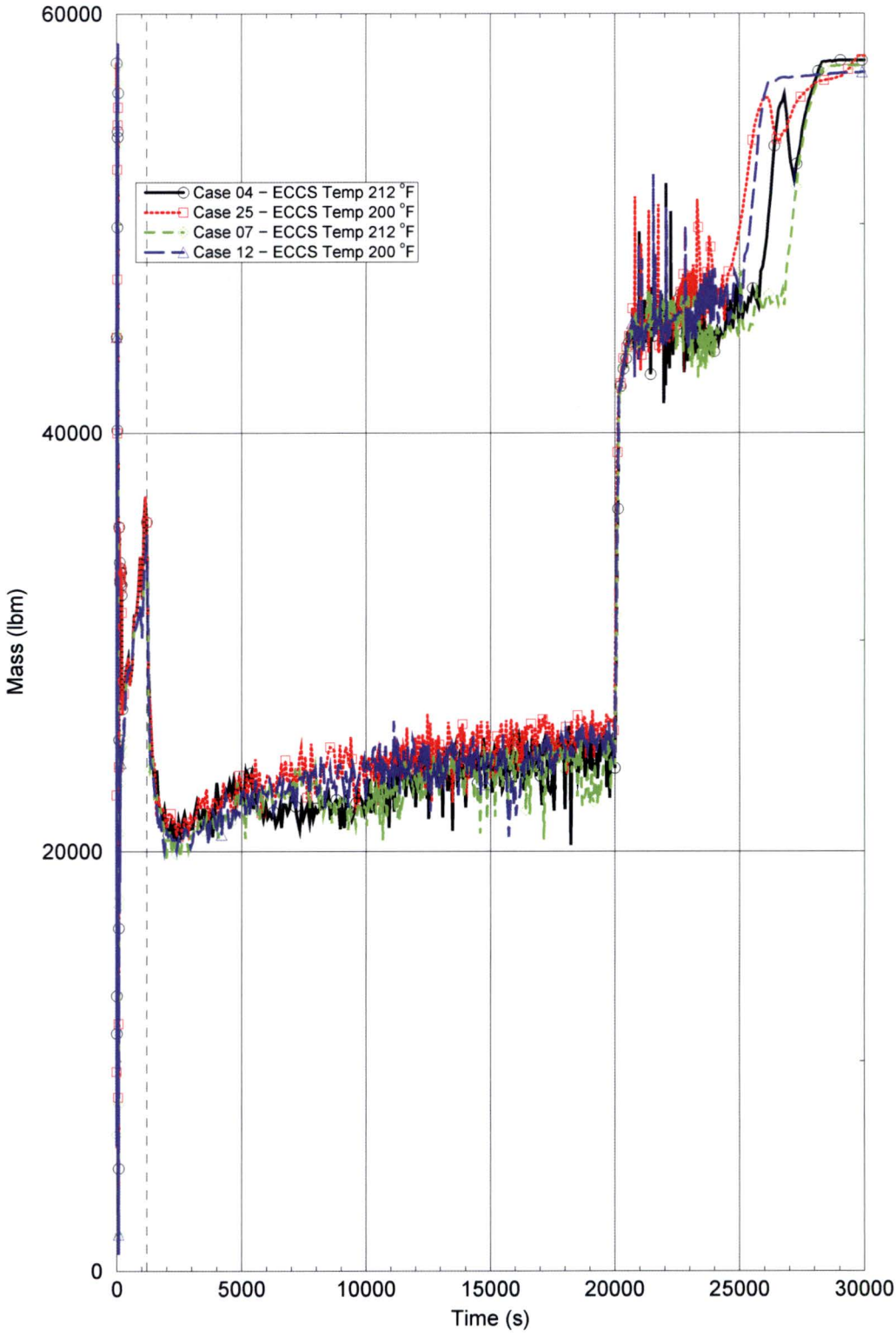

Figure RAI-4.16-3: Average Core Collapsed Liquid Level

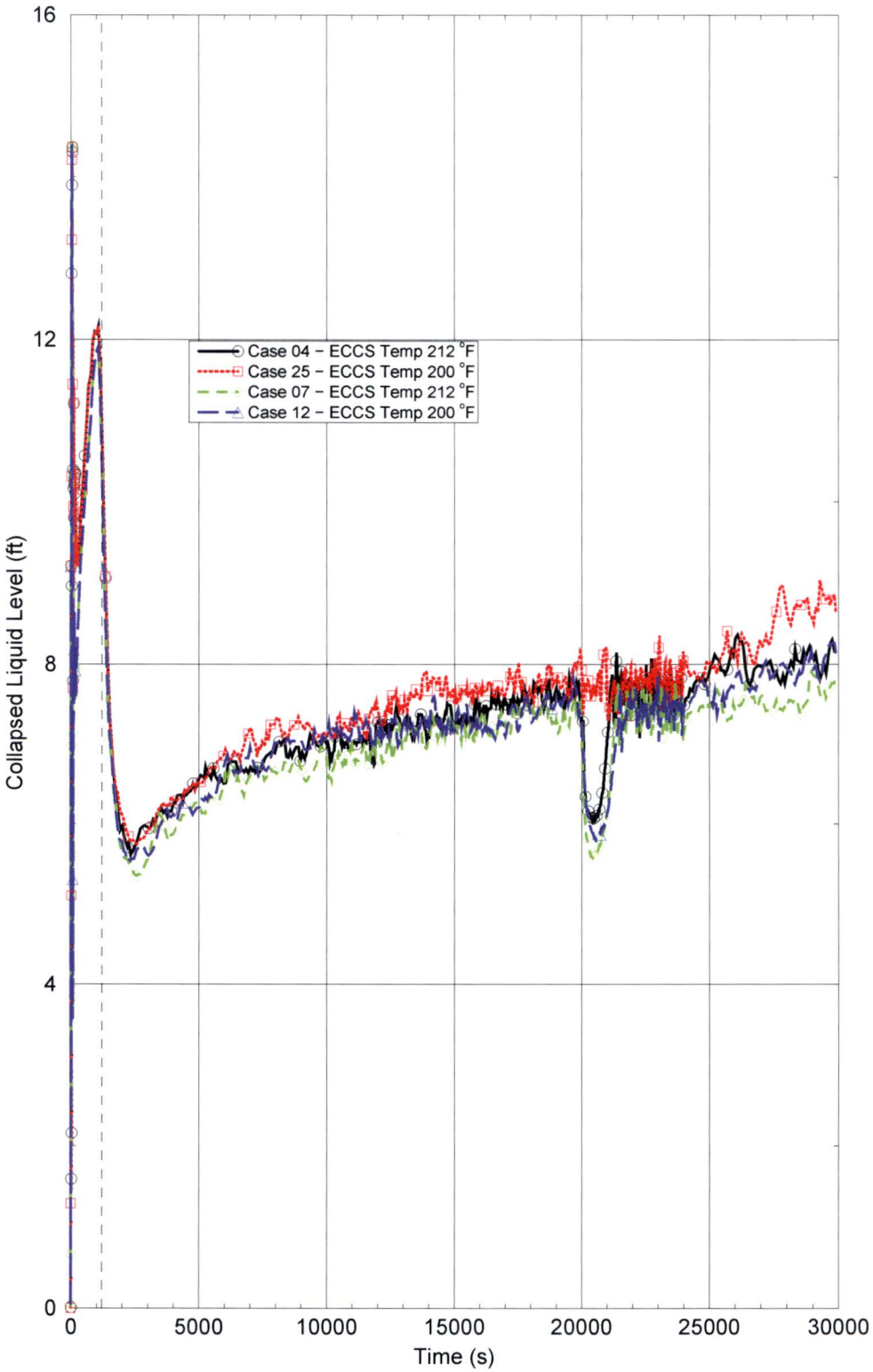

Figure RAI-4.16-4: Reactor Vessel Total Mass

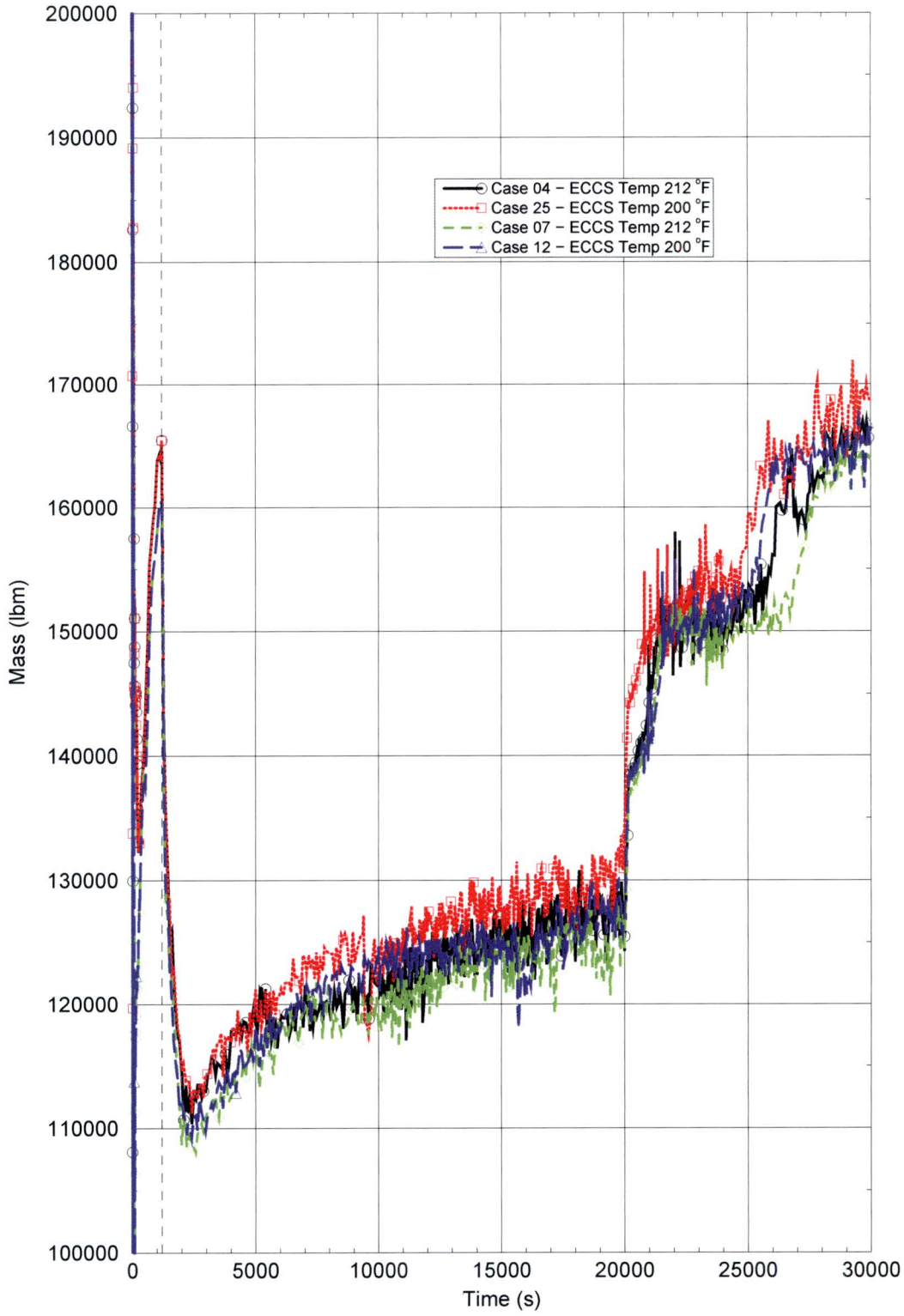

Figure RAI-4.16-5: Boiloff Rate

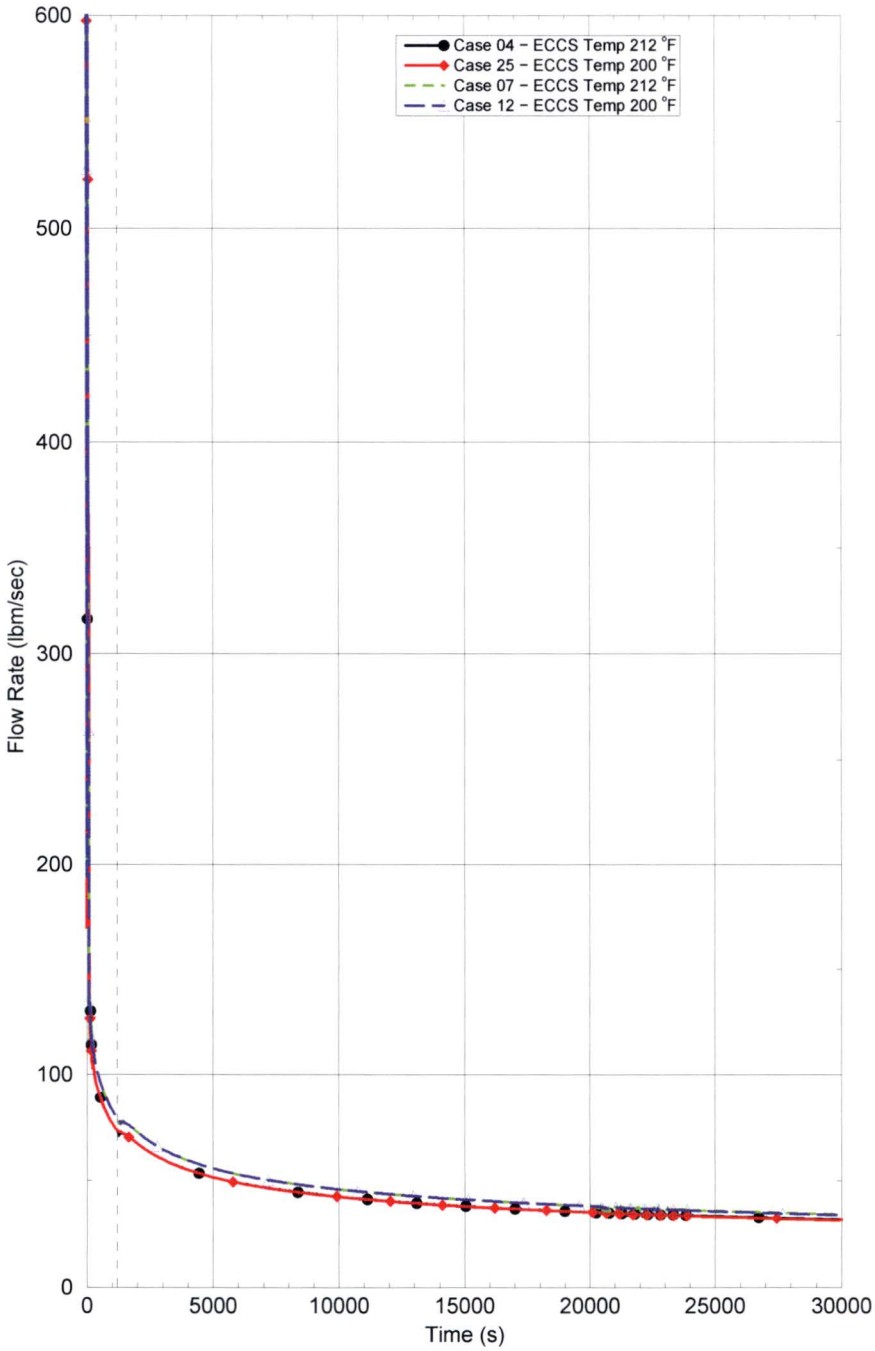

Figure RAI-4.16-6: Integrated Pumped ECCS and Break Flow

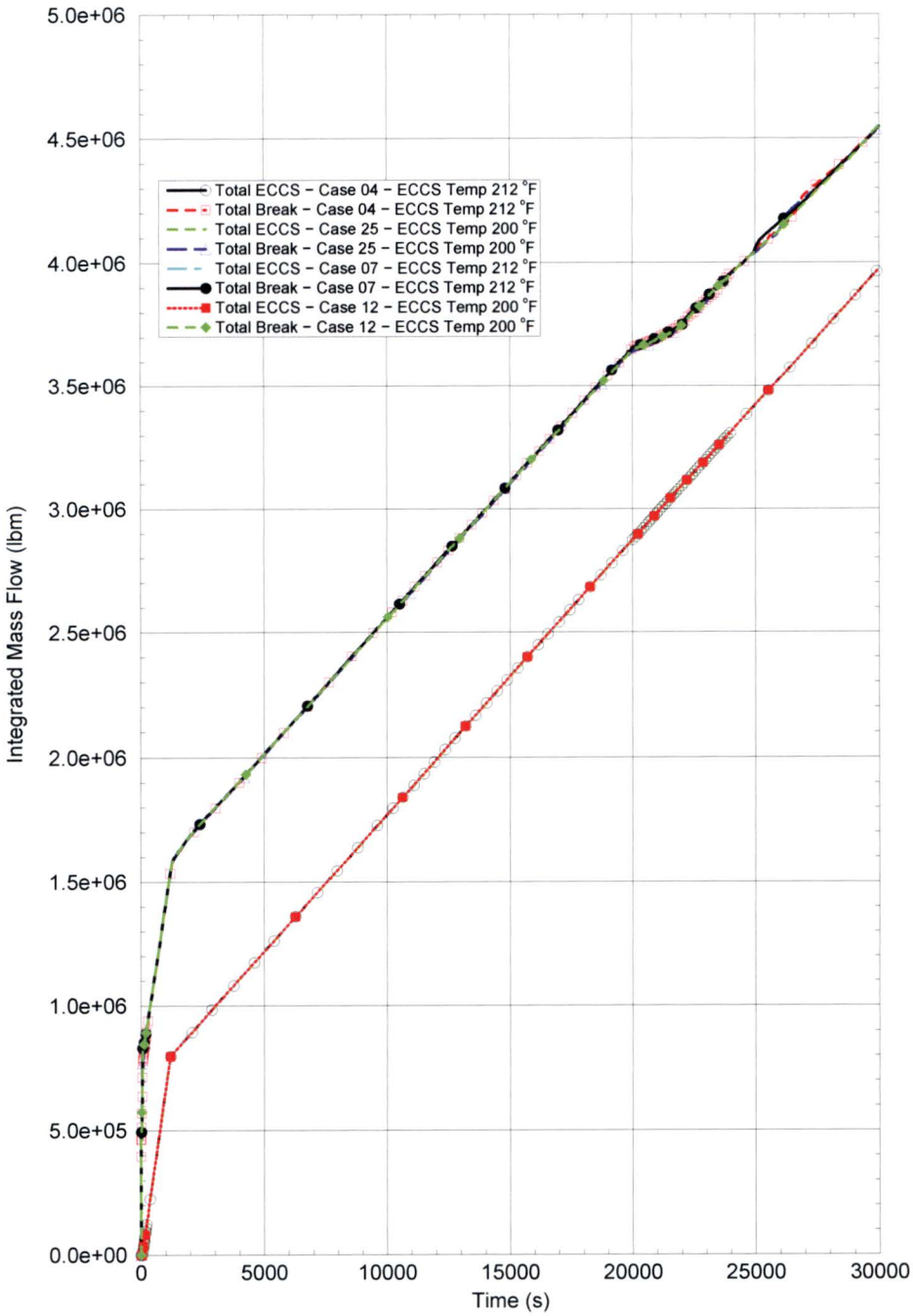

Figure RAI-4.16-7: Integrated Break Vapor Flow

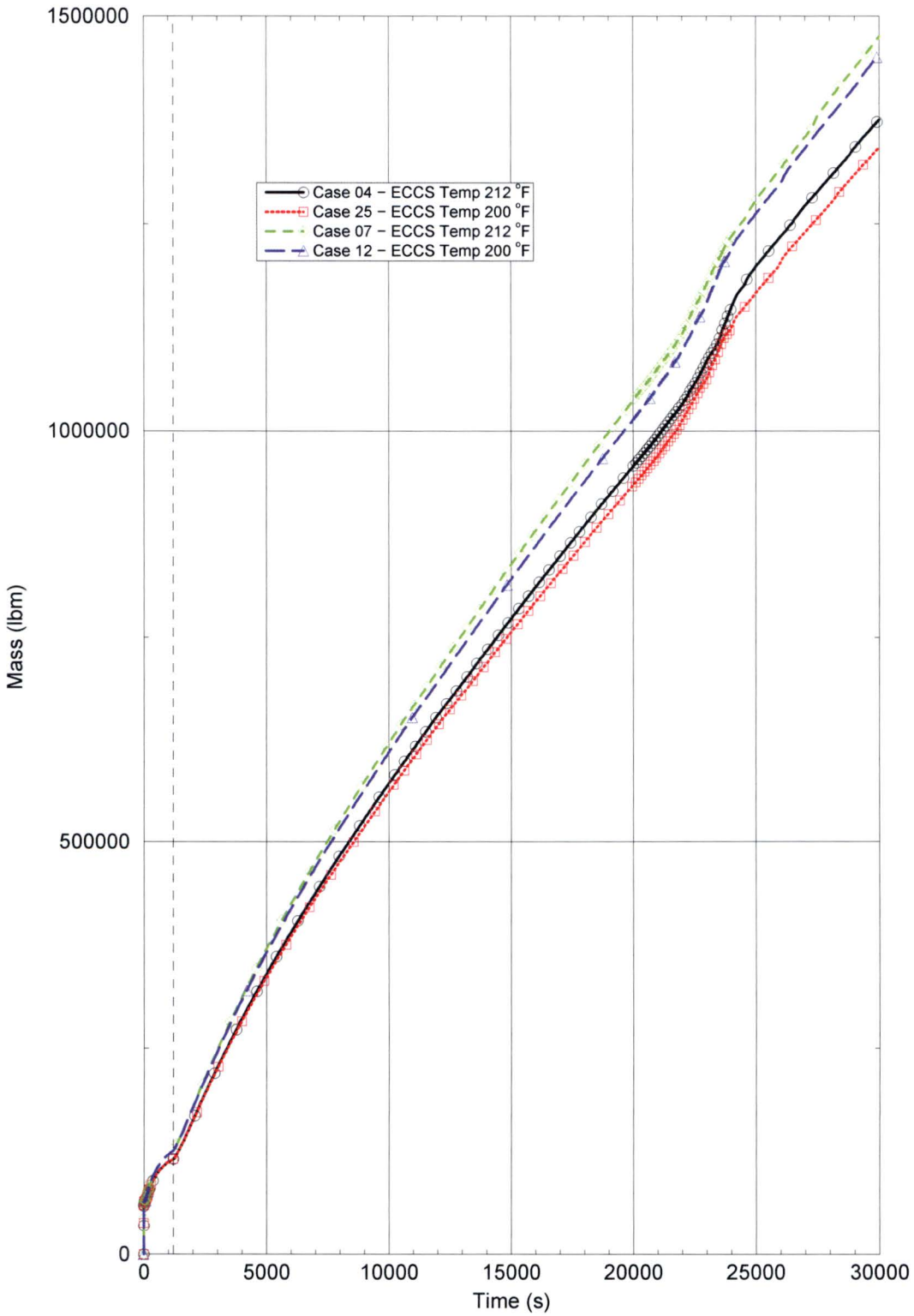

Figure RAI-4.16-8: Integrated Break Liquid Flow

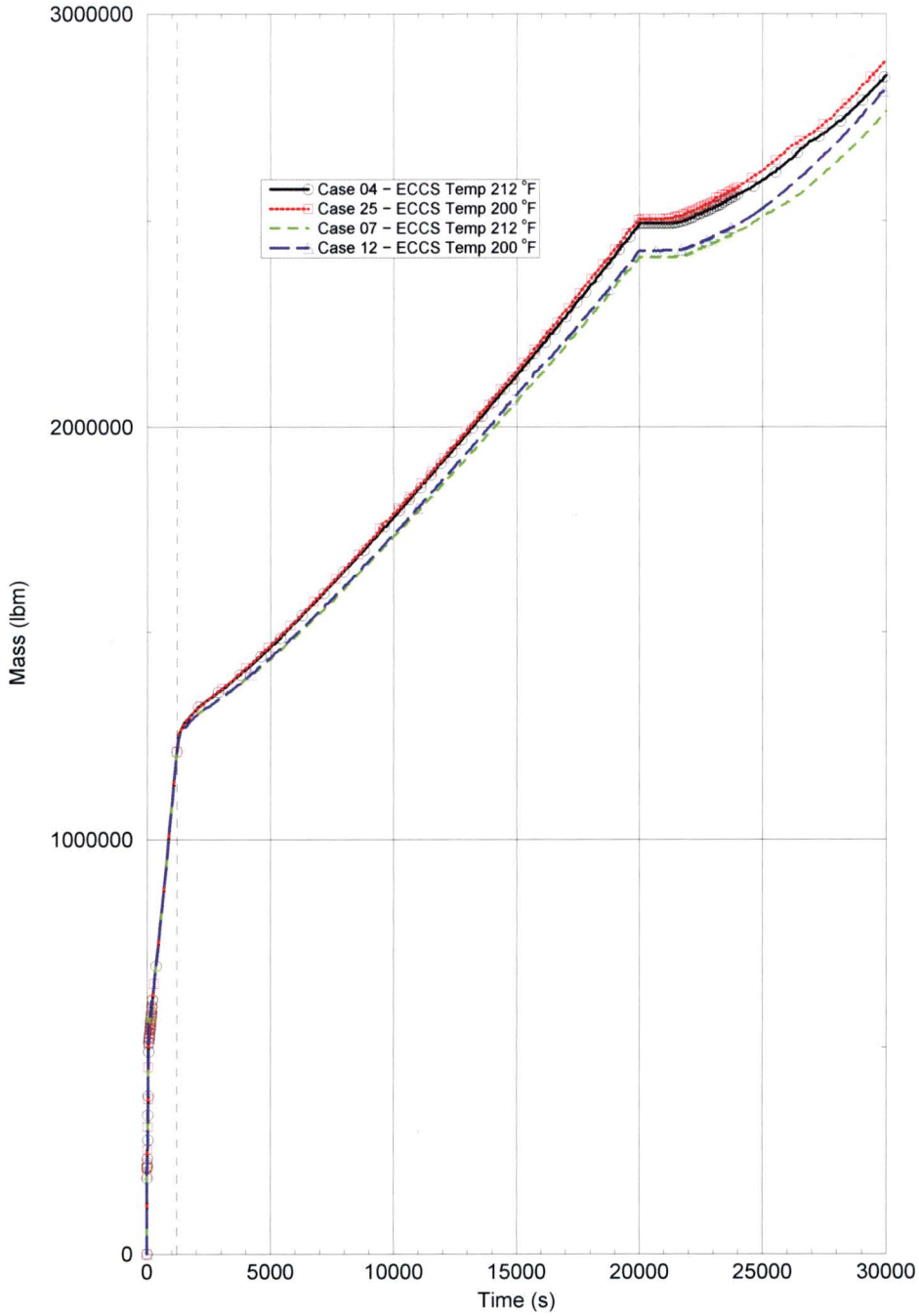

2.16.2.2 Part b

The base analysis has been revised to use a model with a constant 14.7 psia containment pressure after 200 seconds (see the response to RAI 4.1b).

2.16.2.3 Part c

The base analysis has been revised to use a model with a constant 14.7 psia containment pressure after 200 seconds (see the response to RAI 4.1b).

2.16.2.4 Part d

The new base analysis for CE plants, presented above in the response to RAI 4.1b, uses a constant ECCS temperature of 110 °F up to the time of SSO, and a step increase to a constant value of 212 °F at the time of SSO (1200 seconds). A sensitivity study was performed with 70 °F for the ECCS fluid temperature, up to 1200 seconds, followed by a step increase to a constant value of 212 °F at the time of SSO. It should be noted here that the sensitivity study maintained the mass flow rates for the ECCS flows, while the volumetric flow rates are lower, due to the fluid density differences. The sensitivity study shows that the cooler ECCS fluid temperature prior to the time of SSO leads to higher levels in the DC and the core (Figures RAI-4.16-9, RAI-4.16-10 and RAI-4.16-11), with better cooling conditions. Initial expectations about these two cases were to have very little differences, since the changes in boundary conditions are prior to the time of SSO. Analysis of the results show that the balance of the amount of fluid enters and exits the system matches between the two simulations, with the same decay heat and a general system behavior that is very similar. After 10000 seconds, the DC and core collapsed liquid levels track each other between the two cases (Figures RAI-4.16-9 and RAI-4.16-11), except for a small depression in DC level just before t_{block} for the case with an ECCS fluid temperature of 70 °F (Figure RAI-4.16-9). The RV mass also tracks well between the two cases after 10000 seconds (Figure RAI-4.16-12). The base case has more mass in the DC prior to the core inlet blockage time, but less in the core. However, the total RV fluid mass is about the same (Figure RAI-4.16-12). Boundary conditions are similar between the cases (Figure RAI-4.16-14), with ECCS and break flows matching. The individual phases of the integrated flows differ (Figures RAI-4.16-15 and RAI-4.16-16), but the total integrated flow out the break matches, as expected (Figure RAI-4.16-14).

Efforts were made to reduce/eliminate any discontinuities over the years of code development, but some can still exist and perhaps some numerical diffusion at or right before the t_{block} causes some deviation between the two cases. For these two cases, the

PCT results were expected to be similar, but the depression in the DC level prior to SSO may have pushed more mass into the core for the 70 °F case, which made the difference between a subsequent heatup occurring and not.

Table RAI-4.16-2: Pre-SSO ECCS Temperature Sensitivity Cases

Case	ECCS Temperature before SSO (°F)	ECCS Temperature after SSO (°F)	Decay Heat Multiplier	PCT (°F)
04	110	212	1.1	542
15	70	212	1.1	no clad heatup

Figure RAI-4.16-9: Average Downcomer Collapsed Liquid Level

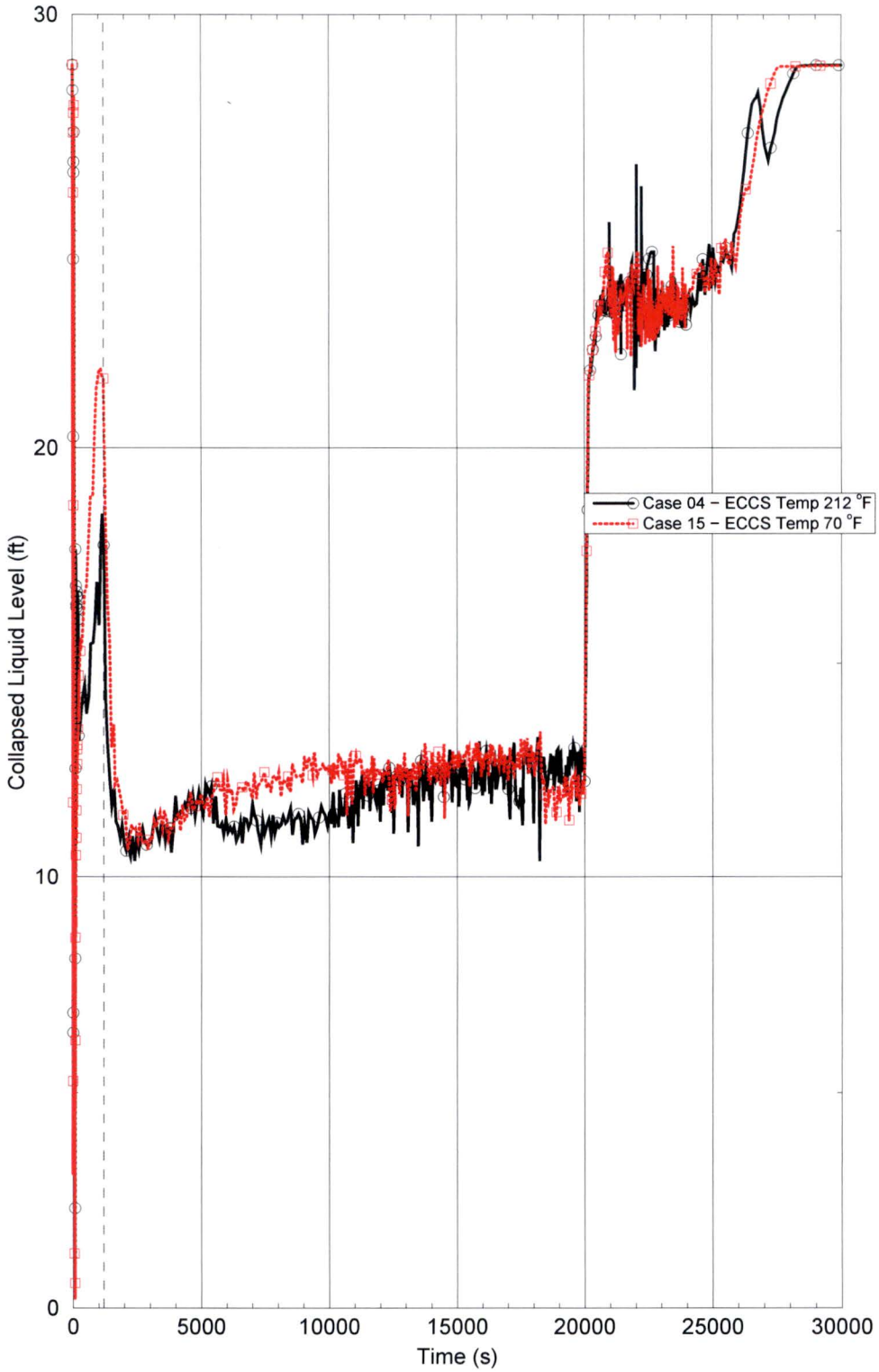

Figure RAI-4.16-10: Downcomer Total Mass

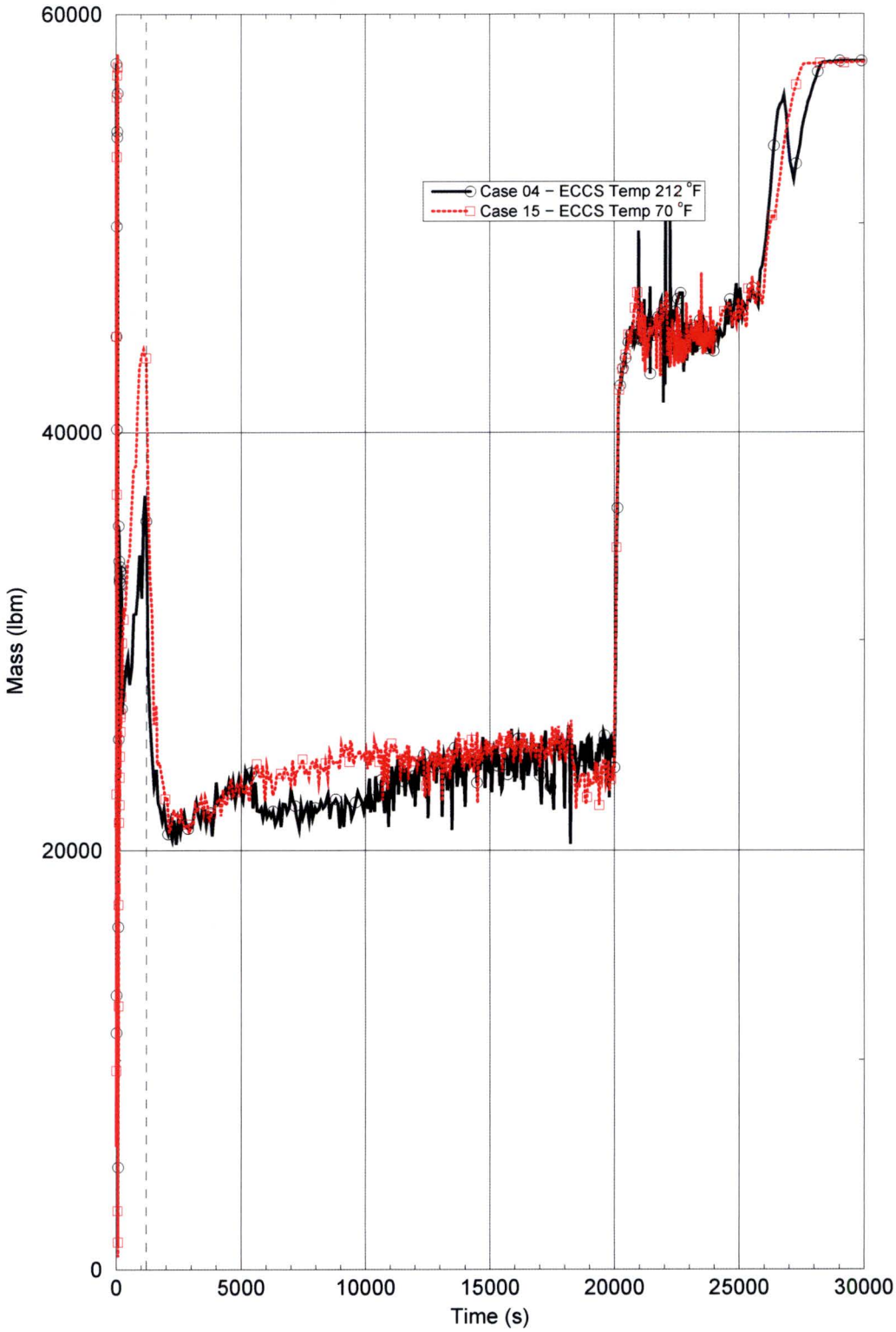

Figure RAI-4.16-11: Average Core Collapsed Liquid Level

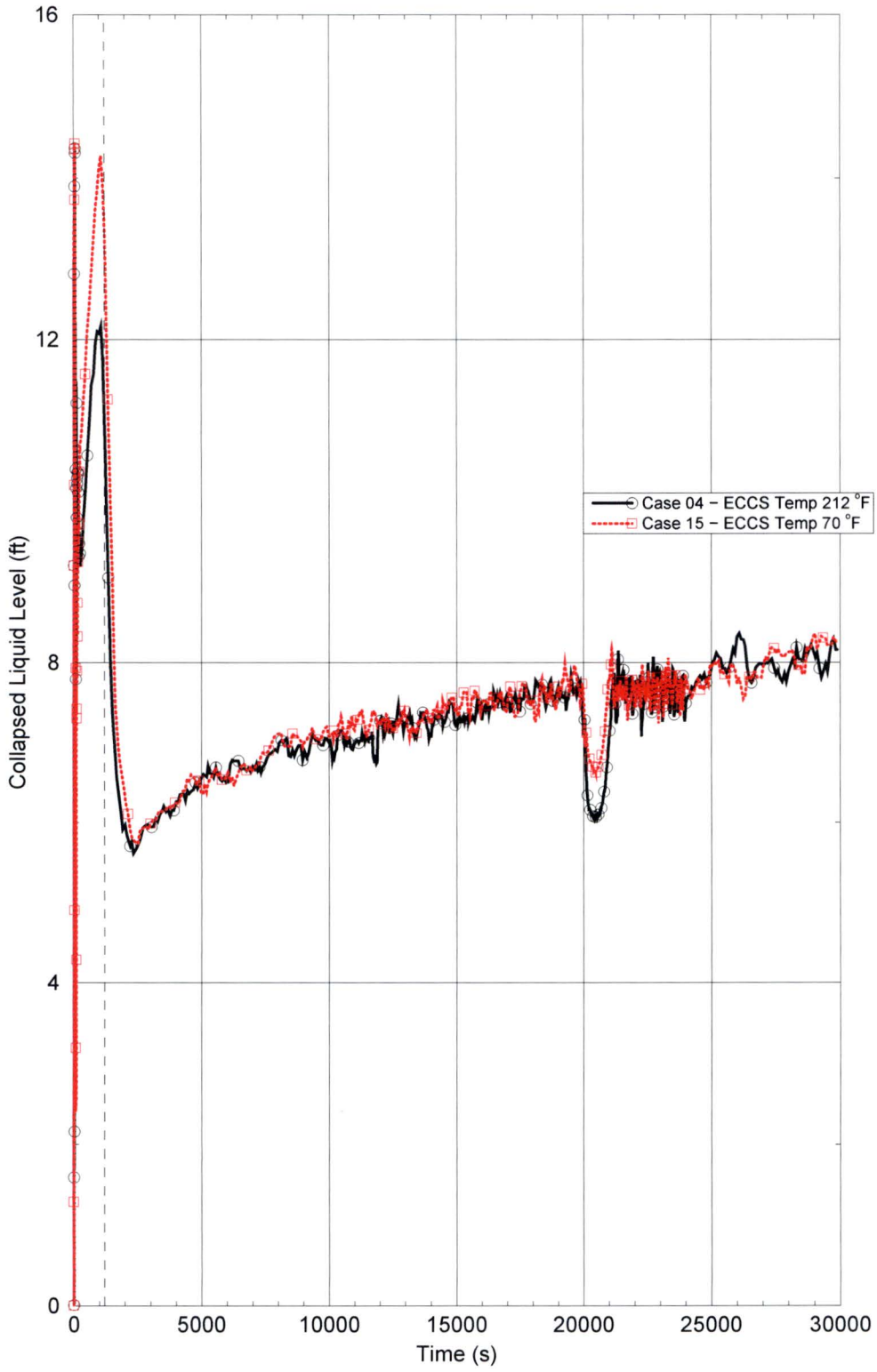

Figure RAI-4.16-12: Reactor Vessel Total Mass

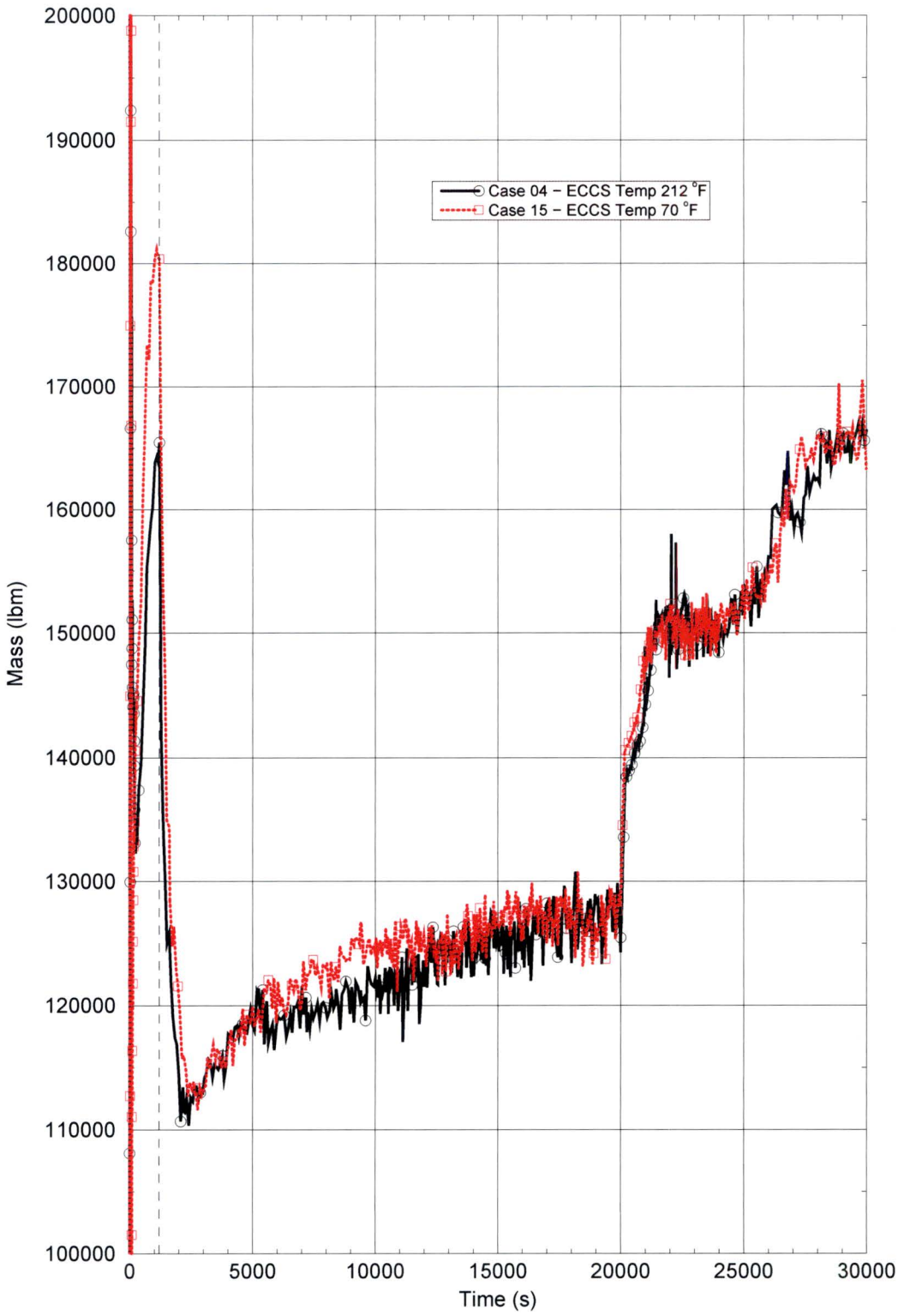

Figure RAI-4.16-13: Boiloff Rate

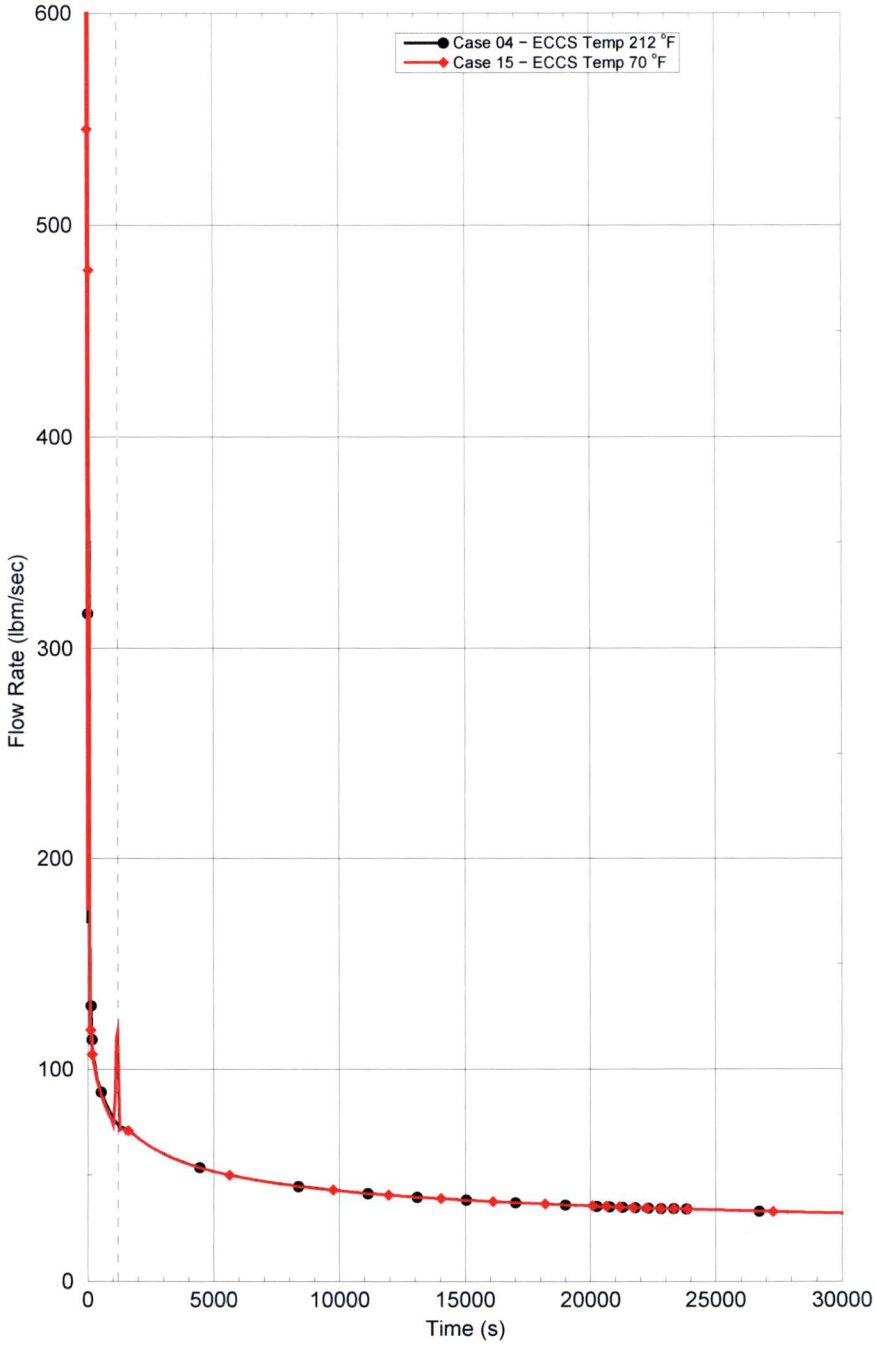

Figure RAI-4.16-14: Integrated Pumped ECCS and Break Flow

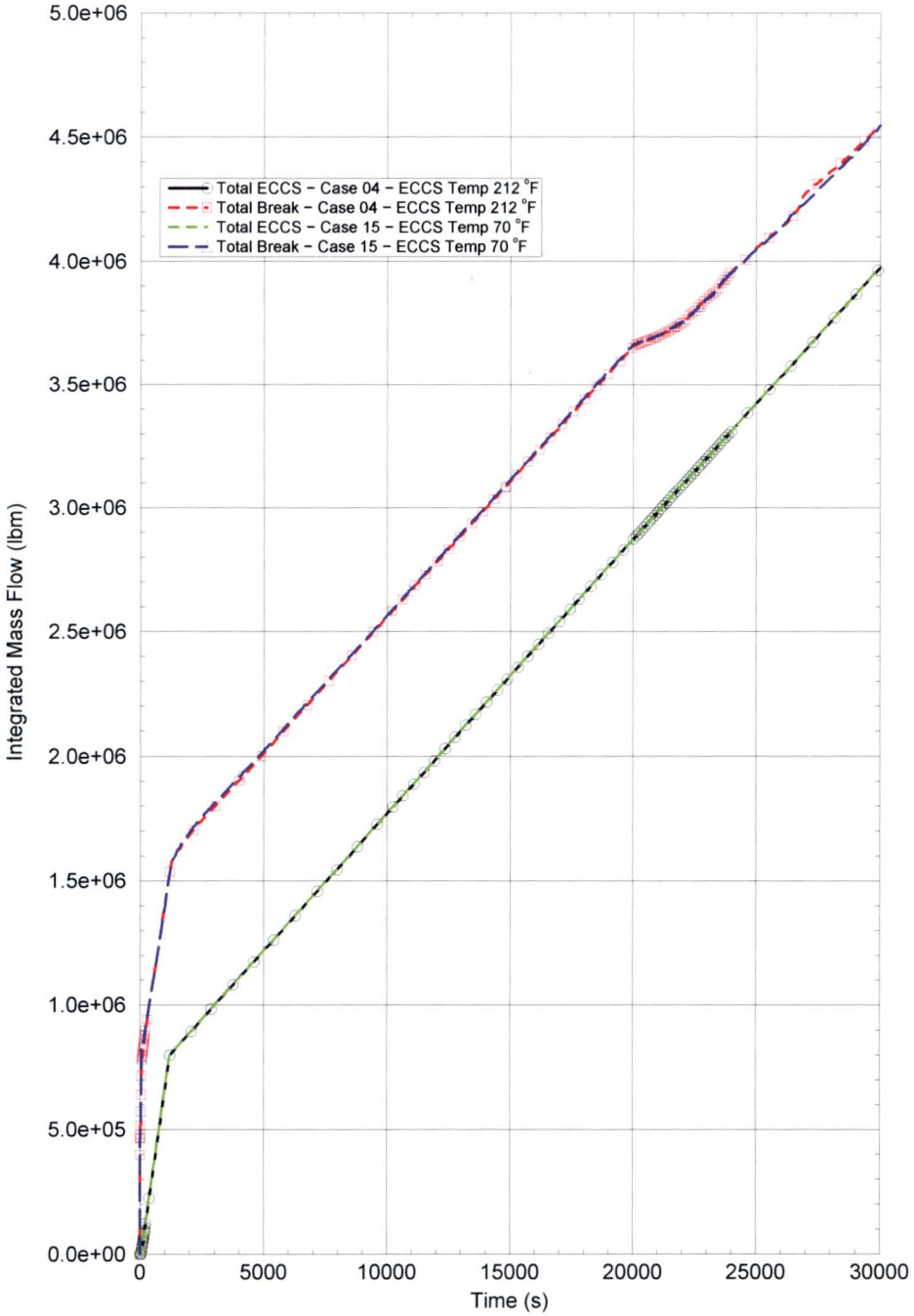

Figure RAI-4.16-15: Integrated Break Vapor Flow

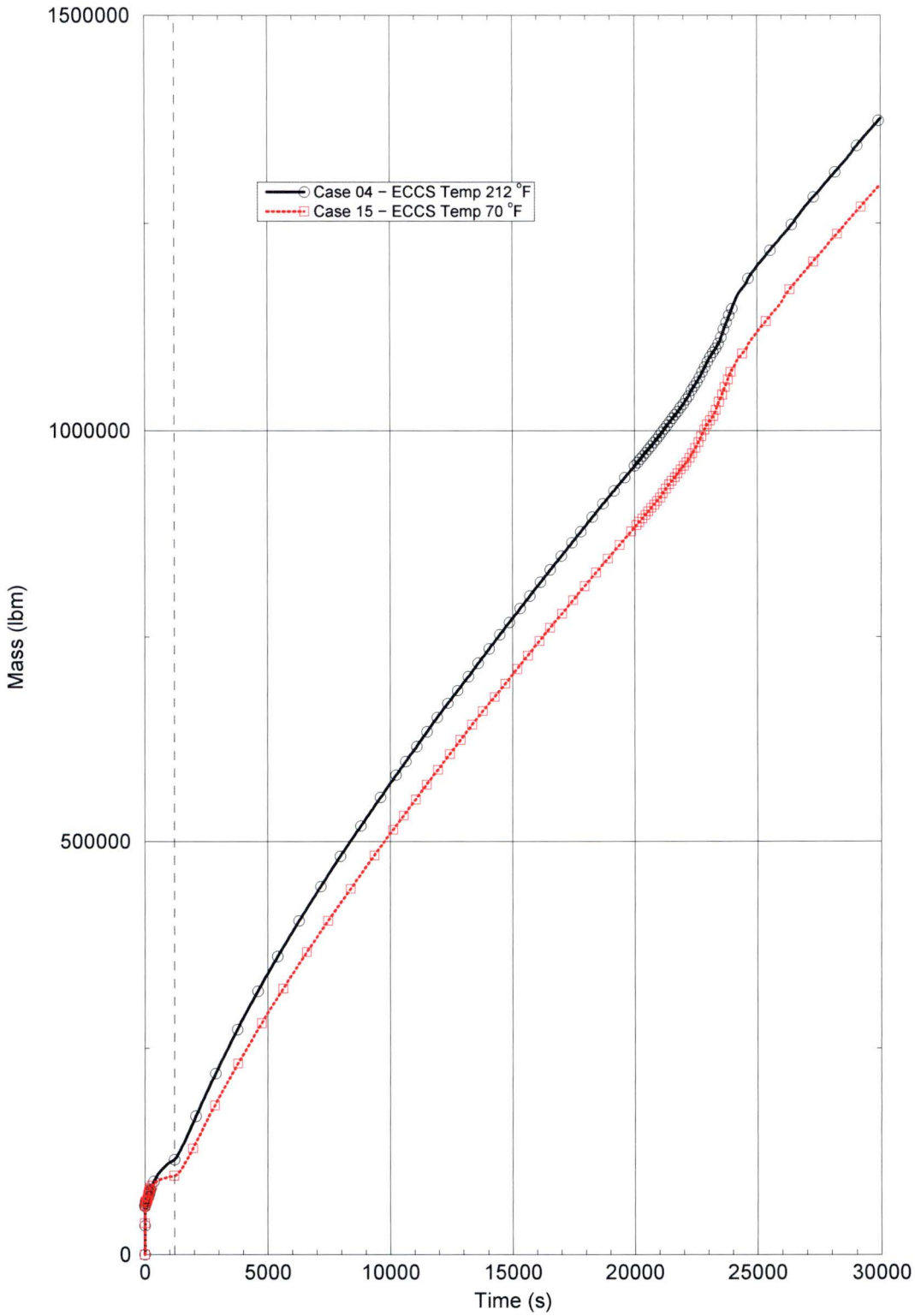

Figure RAI-4.16-16: Integrated Break Liquid Flow

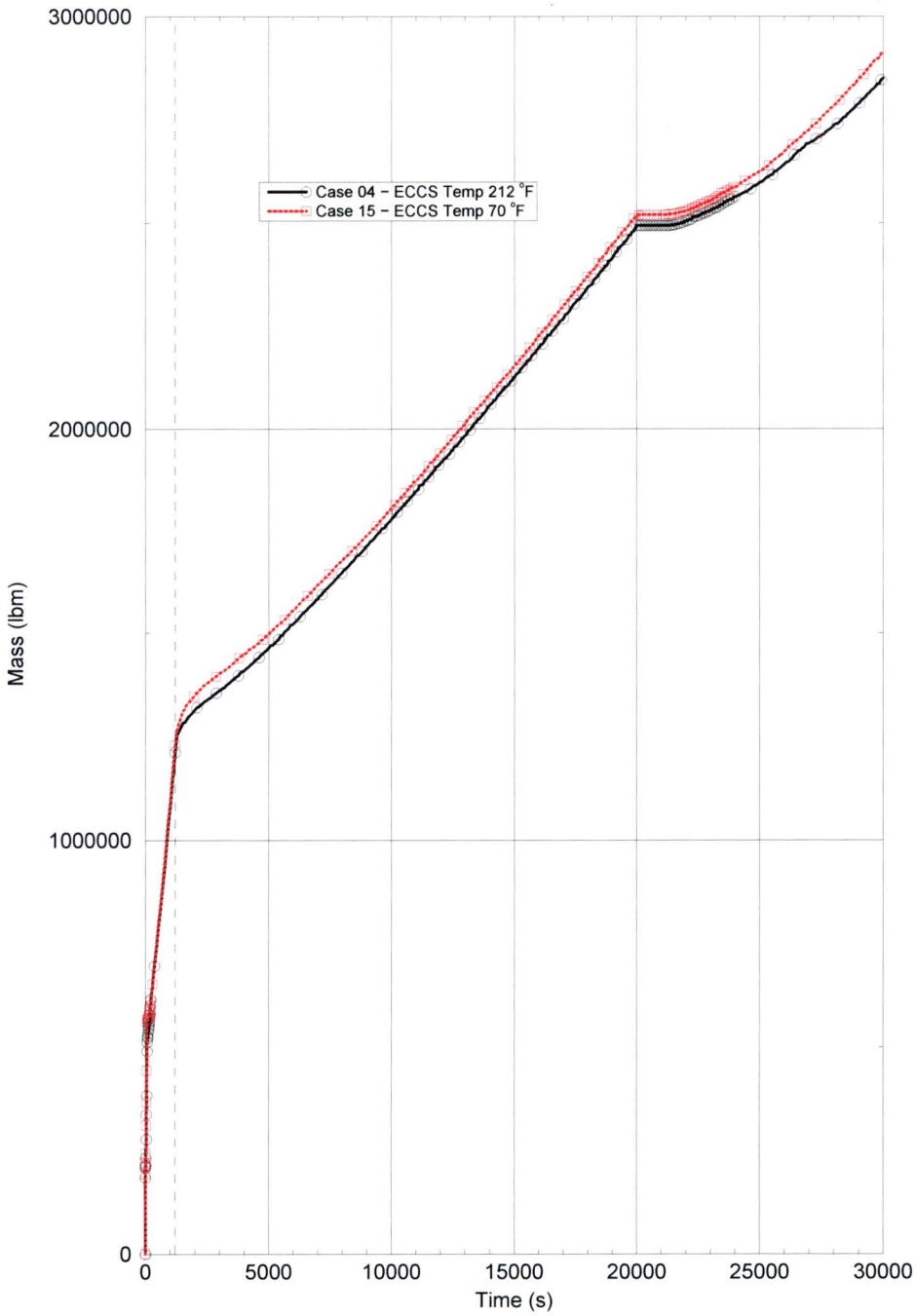

2.17 RAI 4.17

2.17.1 Statement of RAI 4.17

Section 8.2.2 presents T-H results for Case 1B. Case 1B is presented because it represents the limiting time of complete core blockage, t_{block}, for the Westinghouse upflow plant category. In discussing the quantity identified as "reactor vessel fluid mass," shown in Figure 8-17, it is stated that "when complete core inlet blockage is applied, the RV inventory increases quickly, which can be credited to filling of the downcomer". The explanation for the inventory increase following the simulated core inlet blockage appears implausible if the result in Figure 8-17 represents the fluid mass within the entire RV volume. Since a stable ECCS liquid injection rate is expected during the period discussed in the above citation, the increase in accumulated fluid mass in the RV should be attributed to a reduction in the mass rate at which fluid exits the RV though the break, as suggested by the "break exit quality" shown in Figure 8-24, rather than by accumulation of mass in any sub-region within the entire RV control volume. The same observation applies to a similar statement in Section 8.2.3 that "when partial core inlet blockage is applied, the RV inventory increases quickly, which can be credited to filling of the downcomer". This explanation was provided with regard to the predicted "reactor vessel fluid mass" shown in Figure 8-26 for Case 2B, which was used to determine K_{max}. For Case 2B, the corresponding "break exit quality" response appears in Figure 8-34. To understand the role of entrainment and driving processes in the results:

(a) Explain what causes the increase in the RV inventories shown in Figures 8-17 and 8-26. Provide updates to the explanations provided in the text of Sections 8.2.2 and 8.2.3, as appropriate.

(b) Define the parameter "break exit quality" shown in Figures 8-24 and 8-34. Explain whether the same definition applies to any T-H quantity labeled as "quality" throughout Vol. 4. Otherwise, provide definitions and clarifications.

(c) Provide plots showing the following sets of parameters for Cases 1B and 2B in Section 8.

  (i) Mass flow rates of liquid, steam, and total (liquid and steam) fluid discharges through each opening of the double-ended guillotine (DEG) break

  (ii) ECCS liquid mass flow rates injected into each cold leg and the total ECCS liquid mass flow rate injection into the reactor coolant system

  (iii) Liquid mass flow rates entering the RV through each cold leg nozzle and the total liquid flow for all cold leg nozzles

(iv) Mass flow rates of liquid and steam entering the RV through each intact hot leg nozzle and the total (liquid and steam) flow rate for all intact hot leg nozzles

(v) Steam flow quality defined as a ratio of the steam mass flow rate to the total (liquid and steam) mass flow rate for the RV-side opening of the DEG break

(d) Present plots that show integrals for the identified mass flow rates requested in Item c above (liquid, steam, and/or total liquid and steam, as relevant).

2.17.2 Response to RAI 4.17

2.17.2.1 Part a

This RAI pertains to the Westinghouse Electric Company (WEC) plant categories and therefore requires no response for the Combustion Engineering (CE) plant category.

2.17.2.2 Part b

The break exit quality is defined as the mass quality, which is the ratio of the steam mass flow rate to the total mass flow rate. This usage, which is consistent with the standard definition of the term mass quality, is consistent throughout Volume 4.

2.17.2.3 Part c

The requested information for the CE evaluation is provided in the following figures. These results are from the updated analyses described in Request for Additional Information (RAI) 4.1b. The break mass flow rates are provided in Figure RAI-4.17-1. The Emergency Core Cooling System (ECCS) liquid mass flow rates into the cold legs and the total ECCS liquid mass flow rates into the Reactor Coolant System (RCS) are provided in Figure RAI-4.17-2. The liquid mass flow rates into Reactor Vessel (RV) from the cold legs are provided in Figure RAI-4.17-3. The mass flow rates into RV from the intact Hot Leg (HL) are provided in Figure RAI-4.17-4. The steam flow quality for the RV-side of the break is provided in Figure RAI-4.17-5.

Figure RAI-4.17-1: Break Mass Flow Rates for CE Analyses

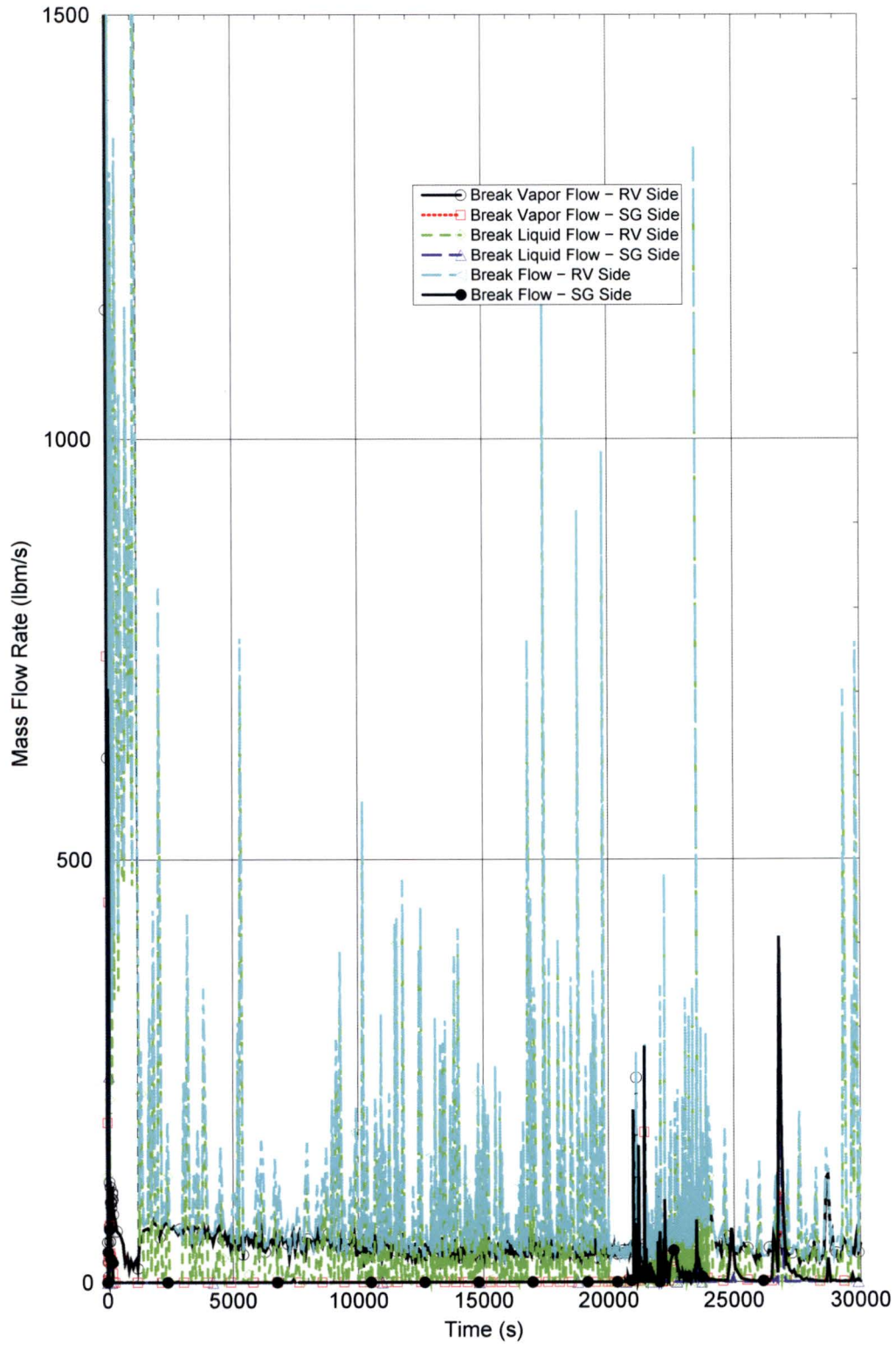

Figure RAI-4.17-2: ECCS Liquid Mass Flow Rates for CE Analyses

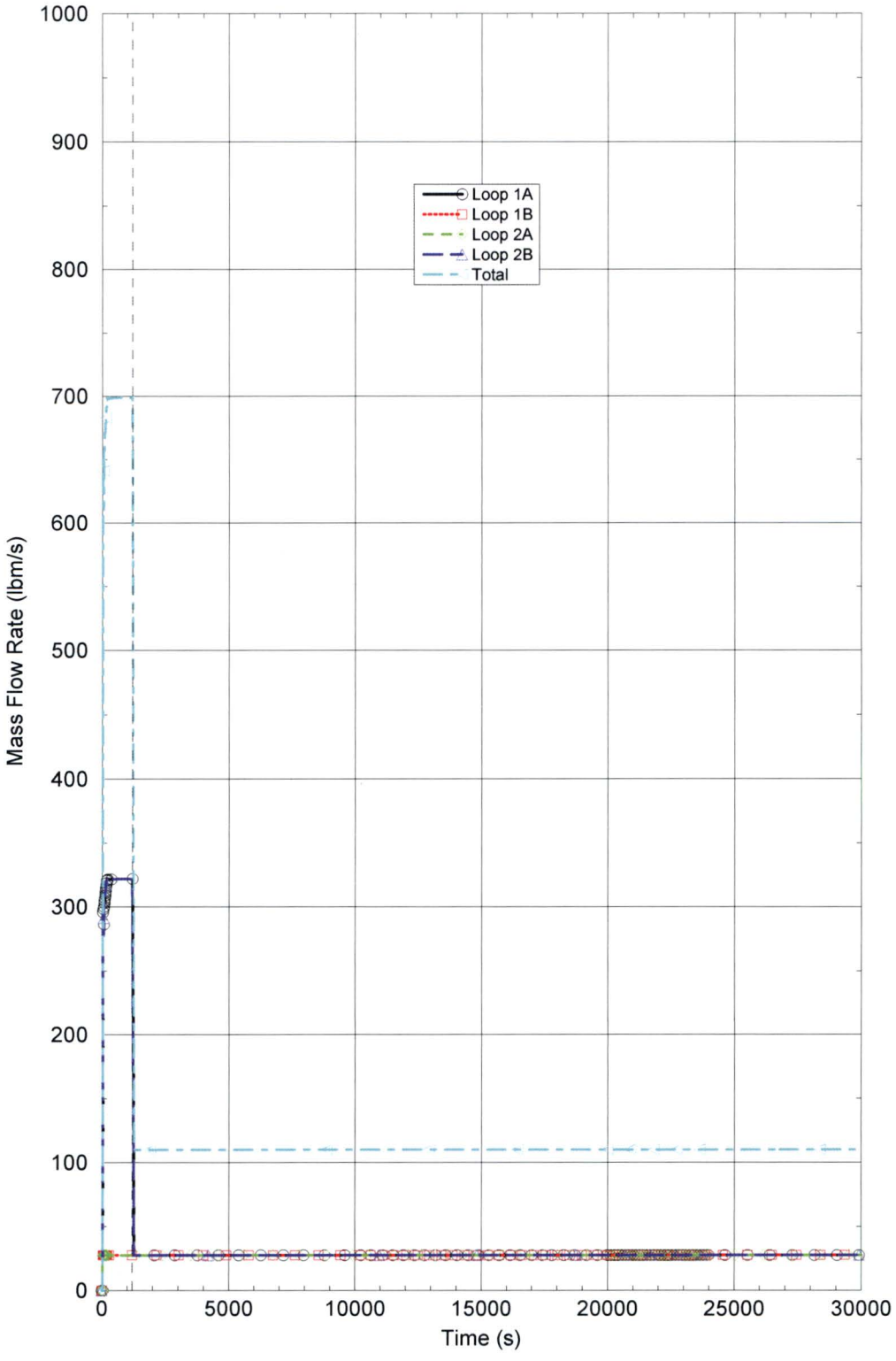

Figure RAI-4.17-3: Liquid Mass Flow Rates Entering RV through CL Nozzles for CE Analyses

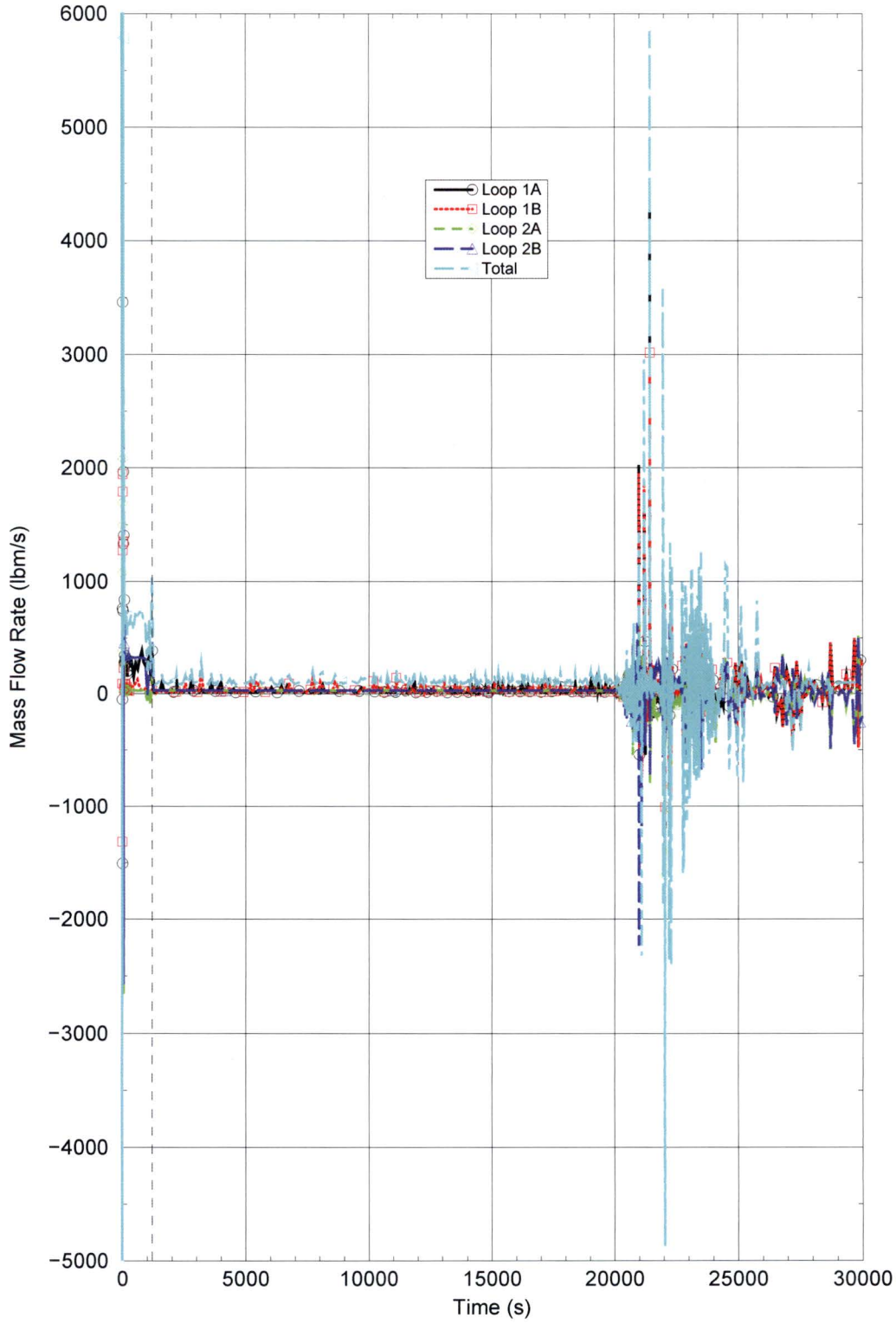

Figure RAI-4.17-4: Mass Flow Rates Entering RV through Intact HL Nozzles for CE Analyses

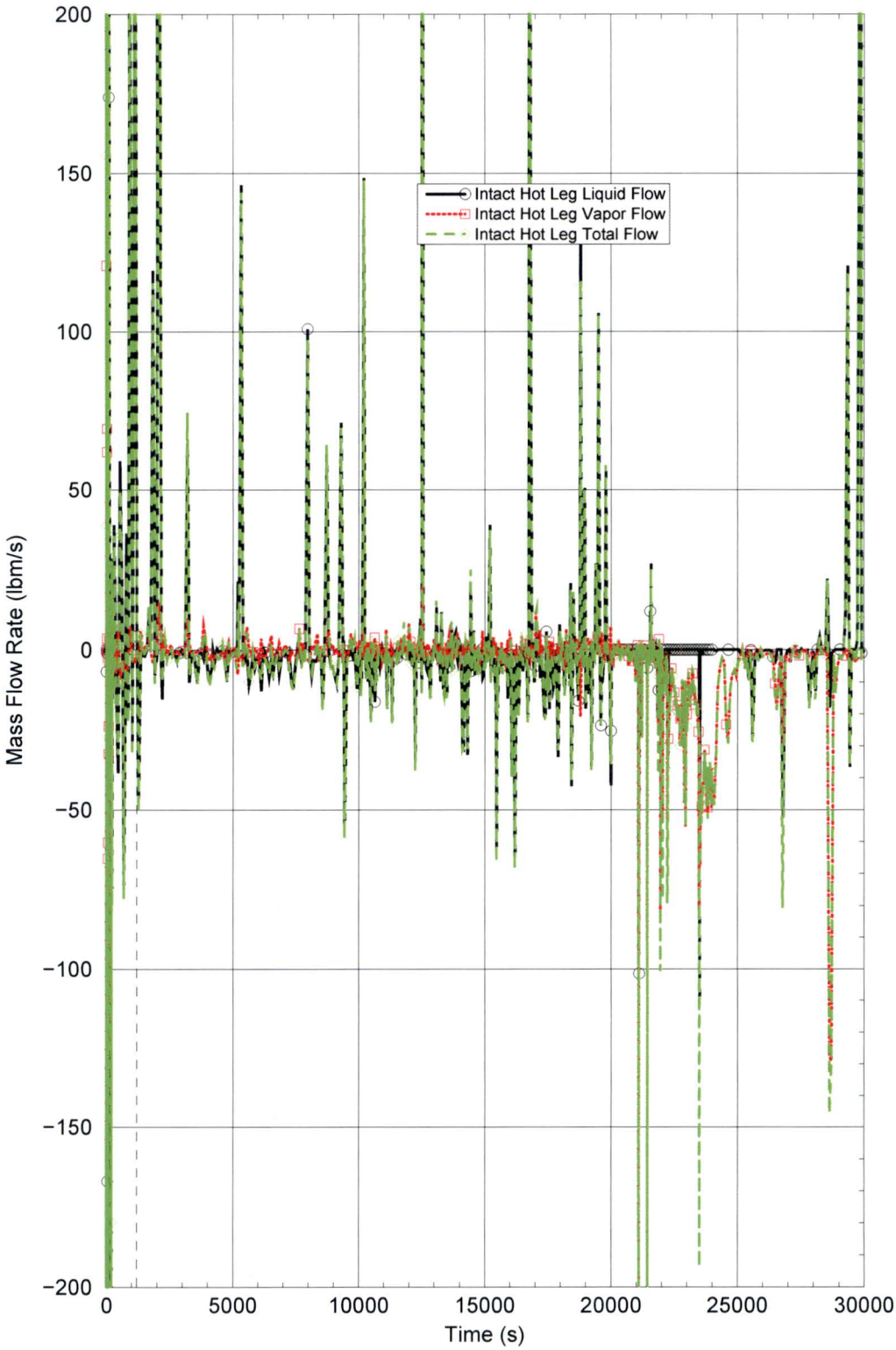

Figure RAI-4.17-5: Steam Flow Quality (Running Average) - RV Side of Flow to the Break

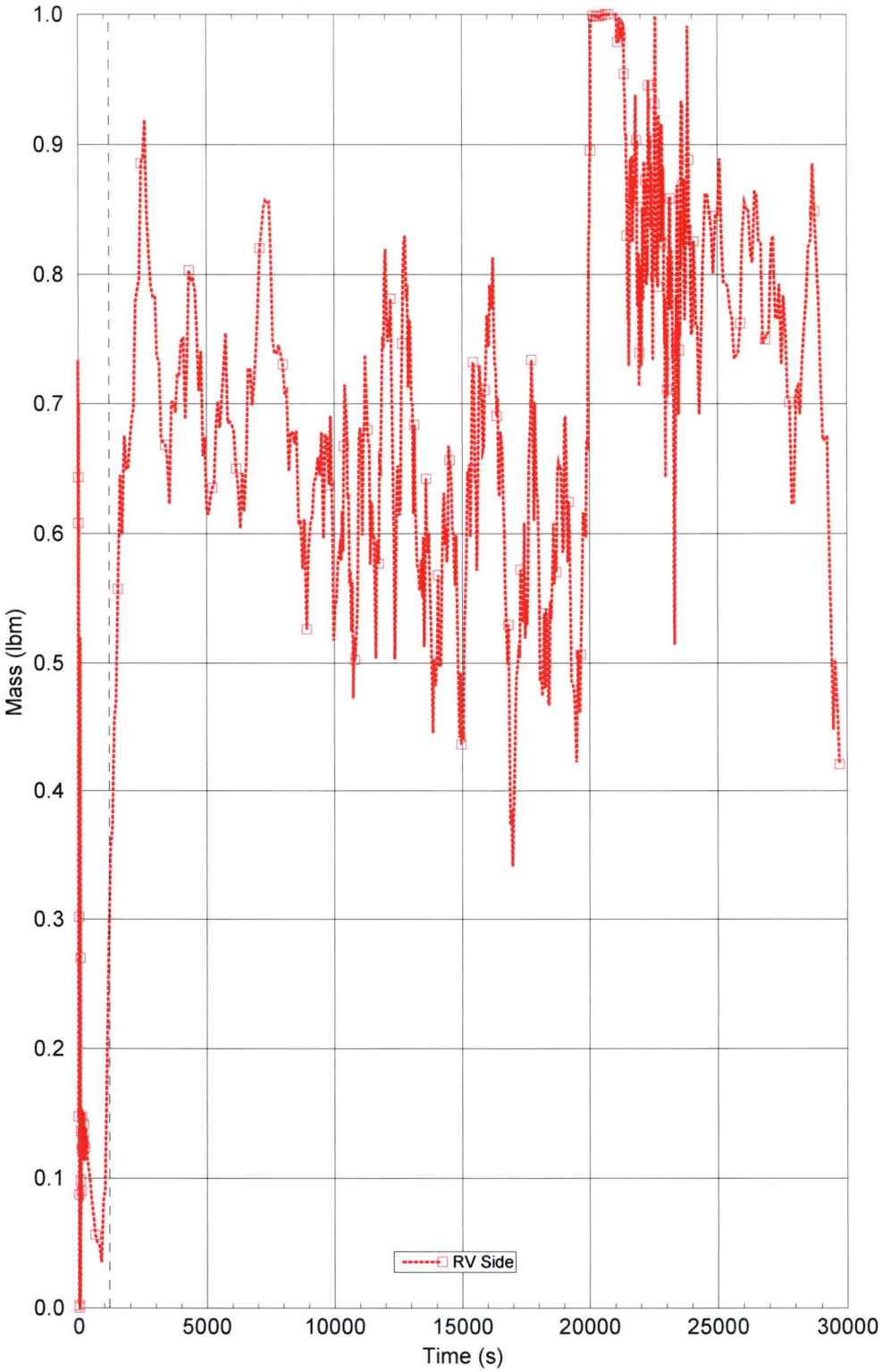

2.17.2.4 Part d

The requested information for the CE evaluation is provided in the following figures. These results are from the updated analyses described in RAI 4.1b. The integrated break mass flow rates are provided in Figure RAI-4.17-6. The integrated ECCS liquid mass flow rates into the cold legs are provided in Figure RAI-4.17-7. The integrated liquid mass flow rates into RV from the cold legs are provided in Figure RAI-4.17-8. The integrated mass flow rates into RV from the intact hot leg are provided in Figure RAI-4.17-9.

Figure RAI-4.17-6: Integrated Break Mass Flow Rates for CE Analyses

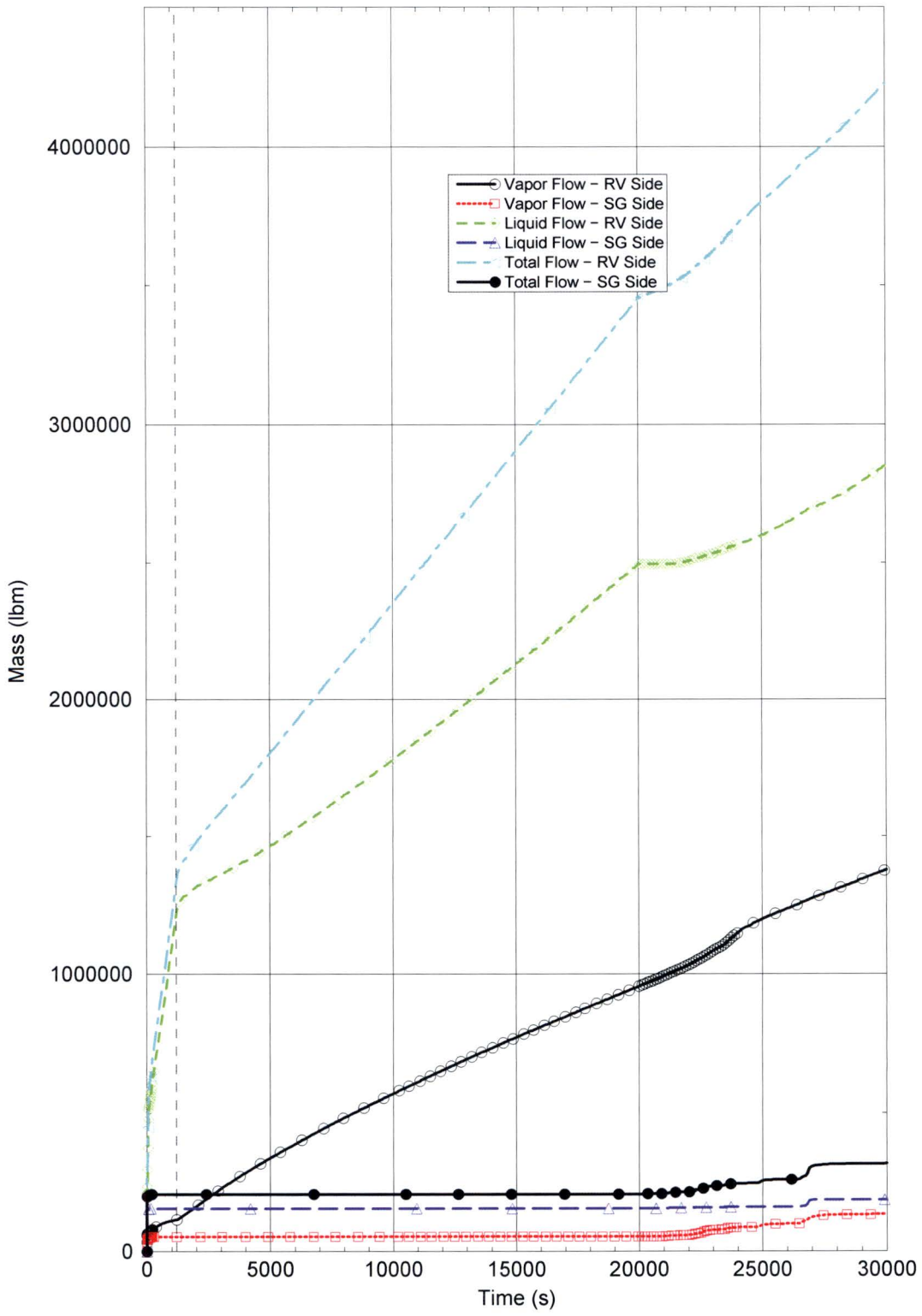

Figure RAI-4.17-7: Integrated ECCS Liquid Mass Flow Rates for CE Analyses

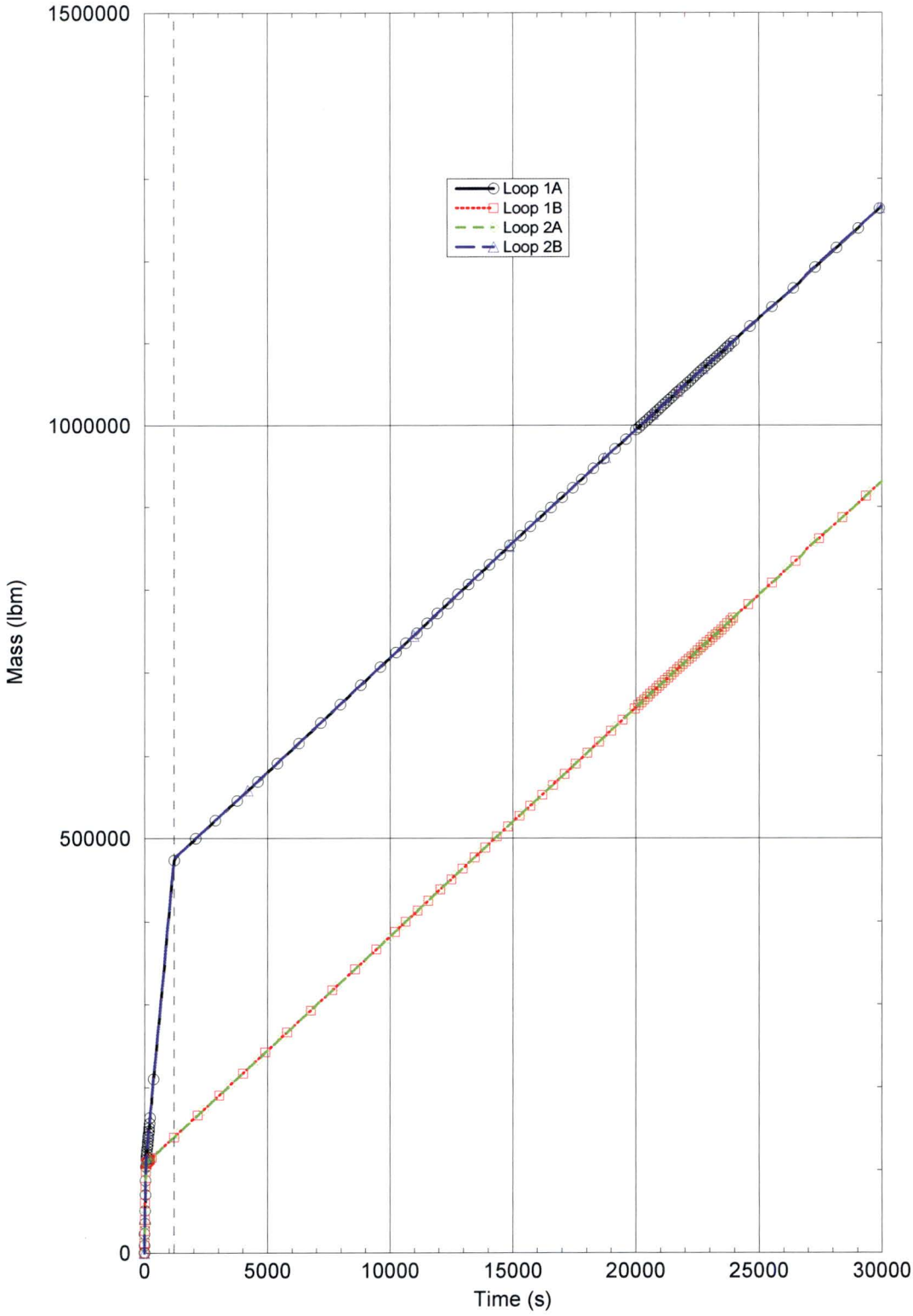

Figure RAI-4.17-8: Integrated Liquid Mass Flow Rates Entering RV through CL Nozzles for CE Analyses

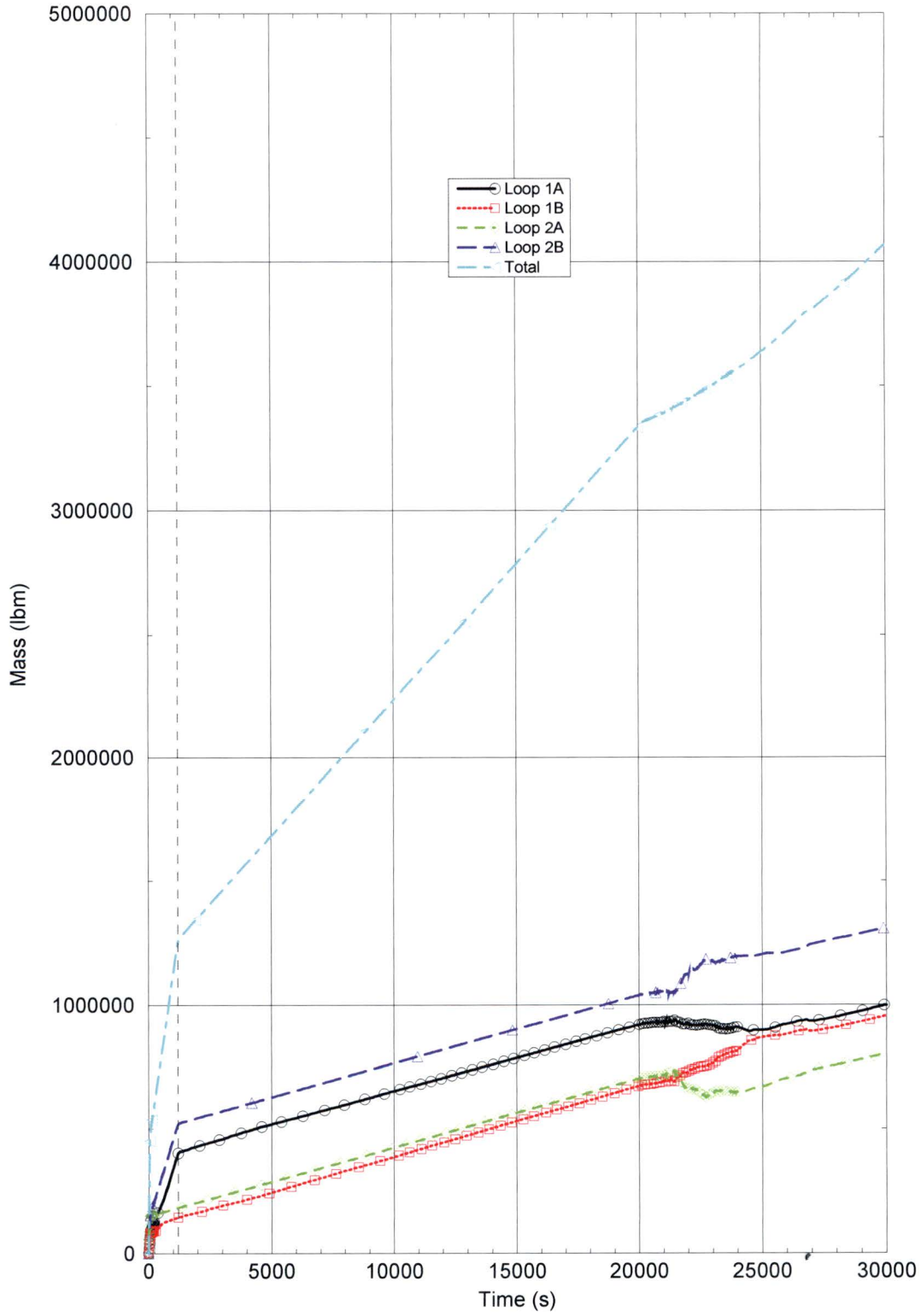

Figure RAI-4.17-9: Integrated Mass Flow Rates Entering RV through Intact HL for CE Analyses

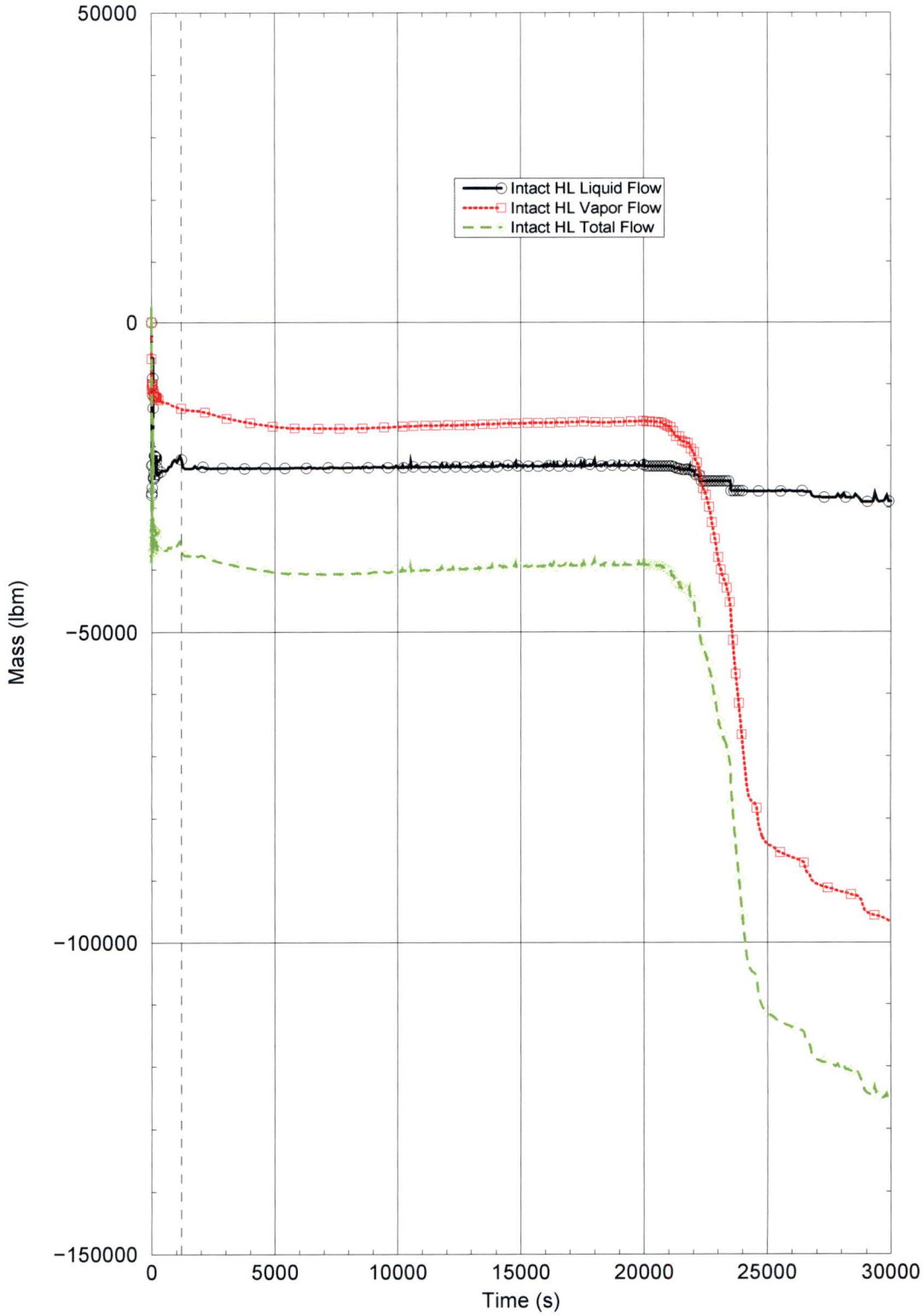

2.18 RAI 4.18

2.18.1 Statement of RAI 4.18

The HLB T-H cases analyzed for the Westinghouse upflow plant category presented in Section 8 include Case 5, which simulated debris blockage for determination of K_{split} and m_{split} at an ECCS recirculation flow rate of 8 gallons per minute per fuel assembly (gpm/FA). As seen in Figure 8-44, following the SSO time, the downcomer and BB collapsed liquid levels decrease relatively rapidly and drop by about 8 ft and 3 ft, respectively, and reach their minimum levels at about 2,100 seconds before starting a gradual recovery. In contrast to all remaining cases presented in Section 8 (Cases 0A, 1B, 2B, 1, and 3), the result for Case 5 shows the predicted downcomer collapsed liquid level decreasing below the BB collapsed liquid level over a period of about 1,800 seconds. Explain the physical processes leading to this prediction based on the code results for this case. Specifically, explain whether liquid entrainment is among the processes. If necessary, implement modeling changes that correct any unacceptable code behavior and present updated results for Case 5.

2.18.2 Response to RAI 4.18

This RAI pertains to the Westinghouse Electric Company (WEC) plant categories and therefore requires no response for the Combustion Engineering (CE) plant category.

2.19 RAI 4.19

2.19.1 Statement of RAI 4.19

The HLB T-H results for the Westinghouse upflow plant category presented in Section 8 include calculations for a single case without debris simulation (Case 0A) and five additional cases that simulate debris for determining t_{block} (Case 1B), K_{max} (Case 2B), and K_{split} and m_{split} (Cases 1, 3, and 5). Regardless of whether debris was simulated or not, the results exhibit a common response as reflected in the plots of collapsed liquid levels for the downcomer, BB, hot assembly, and some plots of predicted RV fluid masses. The response takes place around and following the SSO time. It is characterized by an initial increase in the magnitude of these parameters, which reach maximum levels followed by a relatively rapid decrease. From the predicted collapsed liquid levels, this response is seen taking place around 100 seconds following SSO at 1,300 seconds for Case 0A (Figure 8-7), and within about one minute of the SSO time for Cases 1B (Figure 8-18), 2B (Figure 8-27; it is not easily seen in Figure 8-28 due to core blockage simulated coincidentally with SSO), 1 (Figure 8-36, over a shorter time frame than in the other noted figures due to the high ECCS flow), 3 (Figure 8-40), and 5 (Figure 8-44). A similar response also occurs in Figure 8-17, which illustrates the effect on a predicted RV fluid mass (note that the response is masked in Figure 8-26 due to core blockage simulated coincidentally with SSO).

A similar observation applies to the results presented in Section 9 for the Westinghouse downflow plant category. Figures 9-6, 9-7, 9-17, 9-18, 9-29, 9-33, and 9-37 illustrate the response on predicted collapsed levels and Figures 9-16 and 9-22 show predicted RV fluid masses.

(a) Explain the physical processes leading to this behavior based on the code results for the analyzed cases. This response reflects the system manometric balances and related contributing pressure losses experienced across the core inlet and other simulated flow passages and regions. Describe the effects of each process and explain whether the observed impact from such effects was considered acceptable. Specifically, explain whether liquid entrainment is among such processes. If liquid entrainment has an effect, analyze the degree to which it had an effect on key results from the simulated cases and justify the acceptability of the results.

(b) The maximum resistance, K_{max}, results for the Westinghouse upflow and downflow plant categories are obtained from analyses in which the core blockage is applied simultaneously with SSO. The NRC staff needs assurance that K_{max} results are not affected by processes associated with the above described system response occurring around the SSO time. The NRC staff recommends performing a

re-analyses for the cases presented in Sections 8 (Case 2B) and 9 (Case 2B) used to determine K_{max} with the only change being that the core inlet blockage is applied 200 seconds following the SSO time instead of coincidentally with the SSO time.

2.19.2 Response to RAI 4.19

2.19.2.1 Part a

This RAI pertains to the Westinghouse Electric Company (WEC) plant categories and therefore requires no response for the Combustion Engineering (CE) plant category.

2.19.2.2 Part b

While the RAI specifically pertains to the WEC plant category, an explanation of the process followed in the CE plant category analyses is presented.

In the CE plant analyses, Sump Switch Over (SSO) is modeled to occur at 1200 seconds as described in the response to RAI 4.5a (see Section 2.5.2). This time is selected to be consistent with a minimum switchover time as identified in WCAP-17788, Volume 4, Section 4.2. The K_{max} ramp applied to the CE case is shown in Volume 4, Figure 10-2 and described in detail in response to RAI 4.26. Resistance to debris at the core inlet is not simulated until 1800 seconds, which is 600 seconds after the modeled SSO time. Therefore, the K_{max} results are not affected by processes associated with the changes in Emergency Core Cooling System (ECCS) flow rate and temperature applied at the time of SSO.

2.20 RAI 4.20

2.20.1 Statement of RAI 4.20

The T-H analyses for the large HLB LOCA scenario are used to determine four key parameters, t_{block}, K_{max}, K_{split}, and m_{split}, which are used as inputs to the overall HLB methodology described in Volume 1.

Implementing the high-level process outlined in Figure 4-2, "Overview of Hot Leg Break Methodology," Section 6.5 provides an algorithm that uses K_{split} and m_{split} for calculating in vessel fiber loads and verifying that they comply with the applicable limits for core inlet, in core, and total RV fiber. In particular, the core inlet fiber load is used to determine the core inlet resistance, based on the subscale head loss testing in Vol. 6, so that it can be compared against the applicable K_{max} limit as the accident progresses. This important check is performed in Step 10 of the algorithm. As stated in Step 10, "if the core inlet K factor is greater than K_{max} before the time of t_{block}, then the calculation does not meet the acceptance criteria defined by the TH analyses". The core inlet flow and fiber load after SSO are calculated using both K_{split} and m_{split}. When the core inlet resistance is less than or equal to K_{split}, the flow into the RV passes only through the core inlet where it deposits fiber. When the core inlet resistance is greater than K_{split}, the flow into the RV is split between the core inlet and the alternate flow path (AFP) based on m_{split}. The current core inlet resistance is compared against K_{split} at Step 9 of the algorithm.

The K_{split} and m_{split} critical inputs are determined in Vol. 4 from T-H analyses, which were performed using minimum BB flow resistances "for all plant categories with an upflow BB configuration". Section 4.2 states that "selecting the minimum resistance will minimize the resistance due to debris (and hence the amount of debris at the core inlet) that will begin to divert flow to the AFP". It explains that "minimizing the debris at the core inlet required to divert flow to the AFP will maximize the amount of debris predicted to bypass the core inlet and transport to the core region through the AFP". Section 4.2 further explains that a minimum UHSN resistance "will be applied for cases that are used to determine K_{split} and m_{split}" for the Westinghouse downflow plant category.

Explain if the use of maximum AFP flow resistances result in a conservative mass of debris at the core inlet for all cases. Evidently, using thus determined K_{split} and m_{split} parameters will result in the earliest time of flow diversion through the AFPs and the maximum fraction of ensuing ECCS flow through the AFPs, which will maximize the predicted amount of debris transported to the core region and minimize the amount of debris accumulated at the core inlet. Accordingly, the calculated core inlet debris amount can allow the calculation process to continue, unless stopped due to exceeding the in-core or total RV fiber limits, both of which can be significantly higher than the core inlet fiber limit, and eventually produce an acceptable overall analysis outcome without

detecting possible violation of the applicable core inlet debris limit. Therefore, the generic HLB methodology, using the K_{split} and m_{split} critical inputs established in Vol. 4, could result in non-conservative results for the Westinghouse upflow, Westinghouse downflow, and CE plant categories.

It is possible that an approach based on maximized, as opposed to minimized, AFP resistances for the determination of K_{split} and m_{split} can be considered for implementation in the HLB methodology for assuring satisfaction of the core inlet fiber limit. Provide additional information to justify how the HLB methodology described in WCAP-17788 can be applied to assure satisfaction of the established core inlet fiber based on the t_{block}, K_{max}, K_{split}, and m_{split} results established in Vol. 4. The justification could include sensitivity studies where AFP resistance is minimized for each plant category and plant-specific guidance on this matter.

2.20.2 Response to RAI 4.20

The Thermal Hydraulic (TH) analyses for the large Hot Leg (HL) Break Loss of Coolant Accident (LOCA) scenario are used to determine four key parameters, t_{block}, K_{max}, K_{split}, and m_{split}, which are used as inputs to the overall HL Break methodology described in WCAP-17788-P, Volume 1. These parameters are dependent on a number of input parameters, including the Barrel/Baffle (BB) flow resistance. The response to RAI 4.3 indicates that the BB flow resistance for the Combustion Engineering (CE) fleet varies widely. To that end, a range of resistances was considered for the analyses for the CE plant category.

As described in WCAP-17788-P, Volume 4, Section 4.2, selecting the maximum BB resistance is appropriate for determining t_{block} and K_{max}, because a higher BB resistance will require the largest driving head to force flow through the BB and into the core region. A lower resistance in the BB will allow a higher flow rate through this region sooner such that t_{block} and K_{max} would improve compared to the use of a higher BB resistance. The base analyses for the CE plant category used a bounding high resistance to calculate t_{block} and K_{max}. Therefore, no additional work is required for these analyses.

The previous analyses for K_{split}, and m_{split} were performed with a bounding low BB resistance. The original intent of this selection was to maximize the amount of debris that could be transported to the heated core region. If the Reactor Coolant System (RCS) debris limit is indeed limited by having the maximum amount of debris in the heated core, then this approach is appropriate. However, as discussed in WCAP-17788-P, Volume 1, Section 6.5.4, it is possible that the core inlet debris limit could be limiting. In that case, minimizing the amount of debris diverted through the BB region would be more conservative. Consequently, a higher BB resistance should be analyzed to calculate appropriate values for K_{split}, and m_{split}.

To confirm this assertion and to investigate the sensitivity on the baffle resistance, six new cases were analyzed for the CE plant category. These analyses used the new base case for the CE plants described in the response to RAI 4.1b. The Decay Heat (DH) multiplier was increased from 1.1 to 1.2. A max baffle resistance of [ ] ft^{-4} and a medium baffle resistance of [ ] ft^{-4} were used to calculate K_{split} and m_{split} at 827 gpm, 1654 gpm and 2481 gpm of Emergency Core Cooling System (ECCS) flow. A BB resistance of K/A^2 = [ ] ft^{-4} is the maximum resistance that bounds all CE plants (see response to RAI 4.3). A BB resistance of K/A^2 = [ ] ft^{-4} is a resistance that should bound all but the highest resistance CE plants. The 827 gpm, 1654 gpm and 2481 gpm ECCS flows considered in the new cases are consistent with the ECCS flows of the original K_{split} and m_{split} cases in Volume 4 of WCAP-17788.

Table RAI-4.20-1 shows the new case matrix.

In Volume 4 of WCAP-17788-P, m_{split} was calculated as a function of the core inlet resistance. The calculation stopped when the core inlet resistance reached $5.4x10^5$ or $3.6x10^5$. When the six new cases were analyzed, the m_{split} calculation was extended until the core inlet resistance reached $6.5x10^6$, which is the value of K_{max} as presented in Section 10.2, Volume 4 of WCAP-17788. The core inlet resistances applied for these new cases are presented graphically in Figure RAI-4.20-1. Note that this curve is broken into essentially two segments. The first segment is a fairly slow rate of increase of the core inlet resistance so that an accurate value of K_{split} could be determined. After K_{split} has been determined, the ramp rate was increased in order to reach K_{max} in a reasonable amount of time.

Table RAI-4.20-2 lists the value of K_{split} determined for each new case.

Figure RAI-4.20-2 shows the results of K_{split} as a function of ECCS flowrates per fuel assembly (using the total number of 217 fuel assemblies for the reference plant model) for various baffle resistances. The trendline shown in Figure 10-4, Volume 4 of WCAP-17788-P (K_{split} as a function of ECCS flow):

$$y = 6.416x10^6\, x^{-2.012} \qquad \text{(RAI-4.20-1)}$$

is also plotted in Figure RAI-4.20-2. It can be seen that the scatter data from the new cases follow this trendline fairly closely. K_{split} shows little dependence on Alternate Flow Path (AFP) resistances. The trendline remains on or slightly above the data points of the analyzed cases. A higher value of K_{split} delays the flow diversion to the AFP. This will allow more debris to be accumulated at the core inlet before flow is diverted. Consequently, there will be a greater chance that K_{max} is reached before t_{block}. Therefore, the curve fit of K_{split} presented for CE plants in Section 10 of Volume 4 of WCAP-17788-P remains valid and conservative for continued use in the HL Break methodology described in WCAP-17788-P, Volume 1. Extrapolation of this data to higher flow rates is discussed in the response to RAI 4.21.

As described in responses to RAI 4.30c, m_{split} is calculated by

$$m_{split} = \frac{m_{BB} + m_{UHSN}}{m_{DC}} \quad \text{(RAI-4.20-2)}$$

where,

m_{BB} = The mass flow rate through the BB channel

m_{UHSN} = The mass flow rate through the Upper Head Spray Nozzles (UHSNs)

m_{DC} = The mass flow rate in the downcomer

For the CE plants, $m_{UHSN} = 0$.

Using this formulation, the fraction of ECCS recirculation flow through AFP (m_{split}) is plotted as a function of core inlet resistances minus K_{split} ($K - K_{split}$) in Figure RAI-4.20-3 and Figure RAI-4.20-4 for the maximum baffle resistance K/A^2=[ ] ft^{-4} and the medium baffle resistance K/A^2=[ ] ft^{-4}, respectively. The original bounding curve (based on the minimum baffle resistance of K/A^2=[ ] ft^{-4}) in Figure 10-5, Volume 4 of WCAP-17788 is also shown in the figures as "Volume 4 bound", which represents the following function:

$$y = 0.075\,ln(x) - 0.45 \quad \text{(RAI-4.20-3)}$$

It should be noted that the "Volume 4 bound" curve was designed to bound the low BB resistance results on the high side to maximize the amount of flow and debris diverted to the heated core region. Clearly, the higher BB resistance analyzed in the new cases had the expected outcome of reducing m_{split}, which will minimize the amount of flow and debris diverted to the heated core region and maximize the amount of debris delivered to the core inlet.

New lower bound curves were therefore developed based on the six new cases. These curves are shown in Figure RAI-4.20-3 and Figure RAI-4.20-4 as "Lower bound", which represent the following functions:

$$y = 0.13\,ln(x) - 1.53 \quad \text{for BB resistance } K/A^2 = [\ ]\ ft^{-4} \quad \text{(RAI-4.20-4)}$$

$$y = 0.13\,ln(x) - 1.48 \quad \text{for BB resistance } K/A^2 = [\ ]\ ft^{-4} \quad \text{(RAI-4.20-5)}$$

Utilities should use the appropriate function based on their plant-specific BB K/A^2 value. That is, plants that have a BB resistance that is less than [ ] ft^{-4} should use the

lower bound function described by Equation RAI-4.20-5. All other plants should use the lower bound function described by Equation RAI-4.20-4.

From Figure RAI-4.20-3 and Figure RAI-4.20-4, it can also be observed that the curves of m_{split} are insensitive to the ECCS flowrates once the ECCS flow exceeds 1654 gpm; the curves for 1654 gpm and 2481 gpm are almost superimposed with each other. At lower ECCS flow, such as 827 gpm, the downcomer was never fully refilled during the transient (see Figure RAI-4.20-5 and Figure RAI-4.20-6), causing m_{split} to be lower than the cases with a fully refilled downcomer. Therefore, m_{split} curves with ECCS flowrates of 1654 gpm and higher are expected to be very similar for a given AFP resistance. Use of the lower bound curve for all ECCS flow rates provides a measure of conservatism in the overall calculation of HL debris limit. Utilities that can demonstrate ECCS flow rates above an equivalent 1654 gpm during sump recirculation can improve their debris limits by using a curve that is more representative of the higher m_{split} results. The appropriate equivalent flow rate can be determined using the method provided in the response to RAI 4.5a.

Table RAI-4.20-1: New Case Matrix

Case Name	Baffle Resistance K/A^2 (ft^{-4})	ECCS Flow (gpm)
newcase1	[ ]	827
newcase2	[ ]	1654
newcase3	[ ]	2481
newcase4	[ ]	827
newcase5	[ ]	1654
newcase6	[ ]	2481

Table RAI-4.20-2: Summary of Results for K_{split}

Baffle Resistance K/A^2 (ft^{-4})	ECCS Flow (gpm)	K_{split}
[ ]	827	$3.33x10^5$
[ ]	1654	$1.00x10^5$
[ ]	2481	$4.40x10^4$
[ ]	827	$3.60x10^5$
[ ]	1654	$1.09x10^5$
[ ]	2481	$5.07x10^4$

Figure RAI-4.20-1: Core Inlet Resistance

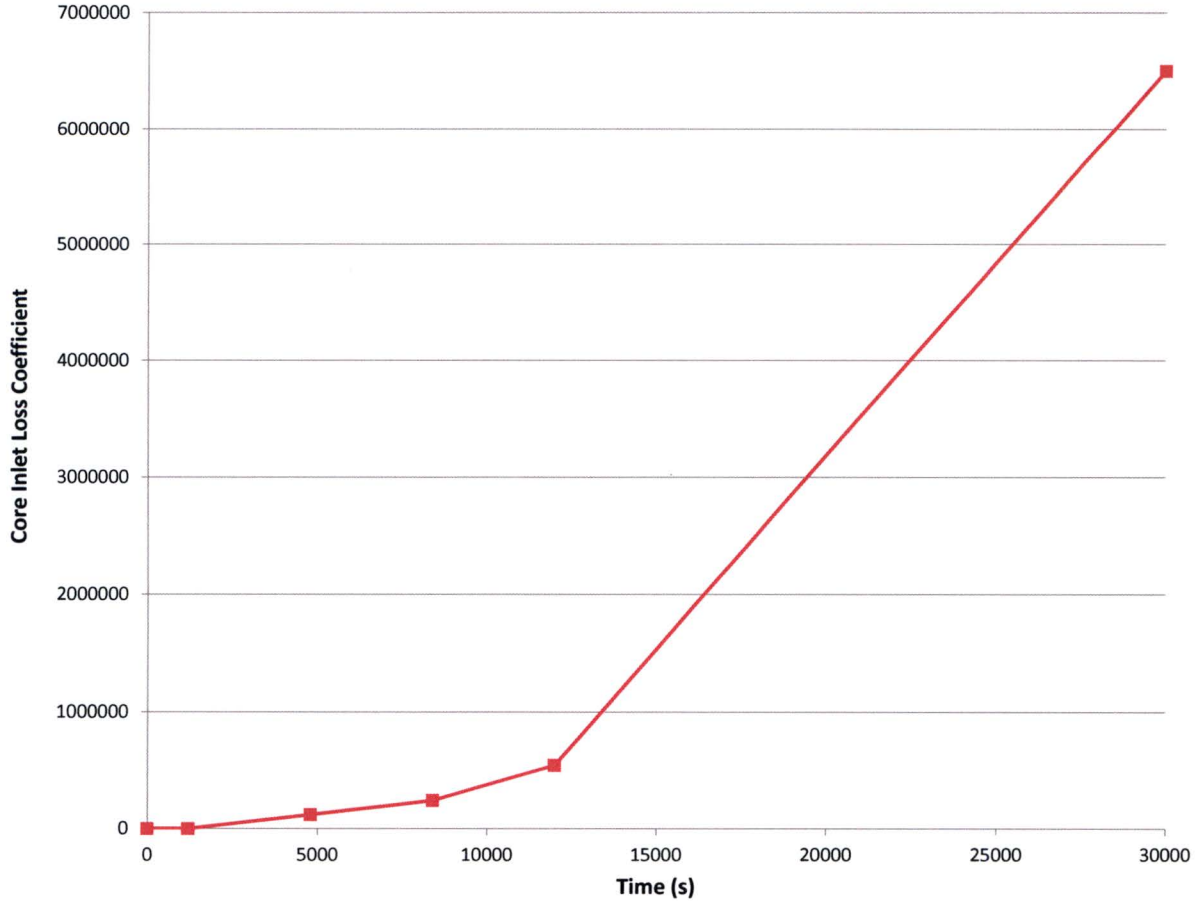

Figure RAI-4.20-2: CE Plant K_{split} as a Function of ECCS Recirculation Flow Rate

Figure RAI-4.20-3: CE Plant m_{split} for Baffle Resistance K/A^2 = [ ] ft^{-4}

Figure RAI-4.20-4: CE Plant m_{split} for Baffle Resistance K/A^2 = [ ] ft^{-4}

Figure RAI-4.20-5: Downcomer Liquid Level for Baffle Resistance K/A^2 = [ ] ft^{-4}

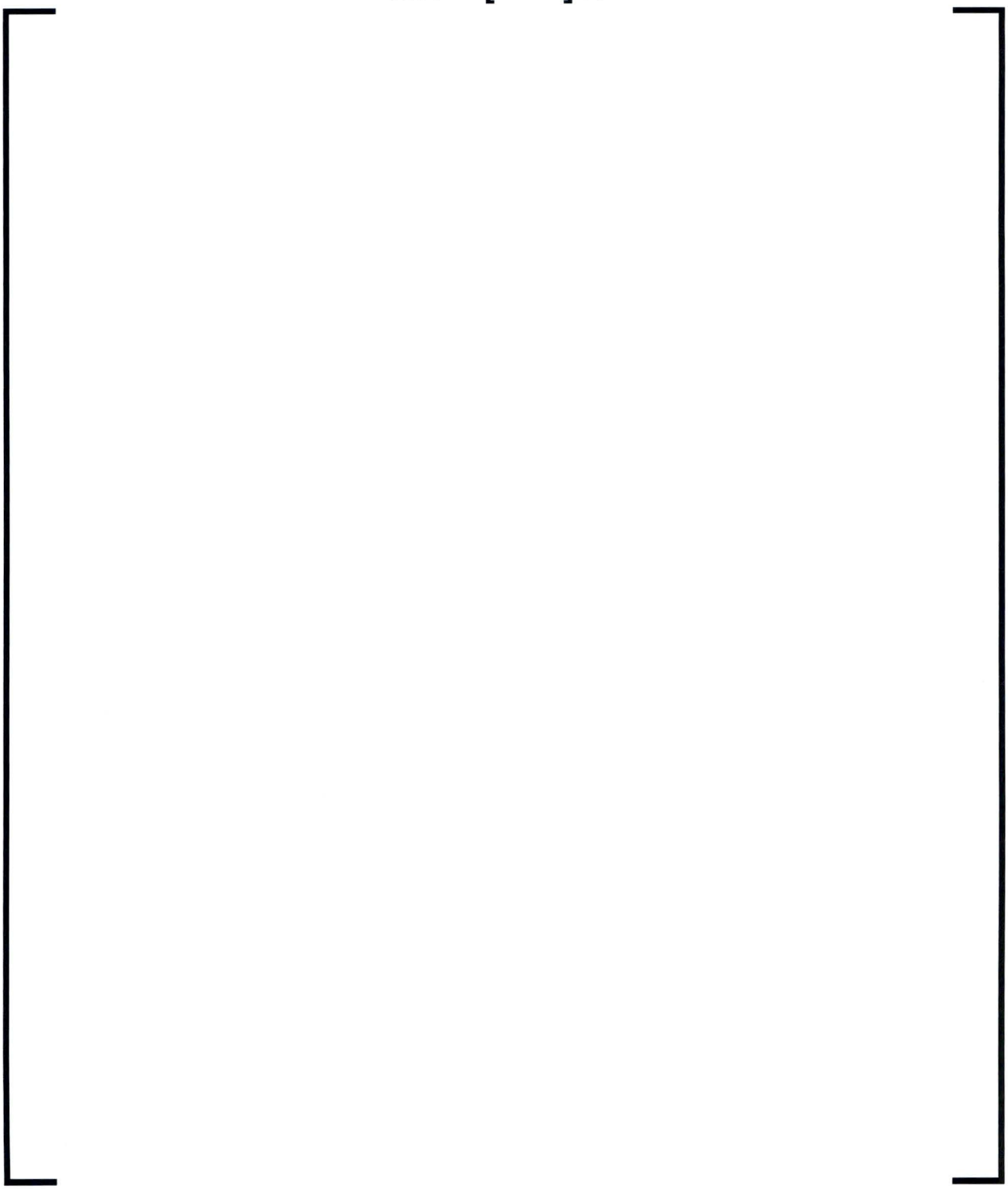

Figure RAI-4.20-6: Downcomer Liquid Level for Baffle Resistance K/A^2 = [ ] ft^{-4}

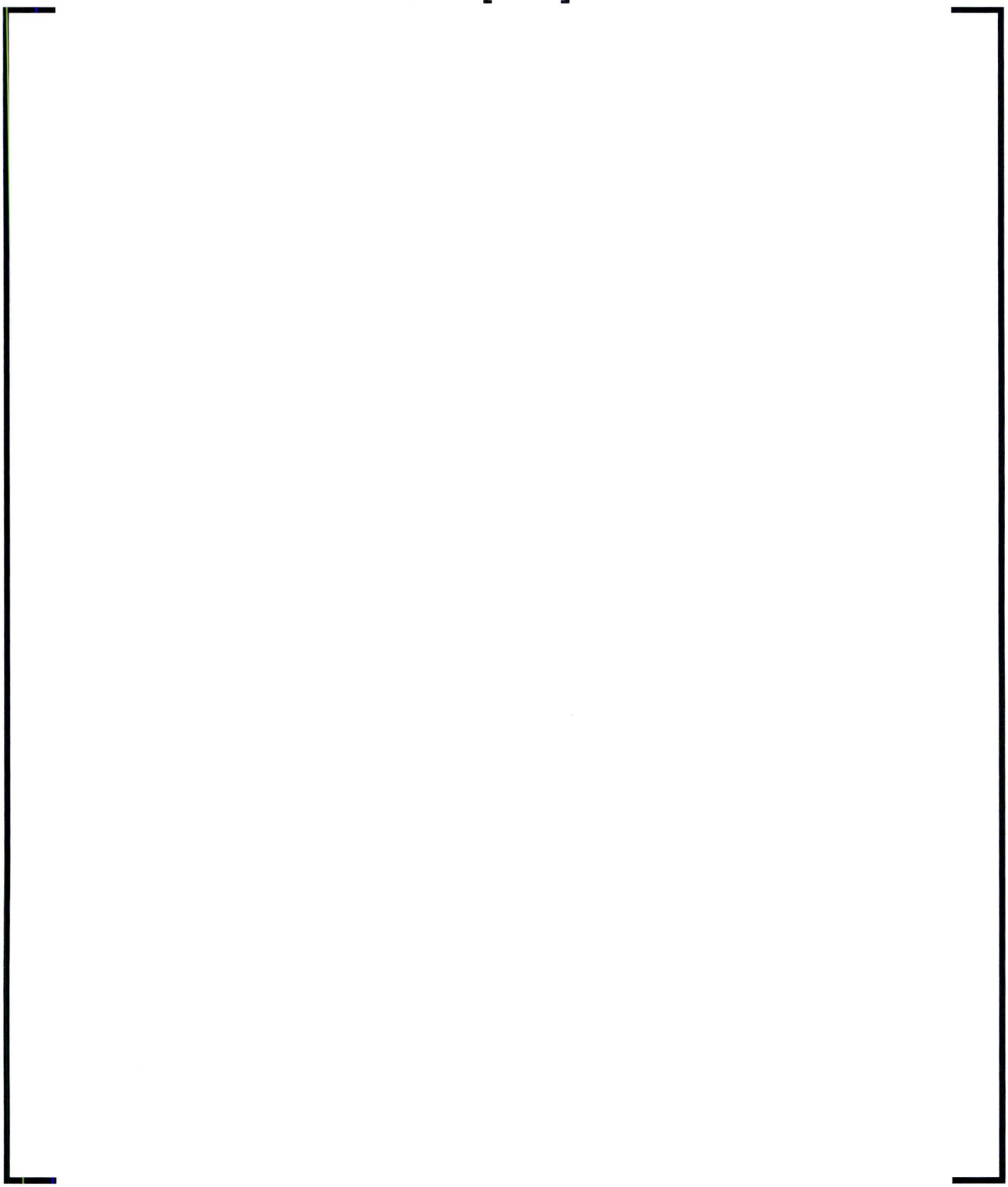

2.21 RAI 4.21

2.21.1 Statement of RAI 4.21

The T-H analyses determine four key parameters, t_{block}, K_{max}, K_{split}, and m_{split}, which are used as input to the overall methodology described in Vol. 1. The K_{split} results are presented in Figures 8-4, 9-3, 10-4, and 11-3 and the m_{split} results are presented in Figures 8-5, 9-4, 10-5, and 11-4 in Vol. 4. Fitting curves to the predicted K_{split} and some m_{split} results are shown in each of these plots. The same plots are reproduced in Figures 6-1 through 6-8 in Volume 1.

The T-H analyses do not provide a basis for extrapolation or interpolation of the calculated K_{split} results as a function of the ECCS recirculation flow rate. Provide the applicability of extrapolating the calculated K_{split} values outside of the analyzed range of ECCS rates for the fitting expressions in Figures 8-4, 9-3, 10-4, and 11-3. Justify the ability to interpolate the expressions to reproduce the calculated K_{split} values between the calculated points.

Similar to the case with the calculated K_{split} inputs, the m_{split} results and the supporting T-H analyses in Vol. 4 do not provide a basis for justifiable extrapolation or interpolation of the calculated m_{split} results documented as a function of the core inlet resistance reduced by K_{split} and the ECCS flow rate. Provide the basis for extrapolating the calculated m_{split} results beyond the maximum core inlet resistances analyzed for each assumed ECCS rate to produce the m_{split} results shown in Figures 8-5, 9-4, 10-5, and 11-4. For the Westinghouse upflow category, the largest core inlet resistance of about $4.0x10^4$ was reached in the case of 8 gpm/FA, whereas the applicable K_{max} is $5.0x10^5$; for the Westinghouse downflow category the largest core inlet resistance of about $1.2x10^5$ was reached in the case of 8 gpm/FA whereas the applicable K_{max} is $6.0x10^5$; for the CE category the largest core inlet resistance of about $5.4x10^5$ was reached in the case of 827 gpm, whereas the applicable K_{max} is $6.5x10^6$; and for the B&W category, a core inlet resistance of about $1.8x10^4$ was reached for each ECCS rate, whereas the applicable K_{max} is $1.0x10^8$. Figures 8-5 and 9-4 each document two fitting expressions for the cases with the lowest and highest ECCS rates for the Westinghouse upflow and downflow categories, whereas Figures 10-5 and 11-4 each show a single fitting curve presumably intended to bound the calculated m_{split} results. Describe how the m_{split} results can be justifiably interpolated to obtain a valid m_{split} input at ECCS flow rates that do not match any of the values analyzed for the Westinghouse upflow and downflow categories (8, 12, 18, 30, and 40 gpm/FA) or for the B&W category (7.5, 12.5, 17.5, 22.5, 27.5, and 43.5 gpm/FA). Also, the significant degree of scatter in the plotted m_{split} points in Figure 10-5 makes the information on the plot hard to interpret.

The NRC staff needs confidence that reliable and valid K_{split} and m_{split} inputs were

obtained. If such assurance is not reached generically, additional T-H calculations to produce applicable K_{split} and m_{split} inputs, including supporting analyses, will be requested on an as-needed plant specific basis.

2.21.2 Response to RAI 4.21

The K_{split} results of multiple cases for Barrel/Baffle (BB) resistances that range from low to high and multiple Emergency Core Cooling System (ECCS) flow rates are shown in Figure RAI-4.20-2 in the response to RAI 4.20. From these results, it can be observed that K_{split} decreases as the ECCS flow rate increases. This trend is expected since higher ECCS flow rates fill the downcomer more quickly (see Figures RAI-4.20-5 and RAI-4.20-6 in the response to RAI 4.20), which will overcome the resistance to flow in the BB region at lower core inlet resistances, resulting in a smaller K_{split}. This trend will continue with diminishing returns as described by the power trend on Figure RAI-4.20-2. Thus, it is a reasonable approach to extrapolate the K_{split} curve to higher ECCS flowrates and interpolate between the analyzed ECCS flowrates.

In Volume 4 of WCAP-17788-P, m_{split} was calculated as a function of the core inlet resistance. The calculation stopped when the core inlet resistance reached 5.4×10^5 or 3.6×10^5. As explained in the responses to RAI 4.20, when the six new cases were analyzed, m_{split} calculation was extended until the core inlet resistance reached 6.5×10^6, which is the value of K_{max} as presented in Section 10.2, Volume 4 of WCAP-17788-P. Once the core inlet resistance reaches K_{max}, no additional debris can be tolerated at the core inlet. Therefore, extrapolation of the m_{split} results to higher $K–K_{split}$ values is no longer needed.

New lower bound curves were also defined for m_{split} in the response to RAI 4.20. As described therein, these new lower bound curves will minimize the amount of flow and debris diverted to the heated core region and maximize the amount of debris delivered to the core inlet. Utilities should use the appropriate function based on their plant-specific BB K/A^2 value. That is, plants that have a BB resistance that is less than [ ] ft^{-4} should use the lower bound function described by Equation RAI-4.20-5. All other plants should use the lower bound function described by Equation RAI-4.20-4.

As described in the response to RAI 4.20, the use of the lower bound curve for all ECCS flow rates provides a measure of conservatism in the overall calculation of the debris limit for a Hot Leg (HL) break. Utilities that can demonstrate ECCS flow rates above an equivalent 1654 gpm during sump recirculation can improve their debris limits by using a curve that is more representative of the higher m_{split} results. The appropriate equivalent flow rate can be determined using the method provided in the response to RAI 4.5a.

2.22 RAI 4.22

2.22.1 Statement of RAI 4.22

The small-break LOCA analysis approach applied for the B&W plant category and the plant analysis results for a 0.5 ft^2 small HLB LOCA presented in Section 11 may not meet the requirements of 10 CFR 50.46(a)(1)(i), which states, "ECCS cooling performance must be calculated in accordance with an acceptable evaluation model and must be calculated for a number of postulated loss-of-coolant accidents of different sizes, locations, and other properties sufficient to provide assurance that the most severe postulated loss-of-coolant accidents are calculated". Specifically, it is questionable whether the RCS T-H conditions, predicted at the time of core inlet blockage and thereafter for a 0.5 ft^2 small HLB LOCA, remain applicable to a DEG HLB LOCA, which represents the limiting scenario as stated in the TR. The three arguments provided in Section 6.4 of Vol. 4 in support of the selected 0.5 ft^2 break size do justify extrapolation of the calculated small-break LOCA results to a full-size DEG HLB LOCA transient considered as the limiting scenario.

Provide additional LOCA calculation results for the B&W plant design category, including results for predicted safety criteria, figures of merit, and supporting analysis results, which demonstrate quantitatively that the requirements of 10 CFR 50.46(a)(1)(i) are met. T-H LOCA calculations should be performed using applicable and appropriately assessed EMs.

2.22.2 Response to RAI 4.22

This RAI pertains to the Babcock & Wilcox (B&W) plant category and therefore requires no response for the Combustion Engineering (CE) plant category.

2.23 RAI 4.23

2.23.1 Statement of RAI 4.23

To assist the NRC staff evaluation of liquid discharge through the break for the large HLB LOCA scenario, provide the following information for each of the four analyzed plant categories for the limiting break size.

(a) Identify key transport mechanisms of liquid discharge through each side of the break that can occur during transient phases of relevance to the T-H analyses. Explain how liquid transport mechanisms caused by liquid spillover under elevated two-phase mixture levels in the reactor upper plenum due to carry-out of dispersed liquid by entrainment under depressed mixture level conditions are accounted for and modeled in the applied codes. Describe whether the liquid transport models are reflective of and dependent on the upper plenum two-phase mixture level and explain how the performance of these models, in terms of their accuracy and sensitivity, depends on the code capabilities to predict the two-phase mixture levels in the reactor upper plenum under conditions representative of the LTCC phase of a large HLB LOCA.

(b) Describe code assessments, including analyses and results, which demonstrate the capability of the codes used in the T-H analyses to adequately predict transport mechanisms that result in liquid discharge through the break during LTCC. Consideration should be given to contribution from mechanisms accounting for both entrainment and deposition (de-entrainment) of liquid that can take place in participating RV regions including the upper plenum and connected broken hot leg piping. Include information identifying test facilities, test runs, and test conditions used in the code assessments. Provide comparisons of code predictions against relevant test data, as available.

(c) Explain if any special liquid entrainment models, modeling options, and related flags were available in the applied codes and if any such features were activated in the T-H analyses to account for liquid entrainment. Examples of such modeling features can be related to special upper plenum entrainment models, mixture level models, and related special interfacial drag models. State whether any break flow multipliers were applied in the analyses. Provide the multiplier values, and explain if the selected inputs were examined for impact on the predicted break liquid discharge.

(d) Identify key models used and the underlying correlations related to the predicted break liquid discharges. Provide the ranges of applicability of these correlations,

and compare them against the conditions predicted in the analyses documented in Sections 8 through 11. Provide the information in a table format for each of the cases analyzed to determine t_{block} and K_{max} in Section 8 (Cases 1B and 2B), Section 9 (Cases 1A and 2B), Section 10 (Cases 1 and 2), and Section 11.

(e) If not provided elsewhere, include plots showing the following sets of parameters for the cases documented in Sections 8 through 11 as a function of transient time:

(i) Mass flow rates of liquid, steam, and total fluid (liquid and steam) discharges through each opening of the DEG break. Include integrals of the identified break mass flow rates.

(ii) Two-phase mixture level on the core side of the RV

(iii) Steam flow quality calculated as a ratio of the steam mass flow rate to the total (liquid and steam) mass flow rate for the RV-side opening of the DEG break

(iv) Predicted pressure difference between the upper plenum cell connected to the broken hot leg pipe and the containment backpressure.

(f) Figure 1 below compares predicted exit qualities for the original analysis of Case 1 used to determine t_{block} for the CE plant category as documented in Section 10 and the revised analysis in Erratum, submitted with the February 12, 2016, letter OG-16-42 (t_{block}=20,000 seconds). It is noted that the results are significantly different following the simulated blockage time in each analysis. The results also differ during some time periods prior to 15,000 seconds, which is the earlier of both simulated t_{block} times. Describe why the results prior to 15,000 seconds are not consistent between the two cases and state which case presents the correct values. Provide similar information for the time period after blockage is simulated. Please describe why the results fluctuate significantly and justify that the code performance provides a valid representation of the system.

(g) During the NRC audit of the AREVA T-H analyses for the CE plant category, entrainment predictions using S-RELAP5 were presented to the NRC staff. Explain whether any code and/or plant input model changes were found necessary to address the code performance. If they were needed, identity and describe any modeling changes that were implemented along with their supporting validation bases. Justify the break liquid carry-out predictions for each of the analyses for the CE plant category in Section 10 including any revisions to these analyses. If necessary, provide updated T-H analysis results.

(h) Investigate whether the substantial scatter in the m_{split} results shown in Figure 10-5 is related to the behavior of the break liquid carry-out result. Note that if the liquid carryover is incorrect, it can render the m_{split} result unacceptable. Describe whether correction of the m_{split} results was found necessary to address the observed scatter

if it was determined that effects from deficiencies in the predicted liquid entrainment were a contributing factor. Provide any updated result if applicable.

(i) Provide assessments demonstrating that t_{block}, K_{max}, K_{split}, and m_{split} results, as obtained from the analyses in Sections 8 through 11 for compliance demonstration with regard to the acceptance criteria, are accurate and not influenced unduly by deficiencies in the entrainment predictions that can be attributed to various factors such as those discussed above in Items a through h. Include consideration of the effects that the ECCS temperatures, both prior and following SSO, and modeling assumptions related to this parameter can have on the prediction results for entrainment.

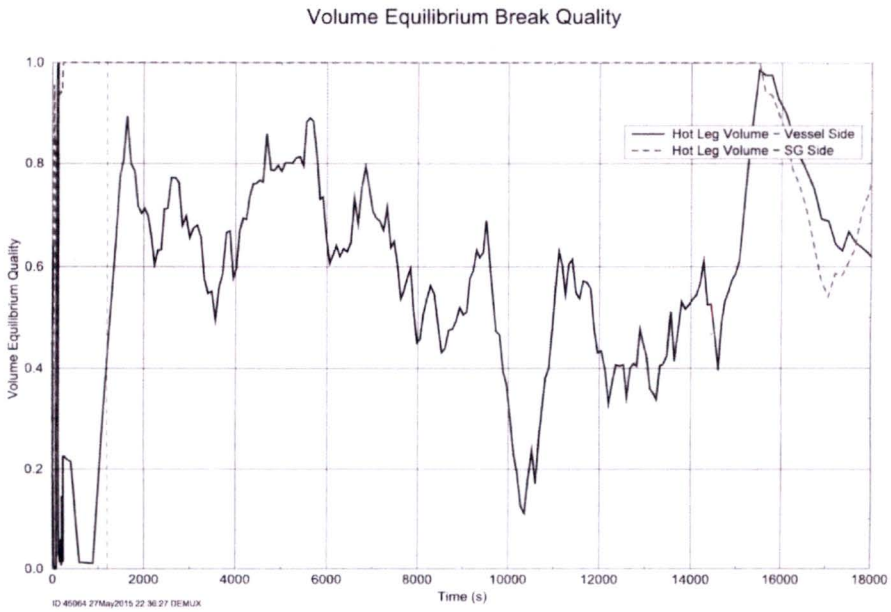

Figure 10-22 Case 1 – Break Exit Quality

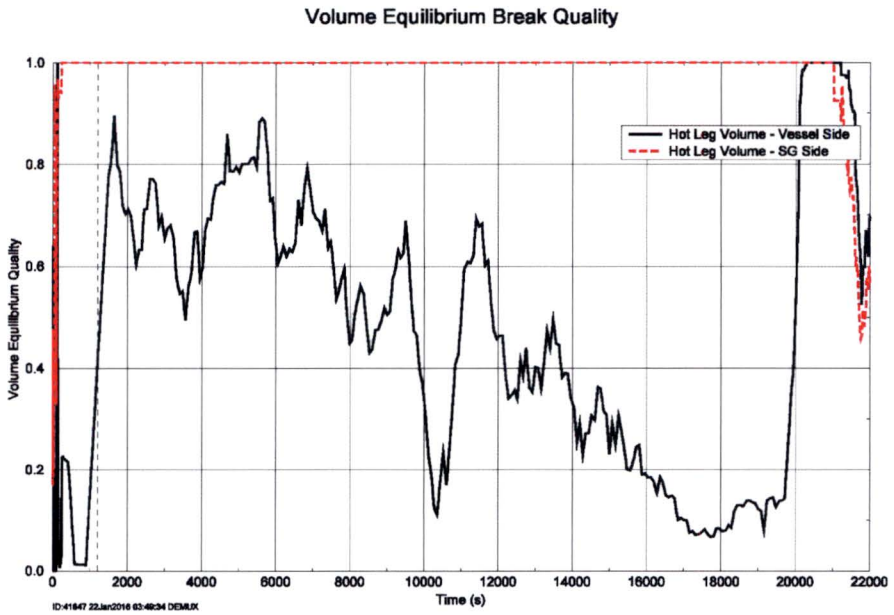

Figure 10-22 Case 1 – Break Exit Quality

Figure 1: Predicted Break Exit Qualities for Case 1 to Determine t_{block} for the CE Plant Category (Top: original result from WCAP-17788 Rev. 0 with t_{block}=15,000 s = 250 min Bottom: corrected result from WCAP-17788, Erratum, OG-16-42 with t_{block}=20,000 s = 333 min)

2.23.2 Response to RAI 4.23

The question asked deals with models and correlations within the S-RELAP5 system code related to the liquid being carried out to the break. Primarily, the underlying question being asked relates to how the mechanisms leading to liquid being carried to the break lead to a conservative, but realistic, prediction in both of the acceptance criteria. The acceptance criteria covers an acceptable Peak Cladding Temperature (PCT) and the avoidance of Boric Acid Precipitation (BAP).

In regards to liquid being carried to the break, having too much liquid being carried to the break is conservative from a PCT perspective, but is non-conservative from a BAP perspective. If too little liquid is predicted to be carried out, the reverse is also true. In order to address this fact, this response will provide background information and a technical justification as to why the BAP acceptance criterion will not present a challenge for the Combustion Engineering (CE) plant category. If BAP is removed from being a concern independent of the calculated liquid carryout to the break, then the focus can be on ensuring the analysis is conservative from a PCT perspective.

Once the background and technical basis relative to BAP is presented, the response to each of the questions asked will be provided.

2.23.2.1 Background

In order to provide a technical basis relative to the BAP criterion, it is helpful to discuss the event progression for common understanding. The event modeled in Volume 4 of WCAP-17788 is a Double-Ended Guillotine (DEG) Hot Leg (HL) break. The HL break scenario progresses as follows:

- **Blowdown, refill, and reflood** – blowdown, refill and reflood are complex Thermal Hydraulic (TH) phenomena and are covered by Realistic Large Break Loss of Coolant Accidents (RLBLOCAs). The break flow is choked during the blowdown phase.
- **Post reflood** – the Reactor Coolant System (RCS) transitions to a quiescent phase and RCS pressure will be close to containment pressure. Pumped-injected Emergency Core Cooling (ECC) water in the cold leg flows into the core through the Downcomer (DC). The water boils in the inner region of the core and the two-phase mixture flows upwards and flows into the Upper Plenum (UP).
  - Part of the liquid flows down through the periphery Fuel Assemblies (FAs) and baffle region. As the water flows down through the periphery FAs, some of the flow will flow radially inwards and mix with the two-phase mixture flowing upwards through the inner region of the core.

- The steam velocity in the UP is expected to be less than the droplet entrainment velocity. Therefore, the remaining water in the UP and steam form a two-phase mixture in the UP and flows upwards and flows out primarily through the broken HL nozzle and flows out to containment through the HL break. A slug flow regime is expected in the UP below the HL nozzle and the swell level will be near the bottom of the HL nozzle.
- There is essentially no steam production in the UP and therefore the superficial steam velocity below the HL nozzle is reasonably constant and therefore the axial void distribution in this region will have to be reasonably constant based on the theoretical basis provided as part of RAI 4.8. The expected void fraction is about 60%. However, this void distribution will also be influenced by the height of the UP below the HL nozzle and the steam velocity in the HL nozzle.
- In a CE plant, during the post reflood phase, the steam velocity in the broken HL nozzle will be more than 100 ft/s, which is substantially higher than the droplet entrainment velocity. In meteorological terms, this velocity is about 70 mph and it clearly shows that it can drag substantial liquid from the UP below the HL nozzle. In addition, the height of the UP below the HL nozzle is about 2.8 ft. As a result of both the relatively short UP height and the large HL steam velocity, the liquid distribution in the UP will skew towards the broken HL as the level approaches the HL nozzle. As a result, there is expected to be a void gradient in the UP below the HL nozzle.
- Following the complete blockage of the core inlet the flow direction in the baffle region reverses and the liquid from the Lower Plenum (LP) flows up to the UP through the baffle and it essentially flows down in the core through the periphery FAs. In the CE analysis, during the early phase, the baffle flow will potentially be lower than the boil-off rate in the core and as a result, the top portion of the core may uncover for a short period. The vessel side break flow during this period will be essentially steam. As the DC fills with water, the baffle flow increases and eventually the core quenches and the mixture level forms in the UP and it will reach close to the pre-blockage level and the two-phase mixture from UP flows out to the containment through the HL break. After this period, the transient progression will be essentially the same as during the pre-blockage period.

After the characterization of the event progression, some background information about the S-RELAP5 system code is provided. The S-RELAP5 code is used for the WCAP-17788-P, Volume 4, analyses for the CE plant type.

While the following section refers to Reference 4.23-3 in several places, for purposes of this discussion, the description also applies to methodology in Reference 4.23-2.

Reference 4.23-3 is a convenient reference since it contains the theory manual, Verification and Validation (V&V) manual, and RLBLOCA methodology all in one spot. Reference 4.23-5 is the theory manual directly tied to the EMF-2103(P)(A), Rev. 0 methodology and can also be consulted for a similar discussion.

S-RELAP5 is an AREVA NP-modified version of RELAP5/MOD2 (Reference 4.23-6), which incorporates the computer portability aspects of RELAP5/MOD3 (Reference 4.23-7) and modifications to the constitutive package to provide congruency with literature correlations and to improve the simulation of key LBLOCA experiments. The S-RELAP5 code solves a two-fluid, six equation model plus one continuity equation of noncondensible gas and a boron tracking equation for flow of a two-phase steam-water mixture, which can contain a noncondensible in the vapor phase and a soluble in the liquid phase. The phasic equations are coupled together via the constitutive models to solve these equations. The field equations are basically in the same form as RELAP5/MOD2, with the addition of full two-dimensional momentum equations. This two-dimensional capability is applied to the RLBLOCA methodology. A summary of the major modifications and improvements incorporated into S-RELAP5 relative to RELAP5/MOD2 are given in Section 7.1.2 of Reference 4.23-3.

The hydrodynamic constitutive models for describing the interphase coupling terms and the wall friction terms in the fluid field equations shown in Section 7.4 of Reference 4.23-3 are discussed in Section 7.5 of Reference 4.23-3. The interphase coupling terms include heat/mass transfer and interphase friction (drag and/or shear). The mass transfer term is further divided into the heat/mass transfer in the bulk fluid and the heat/mass transfer near the wall. The interphase heat/mass transfer near the wall is discussed in Section 7.6 of Reference 4.23-3. As presented in Section 7.4 of Reference 4.23-3, the bulk interphase mass transfer rate is expressed in terms of interphase heat transfer rates to liquid and vapor phase. The interphase coupling terms are formulated within the framework of the two-fluid model and are constructed from the formulations for the basic elements of flow patterns such as bubbles, droplets, vapor slugs (i.e., large bubbles), liquid slugs (i.e., large liquid drops or chunks of liquid), liquid film, and vapor film. The flow regime map, shown in Figure 7-5 in Reference 4.23-3, is used to represent the various complicated flow regimes that can exist in vertical boiling channels below and above the Critical Heat Flux (CHF) locations. Similarly, a simplified horizontal flow regime map is shown in Figure 7-6 in Reference 4.23-3.

As explained earlier, during the post-core quench period following the blowdown, refill and reflood phases of a HL Large Break Loss of Coolant Accident (LBLOCA), the RCS transitions to a quiescent phase and the slug flow regime will be the predominant flow regimes in the inner core regions as well as in the UP below the HL nozzle. The primary system pressure in the RCS will be close to containment pressure. S-RELAP5 was benchmarked under these conditions using the Rod Bundle Heat Transfer (RBHT) level swell tests and developed a technical basis to extend the application to long term. These

tests covered essentially the entire slug-flow regime. Hydraulic diameter difference between the core and the UP is the only difference between the slug flow in the core regions and the slug flow in the UP. It is to be noted that the upper boundary of the slug flow is determined using Equation 7.255 in Reference 4.23-3, which reflects the correlations developed by Taitel and Dukler (Reference 4.23-8) and Wallis (Reference 4.23-9). The equation has taken into account the diameter dependency in the flow regime. The interphase drag in the slug flow regime is described in Section 7.5.2.2 of Reference 4.23-3 and it also reflects the diameter dependency. As explained on page 7-98 of Reference 4.23-3, the transition region between the slug flow and annular-mist flow (shown in Figure 7-5 of Reference 4.23-3) may be considered as equivalent to the highly irregular churn-turbulent flow regime, even though one of the main purpose is an attempt to provide a smooth transition in the interphase drag between the two flow regimes. Therefore, it can be expected that S-RELAP5 will properly calculate the void distribution in the UP during the long term core cooling phase.

2.23.2.2 Technical Basis

The following section describes the recovery of the liquid in the core, as well as in the UP, after t_{block} has occurred. The duration of this recovery can then be compared against a conservative estimate of the BAP time in order to verify that BAP is not likely to be a concern for the CE plant type for the WCAP-17788-P, Volume 4, analyses. Once the BAP aspect of the acceptance criteria can be dispositioned, then the focus can be on ensuring that the WCAP-17788-P, Volume 4, analyses for the CE plant type is conservative from the PCT acceptance criterion point-of-view.

The recovery of the liquid in the UP until the mixture level returns to the bottom of the HL is first calculated using a theoretical UP inventory needed to reach the bottom of the HL and a conservative excess makeup flow. Once the theoretical recovery time is determined, it can be compared to the S-RELAP5 code calculated results. The theoretical approach may have a longer estimated time to get liquid out the break during the recovery as it does not account for the proximity of the HL or the sweep out due to steam flow across the liquid surface. However, the theoretical recovery time is important in order to determine a conservative calculation of the recovery time, in the event that the code may predict liquid out the break earlier than may physically occur. As such, a conservative estimate of the UP inventory recovery to get the mixture level to the HL elevation will use the theoretical approach. This will then be compared to a conservative estimate of the BAP time.

2.23.2.2.1 Estimation of Upper Plenum Void Fraction – Two approaches are used to estimate the UP void distribution below the HL nozzle during the post-core

quench-phase. The first approach is the void fraction calculation using two widely used correlations; Wilson, et al. (Reference 4.23-10) correlation and Cunningham-Yeh (Reference 4.23-11) correlation. Both correlations are also used in the Response to RAI-8. It is to be noted that in Wilson correlation, there is a term that includes the hydraulic diameter. Cunningham-Yeh correlation does not have a hydraulic diameter-dependent term. The second approach is to use the air-water data reported by Zuber and Findlay (Reference 4.23-12) and by Osakabe, Koizumi, and Tasaka (Reference 4.23-13). It is to be noted that the measured void fraction in the air-water tests was below approximately 60%. However, both groups correlated their data using drift-flux formulation (Reference 4.23-12) given by:

$$V_g = C_0\, j + V_{gj} \qquad \text{(RAI-4.23-1)}$$

Where V_g is the gas velocity, C_0 is the distribution parameter, j is the superficial fluid velocity, and V_{gj} is the drift velocity. This linear relationship is then used to extend the application range to higher superficial steam velocities. The results from this study are shown in Figure RAI-4.23-1.

The UP hydraulic diameter typically varies between 6" to 12". Therefore, the void fraction versus j_g is calculated using Wilson correlation using 6" and 12" hydraulic diameters and a 15 psia UP pressure. The void fraction versus j_g is also calculated using the Cunningham-Yeh correlation using the same pressure.

Figure 9 in Reference 4.23-12 shows the air-water test results using a 6" diameter pipe. This paper also correlated the data using the drift-flux correlation with C_0 = 1.45 and V_{gj} = 0.45. This figure also shows that the value for V_{gj} is calculated using the correlation for slug flow (Equation 53 in Reference 4.23-12), given by:

$$V_{gj} = 0.35 \left[\frac{g \Delta\rho D}{\rho_l} \right]^{\frac{1}{2}} \qquad \text{(RAI-4.23-2)}$$

Where V_{gj} is the drift velocity, g is the acceleration due to gravity, $\Delta\rho$ is the density difference between the liquid and vapor phases, ρ_l is the liquid density, and D is the pipe diameter.

Therefore, α_g versus j_g is calculated using C_0 = 1.45 and V_{gj} = 0.45 and plotted in Figure RAI-4.23-1.

Figure 10 in Reference 4.23-12 shows the air-water test results using a 12" pipe. On page 465 of Reference 4.23-12, it is stated that for void fraction above about 26%, the data transition to the drift-flux formulation based on slug flow. Therefore, α_g versus j_g is calculated using the C_0 and V_{gj} values for the 6" pipe data (C_0 = 1.45 and V_{gj} = 0.45) and plotted in Figure RAI-4.23-1.

Osakabe, Koizumi, and Tasaka (Reference 4.23-13) conducted air-water level swell tests using a rod bundle located within a 312mm x 89.4 mm rectangular Plexiglas test vessel. They ran tests with and without the bundle in the test vessel and the results are shown in Figure 2 of Reference 4.23-13. For j_g larger than about 0.1, they correlated the data without the rod bundle using the drift-flux formulation, given by:

$$V_g = 1.3\, j_g + 0.5 \qquad \text{(RAI-4.23-3)}$$

Therefore, α_g versus j_g is calculated using the above equation and plotted in Figure RAI-4.23-1.

From the results shown in Figure RAI-4.23-1, the following observations can be made:

- For diameters above 6", α_g versus j_g variation with diameter is small.
- For diameters above 6", the values calculated using Wilson correlation approaches those calculated using Cunningham-Yeh correlation.
- The air-water data shows that for j_g larger than about 10 ft/s, the void fraction is above 0.6. On the other hand, Wilson and Cunningham-Yeh correlations results show that for j_g larger than about 10 ft/s, the void fraction is larger than 0.5.
- Given the fact that the various void fraction correlations are based on air-water test data, they are well suited to the WCAP-17788-P application as low system pressures.

Since the drift-flux formulation is fitted using the air-water test data, it is concluded that for hydraulic diameters in the 0.5 ft to 1.0 ft range, the void fraction will be greater than about 0.6 for the superficial steam velocities greater than about 10 ft/s.

Figure RAI-4.23-1: Void Fraction vs. Superficial Vapor Velocity

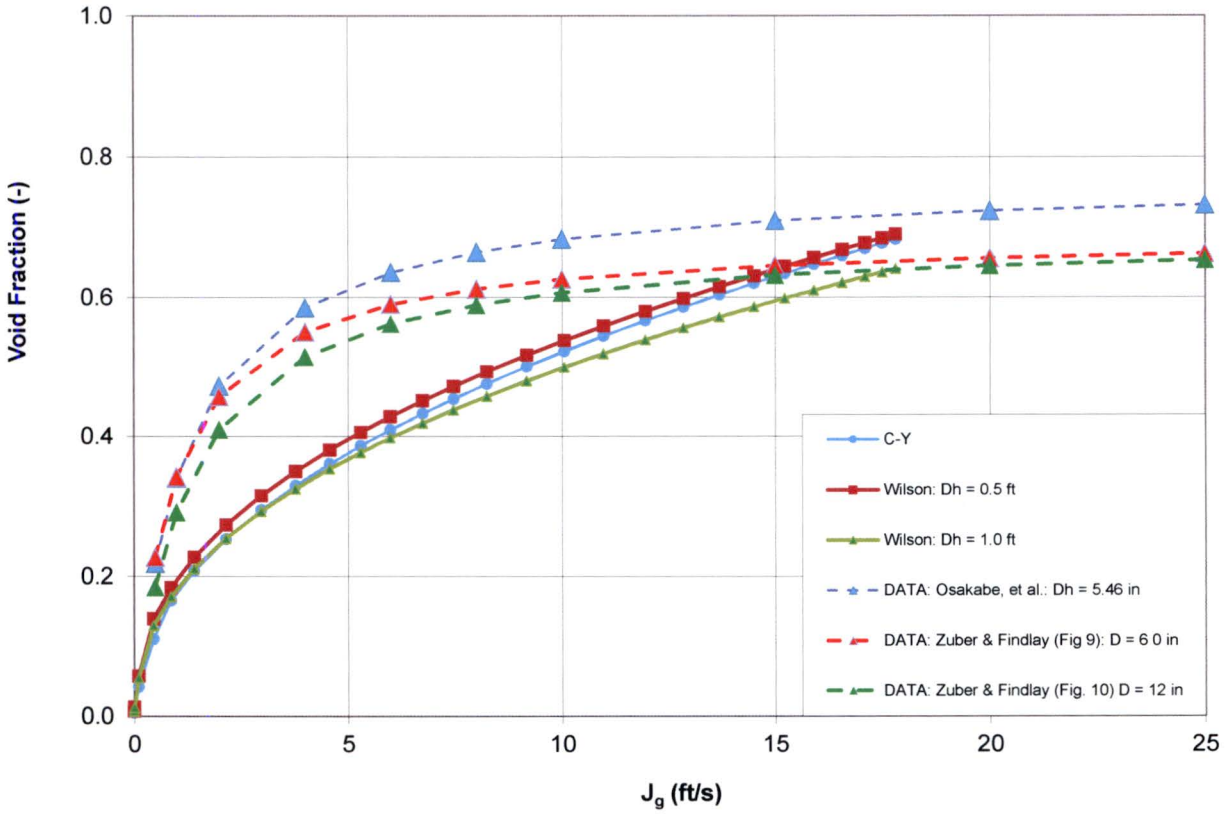

2.23.2.2.2 Plant Transient – Figures RAI-4.23-2 through RAI-4.23-13 show some of the pertinent results for the base CE plant case described in the response to RAI 4.1b that can be used to determine if S-RELAP5 calculates the liquid flow out to the break from the UP. A summary of the results is given below.

- Figures RAI-4.23-2 and RAI-4.23-3 show the void fractions and the superficial steam velocities in the UP second radial sector (above the average core), respectively. A twenty second running average is used in these figure. The superficial steam velocities below the HL nozzle remain above 10 ft/s throughout the transient, except for a short duration after t_{block}. From the air-water data in Figure RAI-4.23-1, the UP void fraction should be greater than 60% during the post core-quench period. It can be seen from Figure RAI-4.23-2 that the void fraction in the first node in UP is about 62% after the mixture level formed in the UP following the core blockage. Figure RAI-4.23-2 also shows that there is an increase in void fraction in the next two nodes. As explained earlier, this is because of the vicinity of

these nodes to the broken HL and the steam velocity in the broken HL exceeds 100 ft/sec, as shown in Figure RAI-4.23-4.

- Based on the UP geometry and a reasonable void fraction of 60% below the HL nozzle with the superficial steam velocities observed, the time for two-phase mixture flow through the vessel side of the break can be estimated. Given the geometry of the CE representative plant case analyzed, the total liquid mass in the UP (including guide tubes) is estimated to be approximately 8000 lbm with saturated fluid conditions at 14.7 psia. This estimation neglects the effects of the proximity of the HL.

- Figure RAI-4.23-5 shows the UP collapsed liquid level. It can be seen that, except for about 1000 seconds after t_{block}, the water level remains reasonably constant from about 10,000 seconds after the start of the transient with a value of about 0.8 ft. Figure RAI-4.23-6 shows that S-RELAP5 calculates about 50% of the maximum possible liquid mass of 8000 lbm in the UP. Given the liquid mass difference between the theoretical UP mass (neglects the effects of the proximity of the HL) and the UP mass calculated by S-RELAP5, a conservative additional delay of the onset of a quasi-steady two-phase flow at the break can be calculated. If a conservative liquid accumulation rate of approximately 10 lbm/s after the core recovery following a complete core blockage is assumed, the break flow will transition to a quasi-steady two-phase flow after about 400 seconds. Figure RAI-4.23-7 compares the baffle exit flow rate against the boiloff rate with a 1.1x multiplier on the ANS 1979 decay heat Standard (Reference 4.23-1). It can be seen in Figure RAI-4.23-7 that the actual excess flow through the baffle is well above 10 lbm/s, which leads to the conclusion that less than an additional 400 seconds is actually needed to reach an UP mass of 8000 lbm.

  From Figure RAI-4.23-8, it can be seen that the vessel side of the break becomes two-phase at about 1500 seconds after t_{block}, where the break quality dropped below 80%. Based on the conservatively estimated uncertainty in the UP mass accumulation, continuous liquid flow from the UP to the break would have initiated prior to 1900 seconds after t_{block}.

  Figure RAI-4.23-9 shows that the core level fully recovers by approximately 1200 seconds after t_{block} and remains nearly constant after this point. This shows the core cannot hold more water and that the excess Emergency Core Cooling System (ECCS) from the Alternate Flow Path (AFP) will go toward refilling the UP.

- Figures RAI-4.23-10, RAI-4.23-11, and RAI-4.23-12 shows the flow regimes in the three UP nodes in the sector above the average core. These reflect the void fraction plots shown in Figure RAI-4.23-2. It can be seen that the bottom two nodes are primarily in slug flow and the third node fluctuates between slug flow, annular mist and mist flow regimes, depending on the void fraction.

It is to be noted that in the RLBLOCA methodology, the vertical stratification model (See Section 7.5.1.1.3 in Reference 4.23-3 for further information on the model) was applied in the UP. However, it was found that for the HL break with the selection of atmospheric pressure containment boundary condition, the flow regimes in UP nodes just below the HL elevation fluctuated between stratified and non-stratified flow regimes that would have introduced numerical flow oscillations. Therefore, that option was not selected for the WCAP-17788-P application.

- Figure RAI-4.23-13 shows that the flow in the Periphery Core (PC) persists in a strong flow in the downward direction throughout the transient. Given a PC flow area of 10 ft^2, this translates into approximately 700 lbm/s in the downward direction. With the flow entering the PC from the baffle exit being only about 80 lbm/s, this strong recirculation within the core shows that the flow from the baffle is directed along this downward flow direction. Thus, the baffle flow is not directly exiting the broken HL. This ensures good predicted mixing in the core and that the flow from the UP is from the core, thereby negating BAP once the level in the UP recovers after t_{block}.

A conservative time to reach BAP is calculated in the following section. This time can then be compared to the estimated time needed to recover the mixture level in the UP to the bottom of the HL elevation, which will determine whether BAP is a concern for the CE plant type.

Figure RAI-4.23-2: Upper Plenum Void Fraction above the Average Core Region

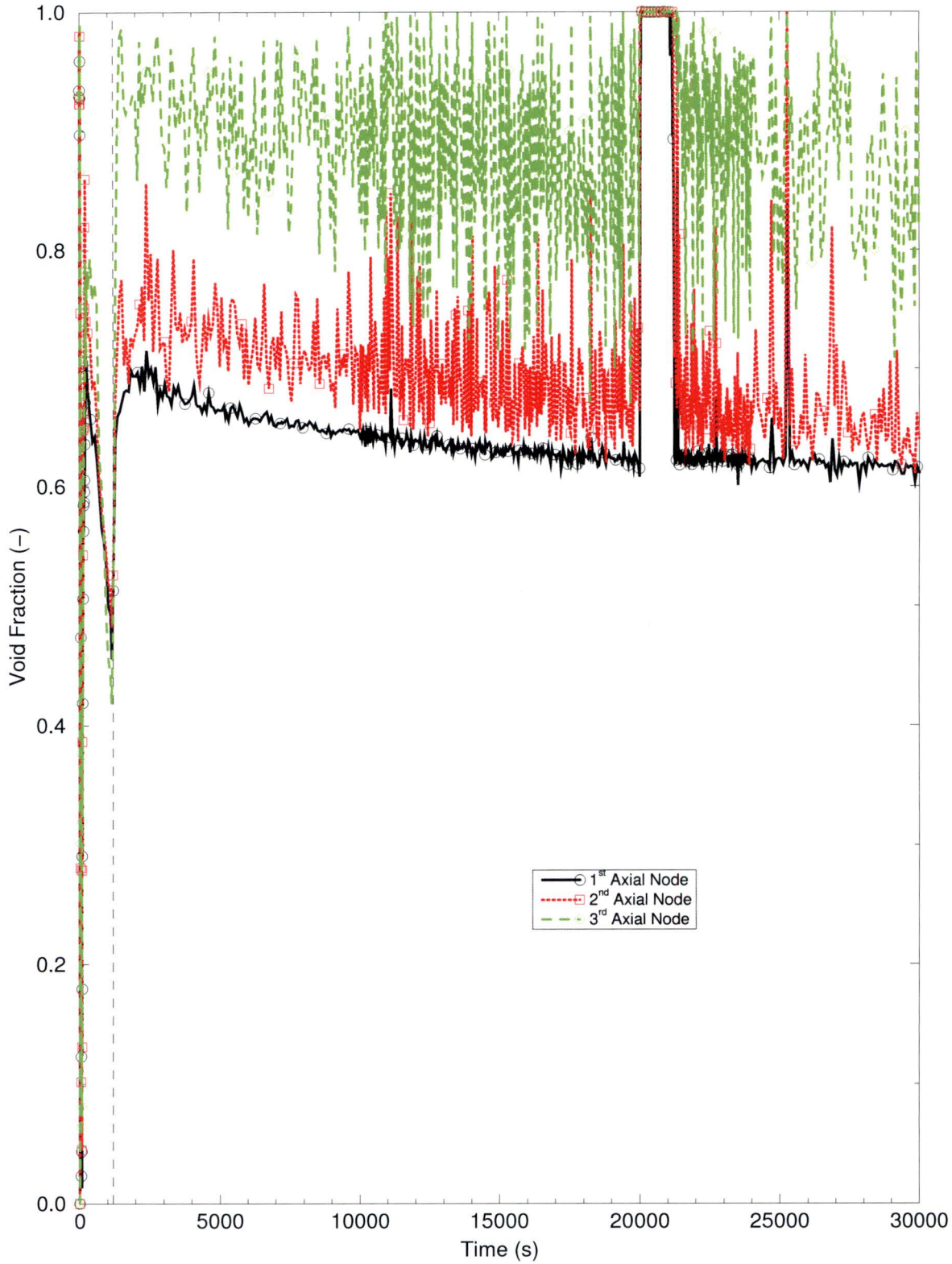

Figure RAI-4.23-3: Upper Plenum Superficial Vapor Velocity above the Average Core Region

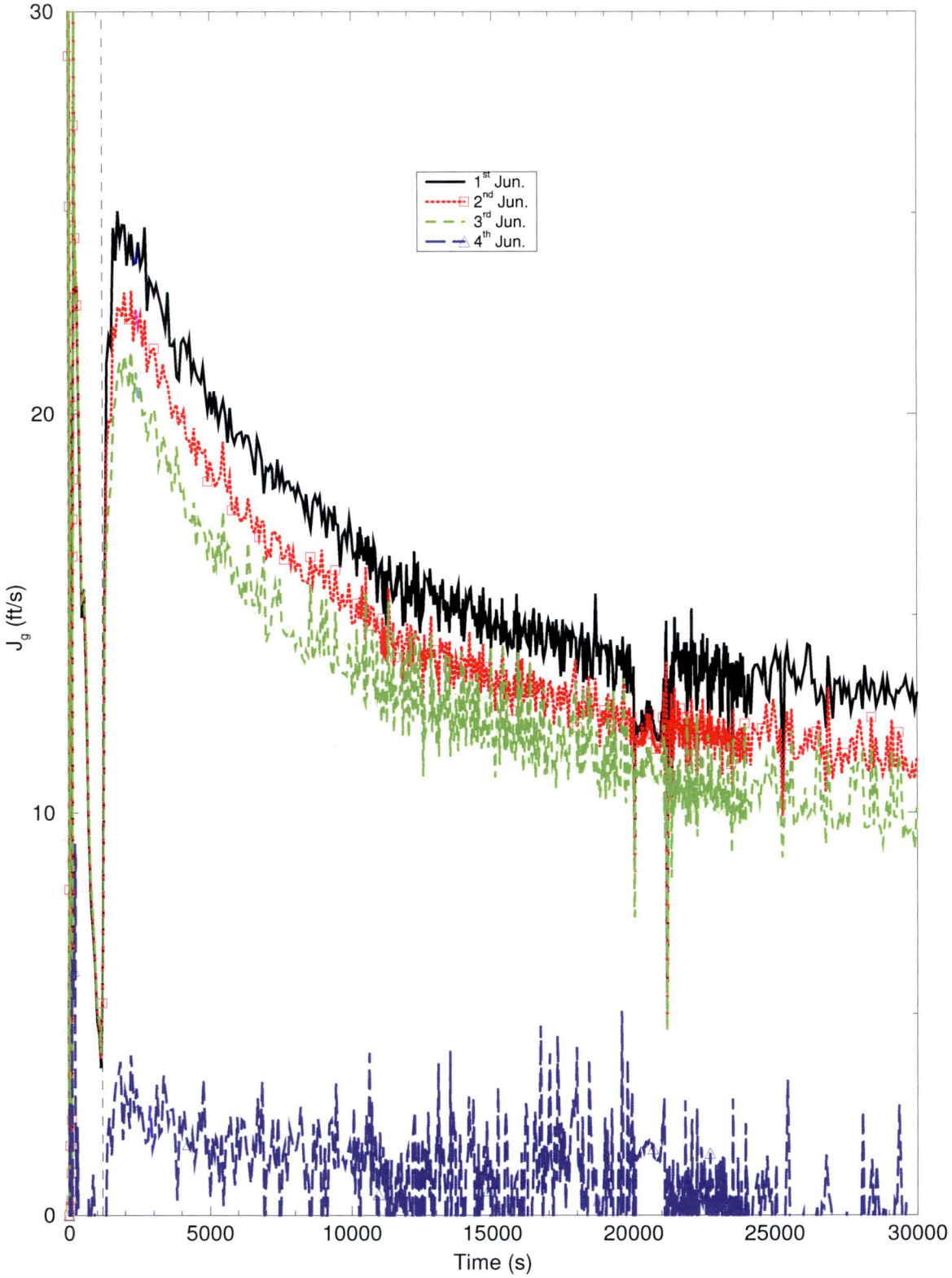

Figure RAI-4.23-4: Upper Plenum to Hot Leg Velocity

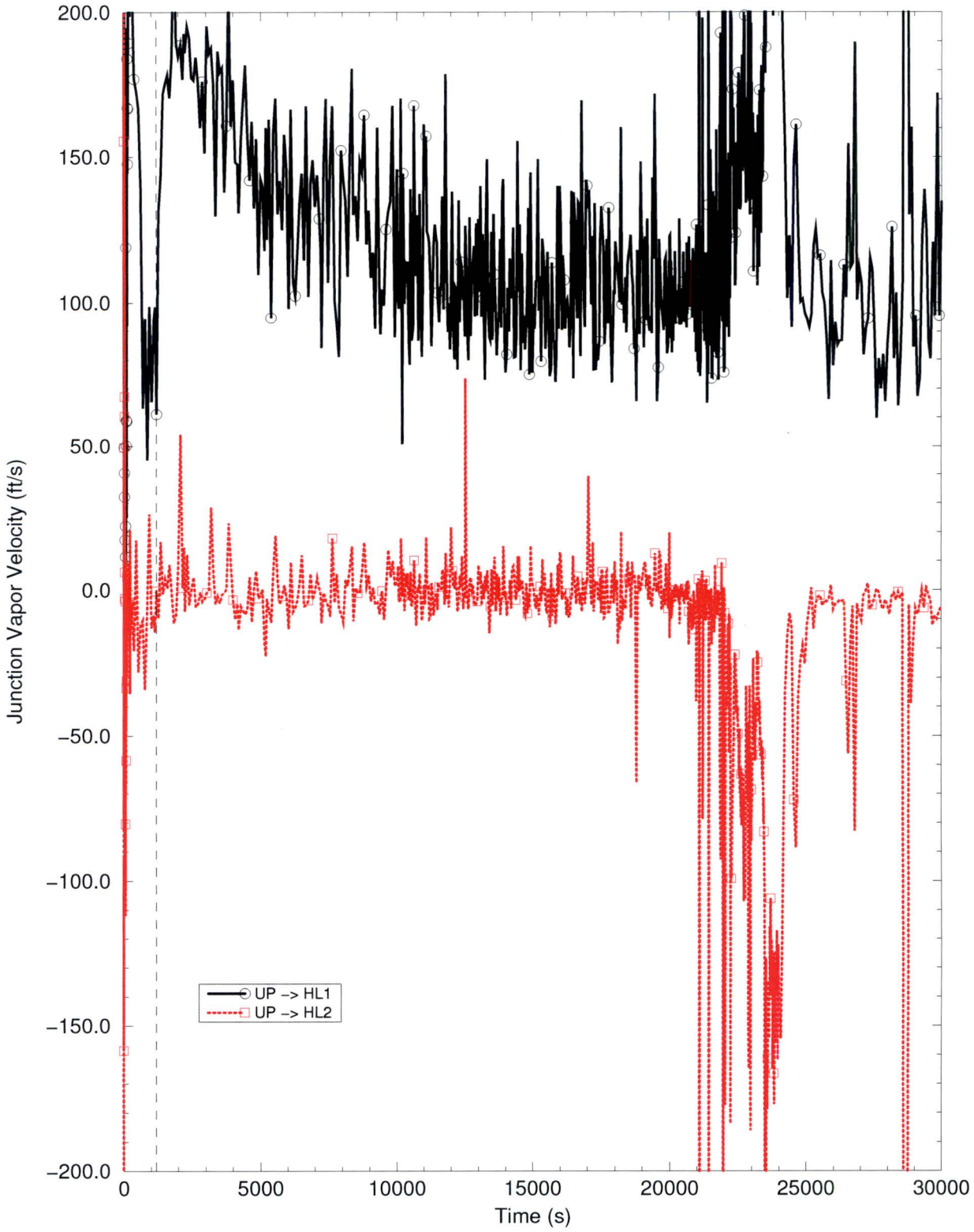

Figure RAI-4.23-5: Upper Plenum Collapsed Liquid Level

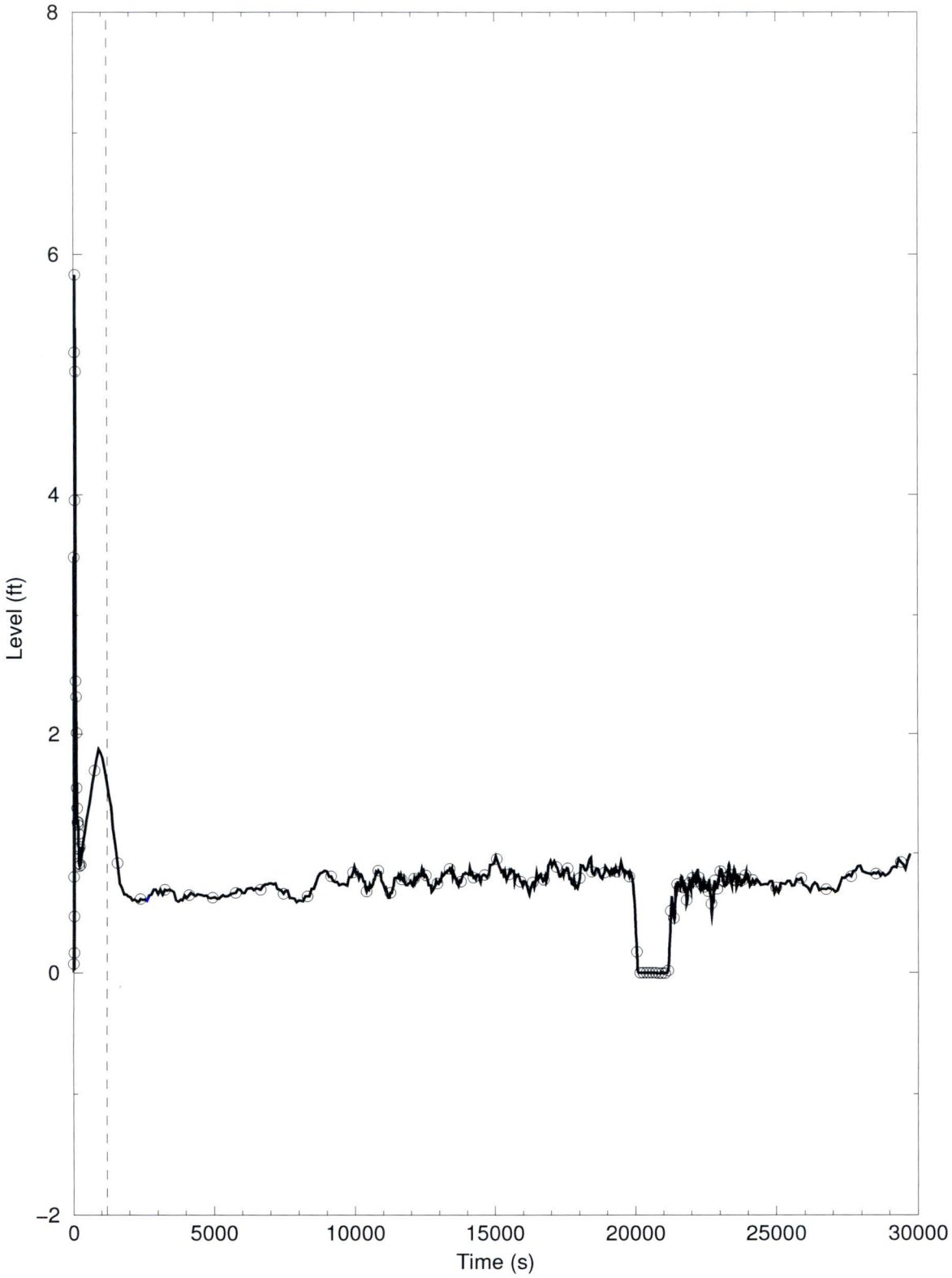

Figure RAI-4.23-6: Upper Plenum Liquid Mass

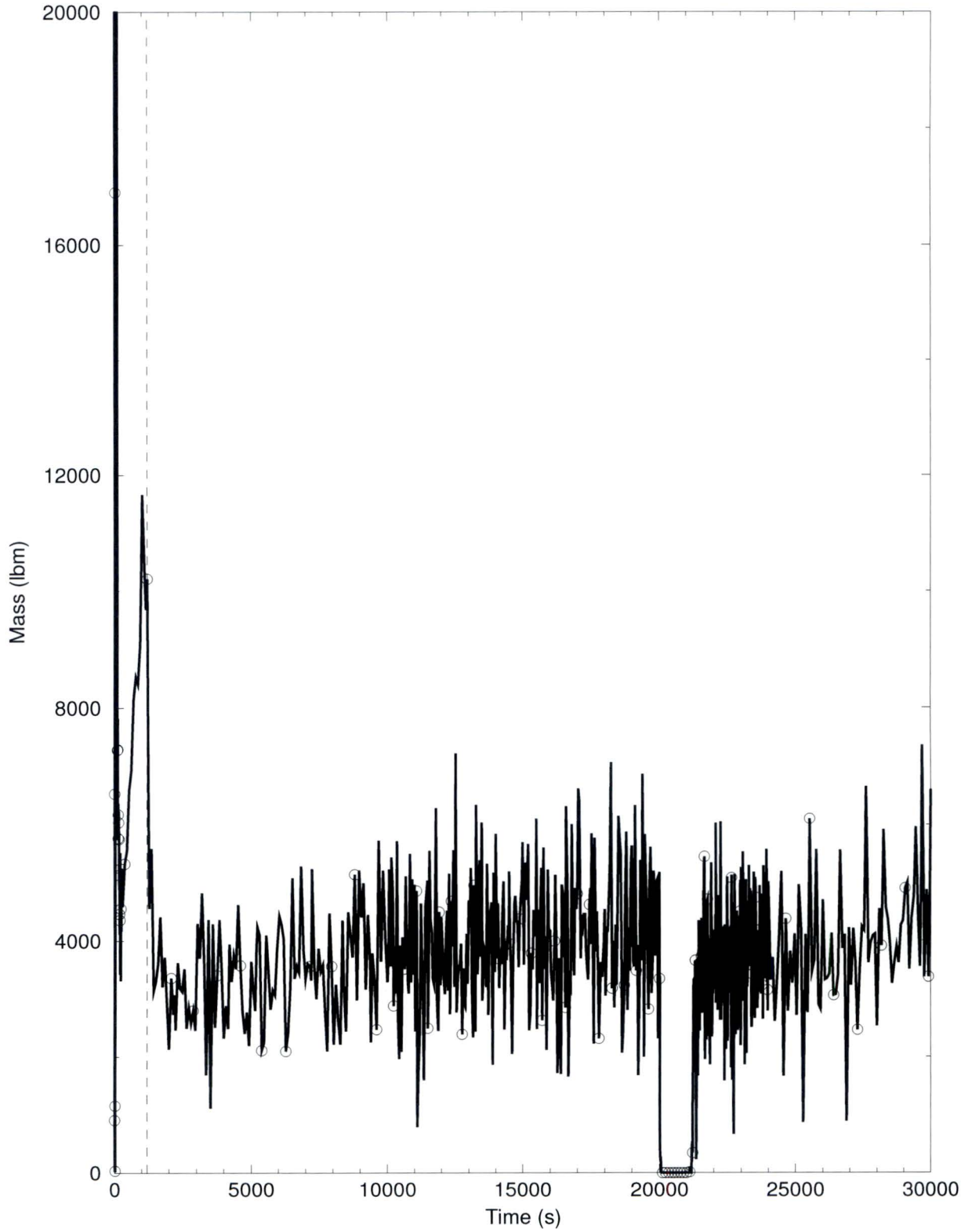

Figure RAI-4.23-7: Baffle Exit Flow and Boiloff Rate

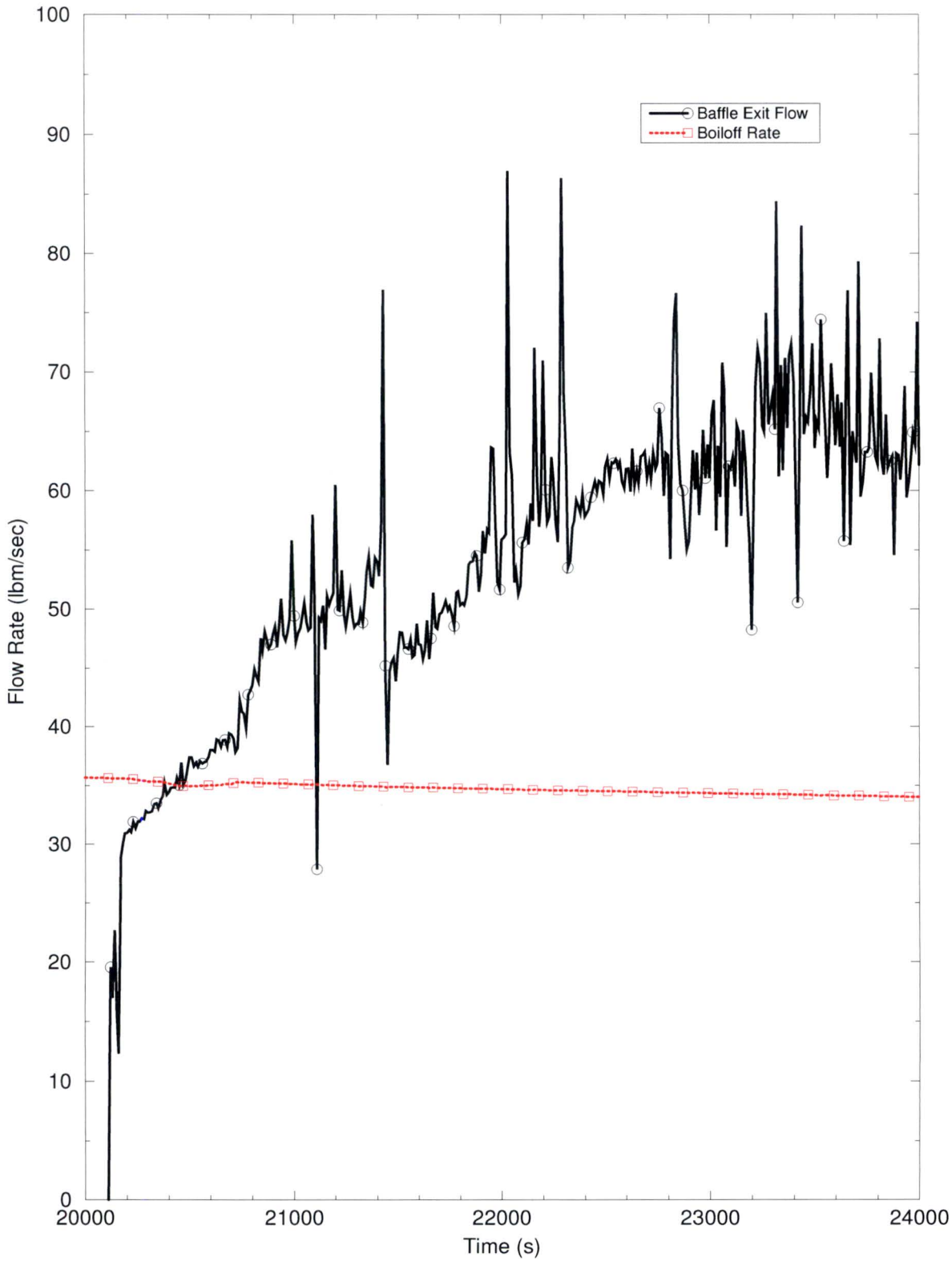

Figure RAI-4.23-8: Vessel Side Break Quality

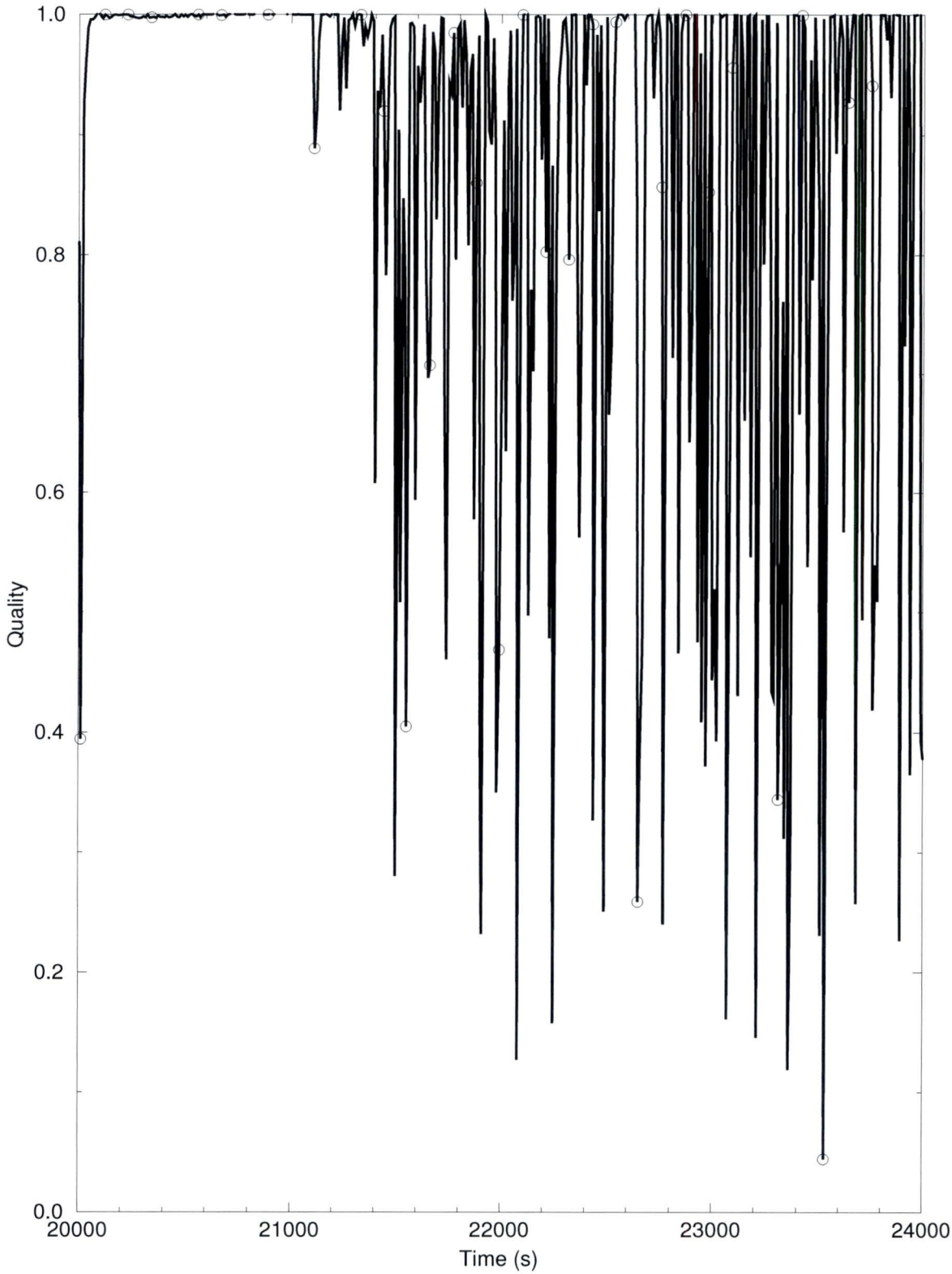

Figure RAI-4.23-9: Average Core – Collapsed Liquid Level

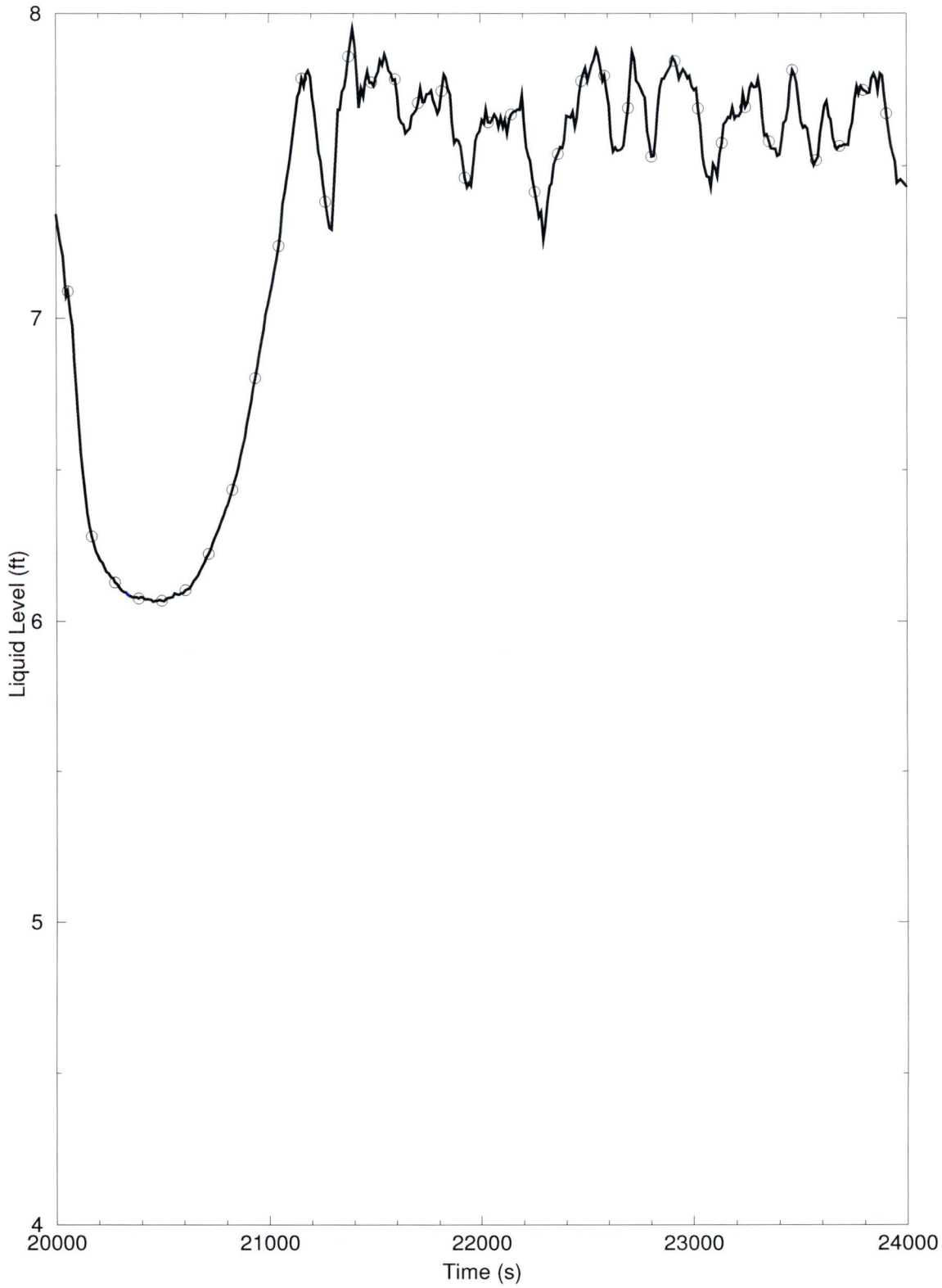

Figure RAI-4.23-10: Upper Plenum Flow Regime - 1st Node above Average Core

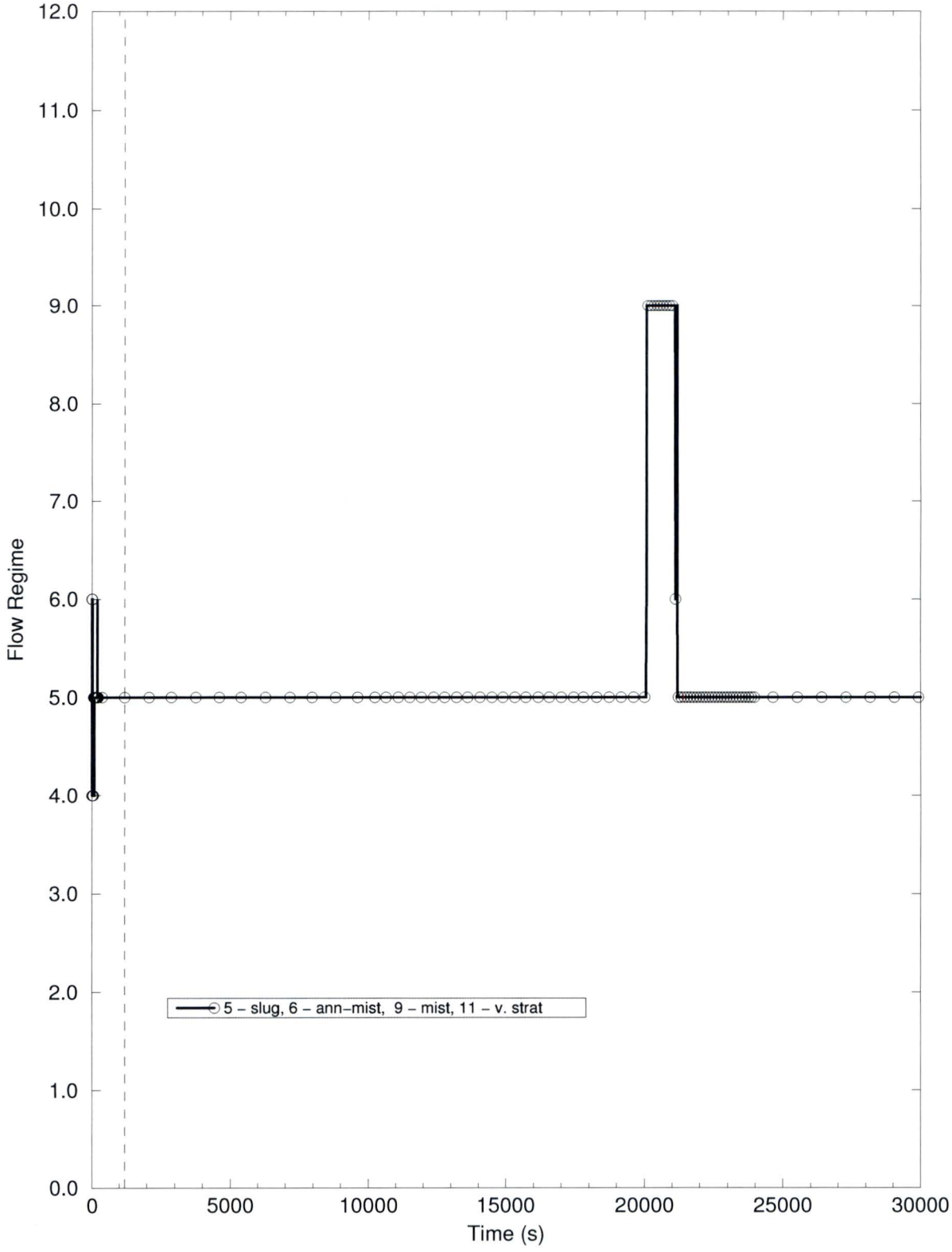

Figure RAI-4.23-11: Upper Plenum Flow Regime - 2nd Node above Average Core

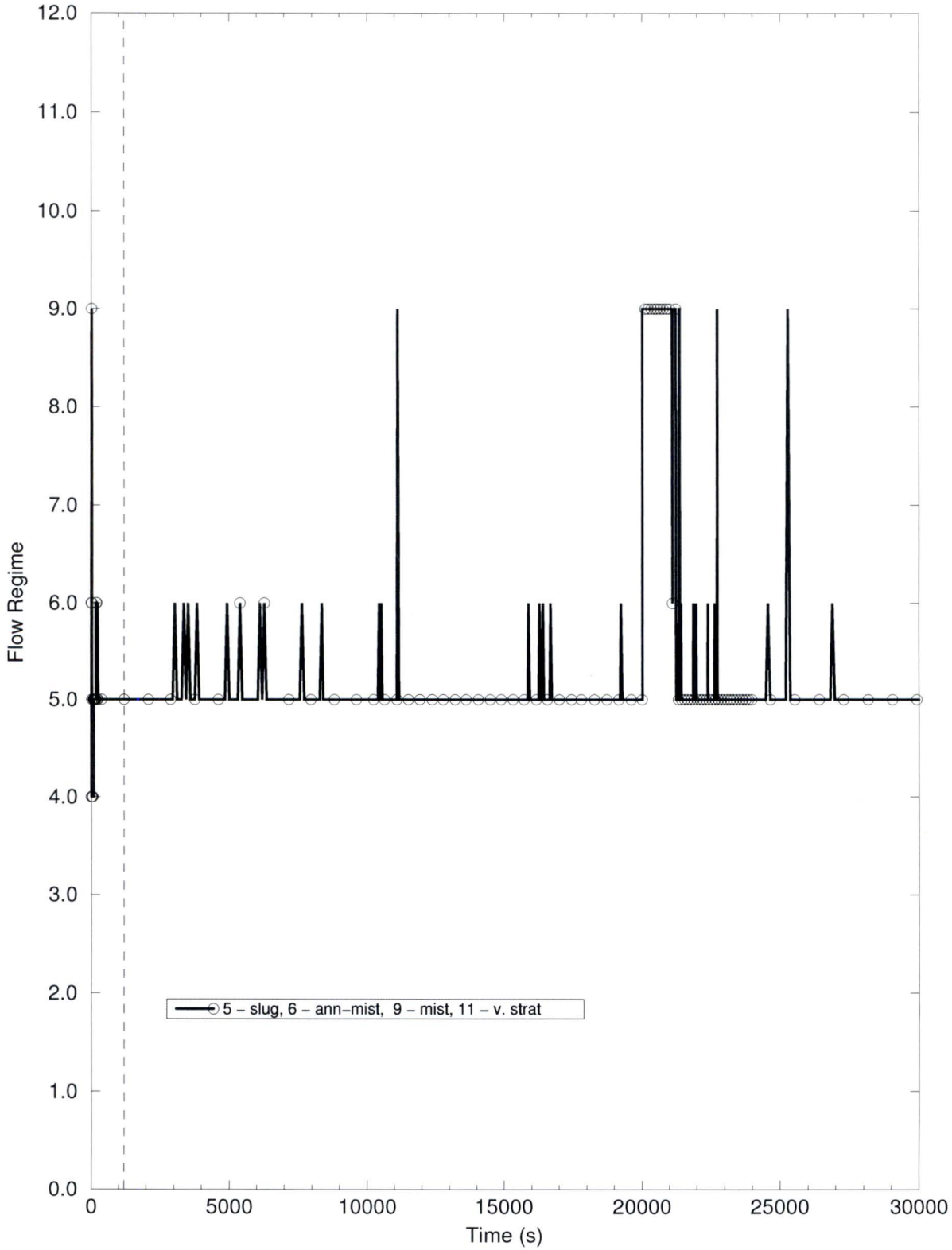

Figure RAI-4.23-12: Upper Plenum Flow Regime - 3rd Node above Average Core

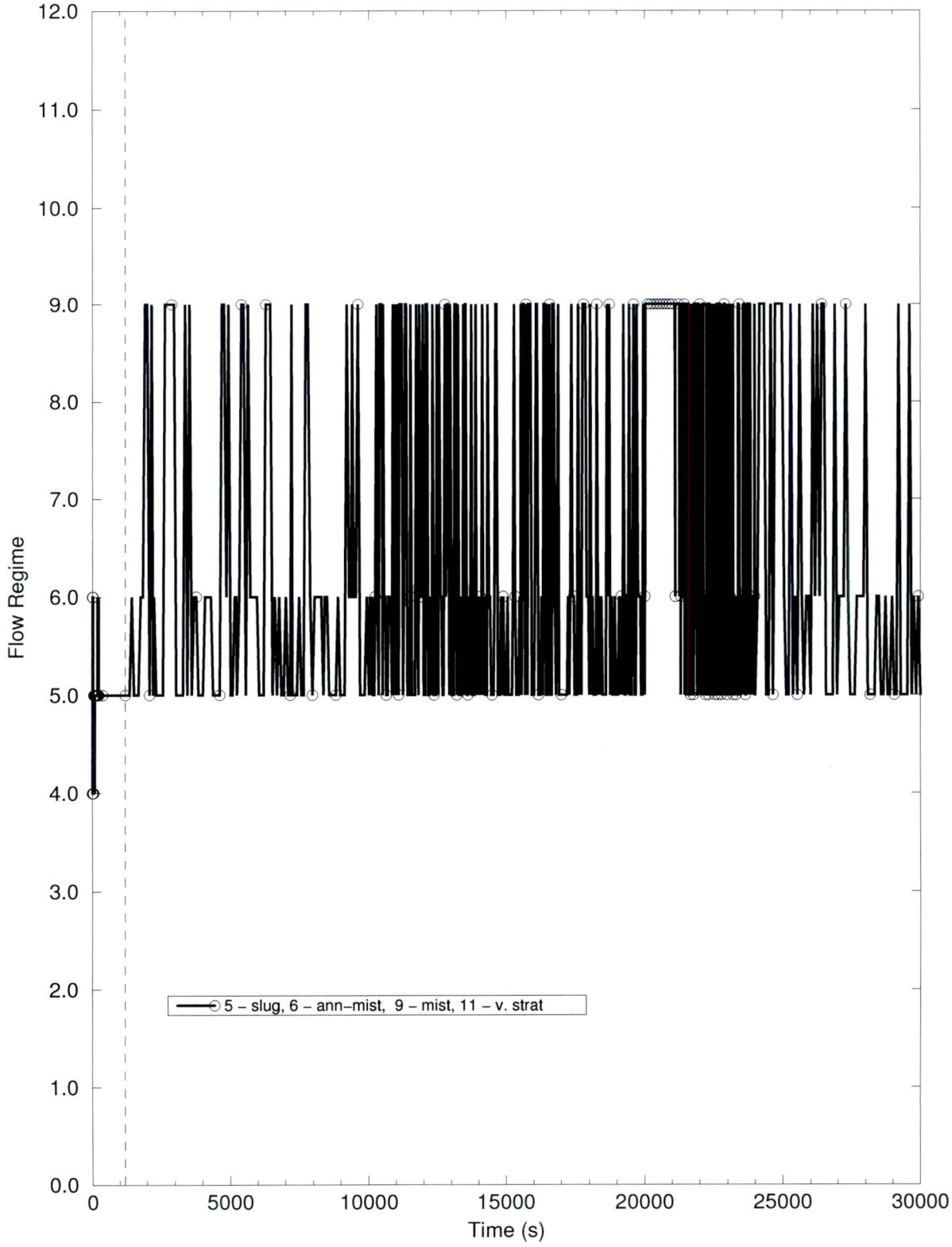

Figure RAI-4.23-13: Average Core vs. Peripheral Core Mass Flux at Core Outlet

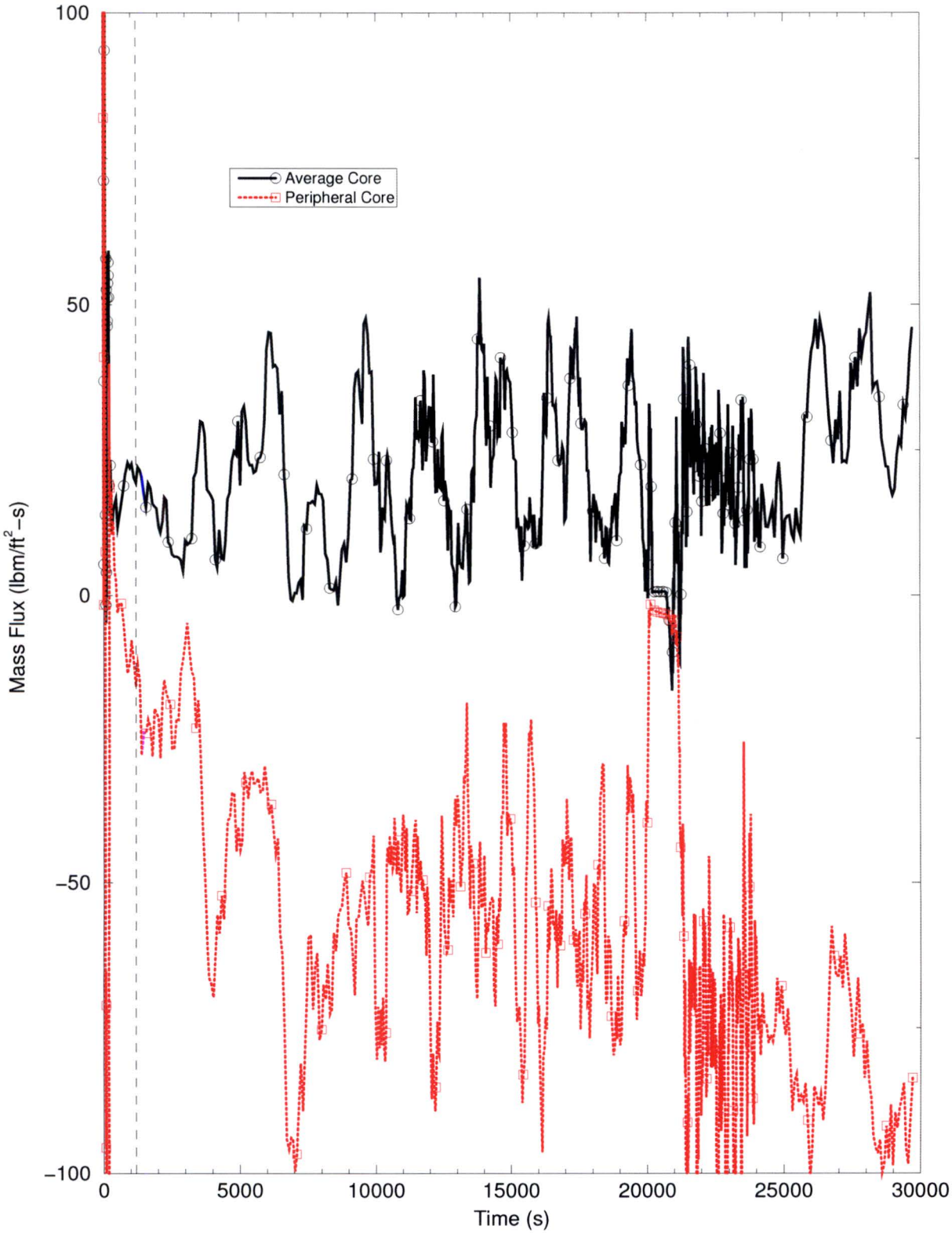

2.23.2.3 Boric Acid Precipitation Time

A simple, but conservative, analysis for the Boric Acid Precipitation Control (BAPC) criteria for GSI-191 was performed for the CE plant-type. The CE fleet were compared by comparing the ratio of the nominal core power to the core fluid volume for each plant (Table RAI-4.23-1). This comparison lead to the conclusion that the use of the GSI-191 representative plant was a justified choice for the BAP analysis since it has the highest core power to volume ratio. A higher core power to volume ratio means that there is a potential to concentrate the boron faster. The goal of this calculation is to provide a conservative estimate of the time the plant can spend after t_{block} without recovering the core mixture back to the HL elevation and reestablish a two-phase break flow condition. If too much time passes before the plant can reestablish flow to the HL, there is a risk that the boric acid concentration to build to such a level in the core that the boron precipitates out of solution as could cause localized blockages within the core.

Table RAI-4.23-1: Core Power to Volume Ratio

Plant Name	Nominal Power (MWt)	Core Volume (ft^3)	Power to Volume (MW/ft^3)
Arkansas 2	3026	558.8	5.415
Calvert Cliffs (1 and 2)	2737	605.5	4.520
Ft. Calhoun	1525	351.0	4.345
Millstone 2	2700	605.1	4.462
Palisades	2565.4	642.8	3.991
Palo Verde	3990	749.4	5.324
SONGS	3438	674.8	5.095
St. Lucie 1	3020	605.5	4.988
St. Lucie 2	3020	619.6	4.874
Waterford 3	3716	683.7	5.435
Representative	3458[2]	607.3[3]	5.694

Table RAI-4.23-2 lists the S-RELAP5 cases (based on the representative CE plant model) that were analyzed to determine the limiting case in terms of BAPC. The first three cases (Case 1 – 3) analyzed were designed more for PCT with a top-peaked axial power shape. Based on these cases (Case 1 – 3), the power shape was changed to a

[2]Includes uncertainty.

[3]Assumes 10% mixing volume reduction from SONGS.

bottom peak since a bottom peaked power shape normally means a lower core inventory, which is conservative for BAP. The bottom-peaked cases analyzed for BAP are Cases 4, 5, and 6. The S-RELAP5 runs were used to determine the minimum core mixing volume after t_{block}. The mixing volume is one of the most important factors in determining the precipitation time. For this BAP analysis, only liquid in the core region is included in the mixing volume. The LP, Lower Head (LH), baffle region, guide tubes, etc. are not included in the volume since there may not be good communication with the core and cannot be guaranteed to be well mixed. Any fluid in the upper region of the vessel (UP, Upper Head (UH), etc.) are also excluded in the mixing volume since the level corresponding to the minimum mixing volume is typically below these regions.

Table RAI-4.23-2: S-RELAP5 Cases Analyzed for BAPC

Case	Description
Case 1	1.0x Decay heat, top-peaked axial, special UP model on
Case 2	1.2x Decay heat, top-peaked axial, special UP model on
Case 3	1.2x Decay heat, top-peaked axial, special UP model off
Case 4	1.0x Decay heat, bottom-peaked axial, special UP model on
Case 5	1.2x Decay heat, bottom-peaked axial, special UP model on
Case 6	1.2x Decay heat, bottom-peaked axial, special UP model off

A variety of conservative assumptions were placed on the BAP calculation performed for all cases. They are listed as follows:

- A 1.2x multiplier on the American Nuclear Society (ANS) 1979 decay heat Standard (Reference 4.23-1) is used for calculating the steaming rate for all cases for the BAP time calculation, except for a sensitivity study performed on the limiting case with a 1.1x multiplier on the ANS 1979 decay heat Standard. This sensitivity study used a 1.1x multiplier on the decay heat for the S-RELAP5 run (for the minimum mixing volume), as well as in the computation of the steaming rate for the BAP time. More power means reaching the BAP time more quickly. Actinides are included.
- Mixing volume only considers the core region. Other regions are not included since they may not mix well with the liquid in the core region.
- Considers cases with a strong bottom-peaked axial power shape. The bottom peak means more level swell and a lower core inventory, which is conservative for BAP.
- The boric acid precipitation limit is set at 50,000 ppm. This is on the low side for the solubility limit at 212 °F. Besides rounding down the limit, this limit also includes a

4% weight reduction on the solubility limits. In addition, the containment pressure may be higher than 14.7 psia at this time, which would result in a higher saturation temperature, and the solubility of boric acid increases with temperature. The use of this limit is conservative. In addition, other chemical species that may form in the sump due to reaction with the buffering agent typically have a much higher solubility limit in water than pure boric acid. Example chemical species are H_3BO_3 and B_2O_3.

- The minimum mixing volume is held constant for this analysis. Makeup water from the sump is just enough to match boil-off due to decay heat and retain this minimum mixing volume. In reality, the minimum mixing volume only occurs briefly. The initial mixing volume (just after t_{block}) is higher and then the mixing volume reduces while the boil-off due to decay heat exceeds the flow though the AFP. After momentarily reaching the minimum mixing volume, the core mixture level begins to recover as the flow through the AFP begins to exceed the boil-off rate after a short period, thereby increasing the mixing volume once again.
- In addition to using the minimum S-RELAP5 calculated mixing volume for this analysis, the minimum mixing volume is reduced by an additional 10% for greater conservatism and to cover the nominal core power density across the CE fleet.
- The core power is held constant at the power calculated at the time of t_{block}. The actual power continues to decay, albeit slowly.
- No boron is carried out of the break after t_{block} for this BAP analysis. In reality, some boron may be carried out in droplets and possibly within the steam itself.
- The sump boron concentration is assumed to be constant. In reality, as the boron concentration builds in the core, the concentration in the sump is reduced.
- Sump boron concentrations of up to 4000 ppm are considered. This is well above the typical maximum mixed sump boron concentration of 3000 ppm.

The most limiting case was determined to be Case 5. This is expected as this case uses a bottom-peaked axial power shape, which promotes additional swell and leads to a lower inventory. This case also uses the special UP model, which increases the amount of water carried out of the HL and to the break. This limiting case was analyzed with both a 1.1x and a 1.2x multiplier on the ANS 1979 decay heat Standard (Reference 4.23-1). A decay heat above nominal leads to a lower minimum mixing volume (more level swell) and also concentrates the boron more rapidly due to the higher steaming rate. A summary of the calculated precipitation time as a function of sump boron concentration is provided in Table RAI-4.23-3 for this limiting case.

Table RAI-4.23-3: Limiting Case Precipitation Time

Sump Boron Concentration (ppm)	Precipitation Time	
	1.1x Decay Heat (s)	1.2x Decay Heat (s)
2000	9044.4	7252.5
2250	7972.9	6387.6
2500	7115.6	5695.7
2750	6414.3	5129.5
3000	5829.8	4657.8
3250	5335.2	4258.6
3500	4911.3	3916.4
3750	4544.0	3619.9
4000	4222.5	3360.4

The earliest BAP time calculated is 4220 seconds after t_{block} with a 1.1x multiplier on the ANS 1979 decay heat Standard. This is with a set of conservative assumptions and assumes a mixed sump concentration of 4000 ppm. In reality, the sump concentration will likely be no more than approximately 3000 ppm using maximum Technical Specifications (TS) boron concentrations for each source of boron. This is because most of the water added to the sump will be below 3000 ppm. For instance, the RCS is typically not more than about 2400 ppm (at Beginning of Cycle (BOC)). The water from the Refueling Water Storage Tank (RWST) will be approximately 2800 ppm. The Safety Injection Tank (SIT) concentration may be a bit higher (3500 ppm, for instance), but the water in the sump is dominated by the RCS water and the RWST water. Therefore, a more realistic time to reach the precipitation limit, even with conservative assumptions, will likely be 5830 seconds, or longer, after t_{block} assuming a 1.1x multiplier on the decay heat. In addition, even if a 1.2x multiplier on the decay heat is used instead, the BAP time at 3000 ppm will be at least 4650 seconds.

If flow can be restored and the core level recovered to the HL elevation within this time frame, there is no risk for BAP. The core will typically recover on its own quickly after after t_{block} as the level in the DC builds, which then leads to sufficient flow through the AFP to overcome the core boil-off due to decay heat and to cover the mixture level to the HL elevation. In the CE analysis presented in the response to RAI 4.1b, the predicted time to recover the UP to the HL elevation by the S-RELAP5 code is approximately 1500 seconds, which is significantly less than the conservatively calculated BAP time. In addition, CE plants may have initiated Hot Leg Injection (HLI) prior to this time. The use of HLI will recover the core inventory rapidly and will provide a flushing flow to preclude a build up in the boric acid concentration.

2.23.2.4 Summary

Liquid accumulation and void distribution in UP and liquid flow from the UP to containment following the complete core inlet blockage were estimated using following approaches.

- Available air-water test data.
- Wilson et al. and Cunningham-Yeh correlation.
- UP geometry of the CE plant model used in the WCAP-17788-P analysis, along with a conservative value for the average void fraction in the UP below the HL nozzle.

The S-RELAP5 models and correlations were reviewed to identify the flow regimes and interphase drag correlations used in the code that is appropriate for the expected flow conditions in the UP during this period. The CE base case calculated using S-RELAP5 was reviewed. From these studies, the following conclusions are made:

- A conservative estimate of the average void fraction in UP below the HL nozzle following t_{block} is 60% before liquid can flow out from UP to containment.
- S-RELAP5 calculates a reasonable void distribution in the UP considering the geometry of the UP and the relatively large steam velocity in the HL nozzle. It is estimated that there is about 400 second uncertainties in the S-RELAP5 calculated timing for the liquid discharge through the vessel side of the break following t_{block}.
- In the base CE model, S-RELAP5 calculated a 1500 second delay after t_{block} for liquid discharge through the Reactor Vessel (RV) side of the break.
- For the CE base model, 1900 seconds is the maximum expected delay after $_{block}$ for liquid discharge through the RV side of the break, once a 400 second uncertainty is applied.

While it is conservatively estimated that the UP inventory will recover and return the mixture level to the HL elevation in no more than 1900 seconds after t_{block}, a conservative estimate of the BAP time assuming a sump mixed-mean concentration of 3000 ppm is at least 5830 seconds. Based on these calculations, BAP is not a real concern for the CE plants in the WCAP-17788-P analysis. As such, the focus on liquid carryout to the break can be on ensuring that the PCT criterion is conservatively met.

2.23.2.5 Part a

On the Steam Generator (SG) side of the break, there are a limited number of liquid transport mechanism of liquid discharge to the break after the initial blowdown phase. There are two main liquid transport mechanisms on the SG side of the break.

- The first mechanism can only transport a limited amount of liquid. The first liquid transport mechanism is due to the fact that the SGs are modeled as bottled up just after the event initiation. Once the reactor trip occurs, a turbine trip is initiated. Once the path to the turbine is closed, no steam is modeled to be released. As such, the SGs remain hot. If liquid makes it into the Cold Leg (CL) side of the broken SG due to the added resistance at the core inlet, the hot walls of the tubes will create steam, which can potentially carry liquid up to the top of the u-tubes and out the break. This process is likely overestimated as the Loss of Coolant Accident (LOCA) SG model has a coarse noding in the u-tubes as it is not designed to be refilled during the transient. The code tends to homogenize the fluid in the nodes and the liquid could be spread over this large surface area and generate more steam than in reality. This liquid transport mechanism is limited as when this steam is produced, it removes energy from the SG secondary side. The secondary side will eventually cool off as this process continues and the mechanism will eventually cease to exist once the secondary side temperature approaches the primary side temperature.
- The second liquid transport mechanism is when the resistance to the core and Barrel/Baffle (BB) are high, and the ECCS flow exceeds what can enter the core and BB with the given available elevation head, the ECCS can eventually fill the SG u-tubes (after going through the first liquid transport mechanism phase) and the excess ECCS can spill over the top of the u-tube bend and exit the break. The majority of the flow will spill on the broken side and go out the break directly, since the pressure is lower on this side. Some liquid may also sporadically spill on the intact SG side, mix with fluid in the UP and then exit the break on the RV side of the break. However, the response to RAI 4.30 shows that the liquid transported through this path is negligible.

On the RV side of the break, the liquid transport mechanisms are more complex.

- In the short term phase (prior to Sump Switch Over (SSO)) droplet entrainment can exist due to high steam velocities.
- As the decay heat reduces, the steam velocities are not high enough for droplet entrainment. Prior to the blockage, the mixture level has a froth that is swept out to the broken HL and that is the primary liquid transport mechanism during this phase.

- As blockage occurs (at t_{block}), the collapsed level and mixture level drops in the core as the decay heat initially exceeds the makeup flow from the AFP and the blocked core. As such, the mixture level falls out of the HL for a period.
- The level in the DC begins to build in order to overcome the higher inlet resistance until the flow through the AFP can exceed that needed to match boil-off due to decay heat. The mixture level then recovers until it reaches near the bottom of the HL. Some liquid can be swept out prior to the averaged core mixture level reaching the HL elevation. This is due to a relatively high steam velocity sweeping across the top of the mixture, which can drag liquid up and out the HL.
- Since the WCAP-17788-P methodology is built from the short-term RLBLOCA methodology, the code/methodology is realistic to conservative relative to leading to a lower core inventory and a higher PCT.

The CE plant model uses a special UP model that is used in the EMF-2103(P)(A) base methodology. This special model enhances the amount of liquid carried to the break, which is conservative from a PCT perspective. In addition, this model was used (along with a bottom-peaked axial power shape) in the BAP time calculation. This minimizes the core mixing volume, which results in an earlier estimated time to reach BAP.

2.23.2.6 Part b

The short-term LOCA behavior is extensively benchmarked for S-RELAP5 in EMF-2102 (Reference 4.23-4) and in EMF-2103, Revision 3 (Reference 4.23-3). The S-RELAP5 code shows good agreement in the short-term LOCA phase, where the phenomena are substantially more complex than what is expected during the Long Term Core Cooling (LTCC) phase.

From the core region, the primary transport mechanism of liquid to the break after the time of SSO is a mixture level (froth) that reaches the HL elevation and is swept out to the break. As such, the primary drivers of this relate to the mixture level swell prediction. The code predicted level in the core region have been benchmarked in EMF-2102 (Reference 4.23-4) and in EMF-2103(P)(A), Revision 3 (Reference 4.23-3), as well as in RAI 4.8. The predicted level swell for the benchmarks performed show a reasonable-to-excellent comparison with the experimental data.

For the majority of the transient (prior to t_{block} and again after the mixture level returns to the HL elevation after t_{block}), the liquid flowing from the core to the broken HL is dictated by the amount of excess ECCS that enters the core. The mixture level will contain a froth that is swept out to the broken HL and the rate is set by the ECCS water that enters the core (through the core inlet or the AFP) minus the water that is boiled off due to decay

heat. The level will swell based on the local steam generation rate along the core, as well as the correlation of that steam production to a local void fraction. During these periods, the transient is in a quiescent pseudo-steady state where the collapsed and mixture levels in the core are approximately constant, with some variation as the decay heat reduces with time. Since whatever excess ECCS enters the core is what spills out during these periods, the most important factors in how much flow spill out is the AFP resistance and the ECCS injection rate (along with the resulting rise in DC level after t_{block}). However, the liquid carry-out during these periods is of little consequence since the core remains covered and a flushing flow is available to preclude any BAP concerns.

During the period where the core mixture level is into the HLs, there is no concern from the PCT aspect, nor the BAP aspect of the acceptance criteria since the core is covered and there is liquid throughput which negates any potential build-up in the boron concentration within the core.

The TH analyses show a relatively short period of time where there may be differences in the liquid the carry-out rate between the code and reality. This is just after t_{block}, where the level starts to decrease due to the boil-off rate due to decay heat exceeding the makeup of ECCS entering the core. When the mixture level is just below the HL elevation, the steam sweeping across the mixture surface can drag liquid towards the broken HL and skew the void fraction distribution in the UP. If the mixture level is not too far below the bottom of the HL, there is a potential for liquid to be swept out. As the level in the core/UP continues to fall, the liquid flow to the break from the core will cease for a period. Once the DC level builds to drive enough flow through the AFP to exceed the core boil-off rate, the level in the core/UP recovers. As the mixture level approaches the bottom of the HLs, there is again potential for steam to sweep the liquid out the break. As the mixture level rises further, it will become more like a froth that is swept out to the broken HL, much like the process before the blockage was imposed. However, as mentioned in the technical basis provided above, there is a substantial margin in the time where there is potentially no liquid flow to the HL and the BAP time.

Because of the reasons above, the effect of liquid carry-out is of no concern as it relates to BAP. In terms of PCT, the model used in the TH analyses for the CE plant follows that of the base RLBLOCA methodology, which is biased towards carrying more liquid out, which reduces core inventory and is conservative from the PCT perspective.

2.23.2.7 Part c

The special UP model used in the base RLBLOCA methodology for the CE plants is activated in the TH analyses to increase the liquid being carried to the break. In the base Evaluation Model (EM), this special UP model is used to enhance carry-out of liquid to the hot leg and steam generator, which enhances the steam binding effect. For the HL

break scenario in WCAP-17788-P, there is no steam binding effect, but this enhanced liquid carry-out reduces core inventory and is conservative from a PCT point-of-view.

Sensitivity studies were performed to determine the impact of the UP special entrainment model. These studies were performed with the special UP model on or off for values of the decay heat multiplier of 1.1 and 1.2. Comparisons of the amount of fluid entrained and expelled out the break show more liquid being lost for the cases with the special model enabled, compared to cases with the special model disabled. This is the natural consequence of the special entrainment model tendency to over-predict liquid carry-over. This is evident regardless of the magnitude of the decay heat multiplier - in both cases the deactivation of the special entrainment model precludes a post-blockage heat-up. The comparisons show that most of that difference in RV due to the UP special entrainment model occurs early on in the transient (in the 1200 to 4000 seconds time range). Consequences of this initial difference are persistent through the later stages of the transient, as the other boundary conditions are unchanged between the cases.

The vertical stratification model in the UP is normally activated in the base RLBLOCA methodology. However, it was determined that the vertical stratification model should be deactivated for the WCAP-17788-P TH analyses for the CE plant-type. The vertical stratification model was deactivated because it was found that for the HL break with the selection of atmospheric pressure containment boundary condition resulted in flow regime oscillations. The flow regimes in the UP nodes located just below the HL connection fluctuated between stratified and non-stratified flow regimes, which would have introduced numerical flow oscillations. Therefore, including the vertical stratification model was not selected for the GSI-191 application.

Break multipliers were used that are consistent with the base RLBLOCA methodology for the CE plants. The break multipliers (break discharge coefficients) were applied to both sides of the break and biased high to maximize the loss of inventory during the short term LOCA phase. However, these discharge coefficients are applied to the subcooled and two-phase choked flow calculations, which only occurs during the early phase of the transient when the break flow is choked. After core reflood, the break flow is unchoked and the break discharge coefficients no longer have an impact on the break flow rate. During this period, the flow out of the break is just the steam flow due to decay heat and excess ECCS liquid flow.

2.23.2.8 Part d

After the initial blowdown phase and the following core reflood, the system is in a pseudo-steady, quiescent state with the boiling in the core and a mixture level that is into the HLs. The rate of liquid being spilled out the break is simply the amount of excess ECCS that reaches the core. As such, there are no special correlations needed to

calculate this. The system can be represented in a macroscopic sense as a simple energy and mass balance calculation.

As mentioned in the response to RAI 4.23b, in the vast majority of the transient, the amount of liquid going to the break is simply the excess ECCS. When the level gets too low after t_{block}, no liquid is carried out. There is only a relatively brief period where the code can sweep liquid out of the break while the mixture level is just below the HL elevation.

As the sweep out period between t_{block} and subsequent recovery of the mixture level to the HL is relatively brief, there is no impact from a BAP perspective, as it has been determined that there is significant margin between the code-calculated mixture level recovery time and the conservatively-calculated BAP time. In addition, from a PCT perspective, the methodology is already skewed towards carrying out more liquid and leading to a higher PCT. This is on top of the other conservative assumptions used in the TH analyses, leading to a conservatively predicted PCT.

2.23.2.9 Part e

The requested plot data for Item e above is the same as that requested for RAI 4.17c, Item i. The instantaneous data are plotted in Figure RAI-4.17-1. The integrated data are plotted in Figure RAI-4.17-6.

The two-phase mixture level on the core side of the RV is into the UP region for the majority of the transient as described throughout this RAI response (see also Figure RAI-4.23-5). The code predicted void fraction in the bottom node of the UP is around 60% (Figure RAI-4.23-2), which is consistent with theory as described in the technical basis section above. After the time of t_{block}, the mixture level decreases since the flow through the AFP is not sufficient to match decay heat just after the blockage is applied. This is due to the nearly instantaneous blockage at the core inlet modeled. This requires the level in the DC to build in order to drive sufficient flow through the AFP to match decay heat. The collapsed liquid level in the core is shown in Figure RAI-4.27-3. This figure shows a smooth behavior with a trending upward value of liquid level as the decay heat decreases. The collapsed liquid level in the core is consistent after the core recovers post-t_{block} with the value prior to t_{block}. The PCT trace in Figure RAI-4.27-7 also shows that the core remains covered, except for a brief period just after t_{block}. Tables RAI-4.9-2 and RAI-4.9-3 in the response to RAI 4.9c provide a snapshot of the void fraction profile close to the time of PCT.

The requested plot data for Item iii above is the same as for RAI 4.17c, Item v., which is plotted in Figure RAI-4.17-5.

The predicted pressure difference between the upper plenum cell connected to the broken hot leg pipe and the containment backpressure is provided in Figure RAI-4.23-14.

Figure RAI-4.23-14: Predicted Pressure Difference between the UP and the Containment Backpressure

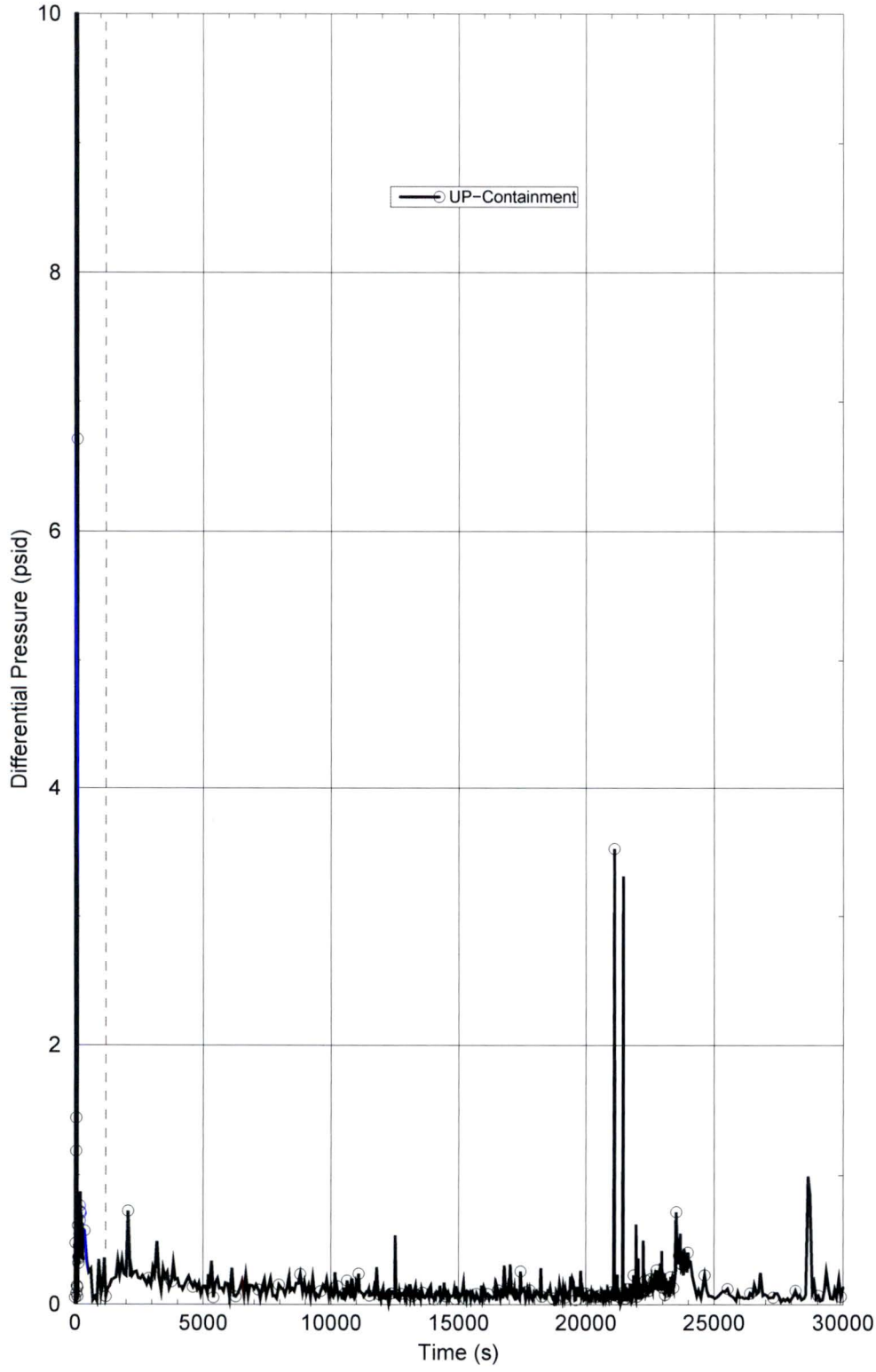

2.23.2.10 Part f

In order to better compare the figures in question, the break equilibrium quality is compared between the original WCAP-17788-P submittal and the errata submitted in the February 12, 2016 letter OG-16-42 (Reference 4.23-14) in Figure RAI-4.23-15 and Figure RAI-4.23-16. It can be seen that the SG side of the break matches between the two cases until the time of t_{block}. On the other hand, the vessel side of the break matches until approximately 11,000 seconds, where the quality starts to differ. The only differences between these two cases during this period is the requested major edit frequency and the restart edit frequency. For the original case, the major edit and restart edit were requested every 1,000 seconds during this period (from 10,000 seconds until $_{block}$) whereas the revised case requested the edits every 10,000 seconds during this same period. As these cases are long and the output files are large, this was an attempt to make the files more manageable in size. The major edit and restart edit frequency has some potential to alter results since the code adjusts its time step to cause a major edit (or a restart edit) at the requested point. The change in time step can lead to a different solution. Although some intermediate trends can change with a modified time step, the overall conclusions remain the same.

In RAI 4.1b, the CE TH analysis is revised to include several updates and is the current and correct analysis for review. Sensitivity studies were performed on t_{block} and the results are confirmed to be identical prior to t_{block}, as expected.

Figure RAI-4.23-15: Vessel Side Break Equilibrium Quality Comparison

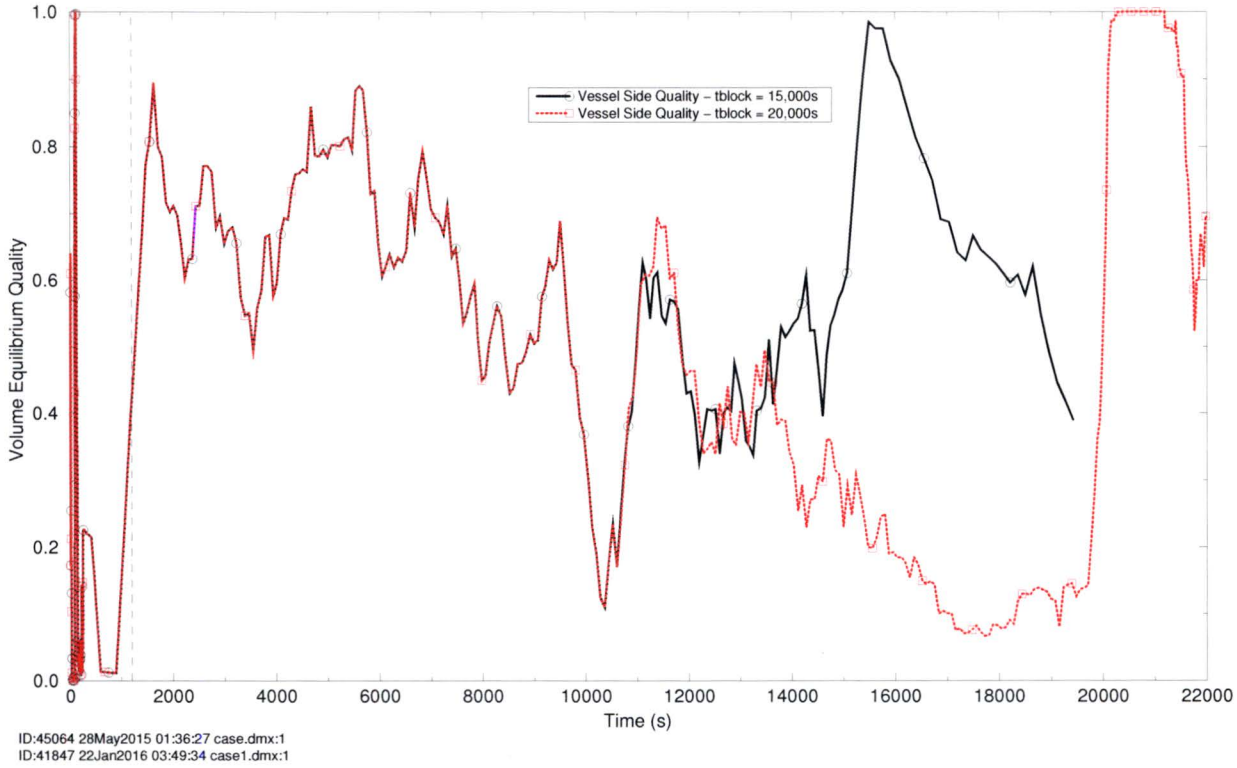

Figure RAI-4.23-16: SG Side Break Equilibrium Quality Comparison

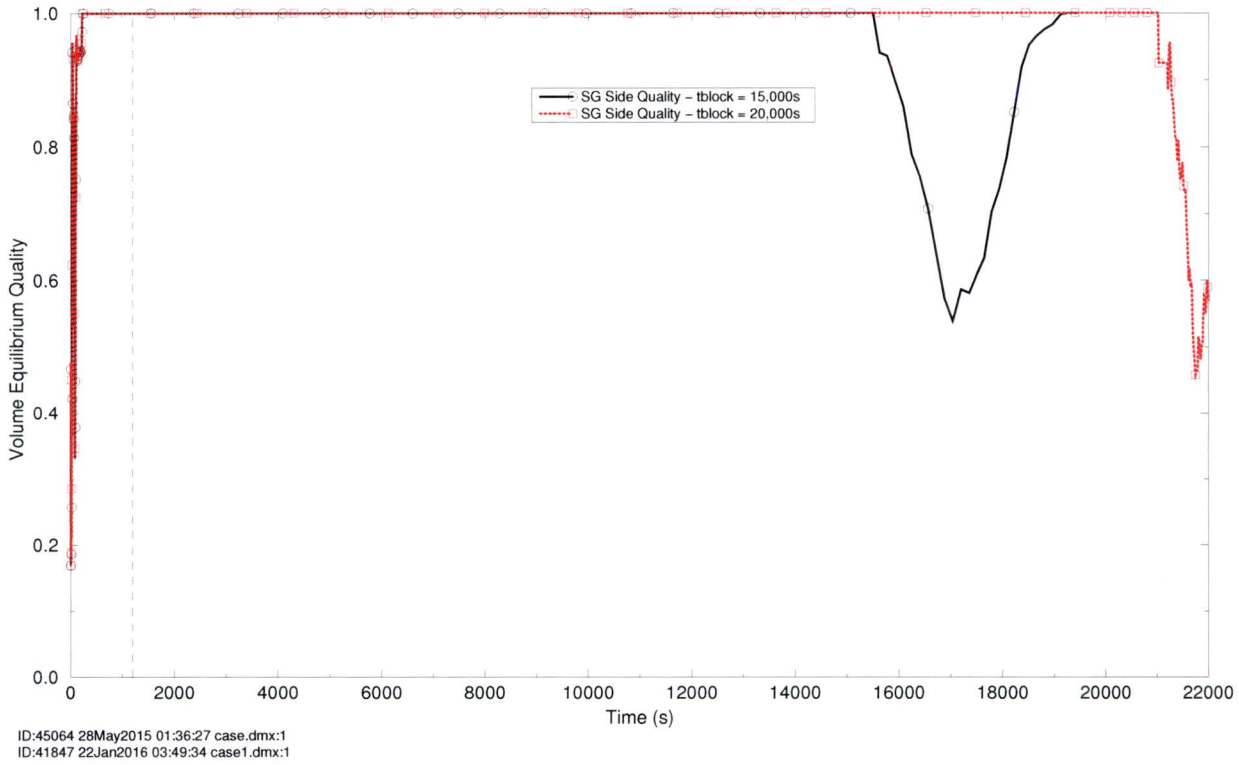

2.23.2.11 Part g

As described in the response to RAI 4.1b, the UP was refined to include [ ] in the vertical direction below the HL connection as opposed to [ ] used in the original TH analyses for the CE plant category. As the code tends to homogenize the fluid within a given node, having the additional nodes in the axial direction better models the void fraction profile below the HL connection.

Several sensitivity studies were performed as part of this set of Requests for Additional Information (RAIs). The most direct sensitivity study related to this particular RAI is a sensitivity on having the special UP entrainment model being activated or deactivated. In either scenario, there is a period where the mixture level falls below the HL elevation where the liquid flow from the core to the HL ceases. However, in the various cases examined, the period of no liquid flow to the break is well below the calculated BAP time. As shown in Figure RAI-4.23-17, there is little impact to the UP level, or the period of no flow to the break from the core, with either option. This is consistent with the expectation described in the response to RAI 4.8a. In addition, it was found that the model with the

special UP entrainment model activated resulted in a higher PCT, as expected. Since BAP was found to be not a concern for either situation and that the PCT is higher when the special UP entrainment model is activated, the special UP entrainment model will remain activated for the AREVA TH analyses for the CE plant category.

Figure RAI-4.23-17: Special Upper Plenum Model Comparison

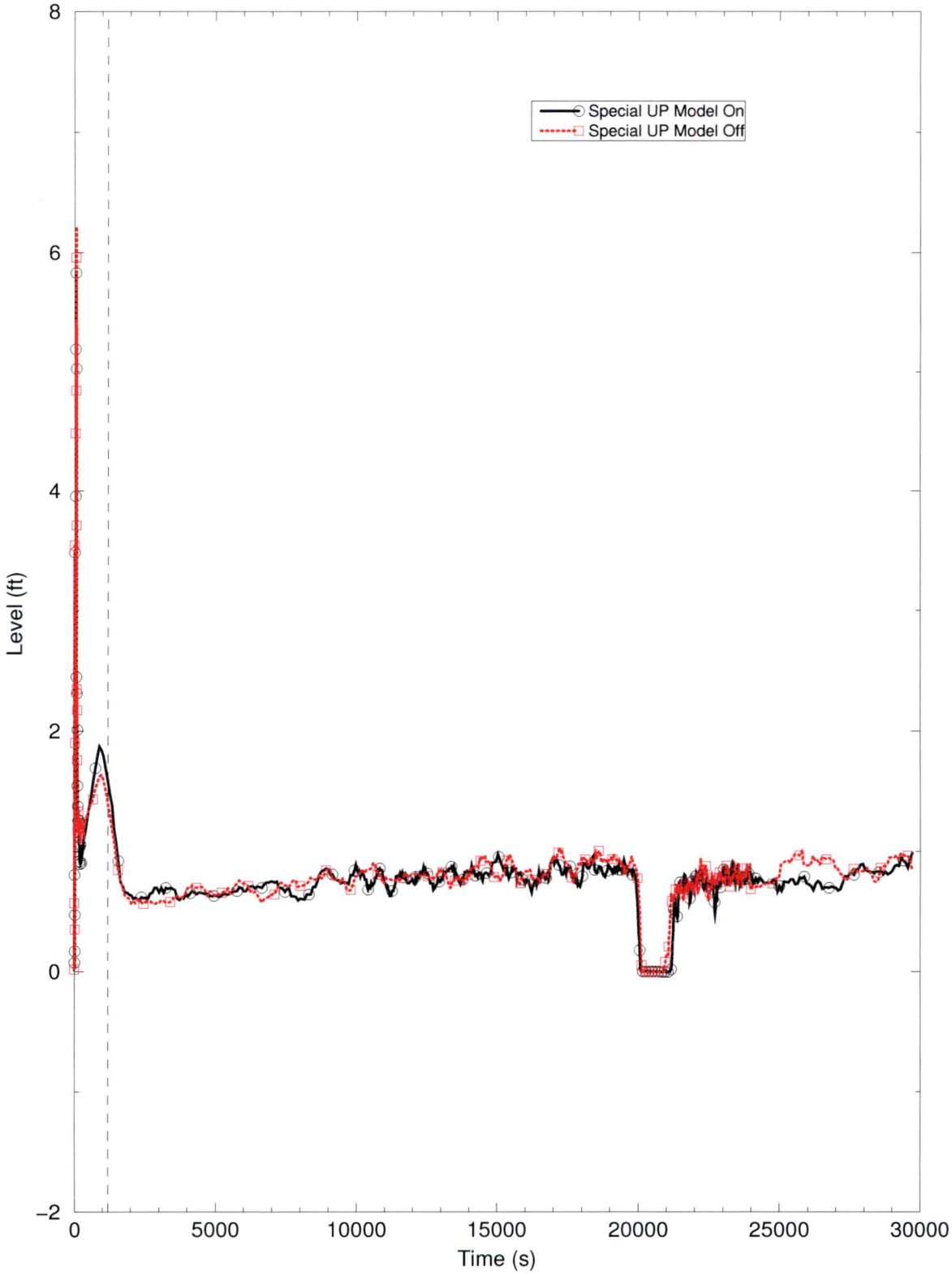

2.23.2.12 Part h

The substantial scatter in the m_{split} results are not related to the break behavior, but are instead related to two-phase instabilities expected in the downcomer and core. Some of these oscillations can be due to the classical "boiling channel instabilities" and instabilities due to flow regime transition. As phase changes occur in the downcomer and core region, the manometric balance is disrupted, resulting in sudden changes in flow. Some of these oscillations can also be numerical due to the discontinuities in the constitutive models. As explained in Section 7.5 of AREVA's topical report EMF-2103(P)(A) Revision 3 (Reference 4.23-3), AREVA's code developers of S-RELAP5, as well as the original Idaho National Laboratory (INL) code developers of RELAP5/MOD2, have made attempts to reduce the discontinuities between the correlations. Similar oscillations are also observed in various reflood benchmarks, including the FLECHT-SEASET benchmarks. These oscillations are amplified by the use of a very low pressure in the GSI-191 cases. Oscillations cause sudden changes in flowrates and make the instantaneous values of m_{split} very noisy.

It can also be observed from Figure 10-5 of Volume 4 of WCAP-17788-P, as well as Figure RAI-4.20-3 and Figure RAI-4.20-4, the oscillation decreases as ECCS flow increases. The CE plants have lower ECCS recirculation flow rates compared to Westinghouse and Babcock & Wilcox (B&W) plants, which makes the oscillation more obvious.

Figure 10-5 of Volume 4 of WCAP-17788-P presents results based on instantaneous values of m_{split} without any data smoothing. Conversely, the results shown in Figure 8-5 (Westinghouse upflow plant model) and 9-4 (Westinghouse downflow plant model) of Volume 4 of WCAP-17788 were smoothed.

To present data in a similar way, the new results presented in the response to RAI 4.20 used a 10 second running average to calculate m_{split} for the CE plants. As seen in Figure RAI-4.20-3 and Figure RAI-4.20-4, the oscillations are greatly reduced. The curves of m_{split} are smoothed out with much less scatter after using this smoothing approach.

2.23.2.13 Part i

Based on a conservative BAP calculation, it was found that the time where no liquid flow exits the core region is a much shorter period than the earliest possible time for BAP for the CE plants. A variety of sensitivity studies were performed, which varied things such as decay heat, the activation of the special UP entrainment model, variation in ECCS temperatures, etc. For all combinations examined, the duration of the lack of liquid flow from the UP to the broken HL is significantly less than the earliest possible time for BAP for the CE fleet. The results related to lack of liquid flow from the UP were found to be

generally insensitive to these changes. This is consistent with the expectation described in the response to RAI 4.8a. Even if the code predicted a liquid flow to the break earlier than reality, a theoretical analysis performed in the initial portion of this response estimates that the estimated additional time to fill the UP to the HL elevation is no more than an additional 400 seconds. This is still well before the BAP time. As such, it is clear that BAP is not a concern in the TH analyses for the CE plants.

Figure RAI-4.23-18 compares the UP level sensitivity with changes in decay heat. Higher decay heat has a slightly longer period before the UP inventory recovers after t_{block}, but is still significantly less than the BAP time. Likewise, Figures RAI-4.23-19 and RAI-4.23-20 compare the impact of changing the ECCS temperature after SSO and before SSO, respectively. For the ECCS temp sensitivity after SSO, the higher ECCS temperature makes the UP level recovery longer, but is still significantly less than BAP time. For the ECCS temperature sensitivity before SSO, there is no obvious difference in results.

From a PCT perspective, the WCAP-17788-P TH analysis for the CE plants closely follows the base RLBLOCA methodology. As such, the model contains certain biases, which cause more liquid to be carried out and result in a higher PCT prediction. For the liquid carry-out for the HL break performed in the WCAP-17788-P TH analysis is enhanced with the use of the special UP model, for example.

Figure RAI-4.23-18: Upper Plenum Level Comparison - Decay Heat

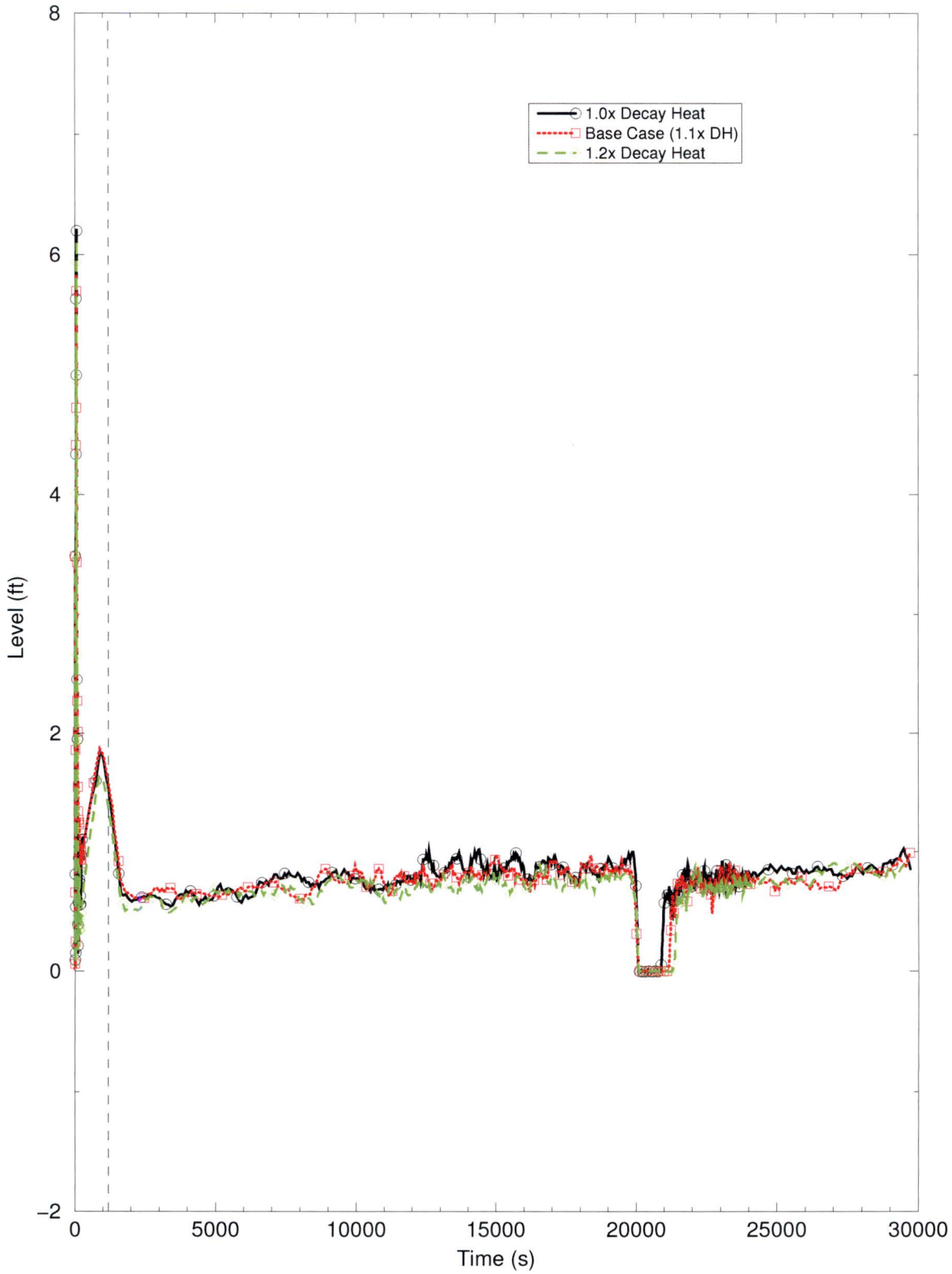

Figure RAI-4.23-19: Upper Plenum Level Comparison - ECCS Temperature after SSO

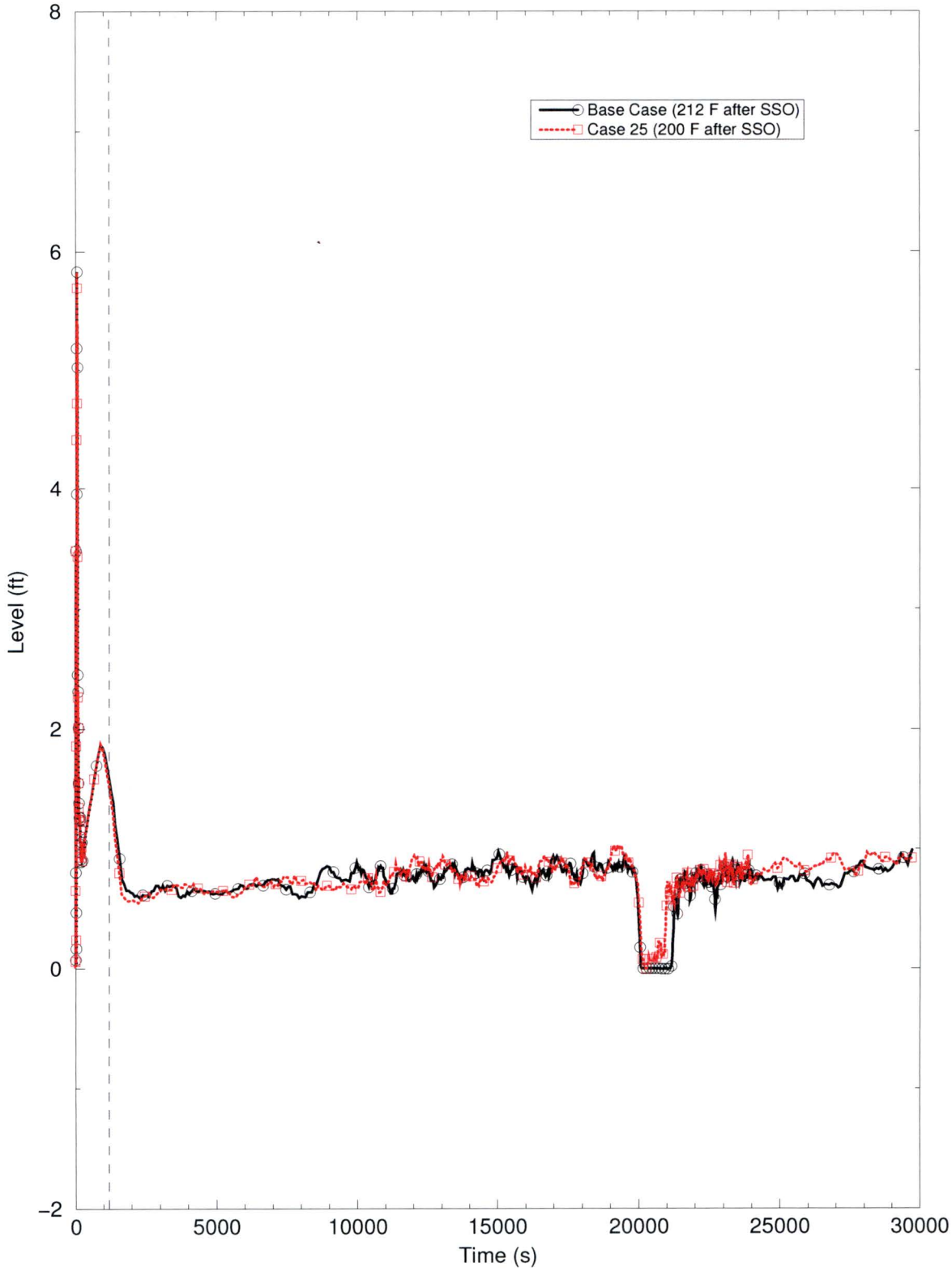

Figure RAI-4.23-20: Upper Plenum Level Comparison - ECCS Temperature before SSO

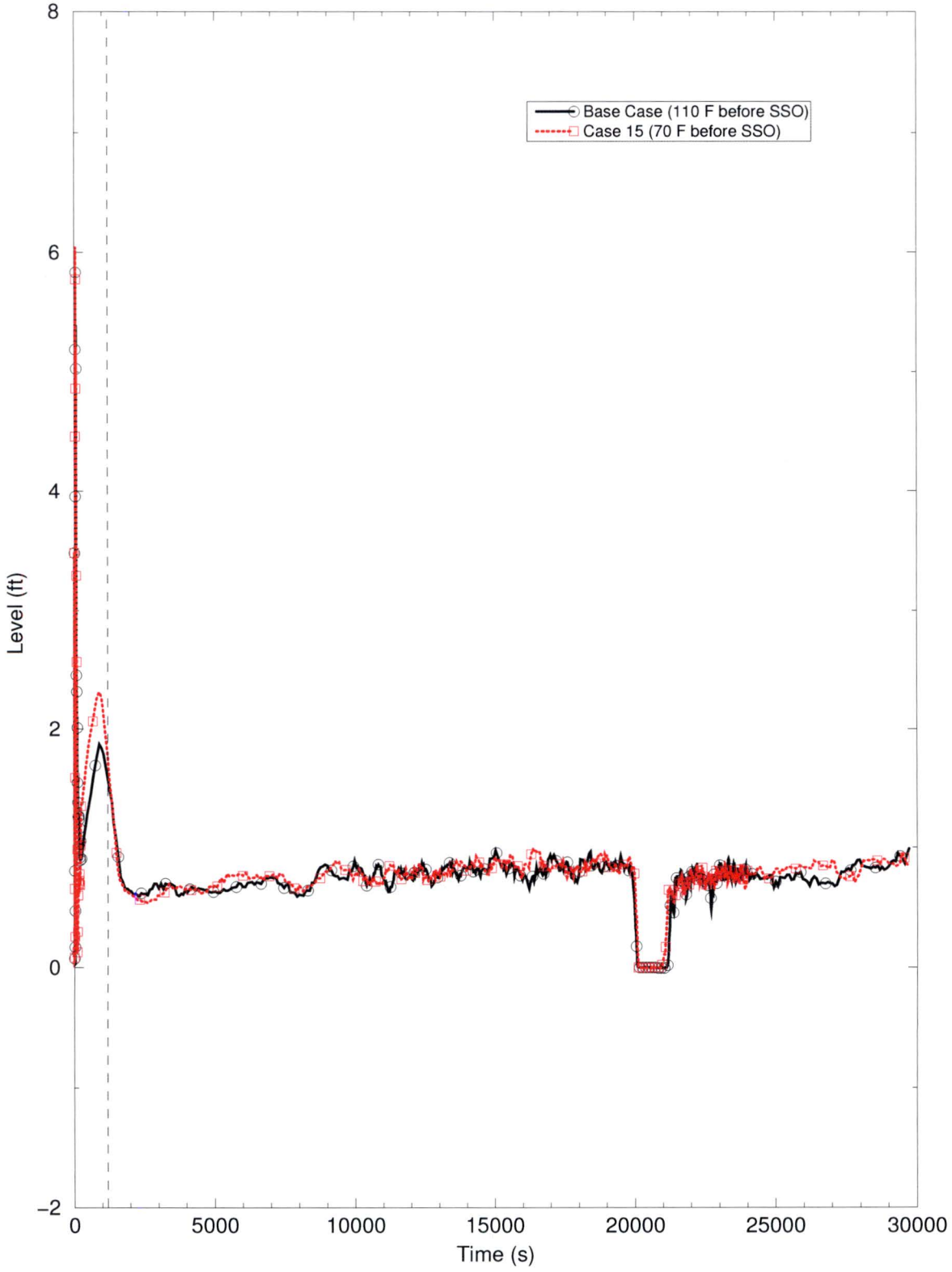

References - RAI 4.23

4.23-1 American Nuclear Society ANSI/ANS-5.1-1979, *American National Standard for Decay Heat Power in Light Water Reactors.*

4.23-2 AREVA Inc. Document EMF-2103(P)(A), Revision 0, *Realistic Large Break LOCA Methodology for Pressurized Water Reactors.*

4.23-3 AREVA Inc. Document EMF-2103(P)(A), Revision 3, *Realistic Large Break LOCA Methodology for Pressurized Water Reactors.*

4.23-4 AREVA Inc. Document EMF-2102(P), Revision 1, *S-RELAP5: Code Verification and Validation.*

4.23-5 AREVA Inc. Document EMF-2100(P), Revision 4, *S-RELAP5 Models and Correlations Code Manual.*

4.23-6 NUREG/CR-4312, EGG-2396, Revision 1, "RELAP5/MOD2 Code Manual, Volume I: Code Structure, Systems Models, and Solution Methods," August 1985.

4.23-7 NUREG/CR-5535, INEL-95/0174, "RELAP5/MOD3 Code Manual, Volume II: User's Guide and Input Requirements," June 1995.

4.23-8 Taitel, Y. and Dukler, A. E., "A Model for Predicting Flow Regime Transitions in Horizontal and Near Horizontal Gas-Liquid Flow," American Institute of Chemical Engineering Journal, Volume 22, pp. 47-55, 1976.

4.23-9 Wallis, G. B., "One Dimensional Two Phase Flow," McGraw-Hill, New York, 1969.

4.23-10 Wilson, J. F., et al., "The Velocity of Rising Steam in a Bubbling Two-Phase Mixture," Trans. Amer. Nucl. Soc., Vol. 5, pp.151, 1962.

4.23-11 Cunningham, J. P., and Yeh, H. C., "Experiments and Void Correlations for PWR Small-Break LOCA Conditions," Trans. Amer. Nucl. Soc., Vol 17, pp. 370-371, 1973.

4.23-12 Zuber, N., and Findlay, J. A., "Average Volumetric Concentration in Two-Phase Flow Systems," J. Heat Transfer, pp. 453-468, 1963.

4.23-13 Osakabe, M., Koizumi, Y., and Tasaka, K., "Interfacial drag Coefficient of Air-Water Mixture in Rod Bundle," J. of Nuc. Sc. And Tech., 21(11), pp. 882-884, November 1984.

4.23-14 Letter OG-16-42, Jack Stringfellow (PWROG) to Document Control Desk (NRC), "Submittal of Errata Pages for WCAP-17788-NP, Revision 0, Comprehensive Analysis and Test Program for GSI-191 Closure (PA-SEE-1090)," February 12, 2016.

2.24 RAI 4.24

2.24.1 Statement of RAI 4.24

Figures 8-9 and 9-8 indicate that the total ECCS injected masses for the Westinghouse upflow and downflow design categories increase significantly at SSO even though the injection rates appear to be constant both prior to and after the observed stepwise change at SSO.

(a) Provide plots of the ECCS injection rates as a function of time for Case 0A for both Westinghouse upflow and downflow plant categories.

(b) Explain the way in which the simulated ECCS pump injection rates prior to and following SSO were determined and identify the factors and assumptions that were considered when determining the flows. Include any temporary safety injection (SI) impediment, single failure assumptions, and pump performance characteristics among the considered factors and assumptions. In the above identified cases, the ECCS recirculation flow rate is much different from the ECCS injection rate prior to SSO.

(c) Clarify if varying the ECCS injection mass flow rate upon SSO had an effect on the analysis results for both plant categories.

(d) Table 7-1 in the revised Section 7.1.1 of Vol. 1 describes the following ECCS performance for a Westinghouse three-loop plant following a large cold leg break. From 0 to 15 min: 1 residual heat removal and 2 high head SI (HHSI) pumps are described as typical injection phase modeling with single active failure; from 15 to 45 min: 2 HHSI pumps, typical SI phase modeling for this plant; from 45 to 47 min: no flow, interruption at cold leg recirculation; from 47 min to termination: 2 HHSI pumps. This represents an ECCS performance pattern, which appears opposite to the one described above (increase vs decrease in ECCS flow rate upon SSO). Clarify if varying the ECCS injection mass flow rate upon SSO following this opposite pattern would have an effect on the analysis results for both plant categories.

(e) Considering the results from Vol. 4, explain the applicable conditions and related requirements for adequately determining the values of ECCS flow. Consider injection and recirculation rates, including interruptions during switchover, on a plant-specific basis to ensure that ECCS performance is adequately represented.

(f) Provide the information requested in Items a through e for the CE and B&W plant categories. It is noted that Table 6-3 lists the “low pressure safety injection (LPSI)

flow rate" as a key input for the CE plant category and Table 6-4 identifies "low pressure injection (LPI) flow rate" as a key input for the B&W plant category thus linking this key input to the performance of specific ECCS components.

(g) Explain the reason for including Note 2 to Table 6-4 relevant to the B&W plant category stating that "the LPI flow rate followed a pump curve in the analysis. The value shown is the flow at run-out conditions". Provide the pump curve and the flow rates used in the analysis. Justify that these parameters are applicable to all plants in this category.

(h) Provide graphs of SI flow rates as a function of time for each individual reactor coolant primary loop for the entire duration of the analysis for the cases included in the case matrices in Tables 8-1, 8-2, 9-1, 9-2, 10-1, 10-2, 11-1, and 11-2. Show the contributions from both high and low pressure SI for the cold and hot legs. Describe all applicable assumptions related to the way in which these flow rates were established and simulated in the T-H analyses.

2.24.2 Response to RAI 4.24

2.24.2.1 Part a

Plots of Emergency Core Cooling System (ECCS) flow rates are included in the response to RAI 4.17c.

2.24.2.2 Part b

The basis for the ECCS injection before and after Sump Switch Over (SSO) is described in the response to RAI 4.5a and below in the response to Part h of this RAI.

2.24.2.3 Part c

As described in the response to RAI 4.5a, the ECCS flow rate before and after SSO is slightly different. Before SSO, automatic actuation of ECCS systems defines the amount of ECCS injection available, consistent with the single failure assumption and a single train of ECCS available (1 High Pressure Safety Injection (HPSI) + 1 Low Pressure Safety Injection (LPSI)). After SSO, the LPSI pumps are isolated leaving only the HPSI

pumps to supply ECCS flow. For the t_{block} and K_{max} analyses, the limiting single failure is of a train of ECCS. Therefore, after SSO, only a single HPSI pump is available. For the base plant model, this represents a ECCS flow of 800 gpm. The analyses presented modeled the minimum ECCS flow rates in an attempt to provide the biggest challenge to core cooling. It should be noted that the 800 gpm figure is based on a fluid density of 61.86 lbm/ft^3, corresponding to fluid conditions around 110 °F. The actual volumetric flow rate will be 827 gpm when sump fluid temperature is at 212 °F.

2.24.2.4 Part d

The base model for Combustion Engineering (CE) plants uses a conservatively low ECCS injection rate corresponding to one train of HPSI + LPSI prior to the time of SSO, and one train of HPSI after SSO.

2.24.2.5 Part e

As previously mentioned, the base model for CE plants uses a conservatively low ECCS injection rate corresponding to one train of HPSI + LPSI prior to the time of SSO, and one train of HPSI after SSO, which represents the minimum ECCS flow rates in an attempt to provide the biggest challenge to core cooling. Sensitivity studies show that the minimum ECCS flow rates are sufficient to provide adequate long term cooling following switchover to recirculation and the postulated formation of a highly resistive debris bed at the core inlet for the nominal case, with a 1.1 decay heat multiplier.

2.24.2.6 Part f

The information requested for the CE plants is provided in the various other sections of this RAI.

2.24.2.7 Part g

This Request for Additional Information (RAI) pertains to the B&W plant category and therefore requires no response for the CE plant category.

2.24.2.8 Part h

The HPSI flows used in the CE model are for 4 injection points with no distinction between flows to the different loops (i.e. imbalance between the loops is not modeled in terms of differences in ECCS piping resistance, but it is taken into account in terms of differences in pressures in the Cold Leg (CL) at the injection point). For this model, flows above 1276 psia are not modeled in Loss of Coolant Accident (LOCA). A loss of a train (bus failure) is equivalent to the loss of offsite power, concurrent with the loss of one emergency Diesel generator. In the CE model used for this analysis, the minimum equivalent flow from a single HPSI pump is distributed to all four cold legs.

The LPSI flows used in the model are for 2 injection points (consistent with the failure of one emergency Diesel generator). For this model, the loss of an emergency Diesel generator is synonymous with the loss of a train associated with an failed offsite-powered bus. The loops available for injection are determined by the bus pairings to the motor operated valves associated with each safety injection line. For this model, the LPSI safety injection lines have the bus pairings such that, assuming the loss of an emergency Diesel generator determines loops 1A and 2B as the loops receiving the LPSI injection. Hot leg injection is not modeled.

The figures requested are provided below. Figure RAI-4.24-1 shows the total pumped ECCS flows for each loop, Figure RAI-4.24-2 shows the HPSI flows for each loop, and, Figure RAI-4.24-3 shows the LPSI flows for each loop.

Figure RAI-4.24-1: ECCS Mass Flow Rates for CE Analyses

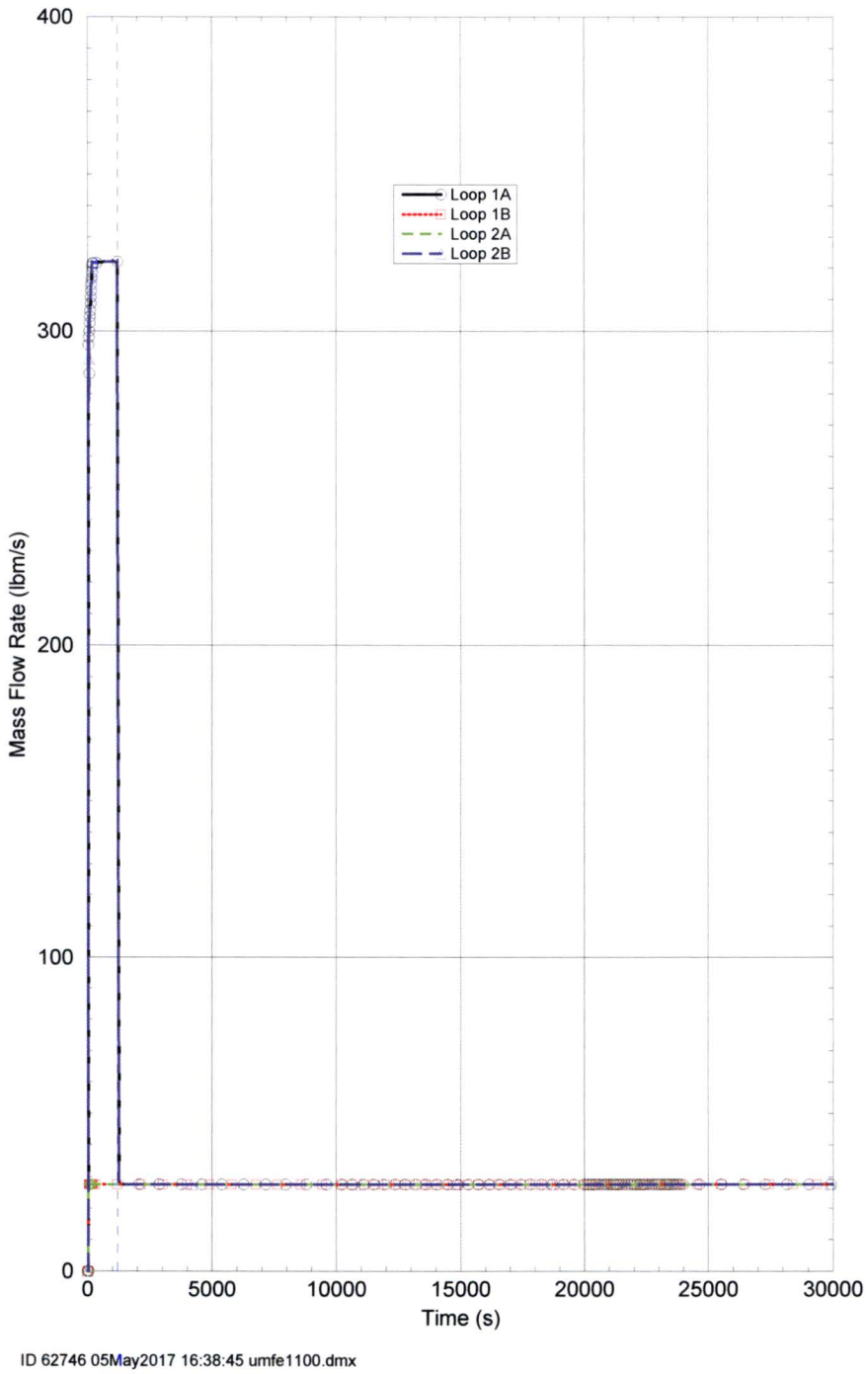

Figure RAI-4.24-2: HPSI Mass Flow Rates for CE Analyses

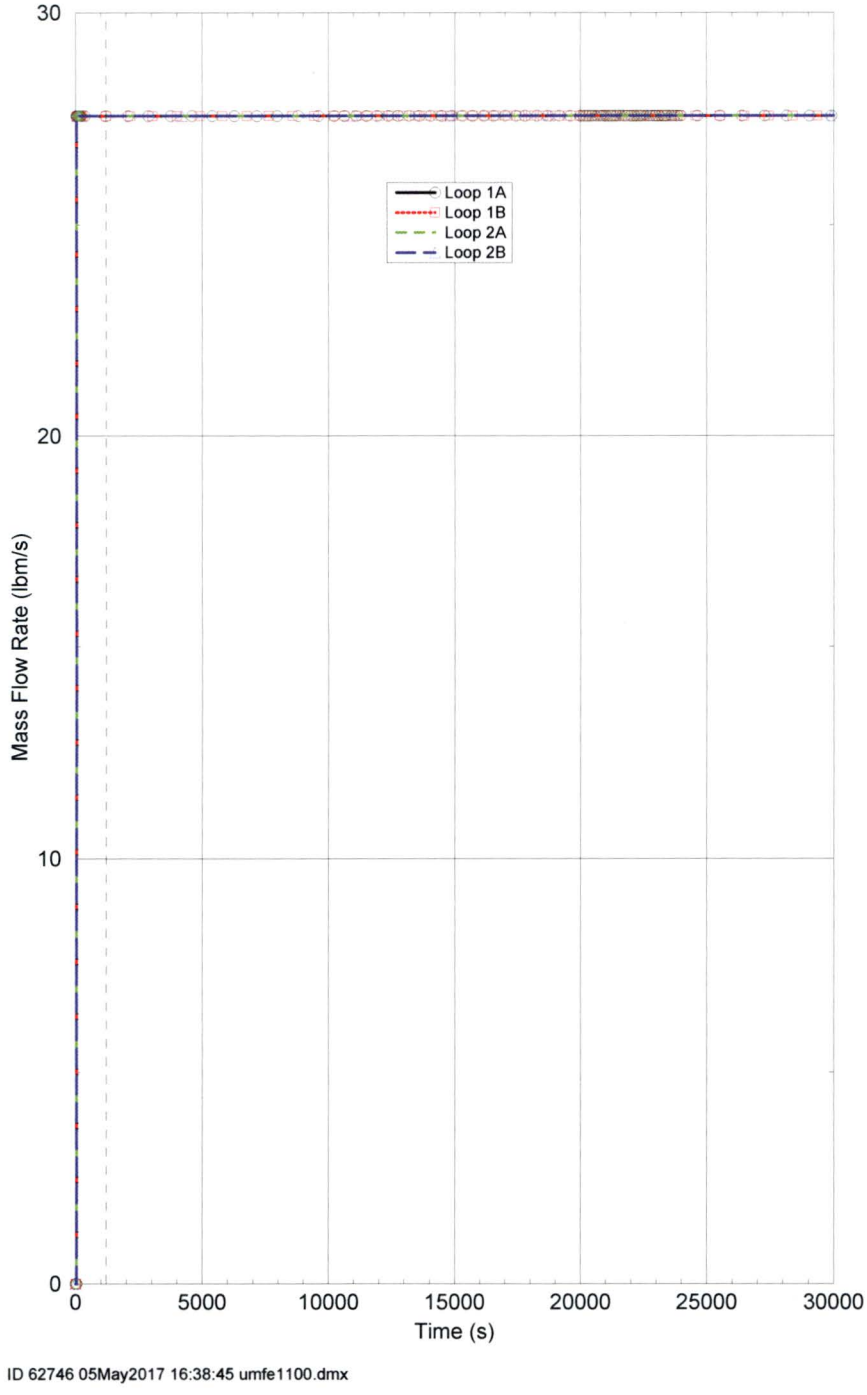

Figure RAI-4.24-3: LPSI Mass Flow Rates for CE Analyses

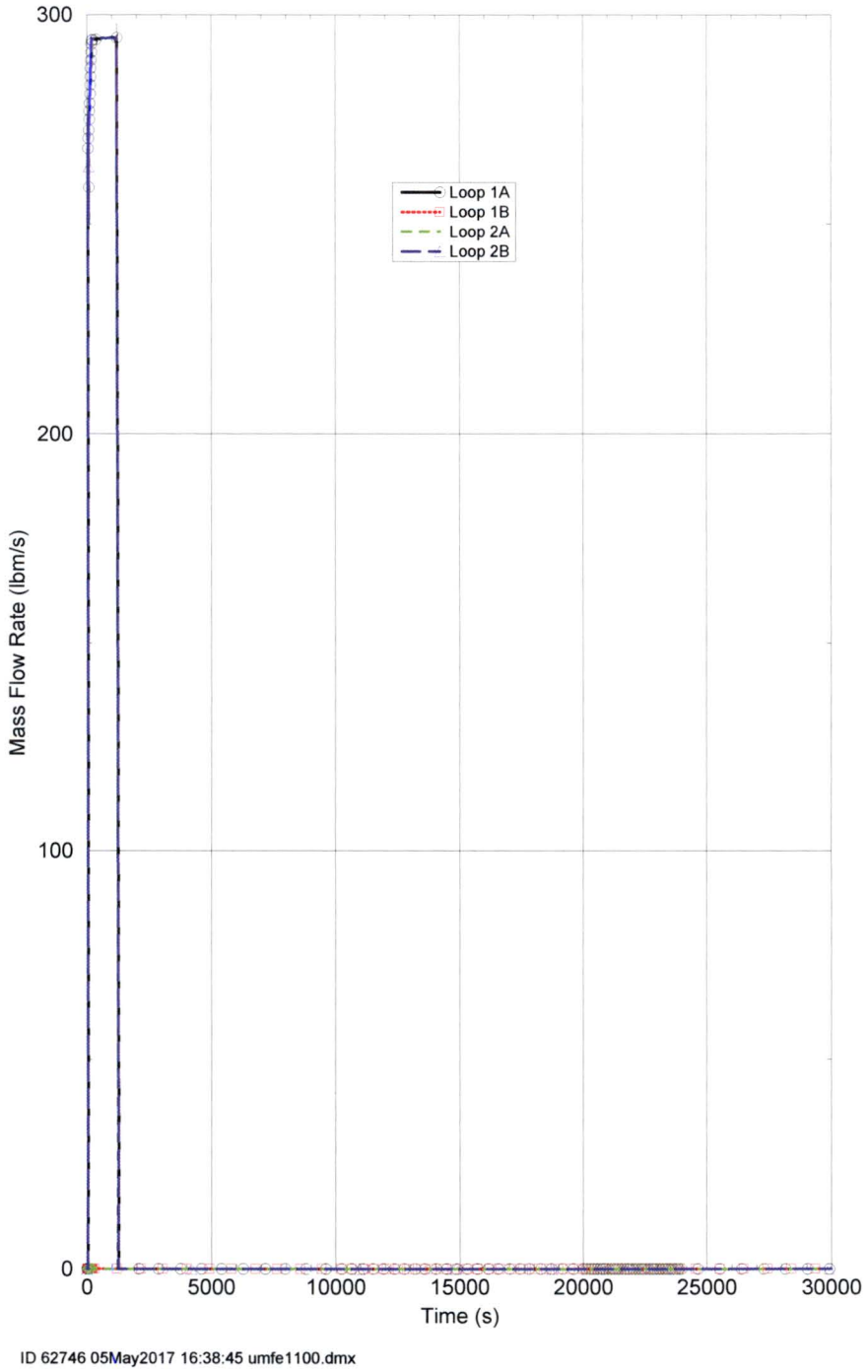

2.25 RAI 4.25

2.25.1 Statement of RAI 4.25

In determining the t_{block} and K_{max} inputs for the Westinghouse upflow category, Section 8.1 provides a simulation matrix of cases considering only two ECCS recirculation flow rates of 18 and 40 gpm/FA. Section 8.2 states that LTCC can be maintained if the time of complete core inlet blockage, t_{block}, occurs 143 minutes, or later, after the initiation of the LOCA event. This time is taken from Case 1B simulating the minimum ECCS recirculation flow rate of 18 gpm/FA and is stated to bound "the range of recirculation flows investigated". The K_{max} input is determined from Case 2B with the same simulated ECCS recirculation flow rate of 18 gpm/FA.

(a) Provide justification that the t_{block} criterion from Case 1B at 18 gpm/FA is valid for the range of flow rates from 8-40 gpm/FA as documented in Table 6-1 for this parameter.

(b) Provide justification that the K_{max} criterion from Case 2B with a simulated ECCS recirculation flow rate of 18 gpm/FA is valid for the range of flow rates from 8-40 gpm/FA as documented in Table 6-1 for this parameter.

(c) Provide justification for using only 18 and 40 gpm/FA flow rates for determining the t_{block} and K_{max} inputs as stated in Note 1 to Table 6-1 and documented in the simulation matrix of cases provided in Section 8.1.

(d) Define the range of ECCS recirculation flow rates for which the t_{block}, K_{max}, K_{split}, and m_{split} results, as obtained in Section 8, are considered applicable to the Westinghouse upflow plant category and provide a justification for this range.

(e) Provide similar responses to Items a through d for the other three plant categories to justify that the t_{block} and K_{max} inputs calculated using a single ECCS recirculation flow rate for each input are applicable to the range of flow rates defined for each plant category. For example, justify for the Westinghouse downflow category that t_{block} is determined from Case 1A simulating an ECCS recirculation flow rate of 40 gpm/FA and K_{max} is determined from Case 2B with a simulated ECCS recirculation flow rate of 18 gpm/FA.

(f) Sections 8-3 and 9-3 state that "the duration and magnitude of the heatup were heavily dependent on the timing of complete core inlet blockage and the ECCS flow rate". Considering the responses to items a through e above, demonstrate that the calculated parameters are valid for the ECCS flow rates and core inlet blockage times used in the analysis.

2.25.2 Response to RAI 4.25

2.25.2.1 Part a

This RAI pertains to the Westinghouse Electric Company (WEC) plant categories and therefore requires no response for the Combustion Engineering (CE) plant category.

2.25.2.2 Part b

This RAI pertains to the WEC plant categories and therefore requires no response for the CE plant category.

2.25.2.3 Part c

This RAI pertains to the WEC plant categories and therefore requires no response for the CE plant category.

2.25.2.4 Part d

The basis for the Emergency Core Cooling System (ECCS) injection before and after Sump Switch Over (SSO) for the CE plants is described in the response to RAI 4.5a. As described therein, the ECCS injection rate during the transient has a direct effect on the core mixture level and cladding temperature response. Higher flow rates will provide significant excess flow above core boiloff. Lower flow rates may be closer to the core boiloff rate such that when blockage is imposed, decay heat removal may be challenged while the flow through the core is reestablished via the barrel/baffle region instead of the core inlet. Studies presented in WCAP-17788-P, Volume 4 confirmed that lower flow rates are more conservative for the Thermal Hydraulic (TH) analyses. Therefore, a minimum flow rate for the CE plants was targeted.

To that end, the CE analyses to define t_{block} and K_{max} are valid for any ECCS flow rate that is higher than the flow rates analyzed and described in the response to RAI 4.5a. As described in the responses to RAI 4.20 and 4.21, the K_{split} curve is a well defined shape and can be extrapolated to higher ECCS recirculation flow rates on a per assembly basis by using the following function:

$$y = 6.416\text{x}10^{6}\, x^{-2.012} \qquad \text{(RAI-4.25-1)}$$

For the values of m_{split}, the response to RAI 4.20 provides two lower bounding curves that can be used as a function of $K–K_{split}$, depending on the baffle resistance of the plant analyzed. In addition, as mentioned in the response to RAI 4.20, the results were found to be insensitive to the ECCS flow rates once the ECCS flow exceeds 1654 gpm. Utilities that can demonstrate ECCS flow rates above an equivalent 1654 gpm during sump recirculation can improve their debris limits by using a curve that is more representative of the higher m_{split} results. The appropriate equivalent flow rate can be determined using the method provided in the response to RAI 4.5a.

2.25.2.5 Part e

The requested information for the CE plant analyses are described above.

2.25.2.6 Part f

The above responses demonstrate that the calculated parameters are valid for the ECCS flow rates and core inlet blockage times used in the analysis. In addition, a sensitivity study was performed on t_{block} for the CE plant category. The study increased the time of t_{block} to 25,000 seconds and analyzed with multipliers of 1.1x and 1.2x on the American Nuclear Society (ANS) 1979 decay heat Standard (Reference 4.25-1). Both cases were less limiting than the base case with t_{block} at 20,000 seconds. Both of the sensitivity cases with a t_{block} of 25,000 seconds showed only a minor secondary heatup. As decay heat reduces with time after reactor SCRAM, it is clear that extending t_{block} to later times results in less decay heat and more excess ECCS available to cool the core. The combination of these results in a lower Peak Cladding Temperature (PCT).

References - RAI 4.25

4.25-1 American Nuclear Society ANSI/ANS-5.1-1979, *American National Standard for Decay Heat Power in Light Water Reactors*.

2.26 RAI 4.26

2.26.1 Statement of RAI 4.26

K_{max} for the CE plant category was determined by applying a gradual ramp in the simulated core inlet resistance starting from 0 at 1,800 seconds and reaching K_{max} of $6.5x10^6$ at 4,200 seconds as shown in Figure 10-2. The profile represents an increase in the resistance value by applying four different constant rates of resistance increase, which change in a stepwise manner with time.

(a) Justify that the K_{max} value of $6.5x10^6$, using the profile from Figure 10-2, represents a robust result and is not an outcome of tuning of the core inlet resistance profile to obtain a desired result. Results from sensitivity analyses can be used to provide the justification.

(b) In the case of the profile shown in Figure 10-2, the core inlet resistance was increased from 0 to $6.5x10^6$ within a time window of 2,400 seconds (40 min). As the result of $6.5x10^6$ for K_{max} was tied to the specific profile from Figure 10-2, justify the K_{max} input for the CE plant category by explaining how it can be assured that the K_{max} value will not be developed within a time window shorter than 40 minutes resulting in K_{max} occurring earlier than 70 minutes into the LOCA transient, which could lead to the PCT acceptance criteria being violated.

2.26.2 Response to RAI 4.26

2.26.2.1 Part a

The base K_{max} study described in Volume 4, Section 10 was performed with the core inlet resistance curve shown in Volume 4, Figure 10-2 and at an Emergency Core Cooling System (ECCS) flow rate of 827 gpm. Since the Combustion Engineering (CE) plant model was updated in response to RAI 4.1b, the K_{max} analysis was redone using the new plant model. This new Thermal Hydraulic (TH) analysis confirmed no core uncovering and a K_{max} of $6.5x10^6$. WCAP-17788-P, Volume 4, Section 10.2.3 will be updated to reflect this new analysis.

As shown in Volume 4, Figure 10-2, the application of the blockage begins at approximately 2000 seconds, which is 800 seconds after the time of Sump Switch Over (SSO). This input was derived from observations of the debris accumulation during the testing process described in WCAP-17788-P, Volume 6. The details of this derivation and the suitability of the curve shown on Volume 4, Figure 10-2 are described in this RAI response.

The fuel assembly testing described in WCAP-17788P, Volume 6 investigated the effect of debris accumulation on the fuel. This testing showed that it takes some amount of fiber accumulation at the lower end fitting before the pressure drop begins to increase. For the limiting case ("Final-Low" flow profile), approximately 3 to 3.5 g of fiber is required (Volume 6, Figures 5-44 and 5-55). From the limiting test results, the fiber buildup (in terms of K_{eq}, which is used to translate between the tested core inlet resistance and the analyzed core inlet resistance as described in WCAP-17788-P, Volume 1, Section 6.3.1) with time after SSO can be calculated (Figure RAI-4.26-1 curves, "AREVA Fuel as Tested" and "WEC Fuel as Tested"). From these results, it can be seen that the accumulation of fiber does not produce a noticeable pressure drop until 800 seconds after SSO. This corresponds to the start of the increased resistance shown in Volume 4, Figure 10-2.

Figure RAI-4.26-1 also shows the rate of resistance as debris continues to accumulate. The increase is initially somewhat gradual. The curve "Used in TH Model" bounds both the AREVA and Westinghouse Electric Company (WEC) fuel until a K_{eq} of approximately 1.0×10^6. Thereafter, the AREVA curve exceeds the curve used in the analysis, while the WEC fuel as tested continues to be bounded. While this may seem non-conservative relative to AREVA fuel, the ECCS flow rate has to be considered as well.

A sensitivity study of K_{max} to flow rate was examined for the WEC plant category (Volume 4, Section 8). The results indicate that a low flow rate produces the limiting results (in terms of Peak Cladding Temperature (PCT) – compare Case 2A and 2B from Volume 4, Section 8). A higher ECCS flow rate increases the Downcomer (DC) fill rate and pushes liquid through baffle more quickly, which is able to remove core decay heat more quickly.

After SSO, the lowest ECCS flow rates for CE plants would consist of flow from a single High Pressure Safety Injection (HPSI) pump (assumes a single failure of one ECCS train and operator isolation of Low Pressure Safety Injection (LPSI) at SSO). As described in RAI 4.5, 827 gpm is expected to be the lower bound on this flow rate. Conversely, the flow could be higher if the single failure is to isolate a LPSI pump. The ECCS flow rate could then be from 2 HPSI pumps and 1 LPSI pump.

Testing in Volume 6 also showed that the "Final-Low" flow rate profile produced limiting results. For the limiting case, the flow rates ranged from a little over 12 gpm/FA at the start of the test to approximately 7.5 gpm/FA at the end of the test. Equating this to the CE plant model used in the TH analysis (which had 217 fuel assemblies), the total flow rate range is approximately 2600 gpm at the start of the test to approximately 1600 gpm at the end of the test. While no testing was done at lower flow rates (827 gpm for example), the limiting results were limiting because they lead to the formation of a single debris bed at the lower end fitting. Testing at lower flow rates would produce the same result (i.e. a single debris bed at the lower end fitting), although the pressure drop would be expected to decrease as the flow rate decreases.

As flow rate in the tests increased, the results became less limiting (Volume 6, Section 5.3). The higher flow rates demonstrated a reduction in the pressure drop due to debris of a factor of three for WEC fuel (Volume 6, Figures 5-43 thru 5-46) and a factor five for AREVA fuel (Volume 6, Figures 5-55 thru 5-57). Therefore, using the limiting case with the Final-Low flow profile will be limiting for K_{max} calculations.

The initial flow rate in the test is when the debris begins to accumulate and will be used for comparison to the plant flow rates.

From this discussion, it is clear that the lowest CE ECCS flow rates are lower than the tested flow rates (827 gpm actual compared to an equivalent of 2600 gpm tested). Since the lower ECCS flow rates will produce the lowest K_{max}, 827 gpm was used in the TH analyses. However, at the lower flow rate, the debris accumulation will be slower. Since debris accumulation is proportional to flow rate, K_{eq} is proportional to flow rate. Therefore, the debris accumulation from the tests can be adjusted by the ratio of the ECCS to tested flow rate to provide a K_{eq} that is appropriate for 827 gpm. The results are shown in Figure RAI-4.26-1, curves "WEC Fuel, Adjusted to 827 gpm" and "AREVA Fuel, Adjusted to 827 gpm". These results indicate that debris does not accumulate until 2800 seconds after SSO (4000 seconds after the break). At the lower flow rate, the rate of debris accumulation is also slower. Given the later time in the transient, the Decay Heat (DH) is lower than at 2000 seconds when the resistance is applied in the base case.

A sensitivity study that applied the adjusted AREVA curve and used 827 gpm of ECCS flow rate was performed. The results show no core uncovering and confirm that the base model remains conservative.

If the ECCS flow rate after SSO is higher than 827 gpm, then the curves shift to the left. At 2600 gpm (the full-core equivalent tested flow rate), the debris accumulation rate is identical to the "as Tested" curve. The pressure drop increases at the same time as that modeled, but would increase at a faster rate. However, the increased ECCS flow rate also fills the DC faster.

A sensitivity study that applied the adjusted AREVA curve and used 2482 gpm of ECCS flow rate was performed. The results show no core uncovering and confirm that the base model remains conservative.

Further, time of SSO is considerably later than 1200 seconds for the CE plants given the lower ECCS flow rates. Given the above delays in debris build up, the application of the blockage would be much later, which further validates that the curve used in the TH model is conservative.

Based on the above discussion and sensitivity studies, it is clear that a K_{max} value of 6.5×10^6, using the profile from Figure 10-2, represents a robust result and is not an outcome of tuning of the core inlet resistance profile to obtain a desired result.

Figure RAI-4.26-1: Core Inlet Resistance for CE Analyses

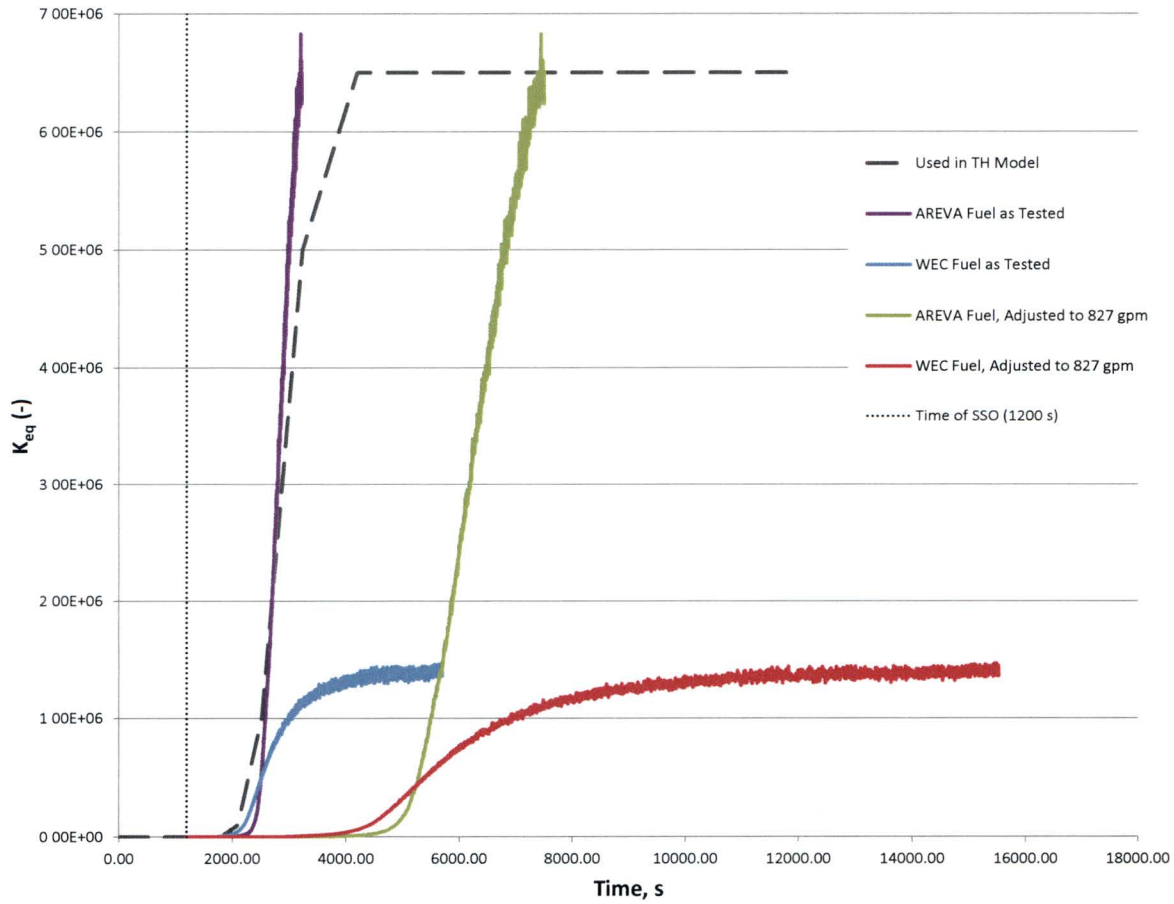

2.26.2.2 Part b

As shown in Volume 4, Figure 10-2, the application of the blockage begins at approximately 2000 seconds, which is 800 seconds after the time of SSO. This input was derived from observations of the debris accumulation during the testing process described in WCAP-17788-P, Volume 6. The details of this derivation and the suitability of the curve shown on Figure 10-2 are described in part "a" of the RAI response.

The fuel assembly testing described in WCAP-17788P, Volume 6 investigated the effect of debris accumulation on the fuel. This testing showed that it takes some amount of fiber accumulation at the lower end fitting before the pressure drop begins to increase. For the limiting case ("Final-Low" flow profile), approximately 3.5 g of fiber is required (Volume 6, Figures 5-44 and 5-55). As described in part "a" to this RAI response, it can

be seen that the accumulation of fiber does not produce a noticeable pressure drop until approximately 800 seconds after SSO.

At higher flow rates, the testing indicated that approximately 2 to 2.5 g of fiber is required to accumulate before the pressure drop begins to increase (Volume 6, Figures 5-45, 5-46, 5-56 and 5-57). At the higher flow rates, the time that this pressure drop is noted will be less than the 800 seconds calculated at the limiting conditions. However, the maximum pressure drop also decreased at the higher flow rates (Volume 6, Section 5.3), resulting in a reduction in the pressure drop due to debris of a factor of three for WEC fuel (Volume 6, Figures 5-43 thru 5-46) and a factor five for AREVA fuel (Volume 6, Figures 5-55 thru 5-57). The lower pressure drop significantly reduces the value of K_{max}. Further, the higher flow rates needed for the debris to arrive sooner will result in a faster rise in the DC level and available driving head to push liquid through the Alternate Flow Path (AFP). The sensitivity study discussed in part "a" to this Request for Additional Information (RAI) response showed that the higher ECCS flow rates offset a faster rate of debris accumulation at the core inlet with no adverse effects. Therefore, the earlier debris accumulation seen for the higher flow rates would not result in more limiting results.

Therefore, using the profile shown in Volume 4, Figure 10-2 for K_{max}, along with the minimum ECCS flow rate, produces bounding results for the CE plant category.

2.27 RAI 4.27

2.27.1 Statement of RAI 4.27

T-H code predictions to demonstrate adequate core coolability under conditions associated with blocked core inlet flow passages require reasonable assurance of adequate code performance under the simulated conditions. The examination of code results during the NRC audit of the Westinghouse T-H analyses in Sections 8 and 9 on January 27-28, 2016, indicates that flow patterns involving parallel cross-connected channels to model the core following a simulated complete core inlet blockage can be complex. It was determined that obstruction of lateral flow passages between fuel assemblies due to the presence of spacer grids was not accounted for in the modeling of the lateral cross-connections between parallel core channels, including the hot channel. In addition, potential effects on the axial flows due to possible localized accumulation of debris at the locations of spacer grids in regions above the core inlet were not modeled to assess such effects.

Cross-flows between parallel channels can be a contributing factor affecting code prediction of local fuel conditions, including PCT, due to their impact on fluid velocities, void fraction, and two phase flow patterns. Provide results from additional T-H analyses for a representative case analyzed in each plant category to assess the effects from the above identified factors related to lateral obstruction of cross-flow passages and impediment of axial flows on the PCT and t_{block} predictions. The analyses should be performed using core modeling changes that account for: (1) reduced flow area of cross-flow passages due to the spacer grids present in the active core region, (2) impact on resistances of cross-flow passages from the spacer grids present in the active core region, and (3) increase in the simulated spacer grid resistances in the axial direction at appropriately selected spacer grid locations, including impact for both axial directions, to simulate the effect from possible local fiber accumulation. Such modeling changes and modifications should be applied to the hot channel and all or some of the channels representing the entire core as found appropriate. If necessary to resolve the impact from the examined factors and processes on the PCT and t_{block} predictions, include sensitivity results related to specific factors and modeling assumptions as applicable. For each simulation, include sufficiently detailed results to explain effects on the predicted core T-H response, PCT, and t_{block} in comparison to the corresponding base cases. Include PCT, void fraction, fluid phase velocities, and two-phase flow patterns for appropriately selected hydraulic channels and cells, as well as integrated mass flows in both lateral and axial directions for selected critical flow passages. Include a description of the implemented modeling changes with a sufficient degree of detail to explain clearly how the physical processes and factors were accounted for in the model along with the introduced assumptions.

2.27.2 Response to RAI 4.27

Debris accumulation in the heated core region is described in Volume 1, Section 6.4.3.1. As described therein, the boiling process, in and of itself, precludes significant debris accumulation. While the general flow patterns in the core are well established by the Thermal Hydraulic (TH) analyses, the local flow patterns are quite complex due to the nature of the boiling process and uniqueness of the cycle specific bundle power distributions. Boiling at any given location in the core produces undulations in the void distributions that vary around a mean void faction. The instabilities of the boiling process introduce energy to the fluid that varies with time and location. In the event that debris begins to accumulate at the leading edge of a spacer grid, the perturbations of the local conditions due to this small debris buildup will lead to changes in boiling that will dislodge the debris before a large, contiguous bed can be established. No significant interruption of the long-term core flow patterns will occur. Therefore, debris beds like those seen at the core inlet will not establish in the presence of boiling. These assertions are supported by the testing presented in Volume 1, Section 6.4.3.1.

As the transient progresses, the core decay heat will decrease, which decreases boiling in the core. In particular, lower power regions of the core (i.e., the core periphery) may decrease boiling while the higher power assemblies continue to boil more vigorously. In any predominately liquid only regions of the core, it may be possible that debris can accumulate on the leading edge of the spacer grid. Subscale testing has demonstrated that flow through a debris bed made of fiber and particulate only will continue for fairly high amounts of fiber (on the order of [ ]). The addition of chemical precipitates may preclude flow through established debris beds of more than [ ]. However, any debris bed that forms in the liquid only region of the core will not extend across the entire core, because boiling continues in the higher power assemblies. The open lattice of the fuel design allows flow redistribution locally around any region that had some additional blockages. Should the flow become stagnant near any region near a blockage tries to form, the fluid will heat up and eventually boil. The boiling will either dislodge a debris bed (if it formed on the top side or bottom of the spacer grid), or the decreased density of the boiling region will draw fluid in to replace the boiled off liquid. In all cases, the open lattice design of the fuel will ensure that the core is cooled and that localized regions with increased boron concentrations will not develop even for complete inlet core blockages and for other limited size local blockages in small portions of the core.

While boiling precludes buildup at the leading edge of a spacer grid, the energy from the boiling process may force debris into internal grid locations such as the spring channels or dimples (see Volume 1, Figure 6-15). The limited size of these geometric features limits the expanse of the debris collection such that the effects would be localized and

have little to no effect on the pressure drop across the spacer grid where they might occur.

Sensitivity studies on the core crossflow resistance were performed. The crossflow resistance was increased by 50% over the base case and was analyzed with a 1.1x multiplier, as well as a 1.2x multiplier, on the American Nuclear Society (ANS) 1979 decay heat Standard (Reference 4.27-1). For the sensitivity study at with the 1.2x multiplier on decay heat, the base case is also ran at this decay heat in order to get a direct comparison of the impact of the increased core crossflow resistance. While the case with the 1.2x decay heat multiplier and the increased crossflow terminated prior to 30,000 seconds, the transient ran long enough to see the important phenomena to draw conclusions.

A discussion of the results of the sensitivity studies follows.

Figures RAI-4.27-1 and RAI-4.27-2 compare the mass flux at the core exit in the average core and the peripheral core with a 1.1x and a 1.2x multiplier on the decay heat, respectively. It can be seen that the increase in the crossflow resistance has nearly no impact on the mass flux at the core exit.

Figures RAI-4.27-3 and RAI-4.27-4 compare the collapsed liquid level in the average core region with a 1.1x and a 1.2x multiplier on the decay heat, respectively. The general behavior of the collapsed level in the average core region is very similar between the cases. For the sensitivity study performed at the 1.1x multiplier decay heat level, the base case shows a greater degree of core uncovery after t_{block}, which explains why the base case resulted in a secondary heatup, while the case with the increased crossflow resistance did not.

Figures RAI-4.27-5 and RAI-4.27-6 compare the collapsed liquid level in the Upper Plenum (UP) region. As with the observations in the collapsed liquid level in the average core region, and the results presented in the response to RAI 4.23, there is almost no difference between the cases.

Figures RAI-4.27-7 and RAI-4.27-8 compare the resulting Peak Cladding Temperature (PCT) traces for the crossflow sensitivity studies performed. The results from the study done with a 1.1x multiplier on decay heat showed no secondary heatup, compared to the PCT in the base case reaching 542 °F. When the decay heat multiplier was increased to 1.2x, a secondary heat up was observed, but the PCT was approximately equal (in both magnitude and timing) to a case where the same decay heat multiplier was applied to the base case.

As described in the response to RAI 4.8a and to 4.23, the void fraction is primarily a function of the superficial vapor velocity, which is directly tied to the decay heat. As stated in the response to 4.8a, the majority of the parameters used in various sensitivity studies conducted in responding to these RAIs, including the sensitivity to crossflow

resistance, have only secondary effects in the core and in the UP thermal-hydraulic behavior. This is consistent with the PCT predictions observed in the sensitivity studies on the crossflow resistance.

Figures RAI-4.27-9 through RAI-4.27-18 provide comparisons of integrals various axial and crossflow flow rate in the core region for the sensitivity study performed with the 1.1x decay heat multiplier. The results with a 1.2x multiplier are similar.

Figures RAI-4.27-9, RAI-4.27-10, RAI-4.27-11, and RAI-4.27-12 provide the integrated flow at the core exit for the hot assembly, central core, average core, and peripheral core regions, respectively.

Figures RAI-4.27-13, RAI-4.27-14, and RAI-4.27-15 show the integrated crossflows between the various core regions near the bottom of the core. Figures RAI-4.27-16, RAI-4.27-17, and RAI-4.27-18 present the integrated crossflows between the various core regions near the top of the core.

While some differences exist in the various integrated flow rates within the core region when the crossflow resistance is increased by 50%, the general trends are quite similar. With these results, and the discussion provided in the response to RAI 4.8a and to 4.23, it is clear that the effects of the crossflow resistance is a second order effect. Due to the low sensitivity of the results on the PCT and general thermal-hydraulic behavior when the crossflow resistance is changed, the thermal-hydraulic analysis in the WCAP-17788-P application for the Combustion Engineering (CE) plants will retain unchanged.

Figure RAI-4.27-1: Core Mass Flux at Core Exit - 1.1x Decay Heat

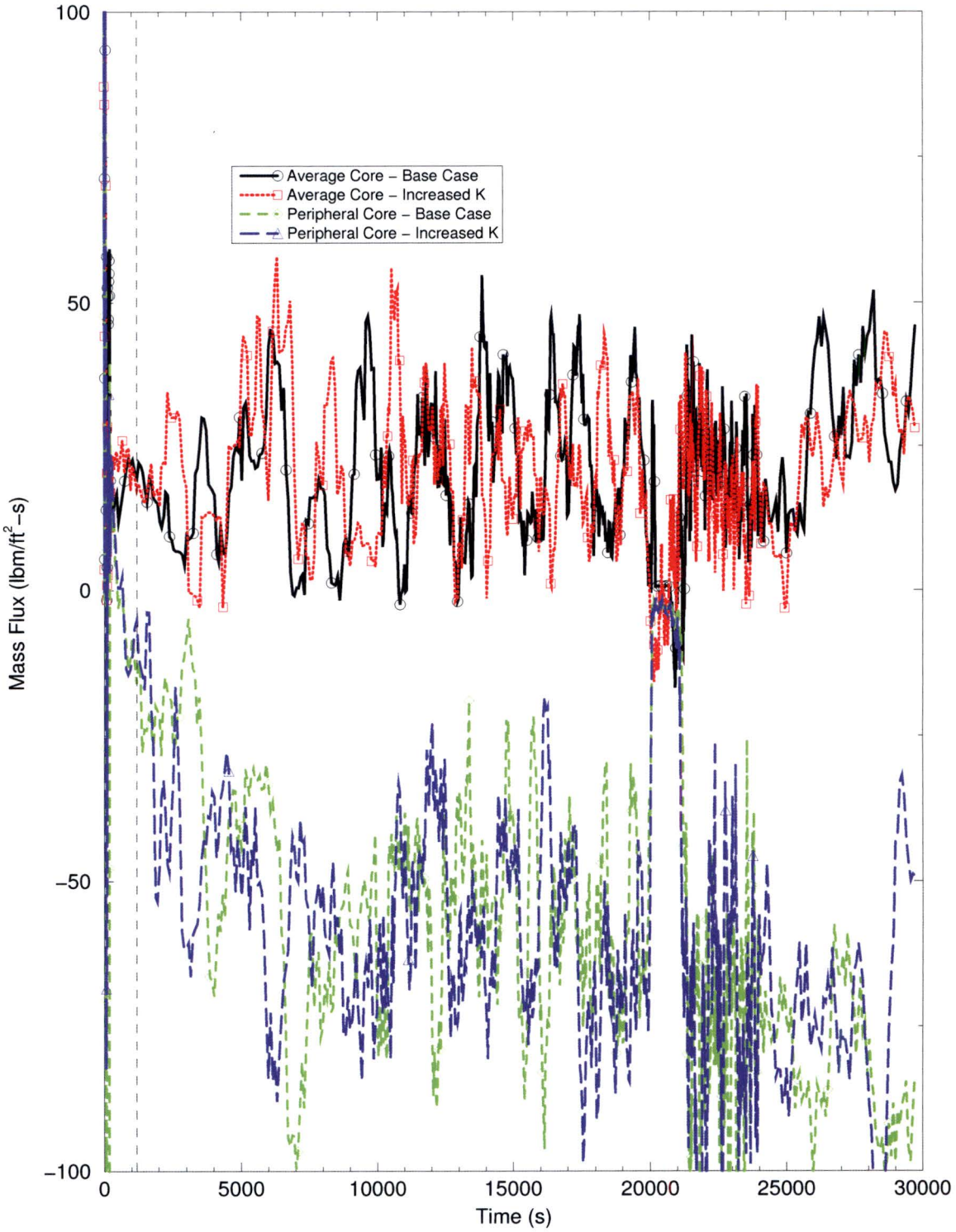

Figure RAI-4.27-2: Core Mass Flux at Core Exit - 1.2x Decay Heat

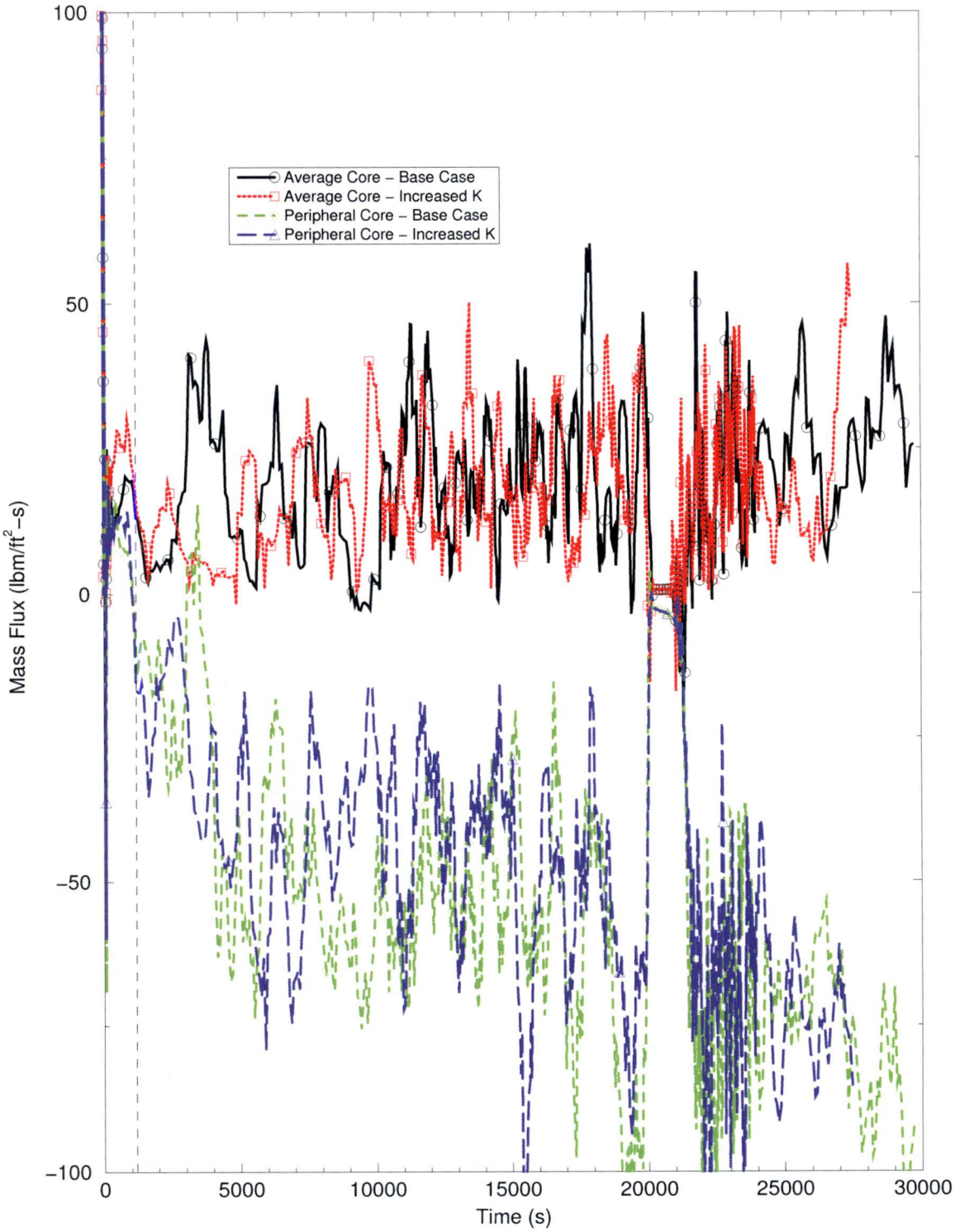

Figure RAI-4.27-3: Average Core Collapsed Level - 1.1x Decay Heat

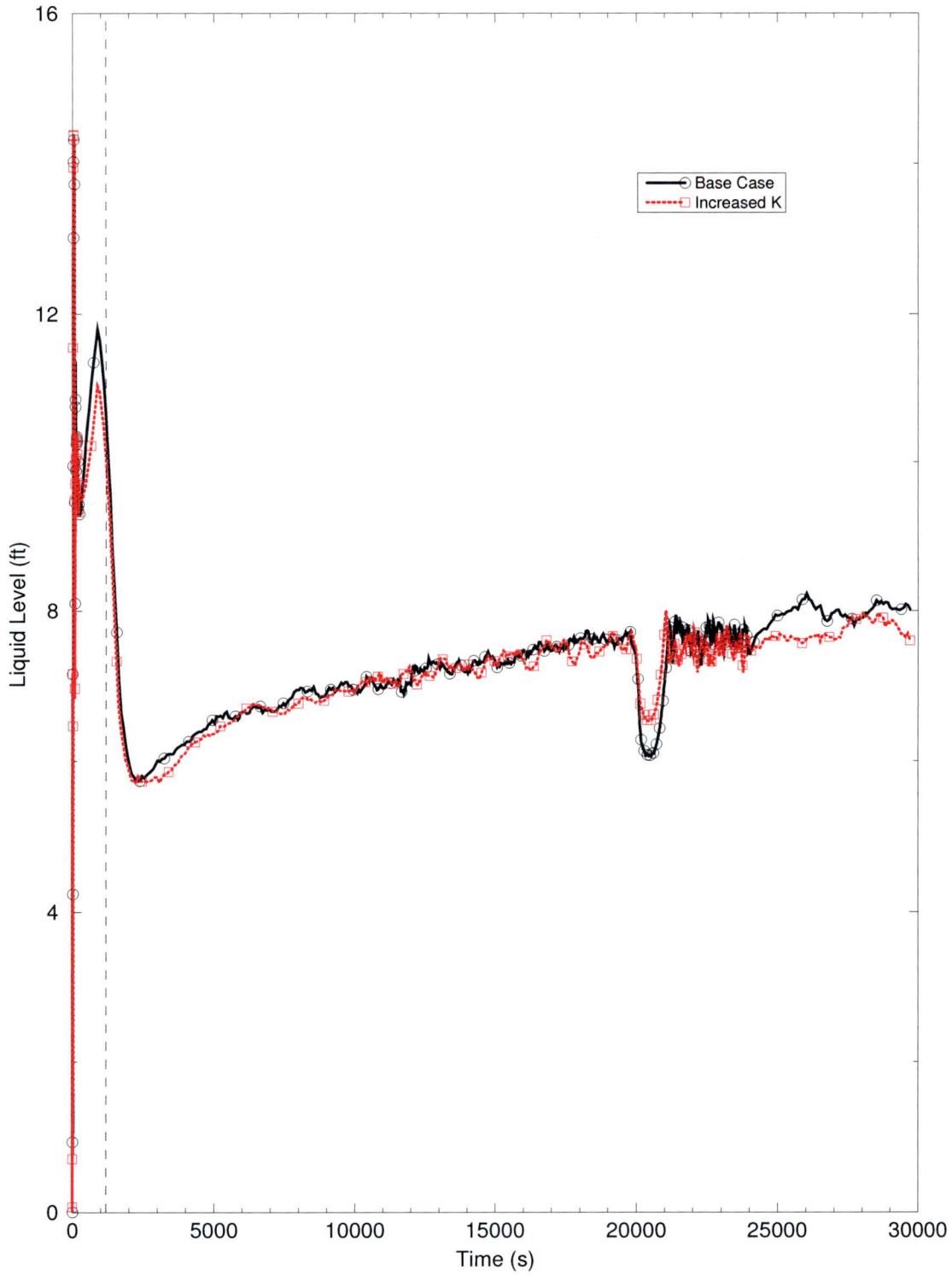

Figure RAI-4.27-4: Average Core Collapsed Level - 1.2x Decay Heat

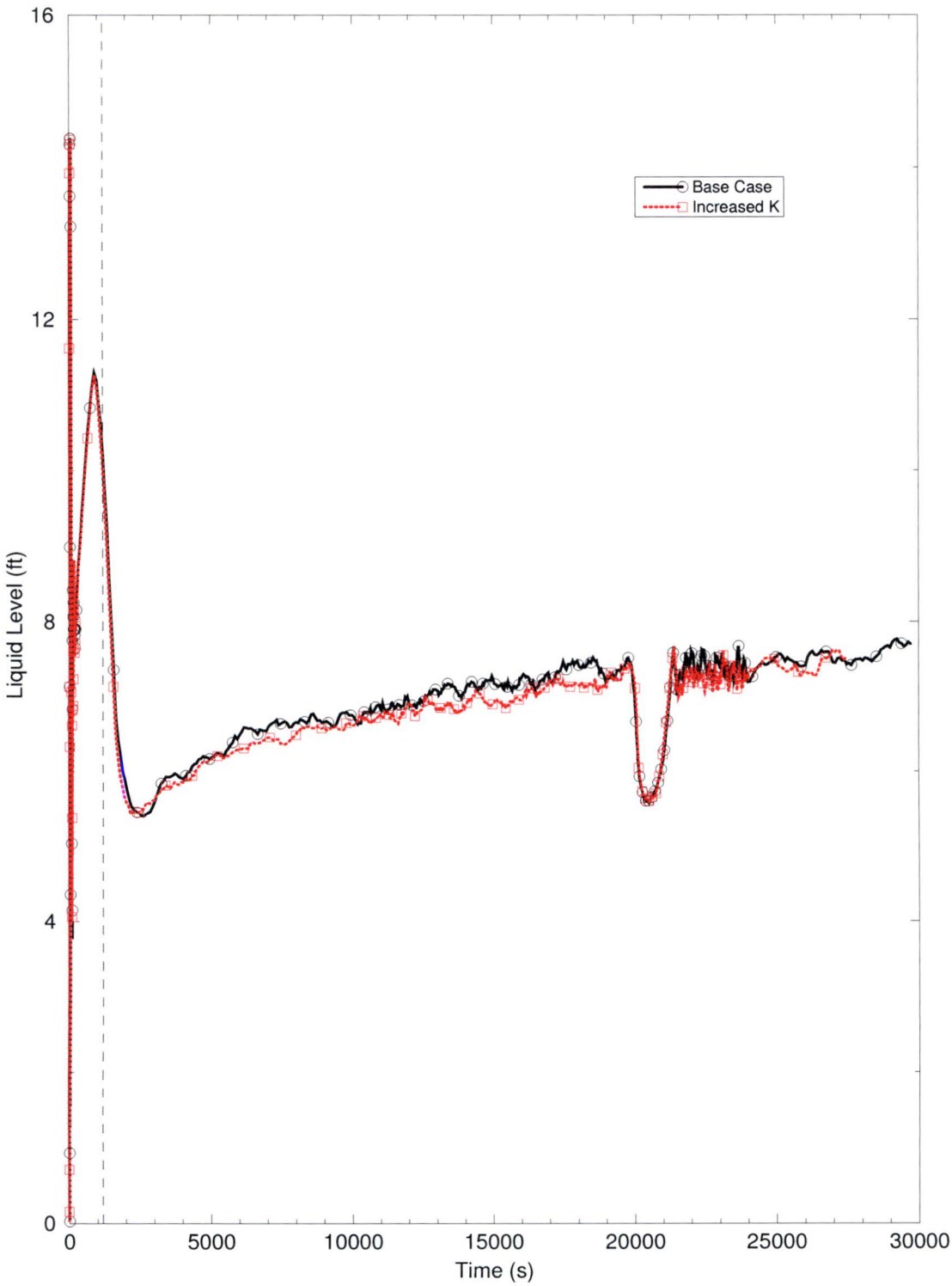

Figure RAI-4.27-5: Upper Plenum Liquid Level - 1.1x Decay Heat

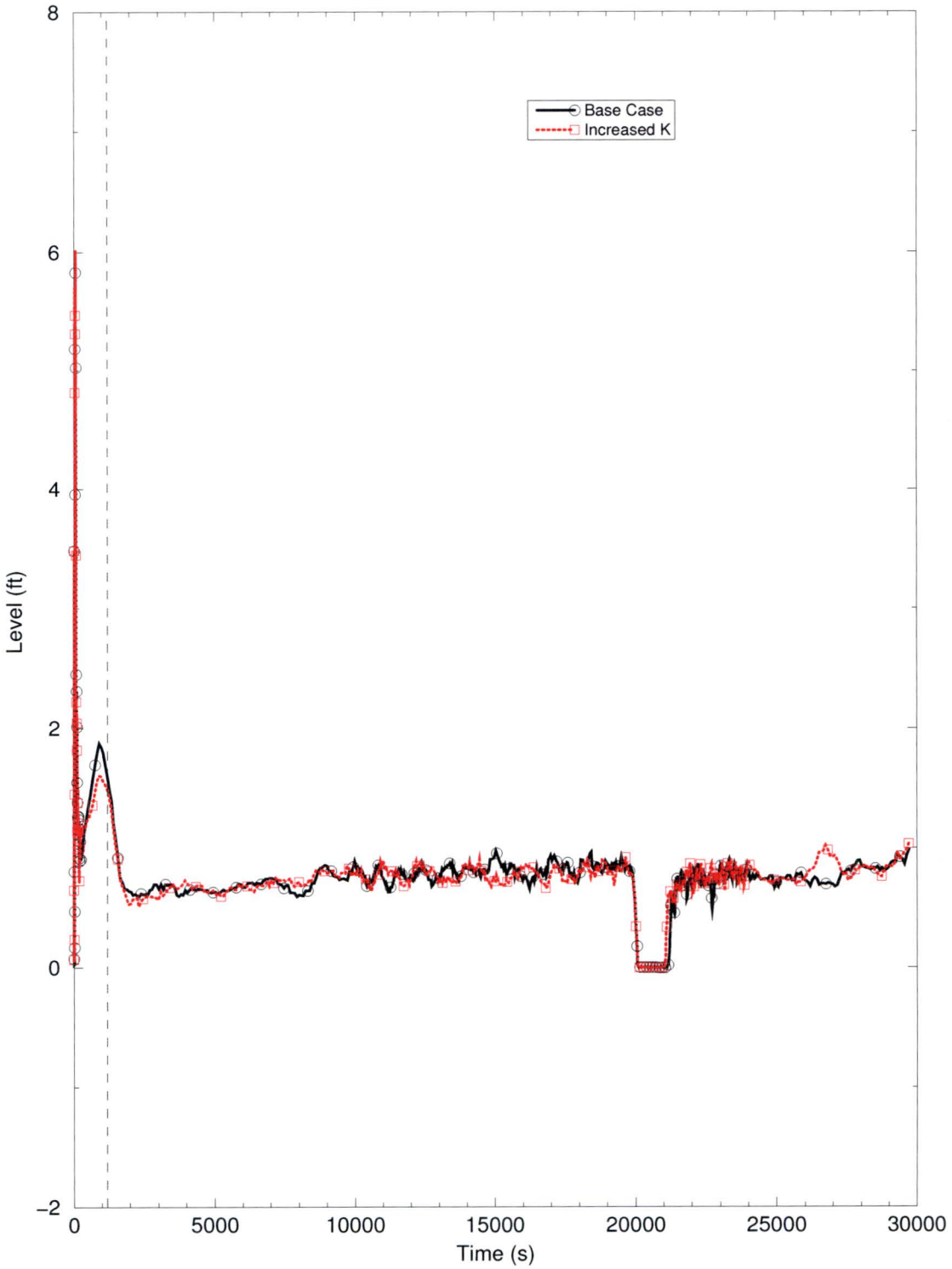

Figure RAI-4.27-6: Upper Plenum Liquid Level - 1.2x Decay Heat

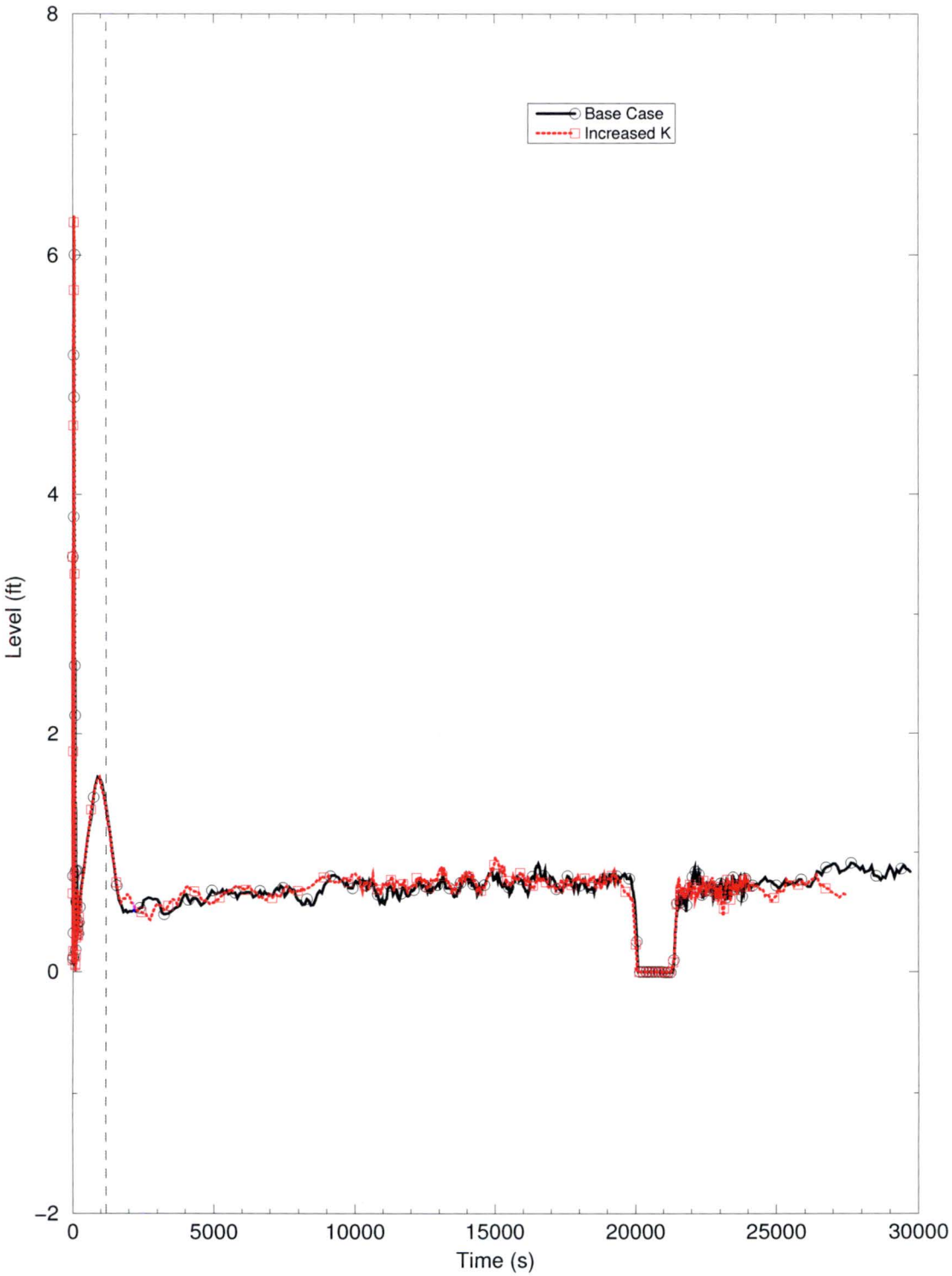

Figure RAI-4.27-7: PCT Trace - 1.1x Decay Heat

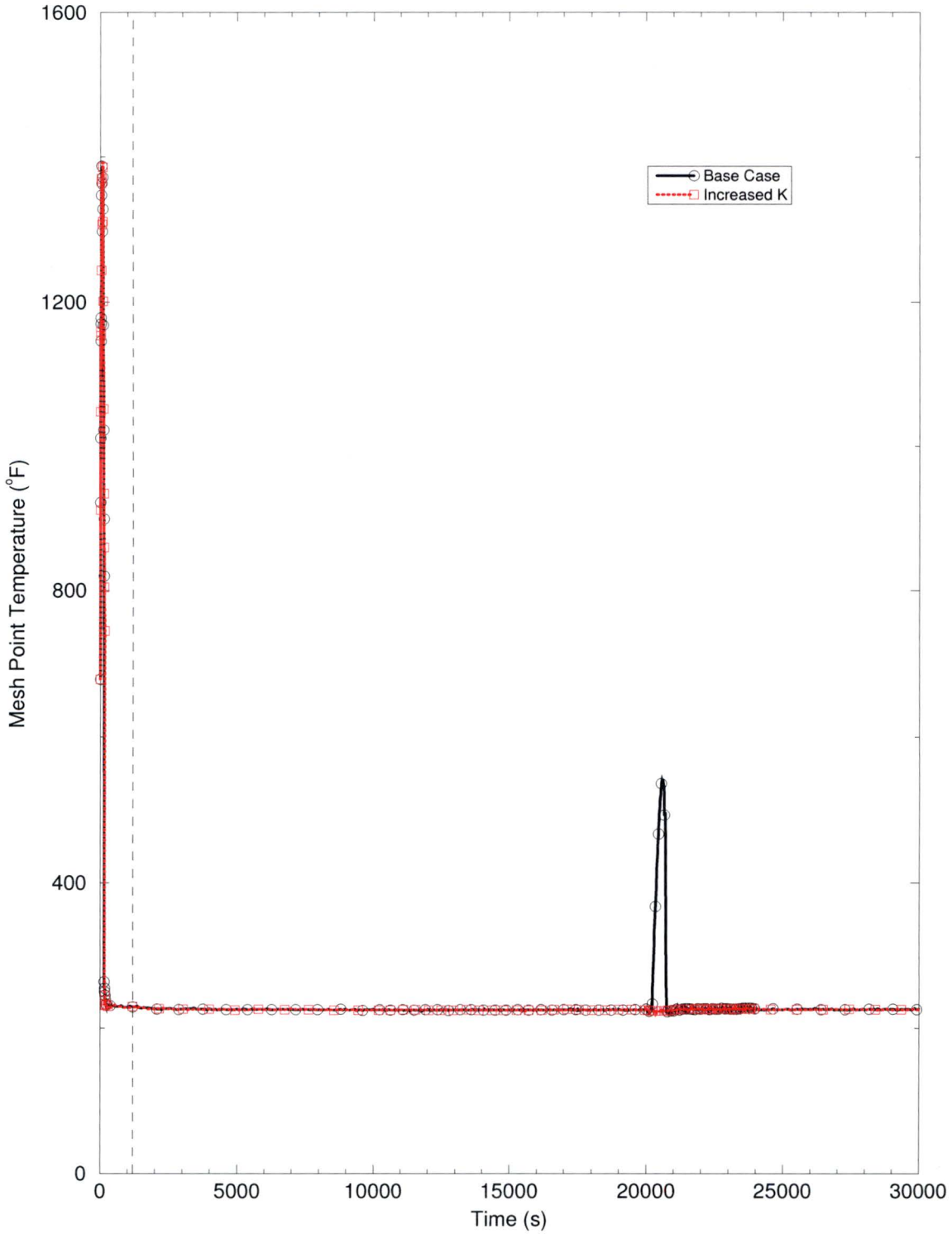

Figure RAI-4.27-8: PCT Trace - 1.2x Decay Heat

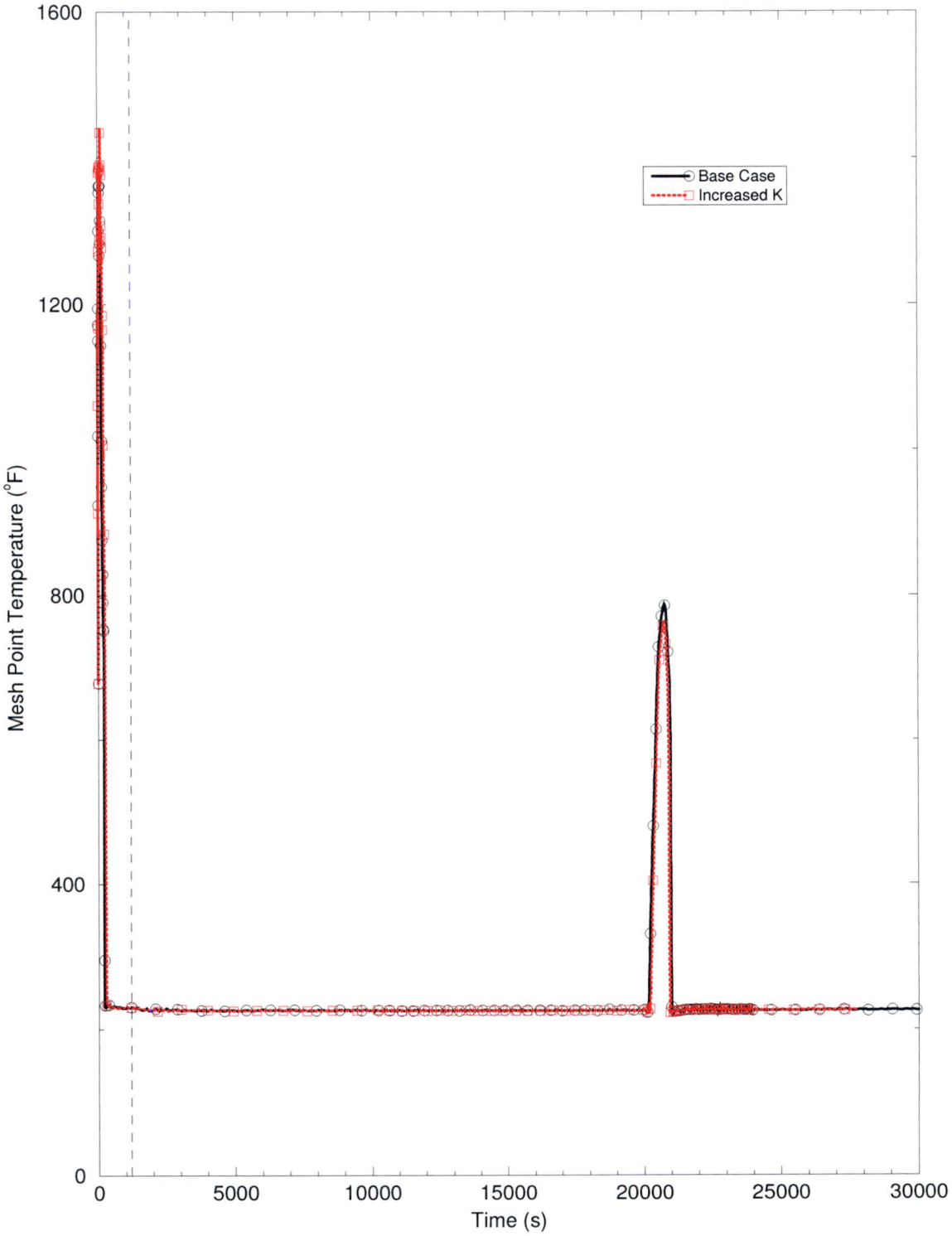

Figure RAI-4.27-9: Integrated Hot Assembly Exit Flow - 1.1x Decay Heat

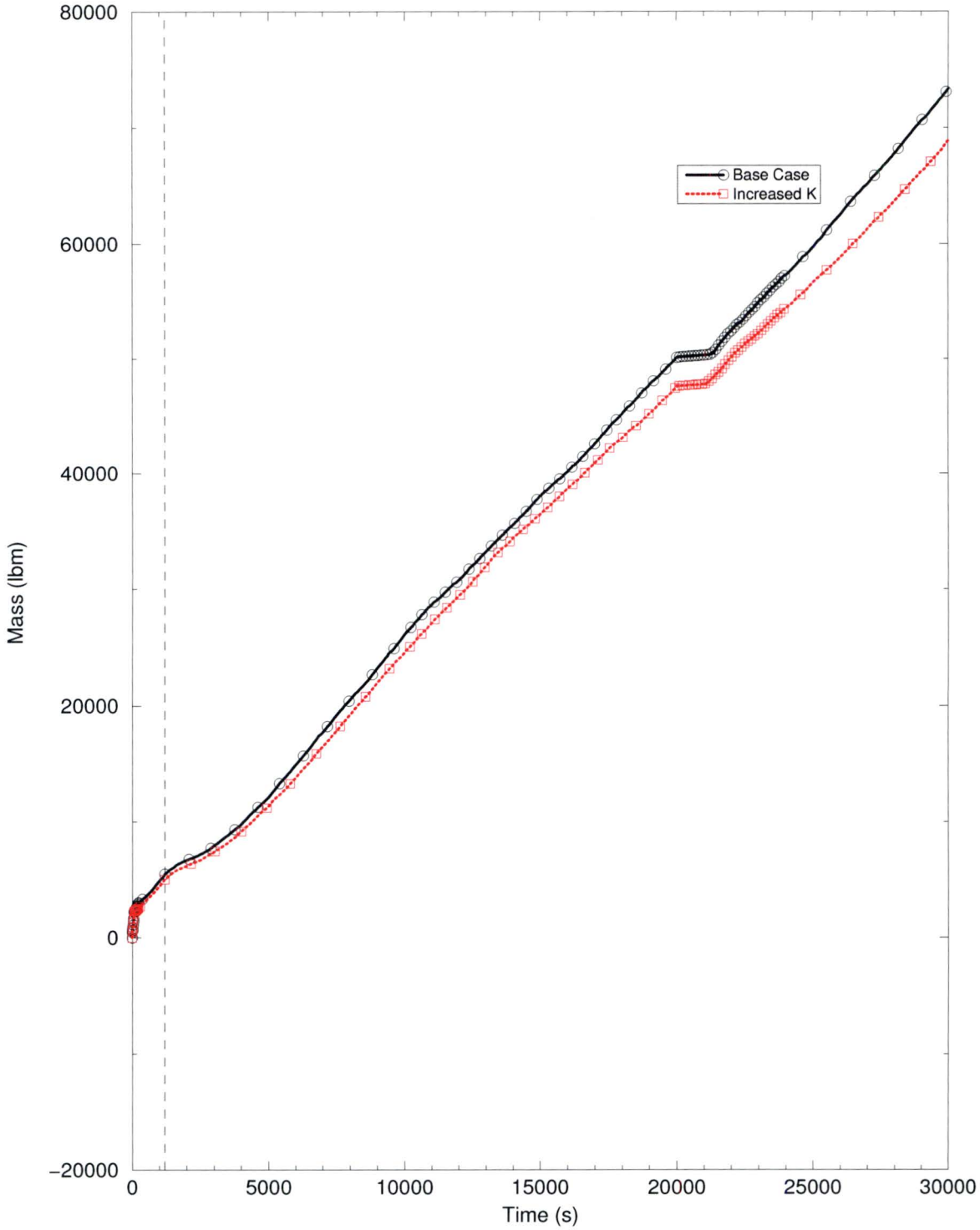

Figure RAI-4.27-10: Integrated Central Core Exit Flow - 1.1x Decay Heat

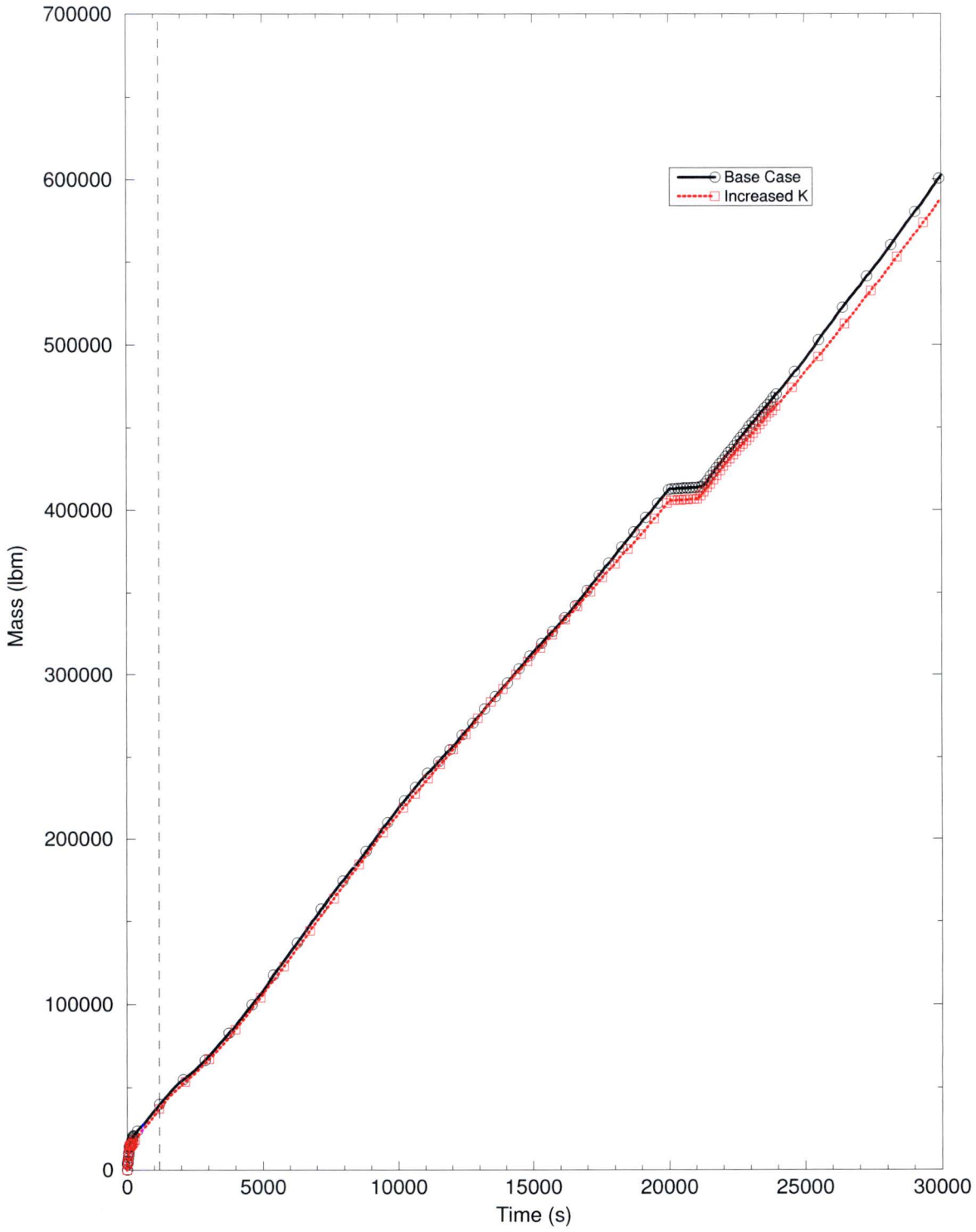

Figure RAI-4.27-11: Integrated Average Core Exit Flow - 1.1x Decay Heat

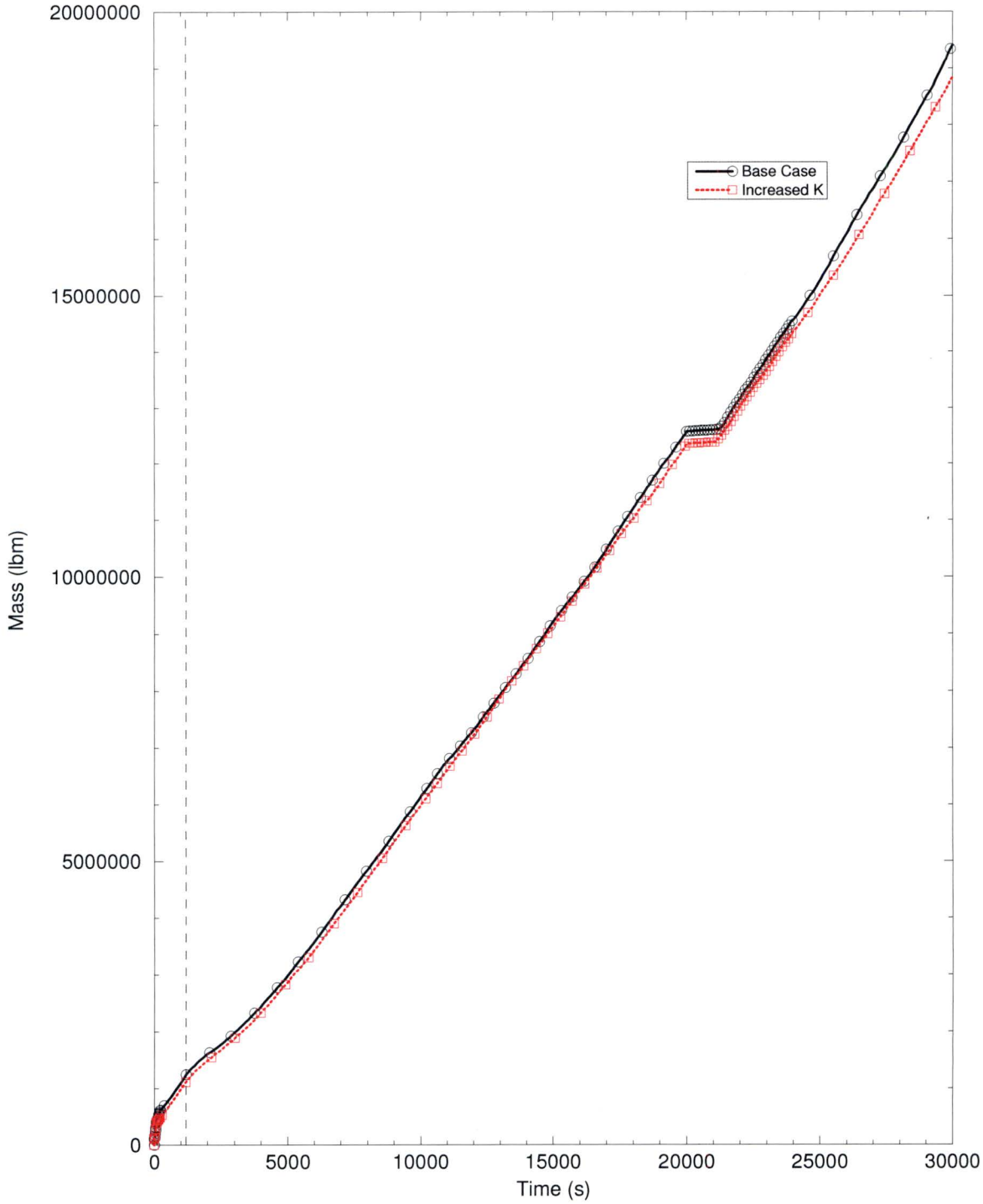

Figure RAI-4.27-12: Integrated Peripheral Core Exit Flow - 1.1x Decay Heat

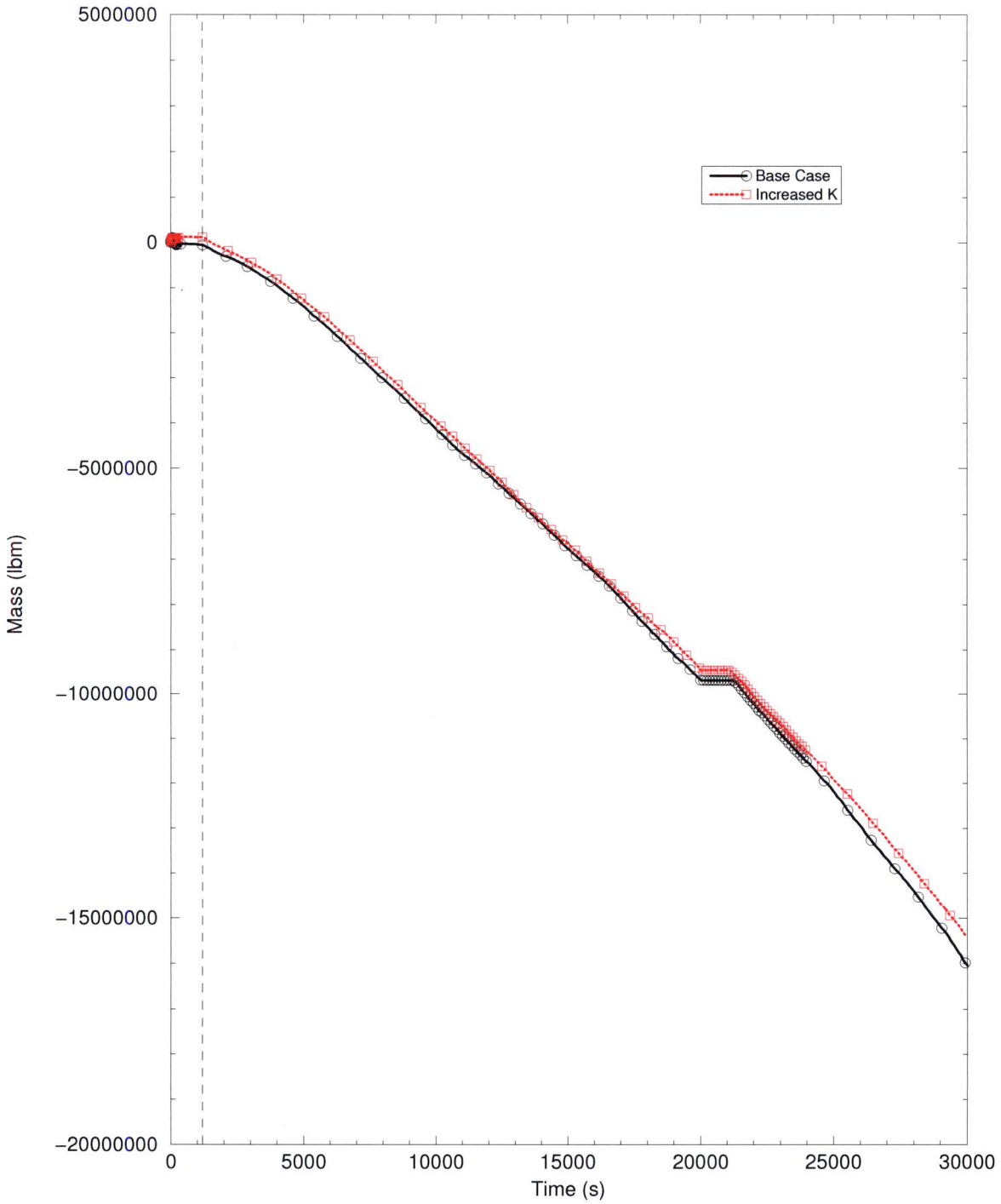

Figure RAI-4.27-13: Integrated Crossflow HA to CC at 0.77 ft - 1.1x Decay Heat

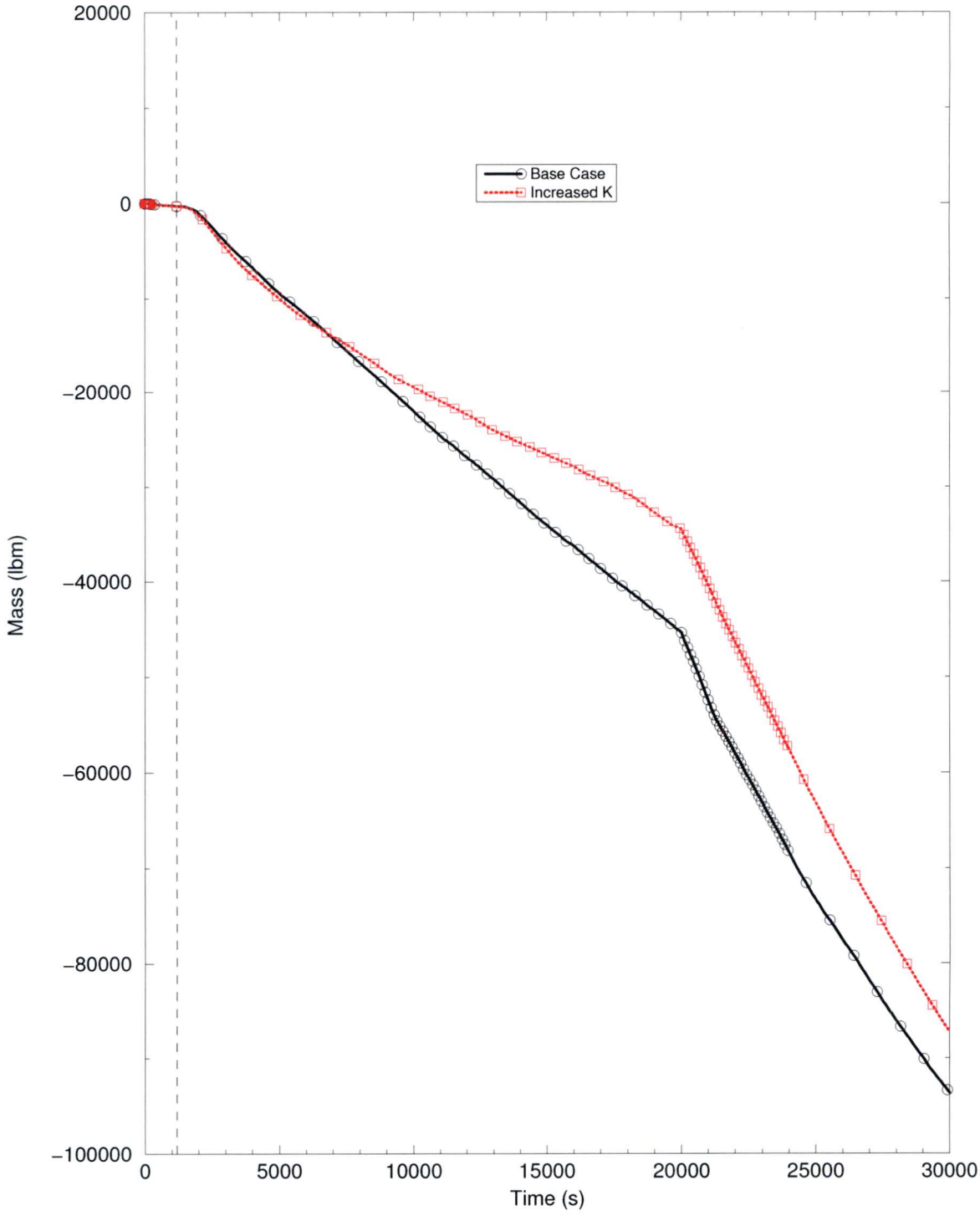

Figure RAI-4.27-14: Integrated Crossflow CC to AC at 0.77 ft - 1.1x Decay Heat

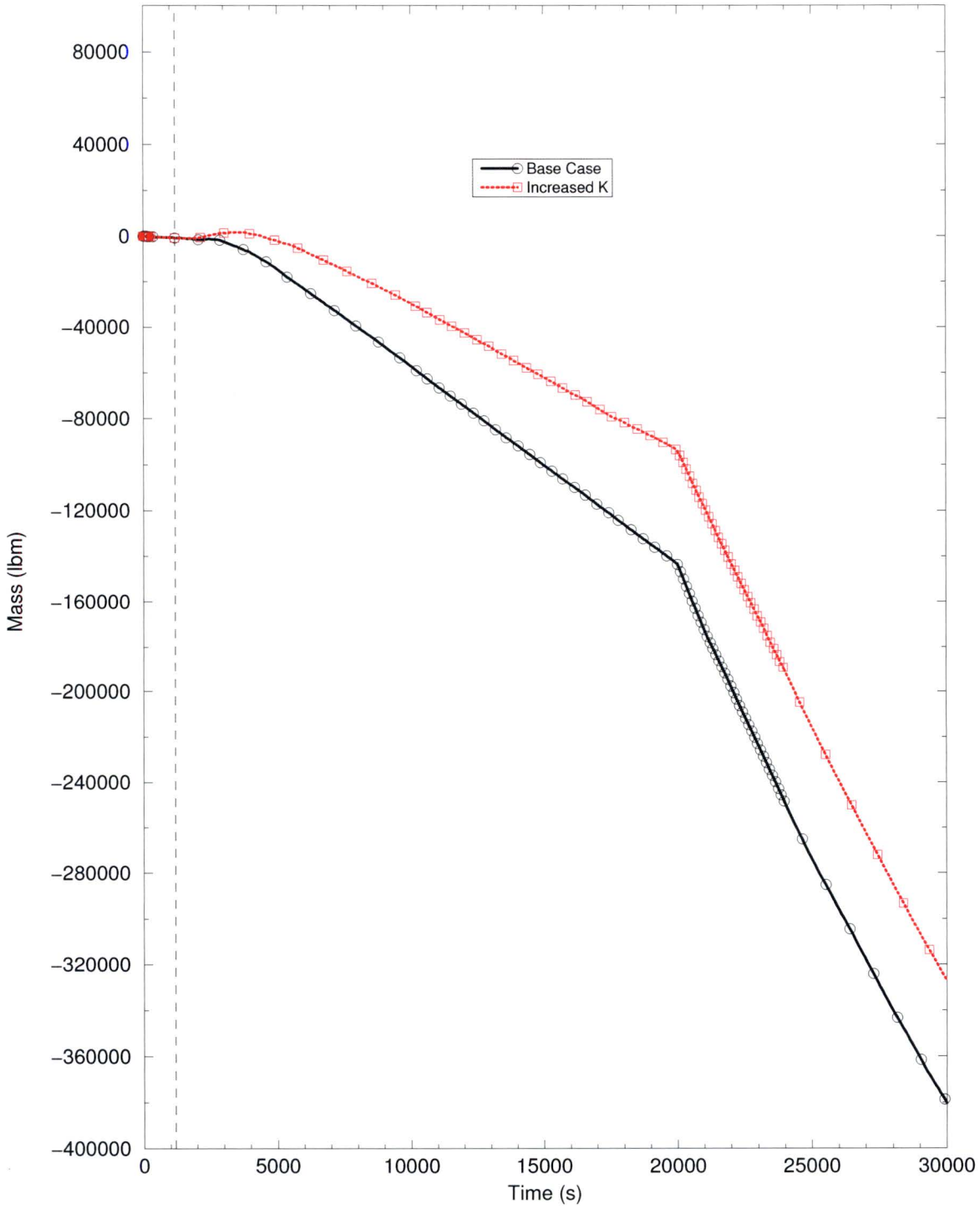

Figure RAI-4.27-15: Integrated Crossflow AC to PC at 0.77 ft - 1.1x Decay Heat

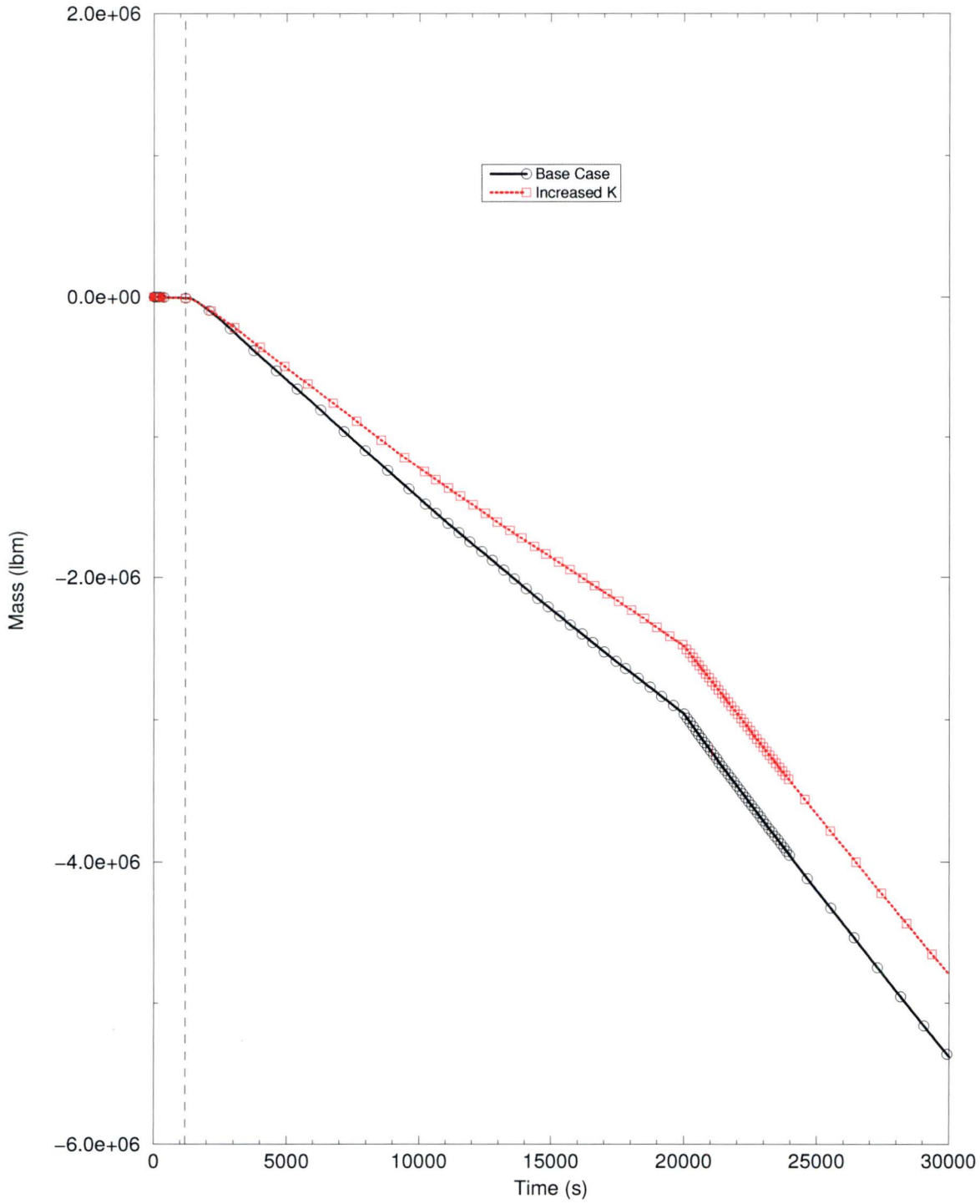

Figure RAI-4.27-16: Integrated Crossflow HA to CC at 10.92 ft - 1.1x Decay Heat

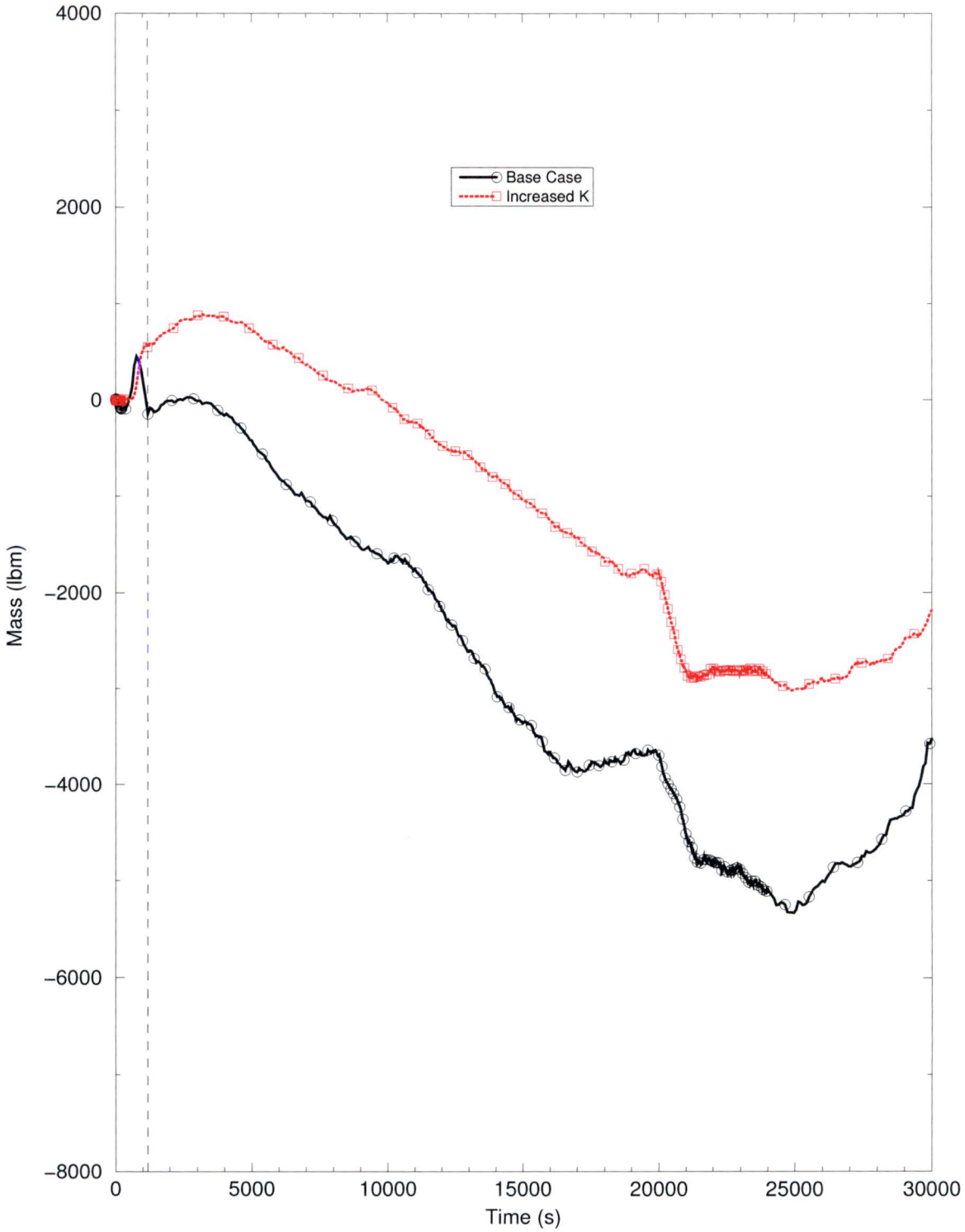

Figure RAI-4.27-17: Integrated Crossflow CC to AC at 10.92 ft - 1.1x Decay Heat

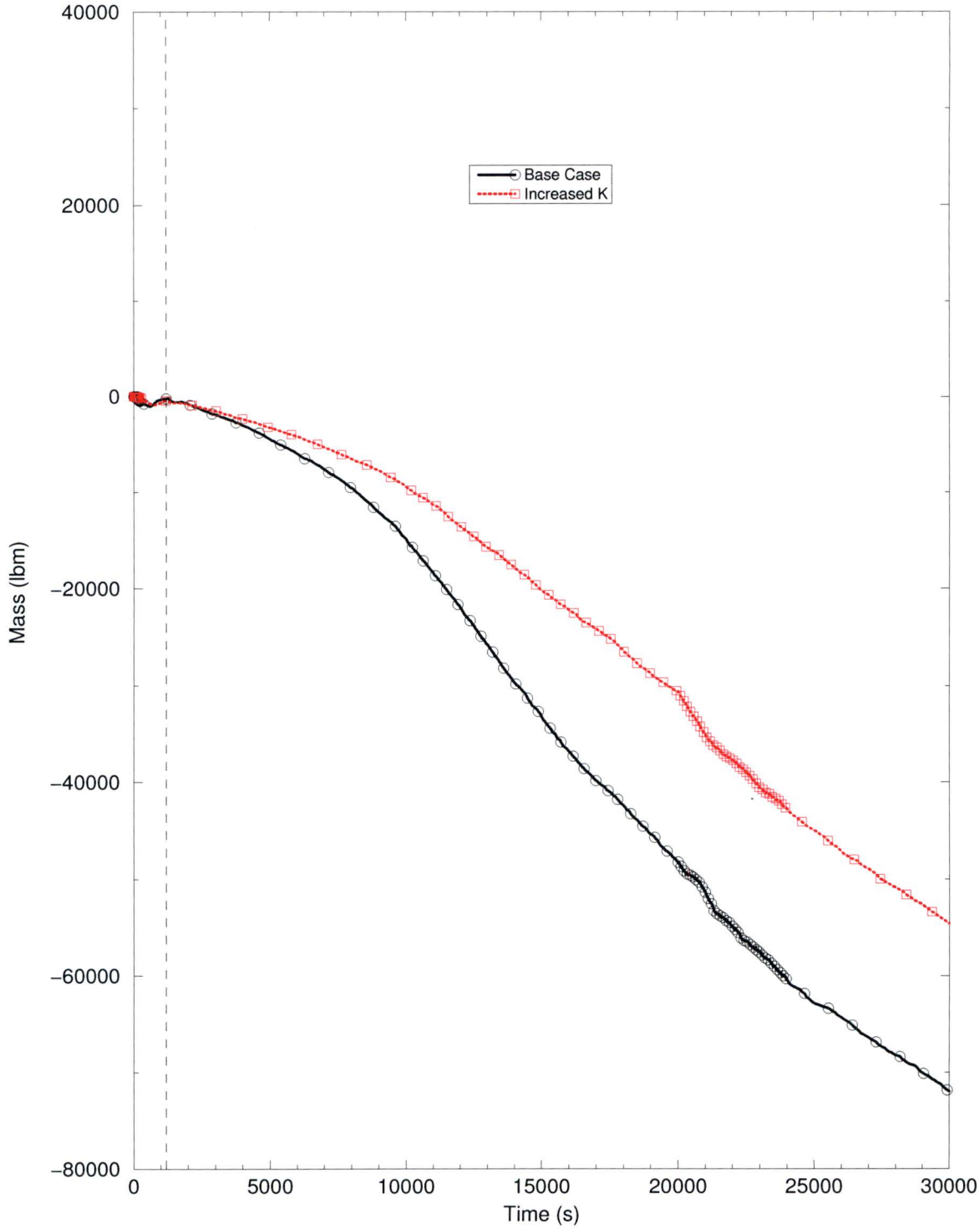

Figure RAI-4.27-18: Integrated Crossflow AC to PC at 10.92 ft - 1.1x Decay Heat

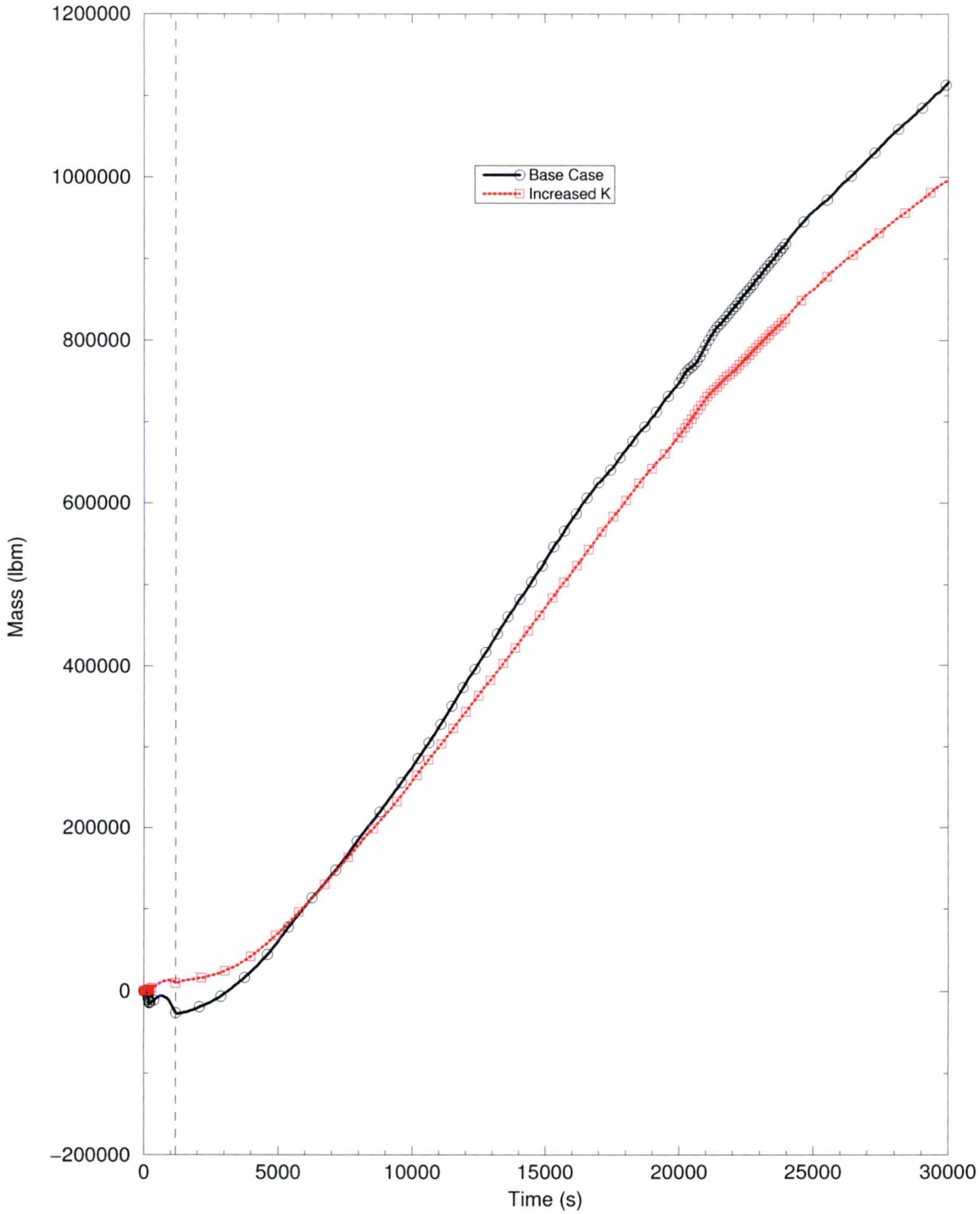

References - RAI 4.27

4.27-1 American Nuclear Society ANSI/ANS-5.1-1979, *American National Standard for Decay Heat Power in Light Water Reactors*.

2.28 RAI 4.28

2.28.1 Statement of RAI 4.28

The Westinghouse upflow, downflow, and CE base plant models were developed for best estimate (BE) PCT and clad oxidation analysis. As discussed in Section 6.1, many of the inputs from the BE models are set to nominal values. Some changes were made to bias the model toward an Appendix K analysis. The use of Appendix K type inputs is intended to add conservatism to the model to account for uncertainties associated with the LTCC phase following a LOCA.

Section 5 notes that the EMs used to analyze debris are based on NRC-approved EMs. For example, Section 5.1 notes that WCOBRA/TRAC MOD7A is used within the Code Qualification Document and ASTRUM EMs. However, the approach of nominal modeling with these codes has not been previously reviewed and accepted by the NRC.

Provide a table of all physical models and plant parameters that were considered in the uncertainty analysis for each computer code's most recently approved EM, and indicate how the uncertainty analysis has been adjusted to use a somewhat nominal, yet somewhat conservative analytic method. For each adjustment relative to the previously approved application, provide detail or justification that explains how the modified approach introduces an acceptable amount of conservatism. This table should expand on the information provided in, for example, Table 6-1, and should compare the current modeling approach to that previously approved for BE analysis.

2.28.2 Response to RAI 4.28

As discussed in Section 5 of the WCAP-17788-P Topical Report (TR), each plant category is analyzed using an approach that is based upon Nuclear Regulatory Commission (NRC)-approved Evaluation Models (EMs). For the Combustion Engineering (CE) plant design, the S-RELAP5 code is used, along with EMF-2103(P)(A), Rev. 0 plus changes referred to as the "transition package" as the base methodology. This was the most recently NRC-approved AREVA EM for Realistic Large Break Loss of Coolant Accident (RLBLOCA) analyses for the CE plant design at the time of submittal of the WCAP-17788-P TR.

Since a deterministic approach is being proposed for the analysis of debris with Generic Safety Issue (GSI)-191, the parameters that may normally be sampled within the base RLBLOCA EM need to be biased to provide a conservative analytic method that is built from a more Best Estimate (BE) methodology. An overview of the sampled parameters in

the base RLBLOCA methodology (includes changes from "transition package") is provided in Table RAI-4.28-1.

The range of the sampled plant parameters for the base San Onofre Nuclear Generating Station (SONGS) RLBLOCA analysis is provided in Table 3-3 of Reference 4.28-2. The range of some of the sampled parameters generic to the EMF-2103(P)(A), Revision 0 are provided in Table 4.19 of Reference 4.28-1. Note that as part of the "transition package", core power, decay heat, and offsite power availability are no longer sampled.

For the WCAP-17788-P TR, each of the sampled parameters described in Reference 4.28-1 is either biased high, low, or kept nominal in an effort to produce a conservative analysis that is built from a BE approach. The following discussion applies to the revised analysis described in RAI 4.1b (see Section 2.1.2).

A summary of the reasons for the way each parameter is treated in the WCAP-17788-P TR is as follows:

- **Axial Skew** - A top-peaked axial power shape is selected for the WCAP-17788-P TR analysis for the CE plants. The top skew raises cladding temperature during any core uncovery. A top-peaked axial shape also minimize the mixture level swell in the core. Details of the power shape are provided in response to RAI 4.5b and 4.5c.
- **Break Type** - A Double-Ended Guillotine (DEG) break type is selected.
- **Break Size** - A full 2A (200% pipe area) DEG break in the Hot Leg (HL) is assumed. The reasons for this selection are provided in Volume 1, Section 3.6 of WCAP-17788-P.
- **Core Power** - The reference CE plant core power (with uncertainty) is 3458 MWt. The response to RAI 4.5a provides additional justification of the selection of this value (see Section 2.5.2).
- **Decay Heat** - The base RLBLOCA uses a fixed (not sampled) value for decay heat. The base EM uses 1.0 x American Nuclear Society (ANS) 1979 Standard decay heat with infinite operation and 200 MeV/fission. The WCAP-17788-P TR increases the decay heat in order to 1.1 x ANS 1979 Standard decay heat with infinite operation. The decay heat is increased to increase Peak Cladding Temperature (PCT) during any core uncovery. The response to RAI 4.5a provides additional justification of the use of increasing the decay heat to 1.1 x ANS 1979 Standard decay heat (see Section 2.5.2).
- **Offsite Power** - The offsite power assumption selected for the WCAP-17788-P TR analysis for the CE plants is with Loss of Offsite Power (LOOP). This was selected as it was the limiting condition for the RLBLOCA PCT analysis and remains as a

justified assumption for the WCAP-17788-P TR analysis. The choice of offsite power has little bearing on the results for the WCAP-17788-P TR analysis as by the time of Sump Switch Over (SSO), any differences wash out between the two options (Emergency Core Cooling System (ECCS) pumps have long been started, so delay times are not a factor, Reactor Coolant Pumps (RCPs) are tripped, etc.).

- **F_Q** - The total peaking (F_Q) is set to a maximum value for the WCAP-17788-P TR analysis. The value of F_Q used was 2.37 (based on Linear Heat Generation Rate (LHGR)) in the original WCAP-17788-P TR analysis. This value has been subsequently increased to a value of 2.545 in the revised WCAP-17788-P TR analysis described in response to RAI 4.1b in order to cover the maximum peak LHGR within the CE fleet of plants. A maximum total peaking drives local cladding temperatures higher, thereby adding conservatism to the calculated PCT during any core uncovery. The axial power profiles use a high radial peaking factor ($F_r^T = 1.81$), high linear heat generation rate (LHGR=13.75 kW/ft). The response to RAI 4.5a provides additional justification of the selection of this value (see Section 2.5.2).

- **T_{min}** - The minimum stable film boiling temperature (T_{min}) is set to the mean value of the sampling range. The value of T_{min} essentially sets the quench temperature and return to nucleate boiling after a cladding temperature excursion. In the short-term Loss of Coolant Accident (LOCA), the cladding heats to some high value. As the reflood process occurs, the cladding temperature gradually reduces until it reaches T_{min}. Once this occurs, the cladding is quenched and returns to a temperature of approximately T_{sat}. For the GSI-191 application, the degree of heatup in the long-term is limited to 800 °F and the heat flux is low by the time of SSO, and therefore cannot maintain boiling in the transition/film boiling regimes. Therefore, the value of T_{min} is of little importance and the use of the mean value is reasonable and justified.

- **Steam Generator Inlet Plenum Fij** - A multiplier applied to the interfacial drag on inlet to the Steam Generator (SG) plenums is set to a value consistent with the base RLBLOCA EM. This multiplier is designed for enhancing steam binding effects, but those effects do not apply in the HL break analyzed in the WCAP-17788-P TR analysis. Therefore, the use of this value is reasonable and justified.

- **Condensation Interphase Heat Transfer Coefficient (HTC) Multiplier** - The condensation interphase HTC multiplier in the Downcomer (DC) region is set to the maximum value normally sampled. Within the "transition package", this value is of little consequence as the "transition package" includes additional condensation interphase HTC multipliers within the cold legs, in order to drive the ECCS fluid towards saturation conditions prior to entering the DC. In addition, after SSO for the

WCAP-17788-P TR analysis for the CE plants, the ECCS fluid is set to saturated conditions. Therefore, the condensation interphase HTC multiplier is of little importance during the period of interest for the WCAP-17788-P TR application.

- **Metal Water Reaction** - Nominal values used for the Metal-Water Reaction (MWR), Baker-Just model replaces Cathcart-Pawel. The Baker-Just model is used in Appendix K applications. As the core stays generally covered in the long term for the WCAP-17788-P application and that the PCT acceptance criteria is relatively low (800 °F), the degree of oxidation (and the contribution of the MWR and the cladding temperature) the impact of the MWR will have little importance. However, the modeling used for the MWR is kept consistent with Appendix K applications (such as Small Break Loss of Coolant Accident (SBLOCA)), thus properly capturing this process.

- **Film Boiling HTC Multiplier** - A value of approximately 1.0 is used for the film boiling multiplier for the WCAP-17788-P TR analysis. Nucleate boiling is expected to dominate the period of interest. The core remains covered for the majority of the transient with the expectation of switching to a steam cooling mode for period after t_{block}, if the core uncovers. As a result, the film boiling multiplier for the WCAP-17788-P TR analysis is not important and the use of a nominal value is reasonable and justified.

- **Dispersed Film Boiling HTC Multiplier** - A value of approximately 1.0 is used for the dispersed film boiling multiplier for the WCAP-17788-P TR analysis. Nucleate boiling is expected to dominate the period of interest. The core remains covered for the majority of the transient with the expectation of switching to a steam cooling mode for period after t_{block}, if the core uncovers. As a result, the dispersed film boiling multiplier for the WCAP-17788-P TR analysis is not important and the use of a nominal value is reasonable and justified.

- **Critical Heat Flux (CHF)** - The CHF multiplier is consistent with the value reported in the base RLBLOCA EM (see Table 4.19 of Reference 4.28-1) and remains appropriate for the GSI-191 application. The heat flux in the long term (after SSO) is relatively low and CHF is not expected. Even if CHF did occur in the WCAP-17788-P TR analysis, the Biasi CHF multiplier will be consistent with the short-term LOCA phase. Therefore, the selection of the Biasi CHF multiplier is appropriate for the WCAP-17788-P TR application.

- **Initial Stored Energy** - While the initial stored energy is of little to no consequence during the period of interest in the WCAP-17788-P TR analysis, the value is biased high to maximize initial stored energy. The break will have removed the initial stored energy from the Reactor Coolant System (RCS) by the time of SSO. Since the initial stored energy will have been removed by the time of SSO, the selection

of the bias placed on the initial stored energy has no influence on the GSI-191 results in the WCAP-17788-P TR analysis.

- **Initial RCS flow rate** - The initial RCS flow rate is set to a minimum flow rate. This reduces the heat transfer in the initial phase of the event (before RCPs trip). The impact of this selection will have no impact once the period of interest is reached for this scenario (after SSO) since the forced RCS flow has long since stopped and the RCS piping is mostly voided. Therefore, the selection of the bias placed on the initial RCS flow rate has no influence on the GSI-191 results in the WCAP-17788-P TR analysis.

- **Downcomer Hot Wall Effects** - The downcomer hot wall effects are included in the WCAP-17788-P TR analysis. Like with other parameters related to initial stored energy, the selection is of no significant consequence as the initial stored energy in the downcomer is mostly removed and discharged through the break before the period of interest (after SSO)in the WCAP-17788-P TR analysis. Thus, the selection of the downcomer hot wall effects has no significant influence on the results for GSI-191 in the WCAP-17788-P TR analysis.

- **Vessel Side Break Discharge Coefficient** - The vessel-side break discharge coefficient for critical flow is biased high, in order to bound the nominal value + 3σ. This maximizes the break flow in the early phase of the transient, leading to a lower RCS inventory in the short term. However, by the time of SSO the break flow is not choked and the value of this break discharge coefficient for critical flow will not influence the results in the period of interest.

- **Pump Side Break Discharge Coefficient** - The pump side break discharge coefficient for critical is biased high, in order to bound the nominal value + 3σ, just like the vessel-side break discharge coefficient. Like the vessel-side break discharge coefficient, this value becomes unimportant by the time SSO occurs.

- **Pressurizer Surgeline Critical Flow Coefficient** - The critical flow coefficient in the Pressurizer (PZR) surgeline is set to the nominal value during the short-term LOCA phase, where the flow may be choked. As with the other critical flow coefficients, this value is not important for the analyses performed in the WCAP-17788-P TR since the effects of this coefficient are over by the time of SSO.

- **Time in Cycle** - The time in cycle for the WCAP-17788-P TR analysis is set to the value used in the limiting base RLBLOCA PCT case. The time in cycle of the fuel is not expected to play an important role during the period of interest.

- **Initial RCS Temperature** - The plant RCS temperature is controlled based on T_{cold}. This temperature is biased high in order to maximize the initial stored energy contained within the fluid. However, like with other parameters related to initial

stored energy, the selection is of little consequence as the effects have been removed well before the period of interest in the WCAP-17788-P TR analysis.

- **Initial Upper Head Temperature** - The CE plant analyzed is a T_{hot} plant. The upper head temperature is varied in the base RLBLOCA EM by sampling flow resistance to the upper head. The upper head temperature used in the WCAP-17788-P TR analysis is set to T_{hot}. The initial upper head temperature is not important in the WCAP-17788-P TR analysis as the effects of the initial head temperature no longer exist by the time of SSO.

- **Initial Pressurizer Pressure** - The initial pressurizer pressure is set to the nominal value. The period of interest in the WCAP-17788-P TR analysis is well after the primary system blows down with the DEG HL break. As such, the initial pressurizer pressure is not important.

- **Initial Pressurizer Liquid Level** - The initial pressurizer level is set to the nominal value. The period of interest in the WCAP-17788-P TR analysis is well after the primary system blows down with the DEG HL break. As such, the initial pressurizer level is not important.

- **Containment Volume** - The containment volume is typically sampled. The initial S-RELAP5 analysis for the CE plants used the ICECON containment model within the S-RELAP5 code. In order to minimize the containment back-pressure, the maximum containment free volume for the entire CE fleet was selected. The updated analysis (see response to RAI 4.1b in Section 2.1.2) was changed to a constant 14.7 psia containment pressure for the period of interest. Therefore, the containment volume is not applicable.

- **Safety Injection Tank (SIT) Temperature** - The SIT temperature is set to the nominal value for the WCAP-17788-P TR analysis. The SITs empty well before the period of interest, given that this is a DEG HL break. As such, the initial SIT temperature is not important.

- **SIT Pressure** - The SIT pressure is set to a minimum value for the WCAP-17788-P TR analysis. The minimum SIT pressure delays injection slightly. However, the SITs empty well before the period of interest, given that this is a DEG HL break. As such, the initial SIT pressure is not important.

- **SIT Volume** - The SIT initial volume is set to a minimum value for the WCAP-17788-P TR analysis. The minimum SIT volume reduces the amount of SIT water during the short-term LOCA phase. However, the SITs empty well before the period of interest, given that this is a DEG HL break. As such, the initial SIT volume is not important.

Table RAI-4.28-1: Sampled LBLOCA Parameters - CE Plant

Phenomenological	
	Time in cycle (peaking factors, axial shape, rod properties, burnup)
	Break type (guillotine vs. split)
	Break size
	Critical flow discharge coefficients (break)
	Critical flow discharge coefficients (surgeline)
	Initial upper head temperature
	Pump 2-phase degradation
	Film boiling heat transfer
	Dispersed film boiling heat transfer
	Critical heat flux
	T_{min} (intersection of film and transition boiling)
	Initial stored energy
	Downcomer hot wall effects
	Steam generator interfacial drag
	Condensation interphase heat transfer
	Metal-water reaction
Plant	
	Pressurizer pressure
	Pressurizer level
	Accumulator pressure
	Accumulator level
	Accumulator temperature
	Containment temperature
	Containment volume
	Initial RCS flow rate
	Initial operating temperature
	Refueling Water Storage Tank (RWST) temperature
	Diesel start (for LOOP only)

References - RAI 4.28

4.28-1 AREVA Inc. Document EMF-2103(P)(A), Revision 0, *Realistic Large Break LOCA Methodology for Pressurized Water Reactors*.

4.28-2 ANP-2975(NP), Revision 0, "San Onofre Nuclear Generating Station, Unit 2 and Unit 3 - Realistic Large Break LOCA Report," Enclosure 6. (ADAMS: ML11215A091).

2.29 RAI 4.29

2.29.1 Statement of RAI 4.29

State whether the base plant models were submitted to the NRC to document safety analysis. Describe how the changes made to the base models regarding core volumes, ECCS model, BB flow resistance, break pressure boundary conditions, break flow multipliers, core inlet blockage, and calculation inputs in Tables 6-1 through 6-4 maintain adequate conservatism.

2.29.2 Response to RAI 4.29

The base model for the Combustion Engineering (CE) plant design in the WCAP-17788-P analysis is the San Onofre Nuclear Generating Station (SONGS) Realistic Large Break Loss of Coolant Accident (RLBLOCA) uncertainty analysis. The SONGS RLBLOCA analysis was performed using the EMF-2103(P)(A), Revision 0 methodology, including modifications as a result of the "transition package". This model was submitted to the Nuclear Regulatory Commission (NRC) staff as part of the SONGS License Amendment Request (LAR) to transition to AREVA fuel with M5 cladding. The review and approval of the SONGS LAR was never completed by the NRC staff as the plant decided to shutdown. However, a similar model was reviewed and approved by the NRC staff for St. Lucie Unit 2 plant (Reference 4.29-1). It also uses the EMF-2103(P)(A), Revision 0 methodology, including modifications as a result of the "transition package". The differences between the St. Lucie Unit 2 plant model and the SONGS plant model are only those that are plant-specific.

The changes made to the base model as part of the WCAP-17788-P Topical Report (TR) and how the changes made maintain adequate conservatism are discussed in RAIs 4.1b, 4.5, and 4.28 (see Sections 2.1.2, 2.5.2, and 2.28.2, respectively.)

References - RAI 4.29

4.29-1 St. Lucie Nuclear Plant, Unit 2 - Redacted - Issuance of Amendment Regarding License Amendment Request for the Transitioning to AREVA Fuel (CAC No. MF5495) (ADAMS: ML16063A121).

2.30 RAI 4.30

2.30.1 Statement of RAI 4.30

Figure 8-19 shows two time periods after complete core blockage during which the downcomer level remains steady (around 19 and 22 ft) before leveling out for the remainder of the transient. This could be explained by an accumulation of injected liquid in parts of the RCS outside of the RV. In addition, possible transport of liquid into the reactor upper plenum via the SG U-tube bundles can take place after filling the cold leg side of the RCS.

The variable m_{split} is defined as the flow split between the core inlet and AFPs. Figures 8-5, 9-4, 10-5, and 11-4 depict the calculated inputs for m_{split}.

(a) Was passage of ECCS liquid into the upper plenum via the SGs predicted for any of the runs used to produce the results shown in Figures 8-5, 9-4, 10-5, and 11-4? For each case that predicted flow into the upper plenum via the SGs, plot (in units of lbm/s) the rate of liquid flow that enters into the core, the AFPs, the reactor upper plenum through each loop, and the total amount into the upper plenum via all loops as functions of time.

(b) Define how m_{split} is calculated in Case 1B considered in Figure 8-19 and illustrate the m_{split} calculation for this case by plotting the rate (in units of lbm/s) of liquid flow into the core and into the BB AFP, the ECCS recirculation flow, the flow into the upper plenum via the SGs, if predicted, and the calculated m_{split} ratio (in dimensionless units) as functions of time.

(c) Provide details of the calculation of m_{split} for any runs that resulted in liquid transport into the reactor upper plenum via the SGs.

2.30.2 Response to RAI 4.30

2.30.2.1 Response to RAI 4.30a

New calculations to determine m_{split} were performed and documented in the response to RAI 4.20. Table RAI-4.30-1 repeats the new case matrix.

For each case, the Steam Generator (SG) primary downside (crossover leg side as opposed to the of Hot Leg (HL) side) levels, instantaneous liquid mass flowrates at the top of the SG U-tubes and their integrals are plotted (Figure RAI-4.30-1 through Figure RAI-4.30-24).

From these figures, sporadic liquid flow can be observed over the top of the U-tubes for both SGs before SG primary downside levels reach the top of the U-tubes. This is because the SG secondary side is bottled up and stays at hot conditions during the transient. When the relatively cold coolant reaches SG tubes, it boils and carries liquid droplets to the top of the U-tubes. For conservatism, it is assumed that these liquid droplets contain debris.

For some cases (newcase2, newcase3 and newcase6), SG primary downside levels reach the top of the U-tubes during the transient and spillover starts to occur (Figure RAI-4.30-5, Figure RAI-4.30-9 and Figure RAI-4.30-21). In these cases, the spillover liquid flowrates in the broken loop SG are much larger than the spillover liquid flow in the intact loop SG (Figure RAI-4.30-6, Figure RAI-4.30-7, Figure RAI-4.30-8, Figure RAI-4.30-10, Figure RAI-4.30-11, Figure RAI-4.30-12, Figure RAI-4.30-22, Figure RAI-4.30-23 and Figure RAI-4.30-24), because the broken loop has a lower exit pressure than the intact loop.

Liquid flow through the broken loop SG will not reach upper plenum and have no impact to m_{split} since the flow will exit to the containment through the double-ended guillotine break on the hot leg.

Liquid flow through the intact loop SG will enter the reactor vessel upper plenum. To quantify the effect of debris that may be carried in such liquid flow, the integrated liquid flow through the intact loop SG is compared to the integrated flow through the downcomer for each case, for the period from the beginning of sump recirculation to the end of the transient. Table RAI-4.30-2 lists the comparison of the integrated flows and their ratio.

It can be seen that the integrated Emergency Core Cooling System (ECCS) liquid flow entering the reactor vessel upper plenum via the intact loop SG is less than 1% of the integrated ECCS liquid flow entering the core inlet and Alternate Flow Path (AFP) through the downcomer. Since mass of debris is transported proportionally to the flow rate, less than 1% of the debris would be carried over the intact loop. Any debris carried in this fluid is not included in the m_{split} calculation (see response to "c" below). It is also neglected in the debris transport to the heated core; however, conservatisms in the debris accumulation calculation more than make up for this negligible additional debris. Specifically, no debris is assumed to exit the break, including the debris that would be in the liquid that spills over the broken loop SG. This flow is much larger than the intact leg flow rate (compare Figure RAI-4.30-23 to Figure RAI-4.30-24, for example). Instead, all debris that enters the Reactor Coolant System (RCS) is assumed to reach the reactor vessel downcomer and approach the core inlet where it will be deposited at the core inlet or transported to the heated core via the AFP. Therefore, the ECCS liquid flow entering the upper plenum via SG and any debris carried by the liquid flow are neglected.

Table RAI-4.30-1: New Case Matrix

Case Name	Baffle Resistance K/A^2 (ft^{-4})	ECCS Flow (gpm)
newcase1	[ ]	827
newcase2	[ ]	1654
newcase3	[ ]	2481
newcase4	[ ]	827
newcase5	[ ]	1654
newcase6	[ ]	2481

Table RAI-4.30-2: Integrated Liquid Flow Comparison after Sump Recirculation Starts

Case Name	Intact Loop SG Integrated Liquid Flow (lbm)	Downcomer Integrated Liquid Flow (lbm)	Ratio %
newcase1	20959.6	2.90E+06	0.72
newcase2	25305.0	5.78E+06	0.44
newcase3	19303.5	7.37E+06	0.26
newcase4	14176.5	2.99E+06	0.47
newcase5	12113.6	5.94E+06	0.20
newcase6	26707.7	7.94E+06	0.34

Figure RAI-4.30-1: SG Primary Downside Collapsed Liquid Levels - ECCS Flowrate = 827 gpm; BB Resistance K/A^2 = [ ] ft^{-4}

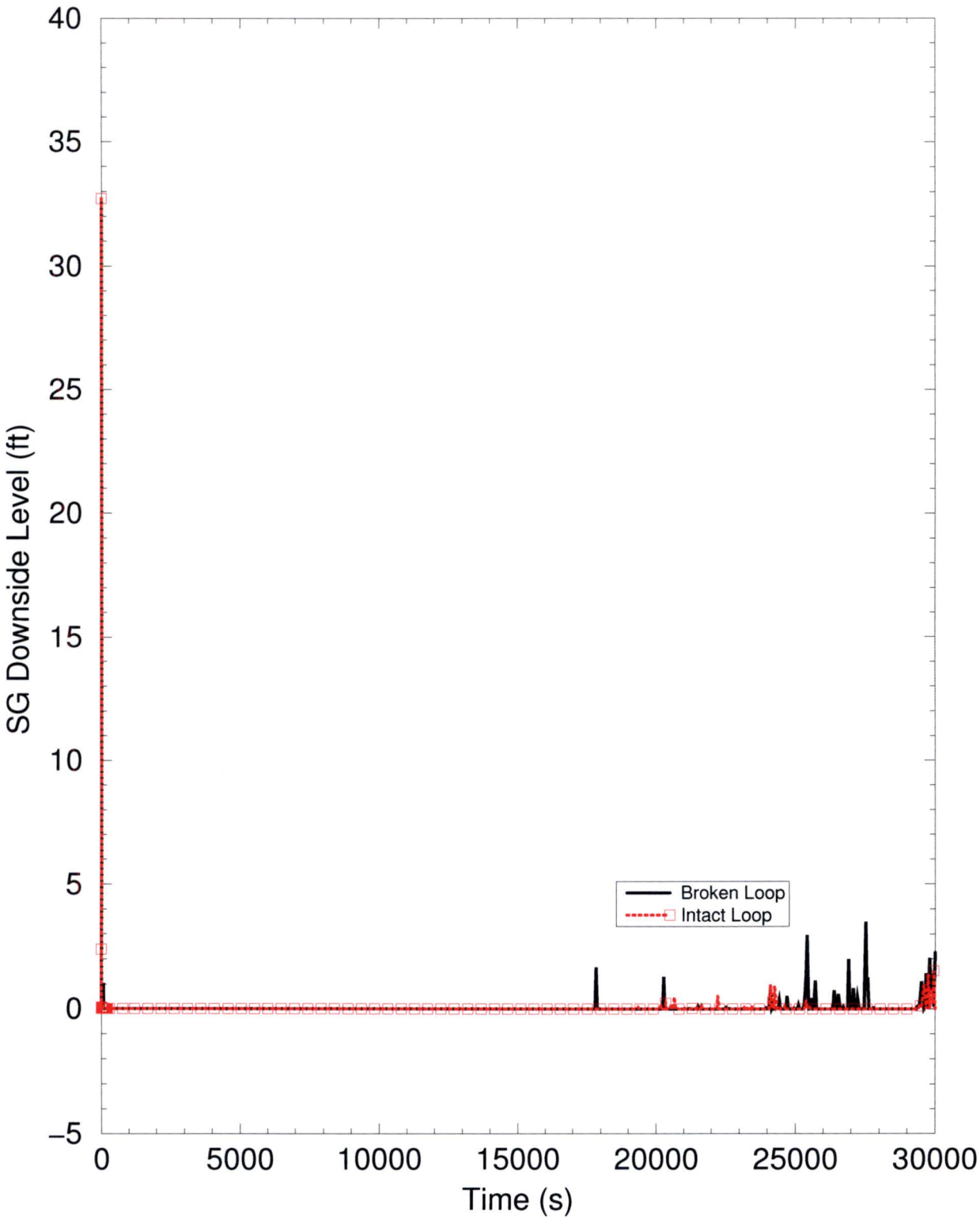

Figure RAI-4.30-2: Liquid Flow at the Top of the SG U-Tubes - ECCS Flowrate = 827 gpm; BB Resistance K/A^2 = [ ] ft^{-4}

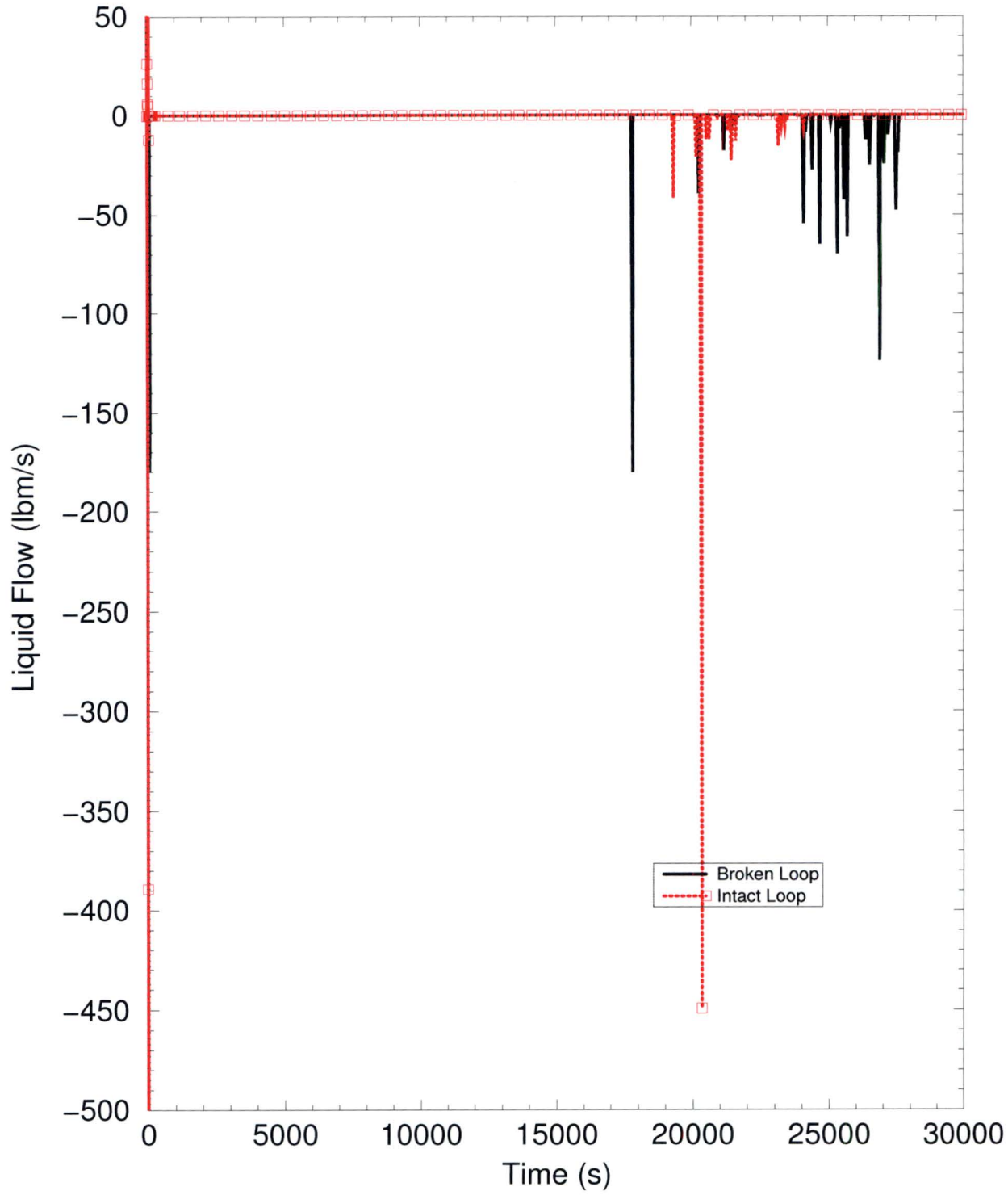

Figure RAI-4.30-3: Integral of Liquid Flow at the Top of the SG U-Tubes on the Intact Loop - ECCS Flowrate = 827 gpm; BB Resistance K/A^2 = [ ] ft^{-4}

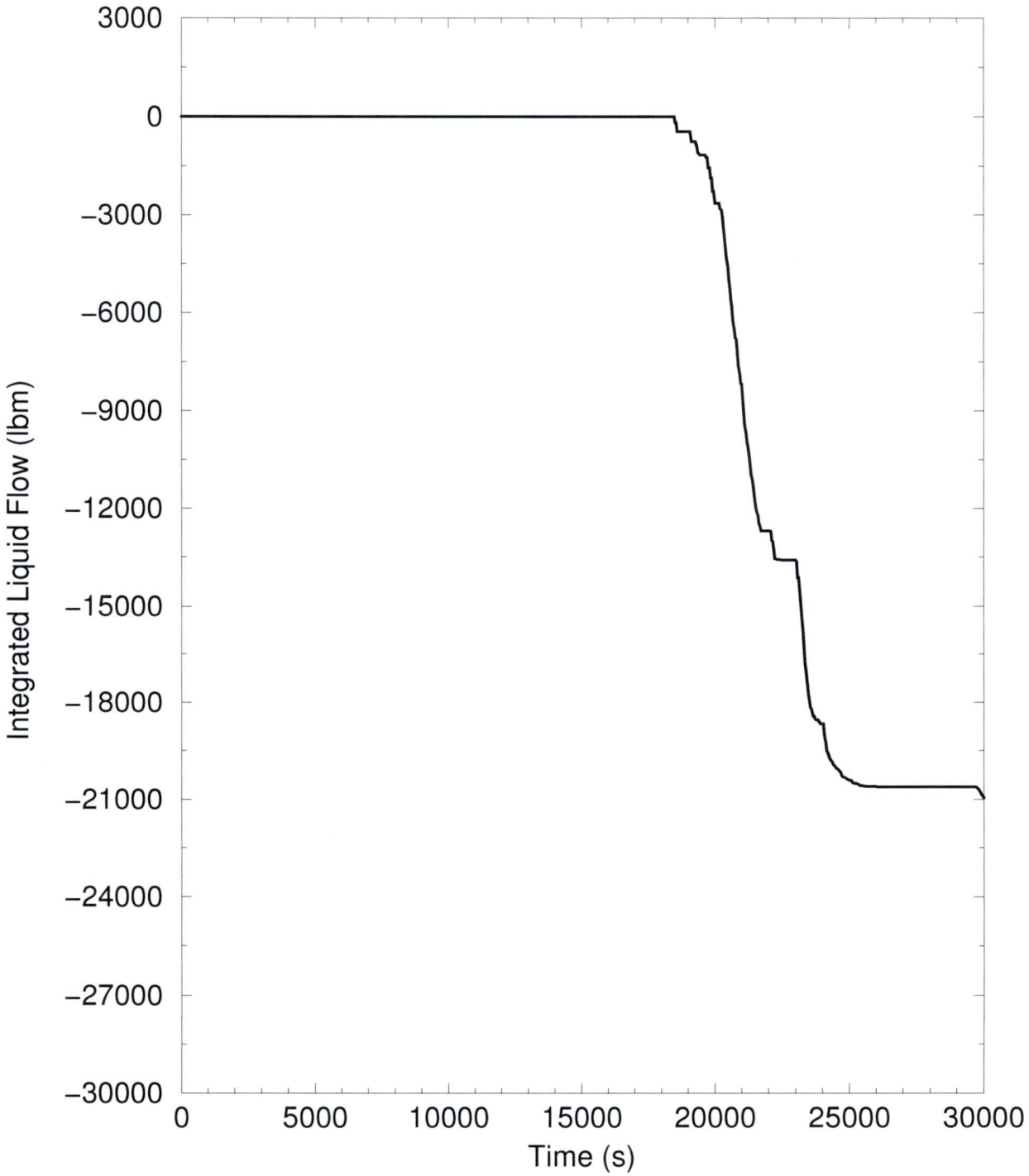

Figure RAI-4.30-4: Integral of Liquid Flow at the Top of the SG U-Tubes on the Broken Loop - ECCS Flowrate = 827 gpm; BB Resistance K/A^2 = [ ] ft^{-4}

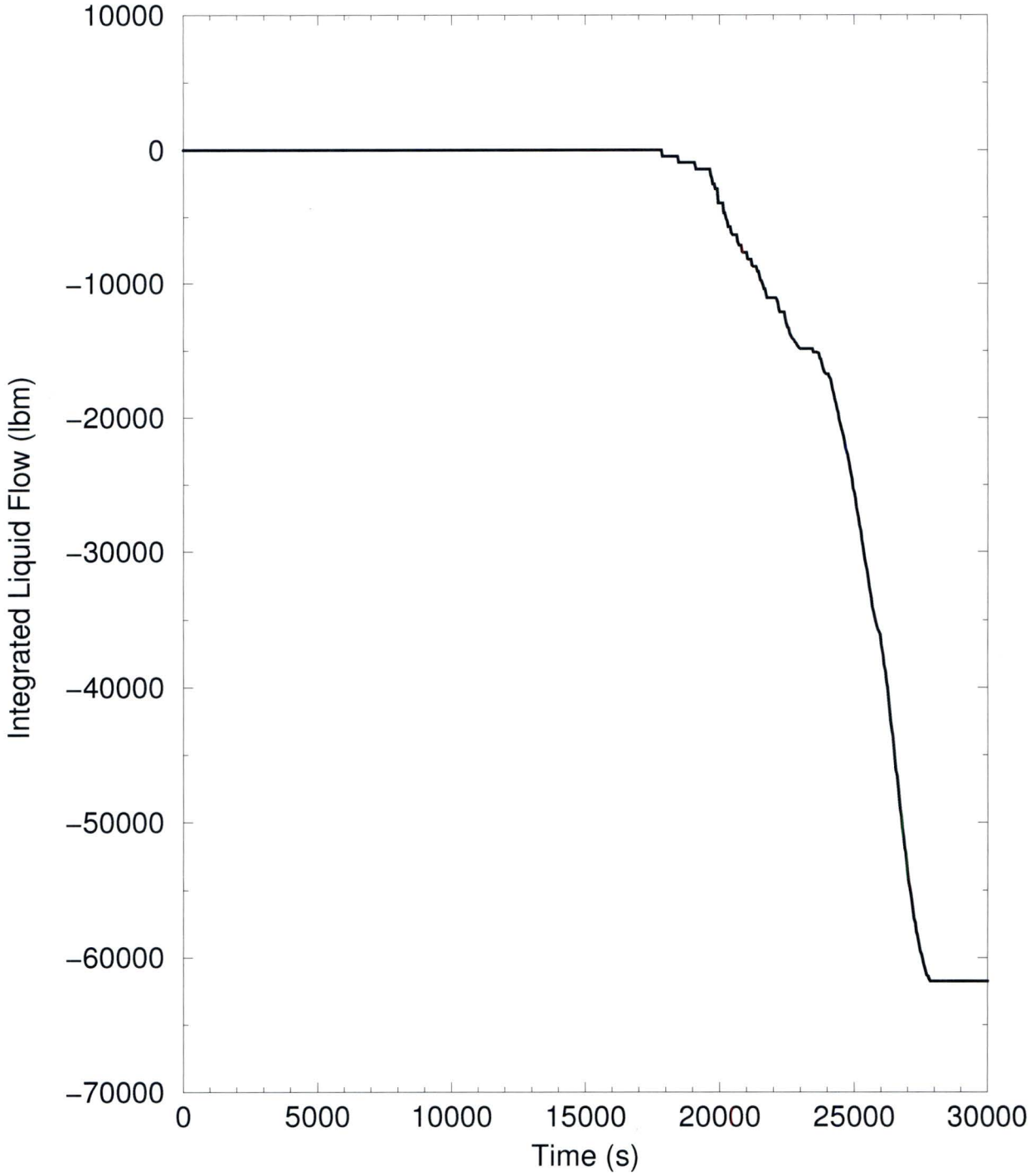

Figure RAI-4.30-5: SG Primary Downside Collapsed Liquid Levels - ECCS Flowrate = 1654 gpm; BB Resistance K/A^2 = [ ] ft^{-4}

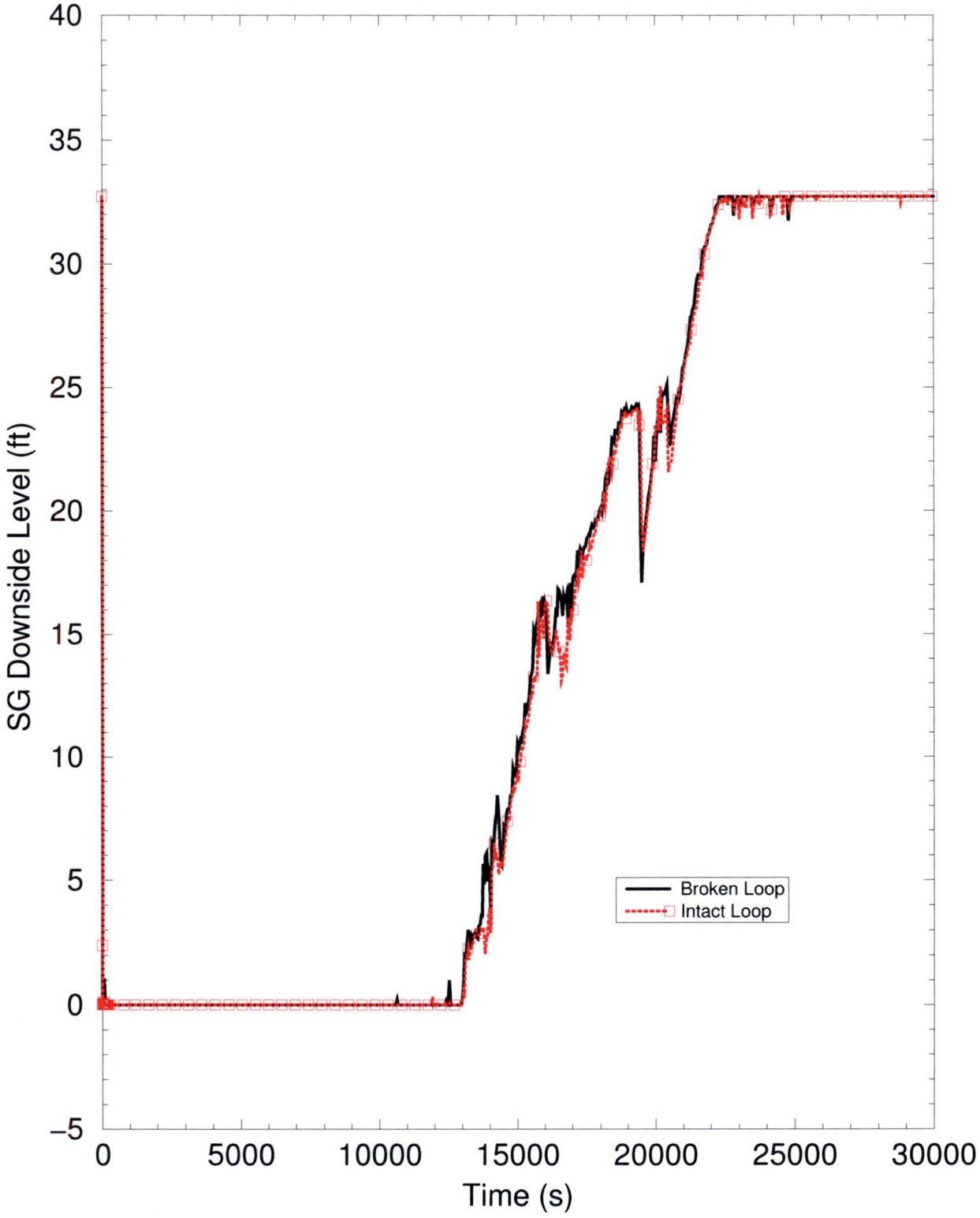

Figure RAI-4.30-6: Liquid Flow at the Top of the SG U-Tubes - ECCS Flowrate = 1654 gpm; BB Resistance K/A^2 = [ ] ft^{-4}

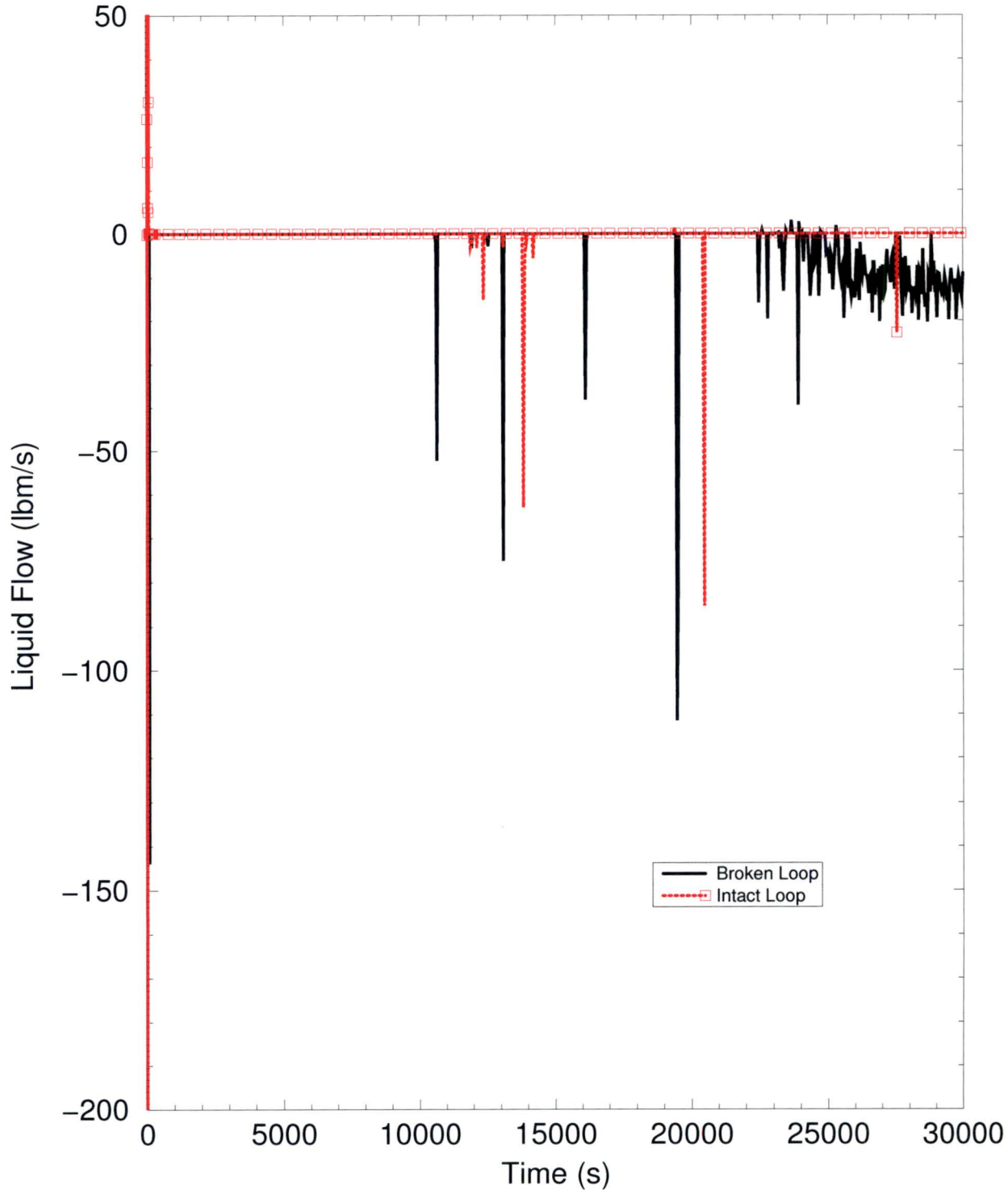

Figure RAI-4.30-7: Integral of Liquid Flow at the Top of the SG U-Tubes on the Intact Loop - ECCS Flowrate = 1654 gpm; BB Resistance K/A^2 = [ ] ft^{-4}

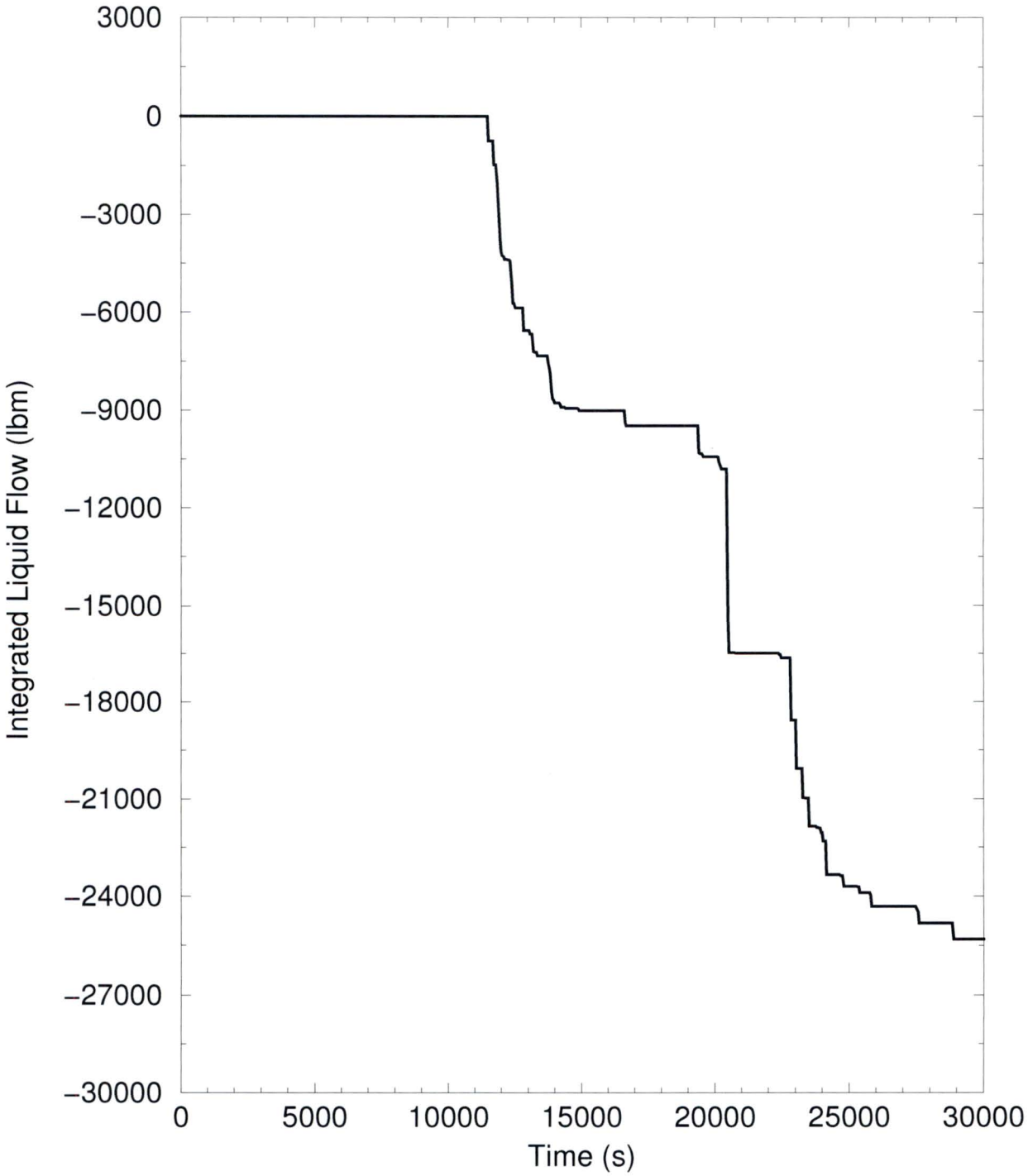

Figure RAI-4.30-8: Integral of Liquid Flow at the Top of the SG U-Tubes on the Broken Loop - ECCS Flowrate = 1654 gpm; BB Resistance K/A^2 = [ ] ft^{-4}

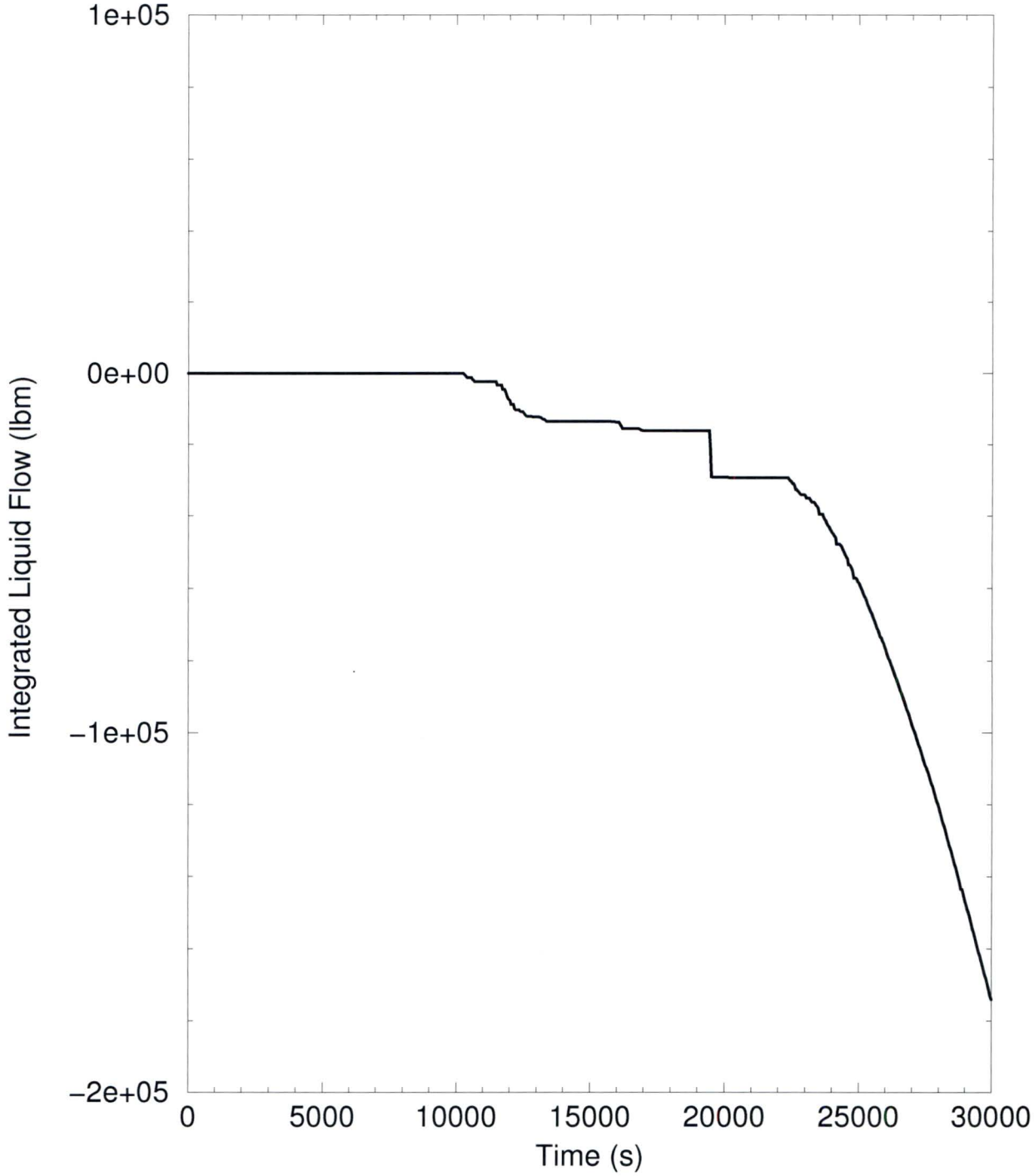

Figure RAI-4.30-9: SG Primary Downside Collapsed Liquid Levels - ECCS Flowrate = 2481 gpm; BB Resistance K/A^2 = [ ] ft^{-4}

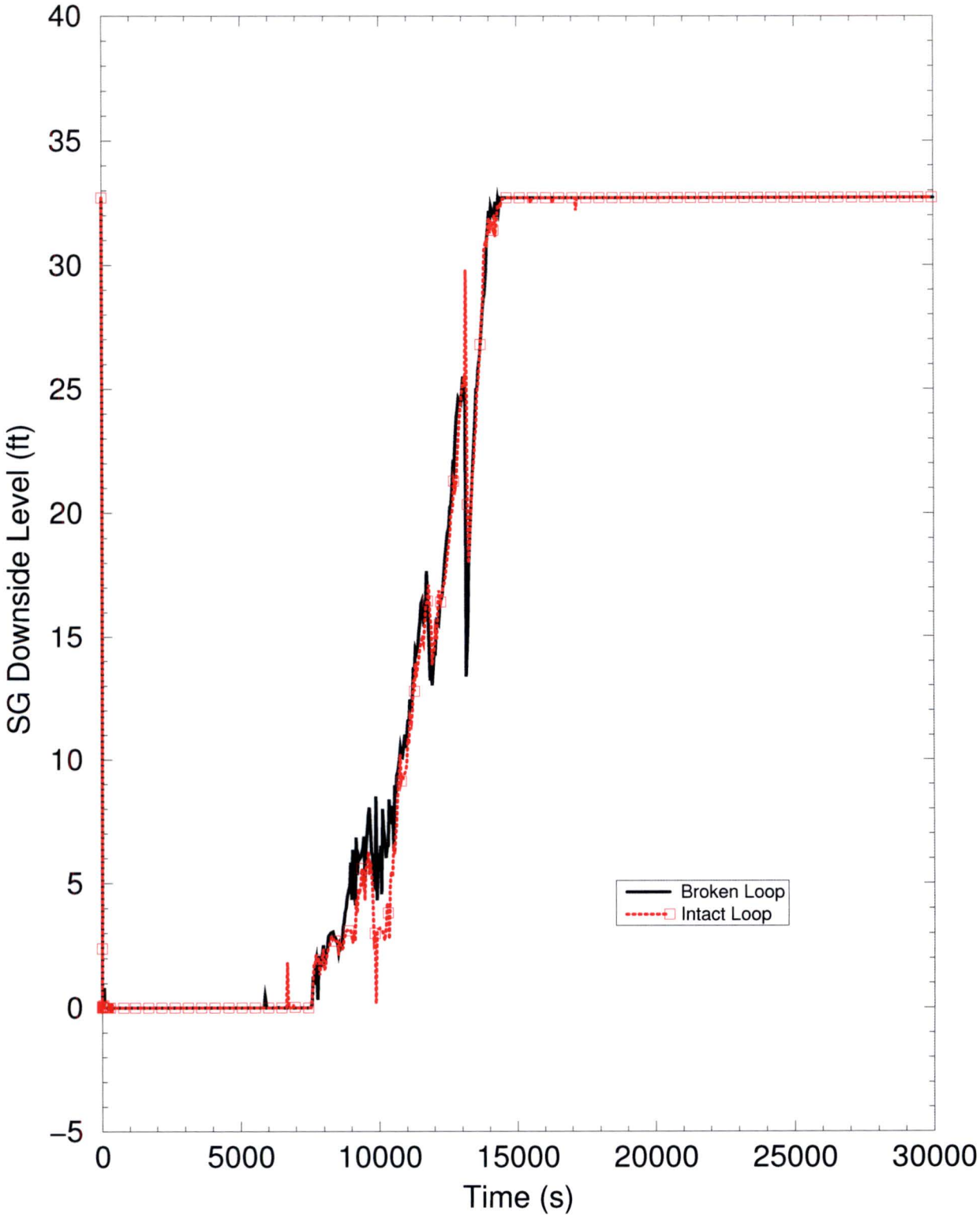

Figure RAI-4.30-10: Liquid Flow at the Top of the SG U-Tubes - ECCS Flowrate = 2481 gpm; BB Resistance K/A^2 = [ ] ft^{-4}

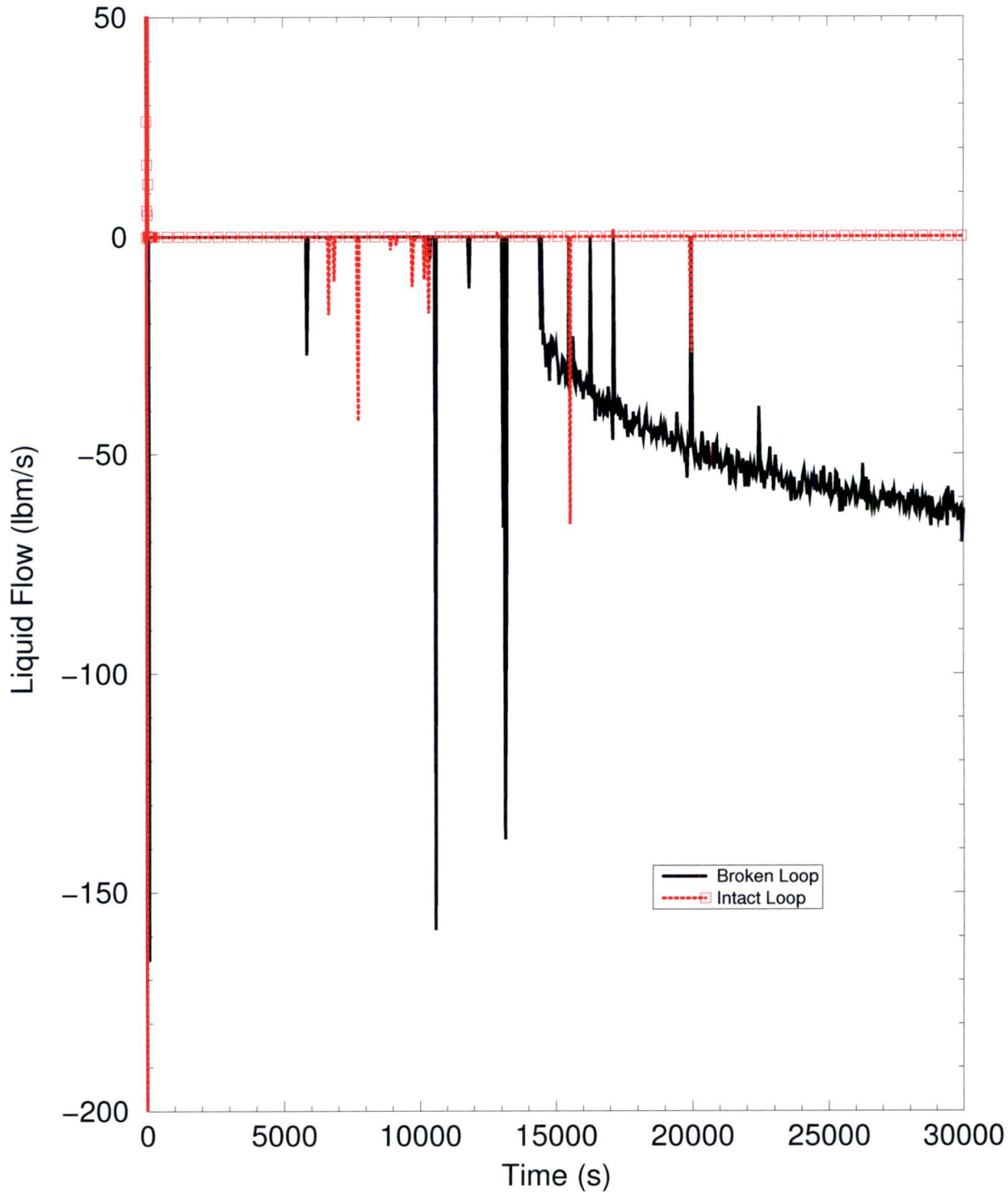

Figure RAI-4.30-11: Integral of Liquid Flow at the Top of the SG U-Tubes on the Intact Loop - ECCS Flowrate = 2481 gpm; BB Resistance K/A^2 = [ ] ft^{-4}

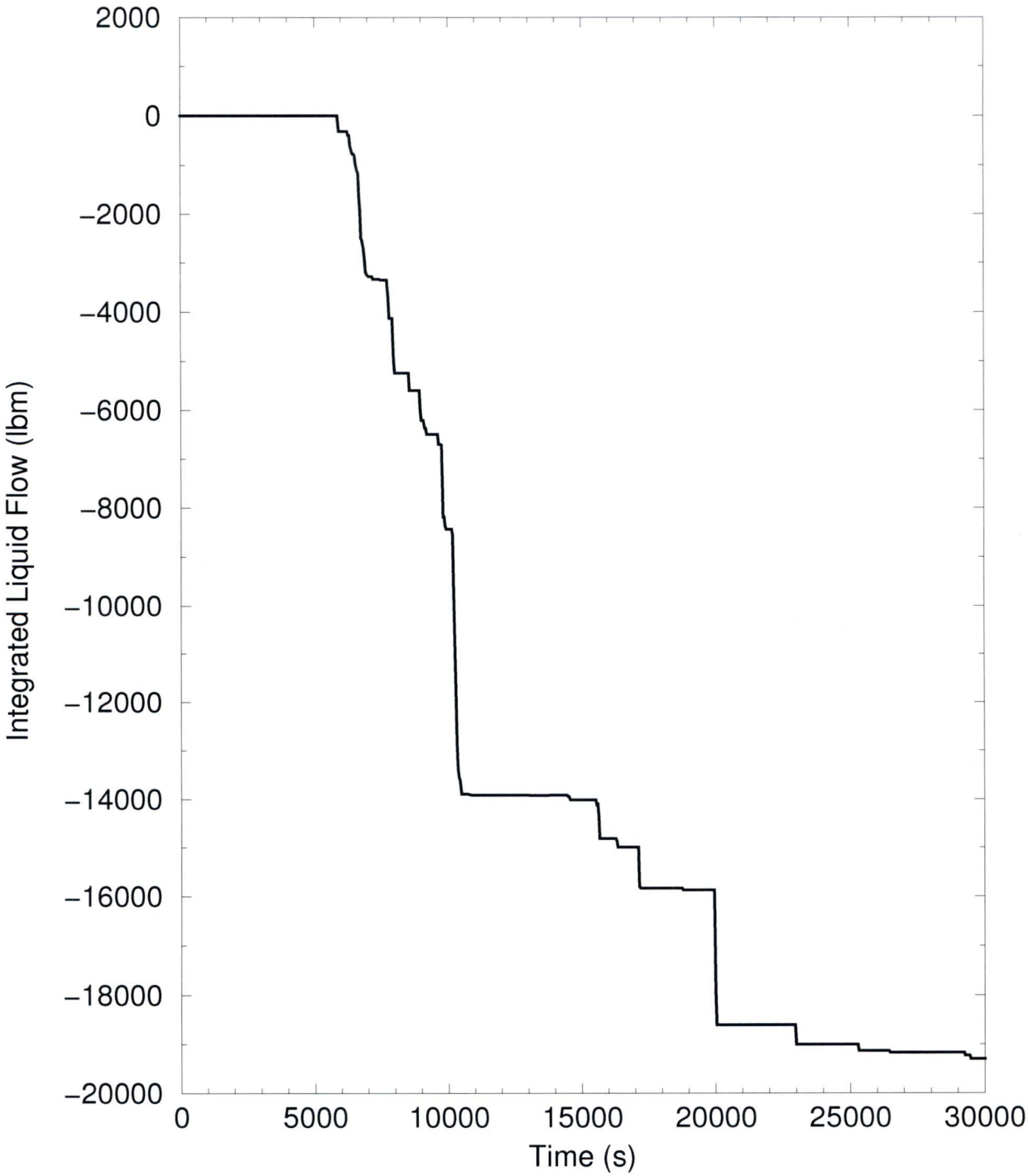

Figure RAI-4.30-12: Integral of Liquid Flow at the Top of the SG U-Tubes on the Broken Loop - ECCS Flowrate = 2481 gpm; BB Resistance K/A^2 = [ ] ft^{-4}

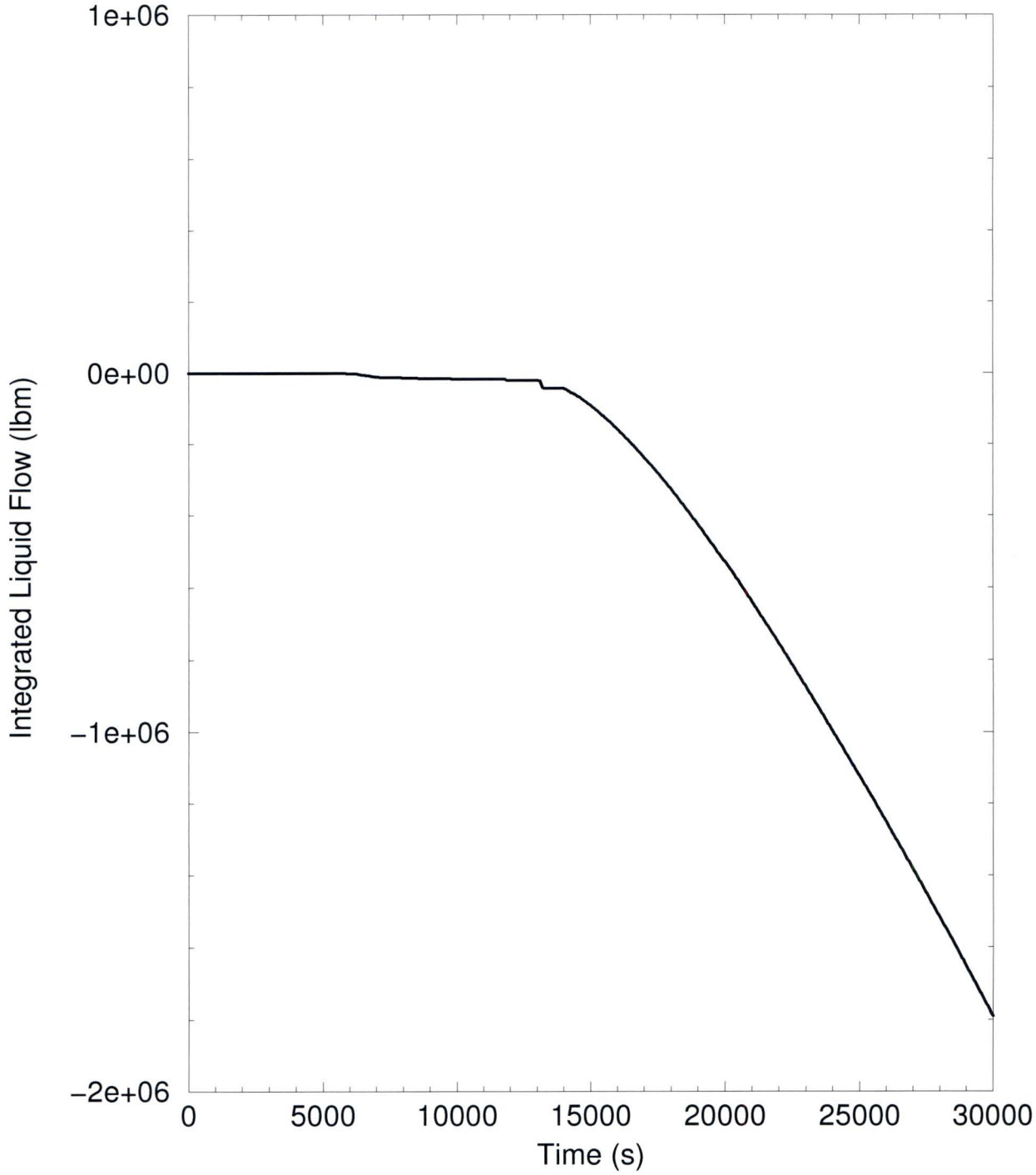

Figure RAI-4.30-13: SG Primary Downside Collapsed Liquid Levels - ECCS Flowrate = 827 gpm; BB Resistance K/A^2 = [ ] ft^{-4}

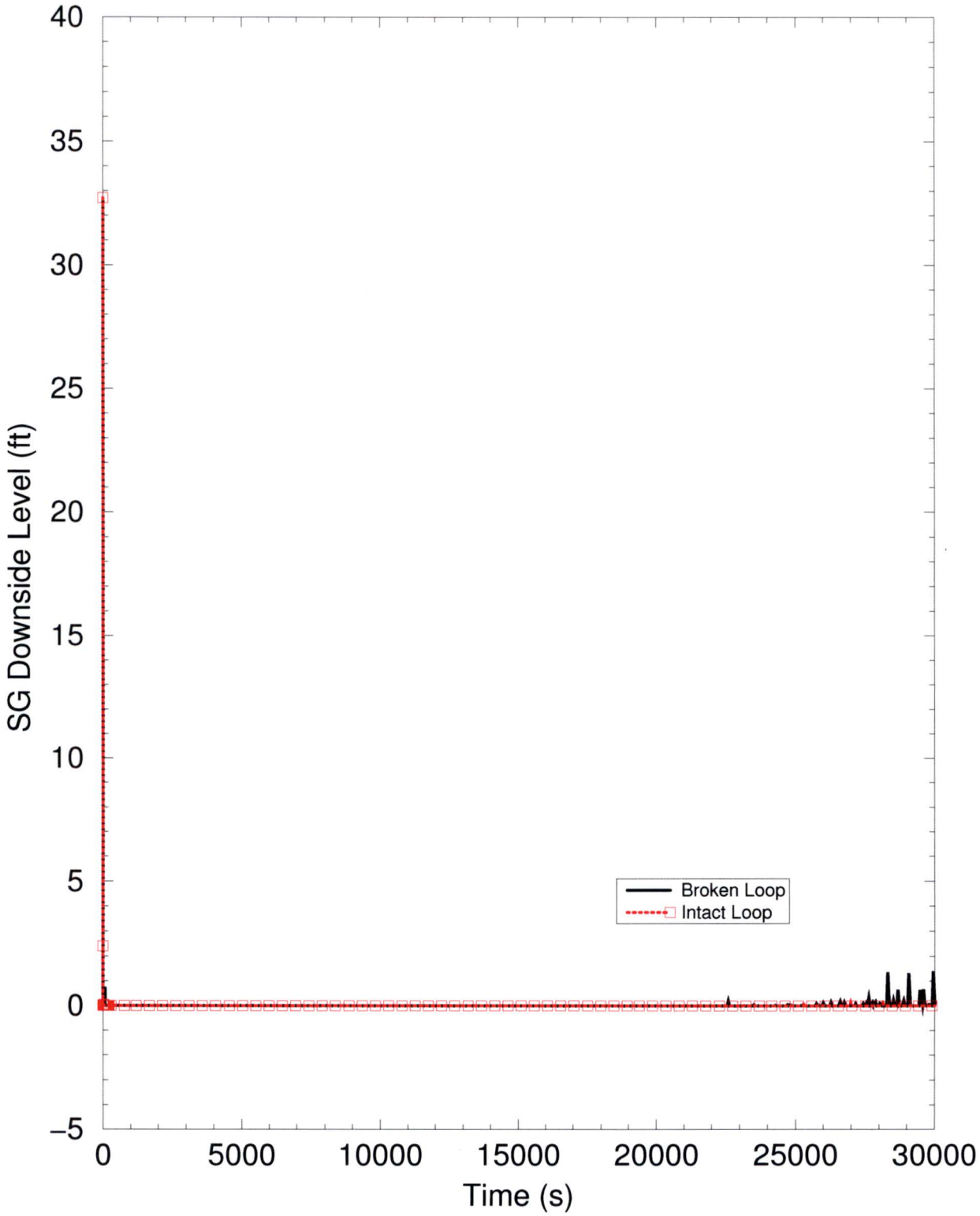

Figure RAI-4.30-14: Liquid Flow at the Top of the SG U-Tubes - ECCS Flowrate = 80gpm; BB Resistance K/A^2 = [ ] ft^{-4}

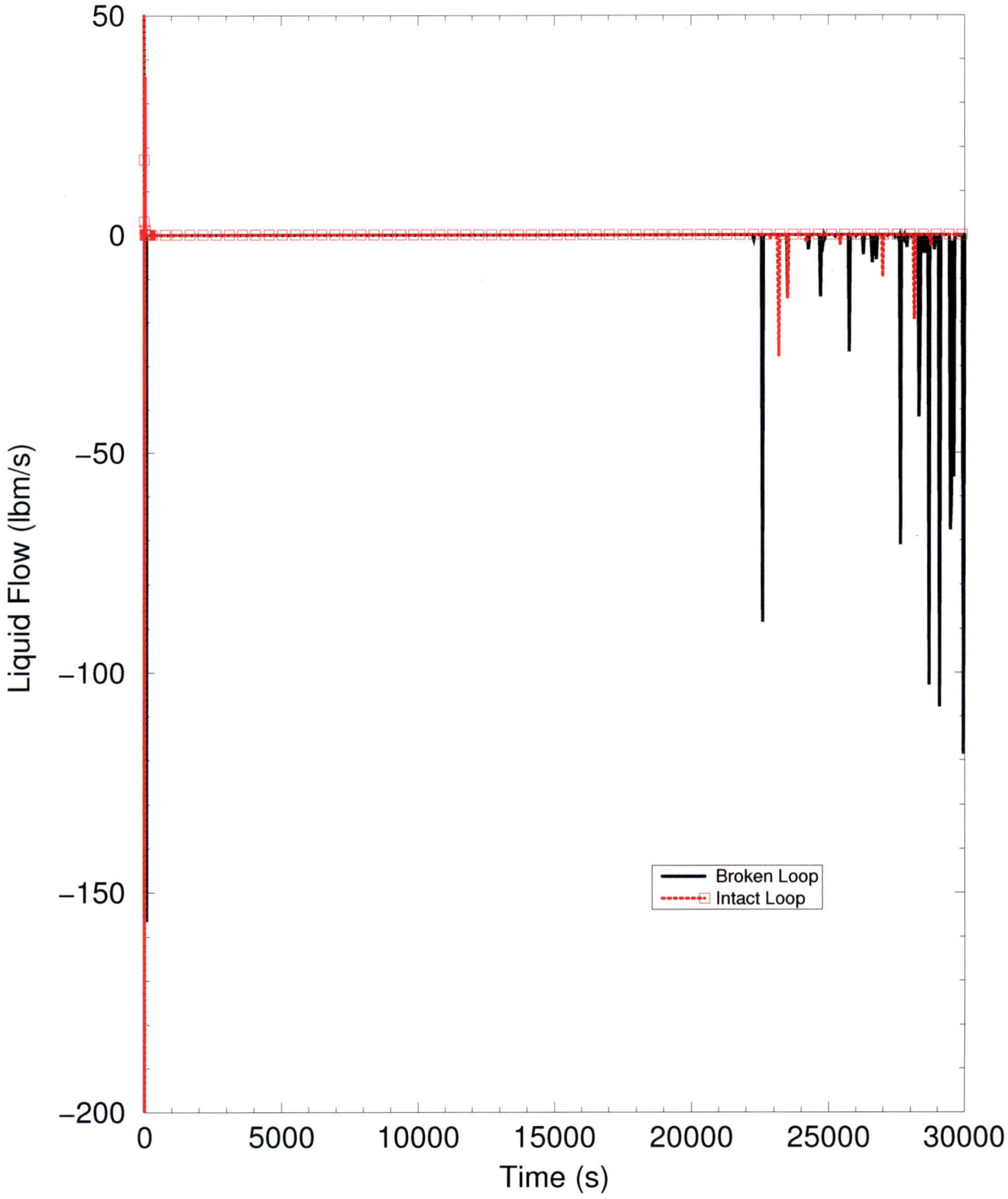

Figure RAI-4.30-15: Integral of Liquid Flow at the Top of the SG U-Tubes on the Intact Loop - ECCS Flowrate = 827 gpm; BB Resistance K/A^2 = [ ] ft^{-4}

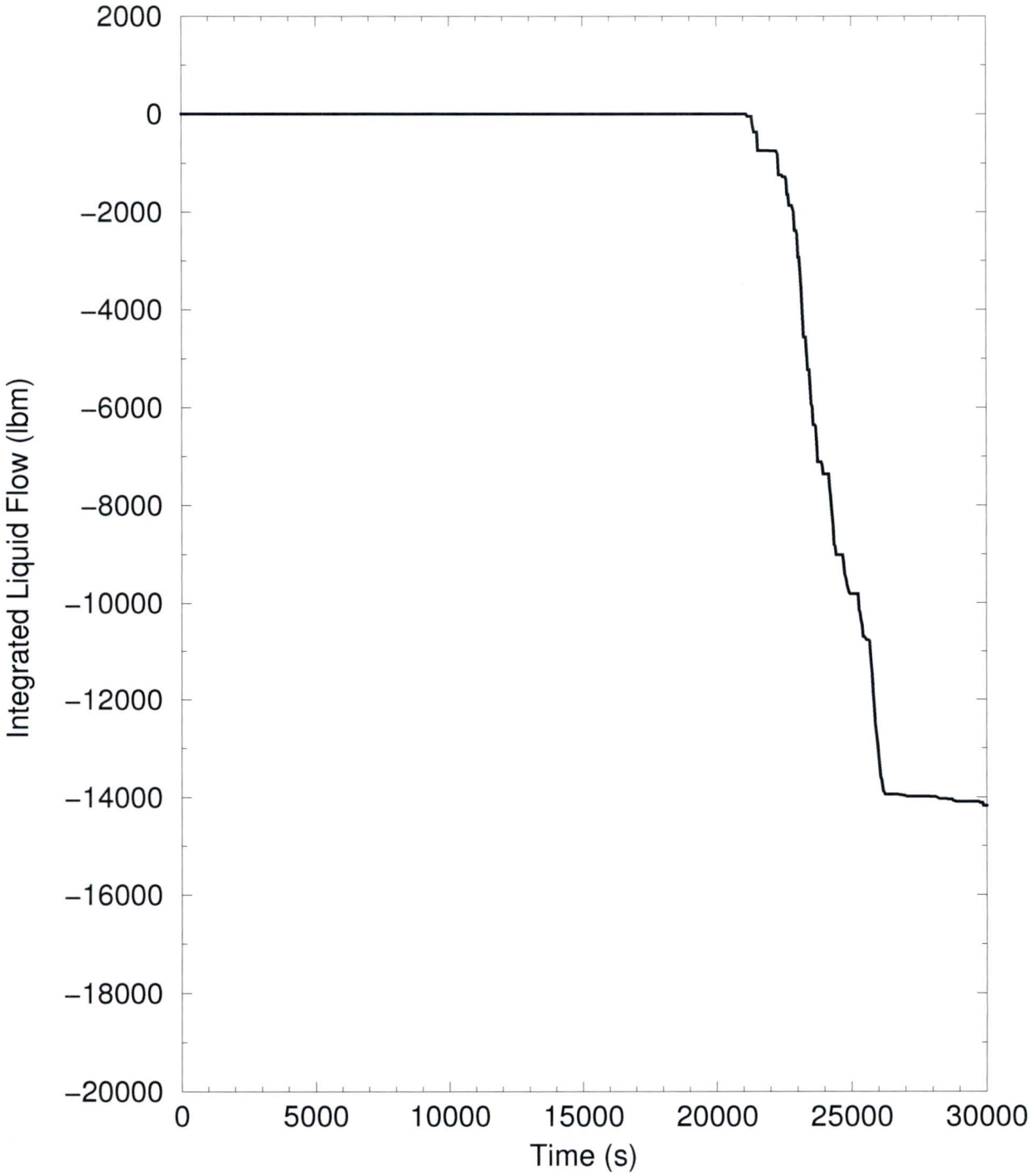

Figure RAI-4.30-16: Integral of Liquid Flow at the Top of the SG U-Tubes on the Broken Loop - ECCS Flowrate = 827 gpm; BB Resistance K/A^2 = [ ] ft^{-4}

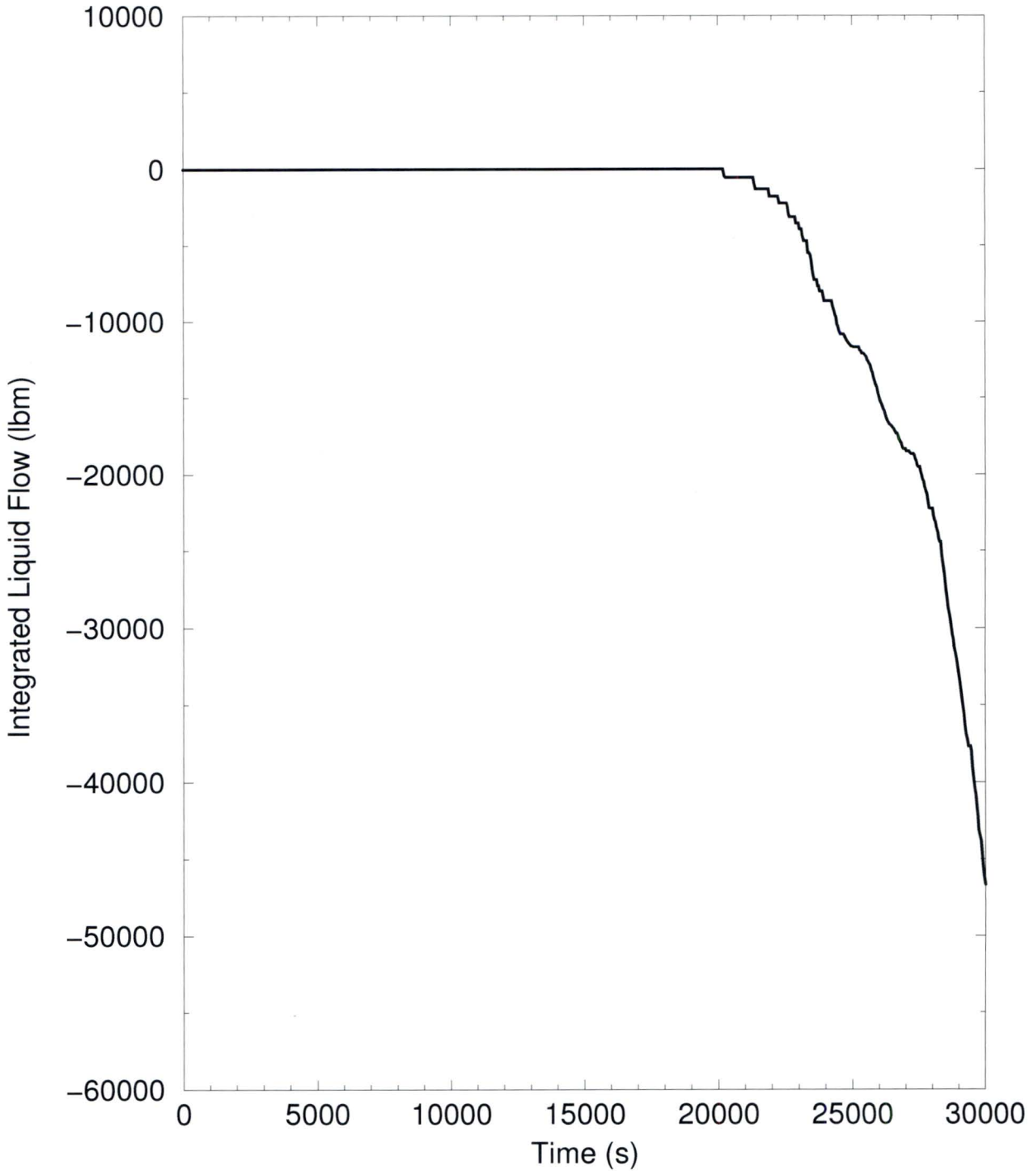

Figure RAI-4.30-17: SG Primary Downside Collapsed Liquid Levels - ECCS Flowrate = 1654 gpm; BB Resistance K/A^2 = [ ] ft^{-4}

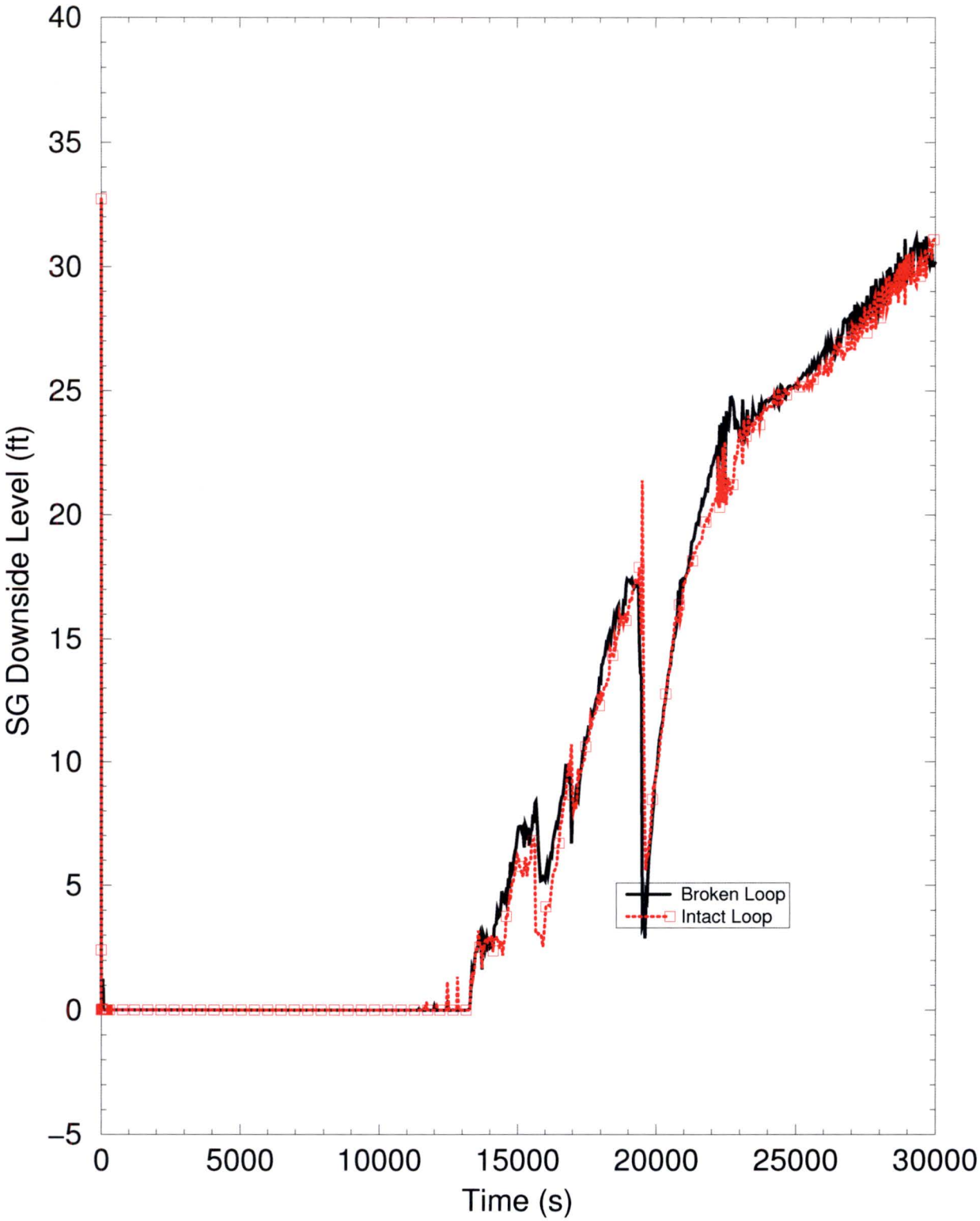

Figure RAI-4.30-18: Liquid Flow at the Top of the SG U-Tubes - ECCS Flowrate = 1654 gpm; BB Resistance K/A^2 = [ ] ft^{-4}

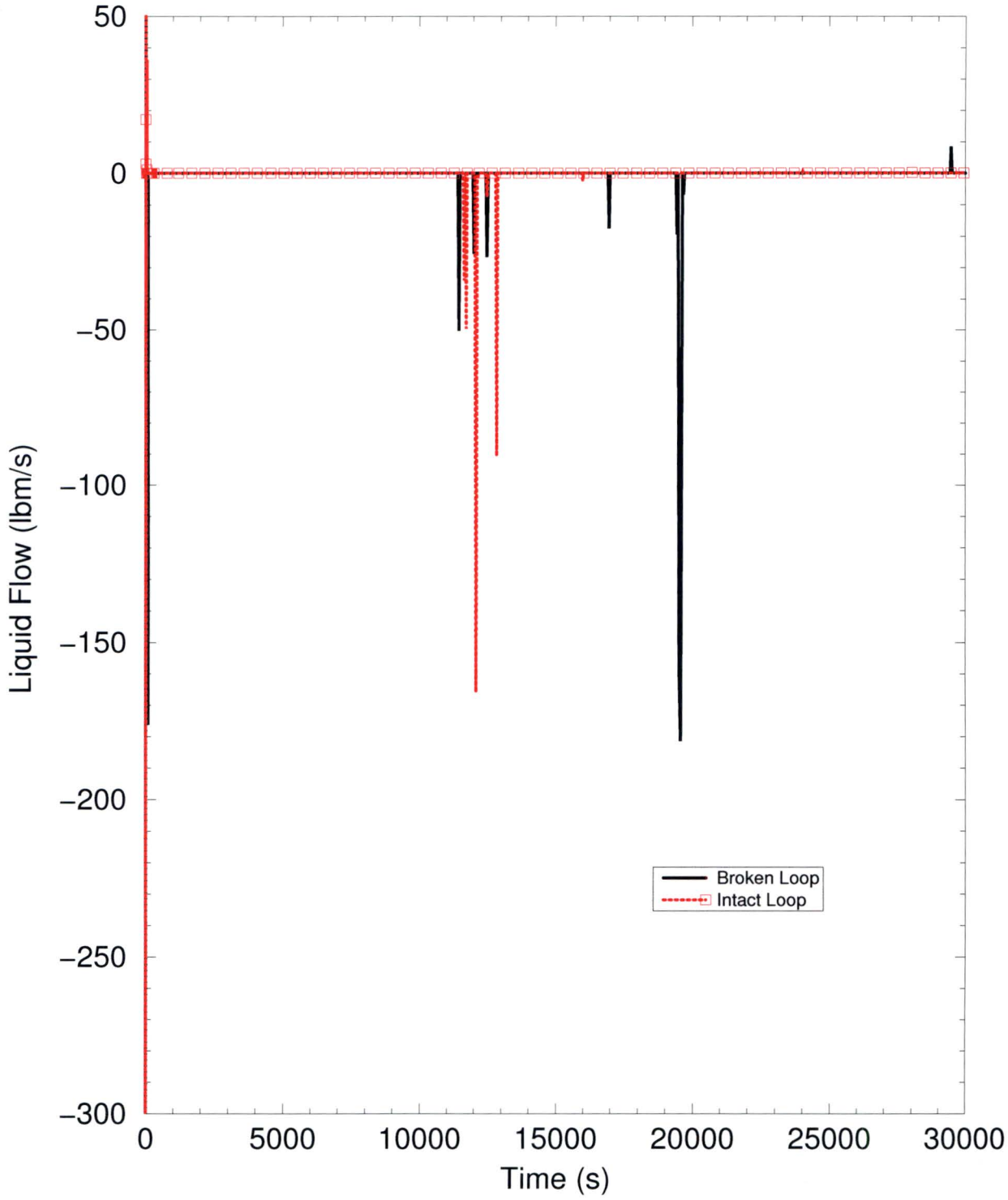

Figure RAI-4.30-19: Integral of Liquid Flow at the Top of the SG U-Tubes on the Intact Loop - ECCS Flowrate = 1654 gpm; BB Resistance K/A^2 = [ ] ft^{-4}

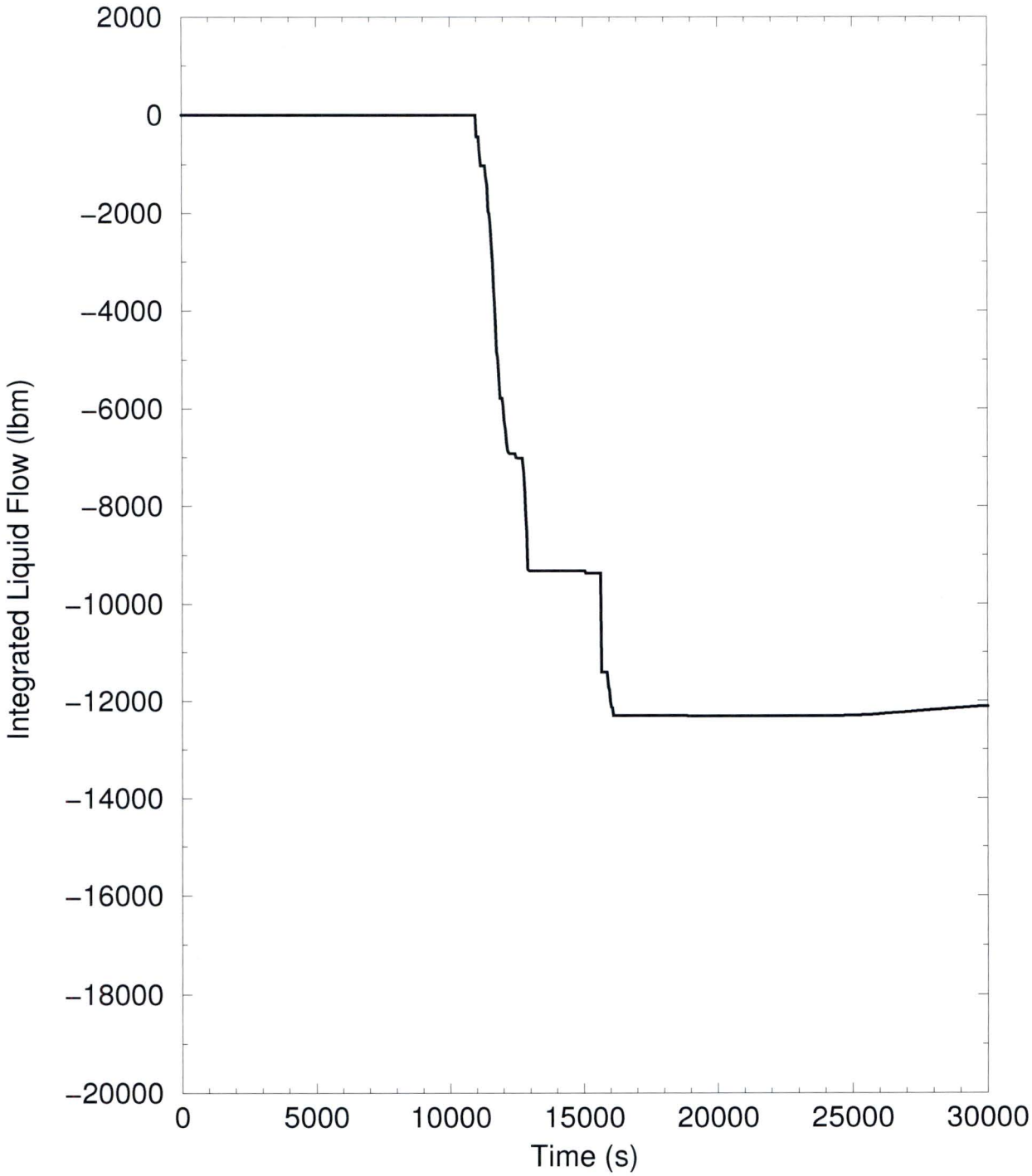

Figure RAI-4.30-20: Integral of Liquid Flow at the Top of the SG U-Tubes on the Broken Loop - ECCS Flowrate = 1654 gpm; BB Resistance K/A^2 = [ ] ft^{-4}

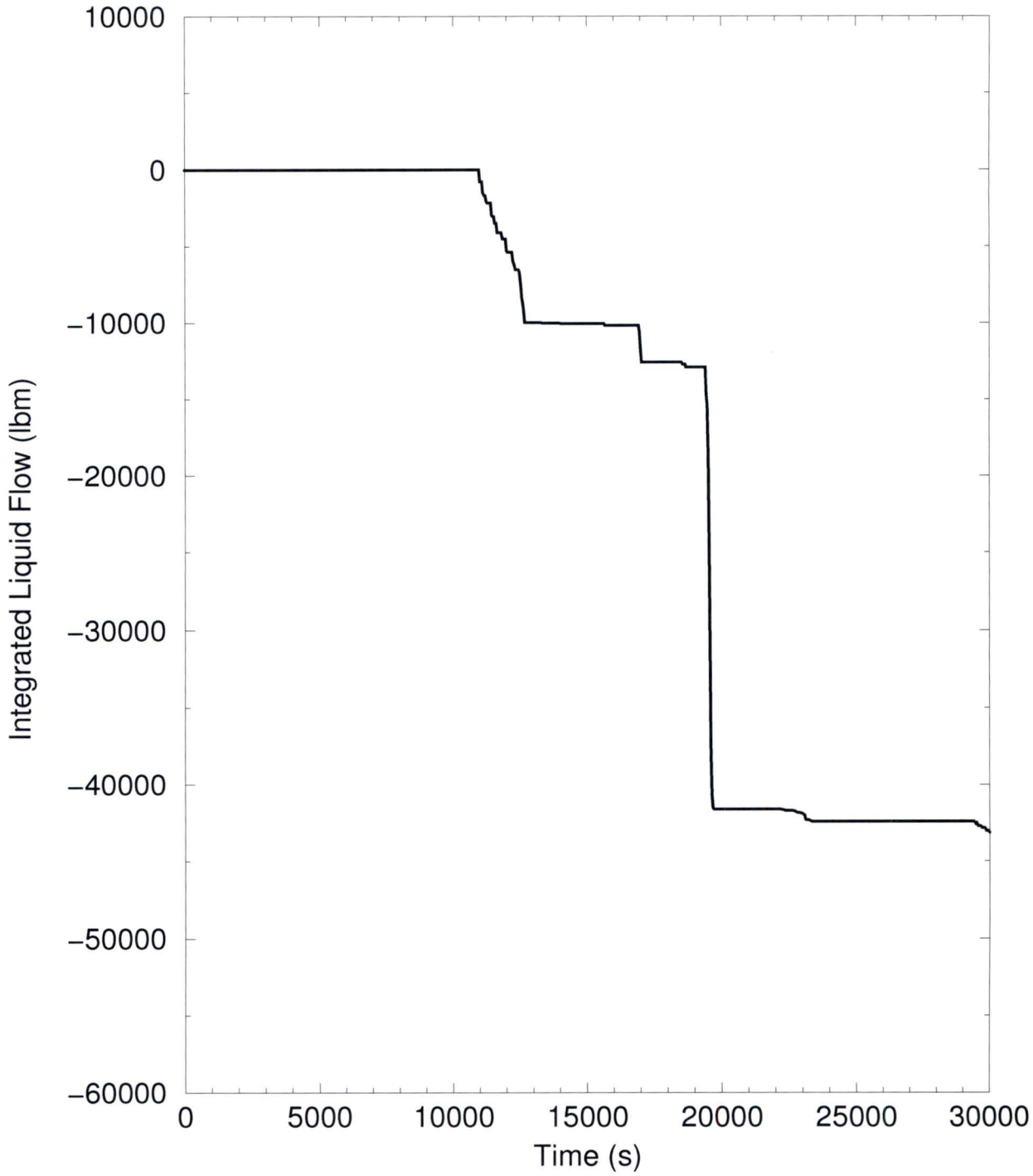

Figure RAI-4.30-21: SG Primary Downside Collapsed Liquid Levels - ECCS Flowrate = 2481 gpm; BB Resistance K/A^2 = [ ] ft^{-4}

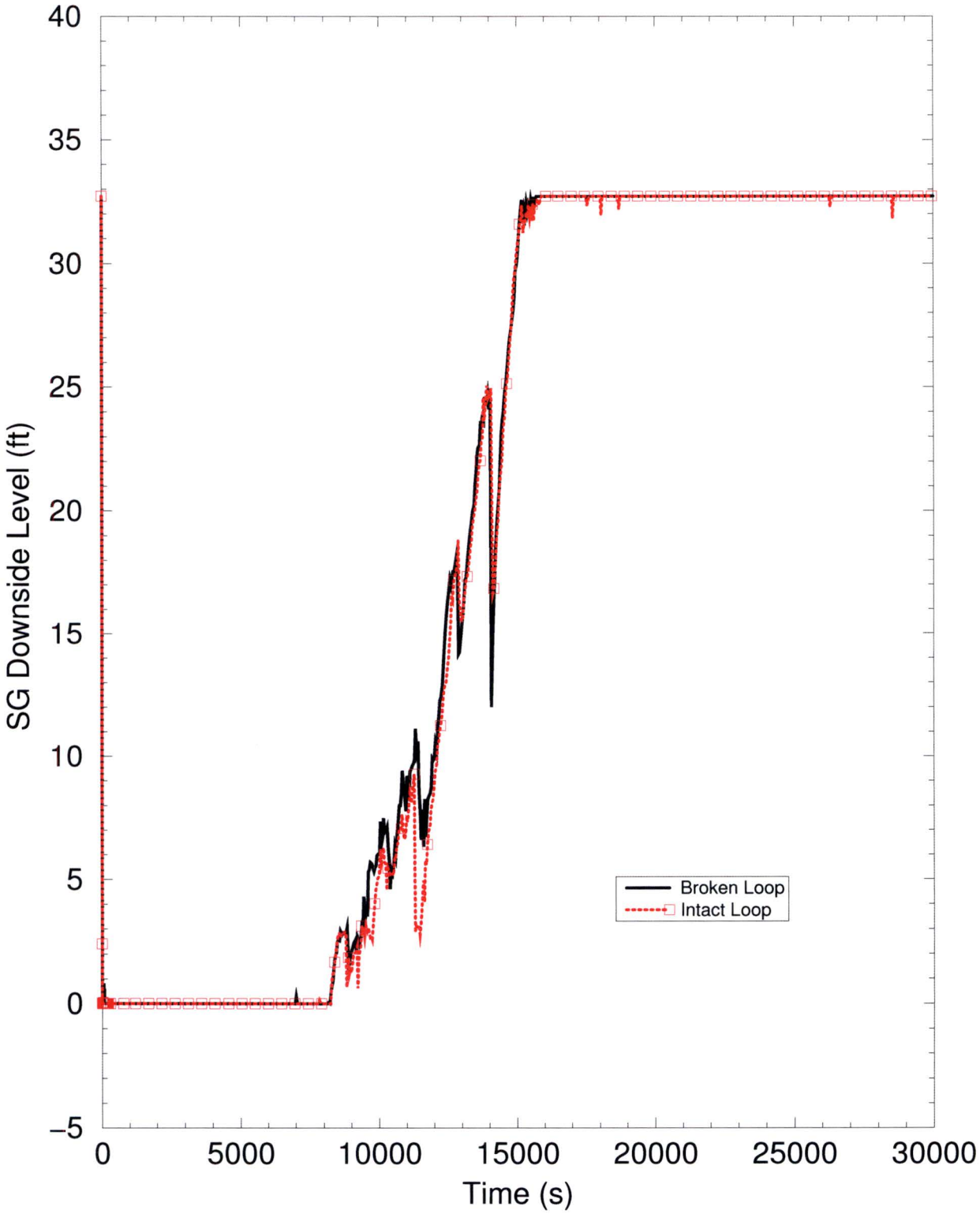

Figure RAI-4.30-22: Liquid Flow at the Top of the SG U-Tubes - ECCS Flowrate = 2481 gpm; BB Resistance K/A^2 = [ ] ft^{-4}

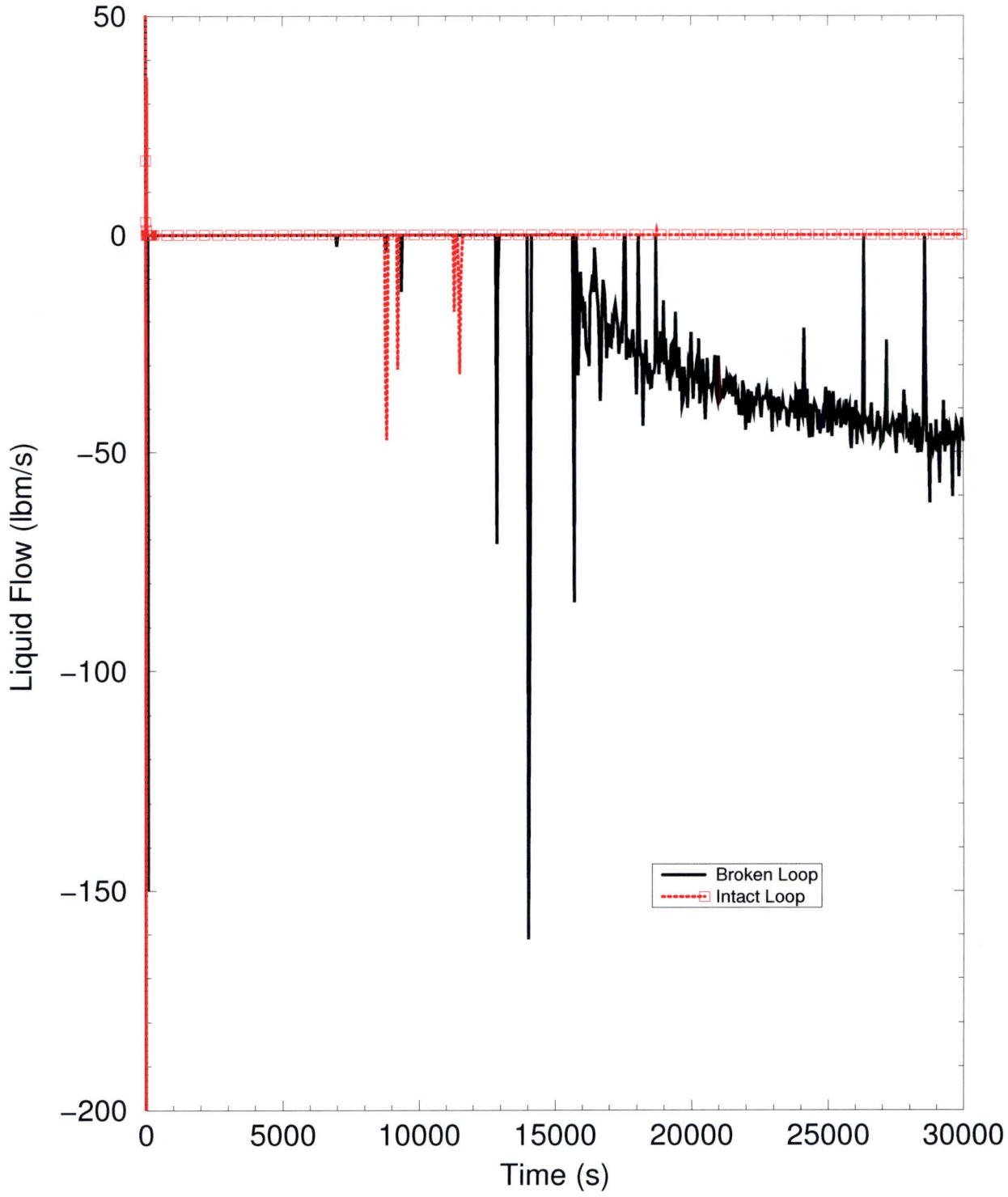

Figure RAI-4.30-23: Integral of Liquid Flow at the Top of the SG U-Tubes on the Intact Loop - ECCS Flowrate = 2481 gpm; BB Resistance K/A^2 = [ ] ft^{-4}

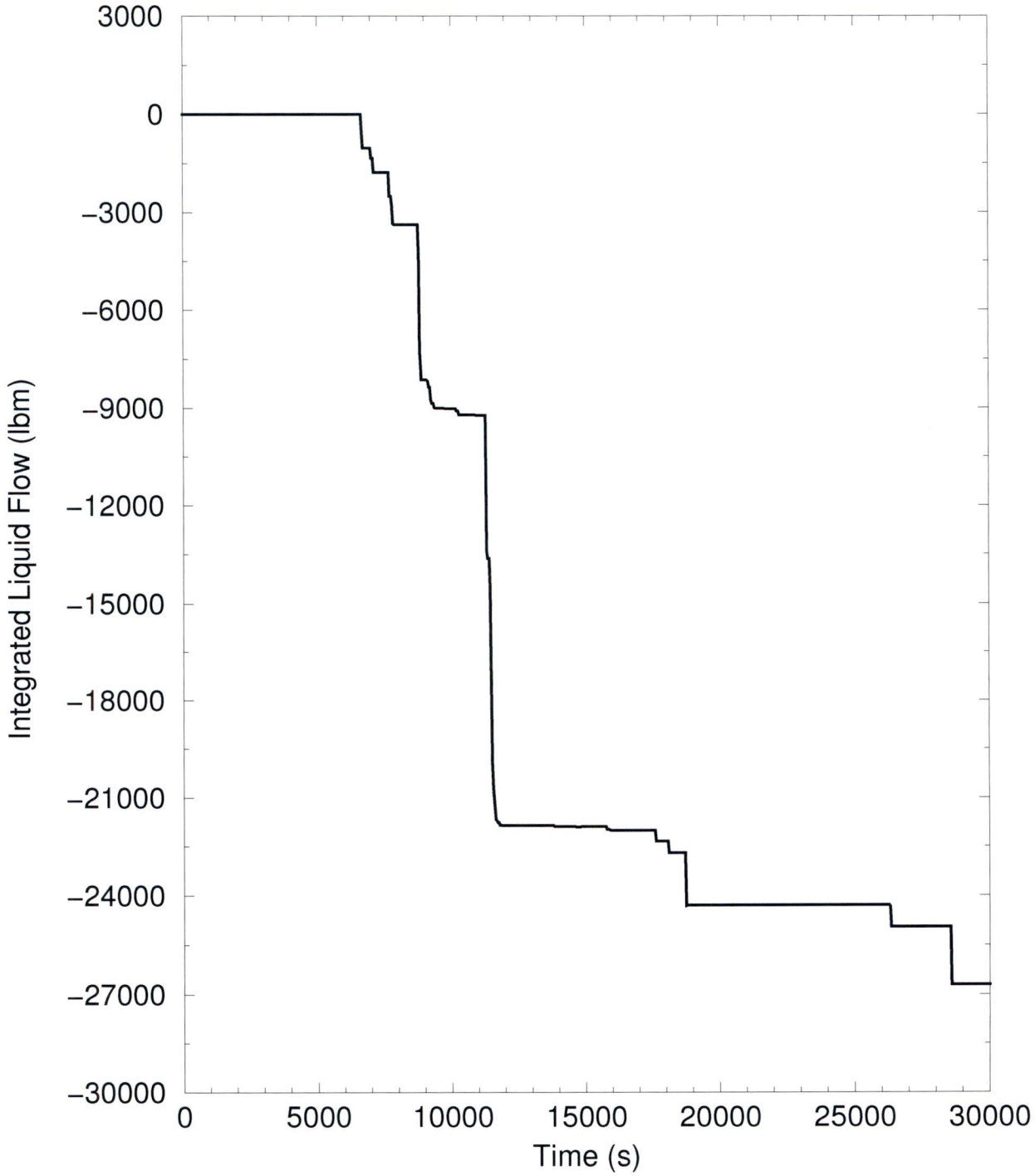

Figure RAI-4.30-24: Integral of Liquid Flow at the Top of the SG U-Tubes on the Broken Loop - ECCS Flowrate = 2481 gpm; BB Resistance K/A^2 = [ ] ft^{-4}

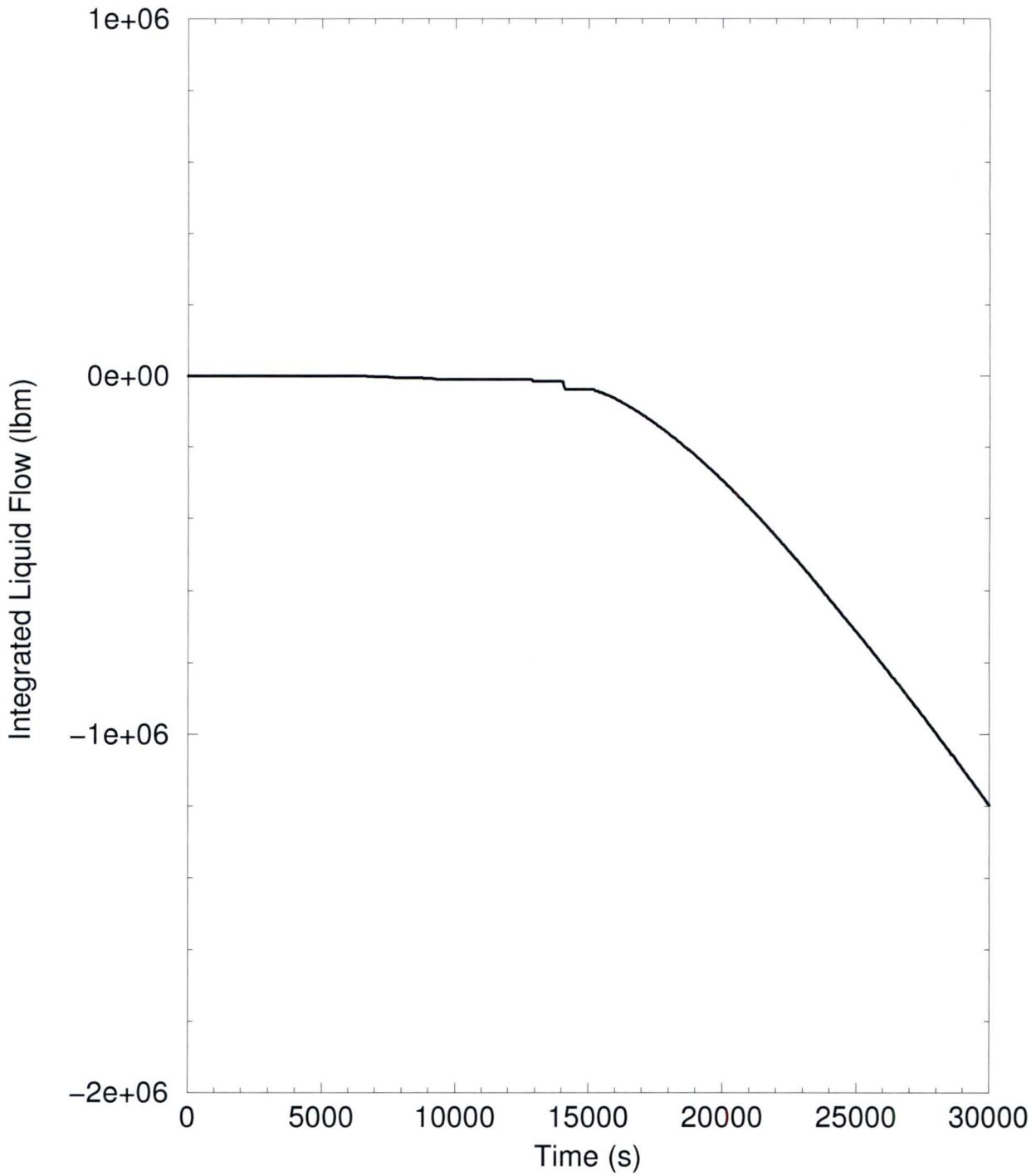

2.30.2.2 Response to RAI 4.30b

The definition of m_{split} is provided in the response to part c of this RAI.

2.30.2.3 Response to RAI 4.30c

For Combustion Engineering (CE) plants, m_{split} is calculated using the following equation:

$$m_{split} = \frac{m_{BB} + m_{UHSN}}{m_{DC}} \qquad \text{(RAI-4.30-1)}$$

where,

m_{BB} = The mass flow rate through the Barrel/Baffle (BB) channel

m_{UHSN} = The mass flow rate through the Upper Head Spray Nozzles (UHSNs)

m_{DC} = The mass flow rate in the downcomer

For the CE plants, $m_{UHSN} = 0$.

This formulation is used to calculate m_{split} shown on Figure RAI-4.20-3 and Figure RAI-4.20-4 in the response to RAI 4.20. As explained in response to RAI 4.30a, the amount of liquid was transported into the reactor upper plenum via the SGs is negligible, and such liquid flow from the SGs is not included in the calculation of m_{split} for the CE plants.